EXPERIMENTAL STUDY OF ADSORBED CATION EFFECTS ON THE FROST SUSCEPTIBILITY OF NATURAL SOILS

A

THESIS

Presented to the Faculty

of the University of Alaska Fairbanks

in Partial Fulfillment of the Requirements

for the Degree of

DOCTOR OF PHILOSOPHY

By

Margaret Marie Darrow, B.S., M.S.

Fairbanks, Alaska

May 2007

EXPERIMENTAL STUDY OF ADSORBED CATION EFFECTS ON THE FROST SUSCEPTIBILITY OF NATURAL SOILS

By

Margaret Marie Darrow

RECOMMENDED:

Advisory Committee Co-Chair

Advisory Committee Co-Chair

Chair, Department of Civil and Environmental Engineering

APPROVED:

Dean, College of Engineering and Mines

Dean of the Graduate School

April 5, 2007

Date

ABSTRACT

Frost heaving is ubiquitous throughout cold regions, causing damage to building foundations, roads, airfields, railways, utilities, and pipelines. Out of the voluminous body of research conducted over the last 80 years, few studies investigated the mineral surface effects on frost heaving. These previous studies were conducted nearly 50 years ago with rudimentary equipment and on homogeneous and artificial soils that have limited applicability to actual field conditions. The purpose of the research presented here is to investigate the adsorbed cation effects on the frost susceptibility of natural soils through experimental testing. A comprehensive suite of laboratory experiments was conducted on five natural heterogeneous soils, including the preparation of divalent and monovalent cation-treated samples. Experimental testing included measurements of engineering index properties, chemical properties, clay content and mineralogy, soil-moisture characteristic curves, unfrozen water content, zeta potential, and frost heave testing. Frost heave tests were conducted using a state-of-the-art laboratory system that demonstrates high repeatability. Soil-moisture characteristic – soil freezing characteristic (SMC-SFC) relations were developed for the five natural soils over an unprecedented range of measurements and using a new approach, which can be related to the Clausius-Clapeyron equation. The SMC-SFC relations yield a new variable, η, which describes the water retention properties of soil at increasing matric potentials and decreasing temperatures. The five untreated soils demonstrated significantly different frost heave ratios, ranging from 0.7 percent to 49.2 percent. Statistical analysis indicates that the frost susceptibility of the five untreated soils is most dependent on adsorbed cations, η, amount of microaggregates smaller than 2 μm, and clay content. For the entire body of untreated and cation-treated samples, statistical analysis indicates that the frost susceptibility is most dependent on adsorbed cations, unfrozen water content, and amount of smectite, kaolinite, and chlorite present in the soil. The results from each cation treatment indicate that the frost susceptibility of: 1) Ca^{2+}-saturated soil is most dependent on zeta potential and unfrozen water content; 2) Mg^{2+}-saturated soil is most dependent on zeta potential and amount of chlorite; and 3) Na^{+}-saturated soil is most dependent on zeta potential, unfrozen water content, and amount of chlorite.

TABLE OF CONTENTS

LIST OF FIGURES

LIST OF TABLES

LIST OF APPENDICES

ACKNOWLEDGMENTS

First and foremost, I thank my co-advisors, Dr. Scott Huang and Dr. Yuri Shur, for pointing me in the right direction, providing me with laboratory support, and offering critical advice. I also thank the other two members of the committee, Dr. Vladimir Romanovsky and Dr. John Zarling, for their words of encouragement and objective perspectives. I am indebted to Dr. Satoshi Akagawa for his unceasing kindness and generosity, and for his invaluable advice gained from years of experience with frost heave testing. Also, I am indebted to Dr. Scott Huang, Dr. Satoshi Akagawa, and Dr. Iwahana Go, for collecting the unfrozen water content data. I also thank Dr. Steve Lin for the use of his laboratory equipment and advice on ζ potential. I am grateful to the National Science Foundation for financial support, and to both NSF EPSCoR and UAF's Civil and Environmental Engineering department for laboratory equipment and the space in which to work.

Several staff members in the Duckering building helped me to solve a myriad of laboratory crises during the "Year of the Lab," including Eric Johansen, Howard Fruhwirth, Tom McCarty, Gary Porter, Joel Bailey, Shane Billings, and Tim Howe. I also thank my office mates, Caroline Maniaci and Matthew Bray, and my coworkers at AK DOT&PF, for enduring my tales of laboratory woes and being continual sources of light-hearted support.

Special thanks go to my father, Dr. Leo Fritschen, and my mother, Eloise Fritschen, for their long-distance guidance, moral support, and understanding. I thank my children, Everett and Eloise, for keeping me grounded in the reality of what playing in the dirt is all about. And finally and most of all, I thank my husband, Daniel Darrow, without whose unlimited patience, support, and enormous self-sacrifice, none of this would have been possible.

CHAPTER 1: INTRODUCTION

1.1 General Overview

Frost heaving is a widespread problem throughout cold regions. This phenomenon causes damage to building foundations, roads, airfields, railways, utilities, and pipelines. With a growing world population and finite natural resources, this problem will become increasingly acute as cold regions see further development.

Frost heaving can be defined as the upward movement of the ground surface during freezing due to an overall increase in soil water content. The requisites for this process are fine-grained soil, freezing conditions, and the availability of water. During the freezing process, excess ice develops in the soil. The ice may be hardly visible, or may form tiny discrete ice lenses or massive ice lenses centimeters-thick, depending on the freezing conditions and soil properties.

Researchers have studied this phenomenon for over 80 years. From the wealth of experimental data and theoretical analysis, we now understand the fundamental elements of the frost heaving process; however, no one theory or empirical approach can fully describe the process nor predict frost heave damage with certainty. Clearly, elements of this complicated phenomenon still remain to be investigated and explained.

1.2 Literature Review

Initially, an attempt was made to create a comprehensive history of frost heave research; however, during the collection of over 300 papers, it became clear that a truly comprehensive history is difficult to produce and would stray too far from the focus of this dissertation. Instead, this generally chronological review focuses on laboratory work, and associated theoretical approaches and numerical modeling, done on fine-grained, saturated soils with a few exceptions: it does not contain discussions of the thermal properties of soils, heaving pressure, or field experiments.

In the past few decades, many excellent summaries and reviews of frost heave tests and theories have been written. In his short book Pipelines and Permafrost, Williams (1979) summarized the current frost heave theories and several fundamental equations common to the frost heave models. MacKay et al. (1978), Loch (1981), and Smith (1985) presented reviews of the capillary theory, the hydrodynamic theory, the secondary heave theory, and the adsorption

force theory. In addition to reviewing these theories, Chamberlain (1981) summarized over 100 frost heave criteria, mostly used by transportation departments. Chamberlain (1986) and Nixon (1987) reviewed the available frost-susceptibility test methods. Kay and Perfect (1988) and Ladanyi and Shen (1989) presented reviews of frost heave theories, and of heat and mass transfer in freezing soils. Anderson and Morgenstern (1973) presented a comprehensive review of physics and chemistry as related to frozen ground. Their paper included summaries of x-ray diffraction studies of clay-water mixtures, experiments using the nuclear magnetic resonance method, as well as other methods used to measure unfrozen water content. Henry (1988, 2000) presented reviews of the chemistry and thermodynamics of freezing soils. Mokwa's (2004) review of the major frost heave theories included segregation potential.

Frost heaving was recognized as a destructive phenomenon as early as the 17th century (Beskow 1935). Research in this area began in earnest in the early 20th century with the work of Bouyoucos, who investigated the behavior of moisture freezing in soil samples (Bouyoucos 1917, 1920). Through freezing experiments using a dilatometer, he determined that not all water in a soil freezes at temperatures below 0°C, and the amount that remains unfrozen depends on the temperature and the soil properties. He noted that fine-grained soil, such as clay, has a higher unfrozen water content at a given temperature than coarse-grained soil, such as sand. Bouyoucos developed a classification for soil moisture in frozen soils, calling water that freezes between -4°C and -78°C "capillary-adsorbed" water, and water that does not freeze below -78°C "combined" water.

Taber was the first to make methodical observations of the frost heave phenomenon (Taber 1929, 1930). He made his initial observations during the winter of 1914-1915, when he placed saturated soil samples out-of-doors during cold nights. For his later laboratory experiments, Taber acquired a freezing cabinet, which allowed him to control the temperature of the freezing tests. He observed that ice lenses typically form perpendicular to the freezing direction, that the rate of freezing affects the size and quantity of segregated ice lenses, and that fine-grained soils are more likely to form ice lenses than coarse-grained soils. He theorized that in order for the freezing front to remain stationary in the soil, the heat coming to the freezing front must equal the heat conducted away from it. Taber determined that frost heaving is not due solely to the volume expansion of water upon freezing, but that the moisture content of certain soils increases during the freezing process. He noted that clay samples would shrink away from the container during freezing, and develop vertical shrinkage cracks that would subsequently fill

with ice. Taber noted that for some soils, a portion of the water does not freeze even when exposed to sub-freezing temperatures for long periods of time. He attributed this observation to the surface effects of the soil particles, calling the unfrozen water "adsorbed water."

Working contemporaneously with Taber, Beskow (1935) published his field observations and summarized the results of his extensive laboratory work. His comprehensive work addressed several different characteristics of the frost heave phenomenon. According to Beskow, the key components of the frost heaving phenomenon are soil grain size and distance to a water table. He observed that, in clayey soil, the soil in between the ice lenses is not frozen. He noted that vertical cracks form ahead of the freezing front in clays, and attributed these to soil desiccation. Beskow noted that increasing overburden pressure decreases both the freezing rate and the freezing point, and that coarse-grained soils experience water expulsion upon freezing. He described these and other observations in terms of the water content and movement within the freezing soil. From his copious freezing tests, Beskow produced several empirical equations and graphs, including formulae to describe the effects of grain size, ground water, diurnal temperature changes, and graphs of unfrozen water content curves. Beskow described soil particles as being surrounded by water layers. The layers closest to the surface are held more tightly to the surface than those at a greater distance, and Beskow attributed the flow of water to the freezing front to these unfrozen water films. The water molecules that are closest to the ice lens eventually freeze onto the ice lens, causing additional water molecules to join this unfrozen film from below. Beskow called this process the "migration of the absorption films." He was also the first to describe the frozen fringe, which is the zone between the warmest ice lens and the freezing front. Alternatively, this area has been called the "freezing fringe" to better describe its dynamic nature (Nixon 1991, Krantz and Adams 1996). Like Bouyoucos, Beskow described different kinds of soil water. He called the water that has the strongest bond to the soil surface "chemically bound," and considered it as part of the mineral surface. The next closest water to the mineral surface is highly susceptible to mineral surface effects, which Beskow called either "adsorbed water" or "hygroscopic water," depending on the degree of saturation of the soil. As a dry soil intakes water, these adsorbed water films increase in thickness, and form "funicular water" between adjacent soil particles. When the pores are completely filled, then this water is called "capillary water." Beskow indicated that there is no clear distinction between adsorbed water and capillary water; rather, a continuum of water states exists between these two end members. Beskow highlighted soil water in his research because he considered the adsorption

forces to be important in the freezing process, affecting the freezing temperature of water and the freezing characteristics of fine-grained soil.

The results of research conducted during the 1930's and 1940's have become fundamental in engineering practice and frost heave theories. Casagrande (1931) indicated that: "Under natural freezing conditions and with sufficient water supply one should expect considerable ice segregation in non-uniform soils containing more than three percent of grains smaller than 0.02 mm, and in very uniform soils containing more than ten percent smaller than 0.02 mm." This statement has been referred to as the Casagrande criteria (Penner 1959), and has been used to develop gradation requirements for non-frost susceptible base course material in pavement structures. In 1943, Edlefsen and Anderson published "The Thermodynamics of Soil Moisture," which has become the defining work on this subject. In the 1950's, transportation organizations began to create apparatus for testing the frost susceptibility of soil, and the results of the subsequent experiments added to the understanding of frost heaving. Jumikis (1957) demonstrated that vapor transport is insignificant in the frost heaving process, and Higashi (1958) determined that the soil moisture content is related to the frost heave ratio, that the form of segregated ice correlates to the frost heaving rate, and that the freezing rate is related to sensible heat loss.

The first frost heave theory was introduced as a result of the wide-spread frost heave testing in the 1950's. Gold (1957) presented a possible mechanism for the upward movement of water in a freezing soil. He based his work on thermodynamic considerations and the pore geometry of the soil. In general, a pressure difference exists across a curved surface, as was demonstrated by Kelvin in his experiment with capillary rise (Hunter 2001). The version of the Kelvin equation that often is seen in frost heave literature is

$$P_i = P_w + {}^{2\sigma_{iw}}\!/_{r_{iw}} \tag{1.1}$$

where P_i and P_w are the pressures of ice and water, respectively, and σ_{iw} and r_{iw} represent the surface tension and the radius of the ice-water interface, respectively (see Appendix A for a comprehensive list of symbols and notation used in this manuscript). Gold used Equation 1.1 and a form of Gibb's thermodynamic potential to discuss the equilibrium conditions in a freezing soil, stating that a positive pressure must develop between the ice and the solid mineral grain in order for equilibrium to be maintained.

Penner (1956, 1957) also published research on this topic, laying the groundwork for what is now known as the "capillary theory." Through his experiments, Penner demonstrated that a soil moisture tension is created as a fine-grained soil freezes. He proposed that the soil moisture tension is the result of the radius of curvature of the ice-water interface in small pores. The Clausius-Clapeyron equation relates the temperature to the pressure at equilibrium between two phases. One generalized form of the Clausius-Clapeyron equation derived by Loch (1978) to explain freezing in soils is

$$\overline{V}_i p_i - \overline{V} p_w = -\frac{L_{fs}}{T_o}\Delta T \tag{1.2}$$

where $\overline{V}_i$ and $\overline{V}$ are the volumes of ice and pore water solution per gram of water, respectively, p_i and p_w are the pressures of ice and water, respectively, L_{fs} is the latent heat of fusion per unit mass, T_o is the melting point of pure water, and ΔT is the temperature difference in °C. Another derivation of several generalized Clausius-Clapeyron equations for freezing soils was presented by Kay and Groenevelt (1974). Combining Equations 1.1 and 1.2 and replacing the specific volumes with density yields

$$\Delta T = \frac{2T_o\sigma_{iw}}{r_{iw}\rho_s L_f} \tag{1.3}$$

where ρ_s is the density of the solid, and L_f is the latent heat of fusion. Penner presented this equation to explain the freezing point depression observed in freezing fine-grained soils. He assumed that the ice formed in the soil pores is roughly spherical in shape, and that the pressure of the ice is atmospheric. As indicated by Equation 1.1, the curved interface of the ice-water contact causes the pressure of the water to be below atmospheric, or in tension. This tension, also called capillary suction, causes water to move towards the freezing front, resulting in the formation of an ice lens. As the temperature decreases (i.e., ΔT increases), Equation 1.3 indicates that the radius of the ice-water interface decreases in size. This allows the ice to penetrate into smaller spaces within the soil. Growth of the existing ice lens stops, and another ice lens forms where the new temperature equilibrium occurs. The capillary suction will be greater in a fine-grained soil than in a coarse-grained soil, because of the pore size and the radius of the ice-water interface. Penner (1959) offered a summary of his experiments and the general frost heave research that had been conducted up to that point in time. He noted that coarse-

grained soils will expel water upon freezing, and emphasized that the adsorbed water in fine-grained soils is the "highway" along which water flows to the freezing front. Based on freezing tests in which he froze samples from the bottom to the top, Corte (1962) demonstrated that a small particle placed on the top surface of ice will remain above the ice as the freezing front progresses upwards. Corte's work provided further evidence of the presence of unfrozen water films surrounding soil particles.

Several authors offered refinements to the capillary model (Everett 1961; Everett and Haynes 1965; Penner 1962, 1963). Everett and Haynes (1965) discussed the application of the model to a number of different geometric arrangements and used the model's principles to predict frost heave pressures, and Takagi (1965) indicated that freezing as described by the capillary theory is a Stefan-type problem. Based on the capillary theory, Bresler and Miller (1975) developed a frost heave model for non-colloidal soils.

Because the soil pore geometry is an essential component of the capillary theory, many researchers saw similarities between this theory and elements of soil physics, namely the soil-moisture characteristic curve. The soil-moisture characteristic curve is a graphical representation of the amount of water remaining in a soil versus matric suction (Hillel 1980). Koopmans and Miller (1966) and Groenevelt and Kay (1977) applied soil physics to the interpretation of the capillary model, suggesting that the soil-moisture characteristic curve could be used to define the frost heave potential of a soil. Hopke (1980) indicated that an equation similar to Equation 1.1 also exists for the water-air interface, and these equations are related via a surface tension ratio that can be determined experimentally. Williams attempted to relate unfrozen water content and the soil-moisture characteristic curve to frost susceptibility (Williams 1963, 1964, 1966). Williams' early experiments indicated that the unfrozen water films near the freezing front create suction in the water pressure, which increases effective stress and causes consolidation in the unfrozen soil, thereby causing an underestimate of the total amount of frost heave. Using a calorimeter, he created unfrozen water content curves, which he related to the corresponding soil-moisture characteristic curves at specific temperatures. Williams measured the pore pressures immediately below a penetrating frost line and the "air-intrusion" value, and calculated pore size, proposing this as a convenient test for determining frost susceptibility as based on capillary theory and the soil-moisture characteristic curve. Miller (1963) proposed that for a given soil there exists a freezing characteristic curve that closely relates to its soil-moisture characteristic curve. From this freezing characteristic curve, the unfrozen water content at a

given temperature can be obtained. Hoekstra et al. (1965) conducted similar experiments from which they attempted to determine the maximum heaving pressure from the soil-moisture characteristic curve. Koopmans and Miller (1966) and Miller (1973b) demonstrated that, for non-colloidal soils, a ratio exists between the pressure differences and the surface tensions between water and ice. These can be compared to the soil-moisture characteristic drying curves. They proposed that the pore geometry can be used to describe the temperature and amount of water present during freezing. Penner (1967, 1976), working with granular artificial "soils," concluded that the soil structure and gradation are the single most important physical characteristics in assessing frost susceptibility.

The capillary theory is a simple approach to understanding frost heaving. While it explains some of the processes observed, it is not without shortcomings. The capillary theory indicates that ice lenses form at the same elevation as the freezing front, which was disproved by later experimentation. Also, the theory underestimates the maximum frost heave pressure, as it does not account for the temperature, temperature gradient, or frost penetration rate (Ladanyi and Shen 1989).

Much of the early research that supported the capillary theory did not include the effects of the mineral surfaces on the adsorbed water films (Henry 2000), because the soil was assumed to be an ideal granular material. Research on mineral surface effects was being conducted concurrently with the development of the capillary theory, and would later prove that the capillary theory does not adequately describe the frost heave phenomenon. Grim (1952) discussed the role that clay minerals play during the freezing of soils. Grim determined that different clay minerals have different frost susceptibilities, and that the frost susceptibility will be further affected by the type of cation adsorbed to the mineral surface. He determined that the water immediately adjacent to the surface of a mineral is in a different physical state than the water in the center of a pore, and explained differing frost susceptibilities by how tightly the water is held by the mineral surface.

Jackson et al. (1957) and Chalmers and Jackson (1970) presented arguments that the free energy of the mineral surface is the driving force behind frost heaving, and indicated that supercooling is required for the energy to resupply the unfrozen water films. Cass and Miller (1959) disagreed with Jackson et al. (1957) about the necessity of supercooling in the frost heaving process, and instead proposed that frost heaving was akin to osmotic swelling in clays. Cass and Miller (1959) described the phenomenon in terms of electric double layer theory,

noting that the double layer contains a concentration gradient of ions. This concentration gradient may explain the freezing of water films from the open pore inwards towards the mineral surface. Cass and Miller postulated that monovalent cations may increase the dimensions of the double layer, increasing the tendency of the soil to heave. Conversely, these authors suggested that the addition of polyvalent cations would result in a contracted double layer, reducing frost susceptibility.

Linell and Kaplar (1959) published a review of frost heave research, with the focus on the influence of soil grain size and mineralogy. They noted that criteria based solely on grain size distribution were inadequate, as the mineral composition of the soil is also critical in determining frost susceptibility. Lambe et al. (1969) published comparable findings, and ranked clay minerals by their inherent frost susceptibilities. From freezing tests, these authors determined that the exchangeable cation present in the clay mineral can cause the rate of heave to vary over a considerable range. Horiguchi (1979) produced similar results from frost heave tests on zeolites, and Nersesova (1961) produced similar results from extensive frost heave tests on a variety of natural soils. Her test results indicated that the composition of exchange cations determines the intensity of water migration, ice lens formation, and frost heave. From her systematic experiments, Nersesova determined that soils saturated with multivalent cations heave more than those saturated with monovalent cations, and demonstrated that a frost susceptible soil can become non-frost susceptible and visa versa, by exchanging the cations. Nersesova attributed this to the effect of the cations on the soil surface energy. Nersesova and Tsytovich (1963) reiterated Nersesova's earlier findings. These authors noted that the soil cations affect the degree of aggregation of soil particles, the thickness of the unfrozen water films, and the zeta potential of the mineral grains. They emphasized that the unfrozen water content is dependent on the soil gradation, the mineralogical composition of the clay fraction, and the exchangeable cations, and that none of these characteristics can be considered independently as they are all interconnected for a given soil. Tyutyunov (1963) also suggested that the amount of frost heave depends on the surface energy of the soil, which depends on the cations present. He proposed that adsorbed water is structurally different than pore water, as its structure reflects the spatial coordination of molecules in an ice unit cell. Anderson (1967) utilized the x-ray diffraction method (XRD) to investigate the unfrozen water interaction with a clay mineral surface. He determined that the amount of unfrozen water present in a soil is independent of the initial water content, and instead is controlled by the specific surface area and

the intensity of the mineral surface's interaction with water. His XRD experiments indicated that the interlamellar water in a double-layer clay possessed high mobility as the soil was frozen.

Takagi (1963, 1963b) indicated that irreversible thermodynamics are necessary to explain the presence of the thin unfrozen water films and the freezing point depression in soils. He disagreed with Cass and Miller (1959), stating that the electric double layer does not represent the true physical situation in a freezing soil. An unusual approach to the frost heave problem was taken by Palmer (1967), who compared the development of ice lenses in a freezing soil to the development of Liesegang rings.

The cause of the unfrozen water content in a soil and the flow of moisture to the freezing front continued to be the focus of much research and debate. Hoekstra (1966, 1969) was the first to observe that ice lenses form at some distance behind the freezing front, thereby shedding doubt onto the capillary theory. Like previous authors, he noted that water movement occurs in freezing soils through the unfrozen water films, and that vapor transport provides an insignificant contribution to the amount of heave in a freezing soil. Hoekstra stated that since the unfrozen water content is directly related to the permeability of the frozen soil, it controls the amount of moisture migration to the freezing front. By measuring pressures developed by freezing soils, Hoekstra (1969) noted that, while a freezing sand or silt may reach a constant value, the pressure in a freezing clayey soil will continue to grow throughout the test. He attributed this characteristic to the thicker and more continuous unfrozen water films present in clays. Penner (1967) and Sutherland and Gaskin (1973) indicated that measured frost-heaving pressures were larger than those predicted by the capillary theory. Experiments by Kudryavtsev and Yershov (1973) and Penner and Walton (1979) reiterated that ice lenses grow behind the freezing front, which indicates that a freezing soil possesses a zone of freezing rather than the freezing plane proposed by the capillary theory.

The nature of the water comprising the unfrozen water films was discussed at great length by Russian authors at the Second International Permafrost Conference held in 1973. Orlov (1973) indicated that surface area and free energy are critical elements in describing the frost susceptibility of a soil. Kiselev et al. (1973) used nuclear magnetic resonance (NMR) to investigate the water film on an ice surface. They found that a "moving water phase" develops on the ice surface as the sub-freezing temperature approaches the phase change temperature. Several authors presented findings on the nature of unfrozen water in fine-grained soils, including Ananyan (1973), who stated that unfrozen water has unique properties compared with

bulk water, and Volkova (1973), who indicated that the proximity of the mineral surface distorts the water molecules and increases the viscosity of the film water. Dostovalov (1973) proposed that water adsorbed on the mineral surface is analogous to "hot ice," having a different structure than bulk water. Tyutyunov (1973) suggested that the film water in direct contact with soil particle surfaces has an increased electron density and structural distortion. He related this unique water phase to the hydration energy of soil cations.

Burt and Williams (1976) measured the hydraulic conductivity of frozen soils, and their publication since has become a widely-referenced work. Dirksen and Miller (1966) determined that certain soils can experience frost heave within a closed system, due to the reorganization of existing soil moisture. Low et al. (1968), Anderson and Tice (1972), Anderson et al. (1973), and McGaw and Tice (1976) presented empirical formulae that predicted the unfrozen water content of frozen soil. Williams (1976, 1977) presented experimental results and a general overview of the freezing process in soils. He noted that heave depends on the hydraulic gradient within the soil, which is determined by soil suction. Loch (1978) attributed the source of soil suction to the diffuse double layer present in clays. Horiguchi and Miller (1983) conducted experiments with a constant-volume permeameter/dilatometer to obtain data on unfrozen water content and hydraulic conductivity. Several other researchers investigated the flow of moisture through both saturated and unsaturated freezing soils, calculating and predicting values of hydraulic conductivity. Papers in this area include: Jumikis (1973); Kudryavtsev and Yershov (1973); Kudryavtsev et al. (1973); Kay and Groenevelt (1974); Groenevelt and Kay (1974); Jame and Norum (1976); Zhestkova (1978); Mageau and Morgenstern (1979); Reed et al. (1979); Berg et al. (1980); Fukuda (1980); Perfect and Williams (1980); Ratkje et al. (1982); Aguirre-Puente and Gruson (1983); Jinsheng and Rong (1983); Nakano et al. (1984); Ingersoll and Berg (1985); Nakano and Horiguchi (1985); Yanagisawa and Yao (1985); Xu et al. (1987); Tarnawski and Wagner (1996); and Cheverev et al. (1998).

Frost heave testing apparatus improved with the ever-growing interest in this area of research. Many researchers presented summaries of testing results, discussions of improvements to laboratory systems, and proposals for new frost-susceptibility tests. Such discussions include those by: Croney and Jacobs (1967); Leary et al. (1968); Kaplar (1968); Penner (1972); Zoller (1973); Berg (1975); Penner and Ueda (1978); Jones and Dudek (1979); Loch (1979, 1979b); Lomas and Jones (1981); Ingersoll and Berg (1981); Jones (1981); Penner (1981); Pietrzyk (1981); and Tester and Gaskin (1996).

Kaplar (1970) presented a qualitative model to describe the frost heave process, in which he attempted to explain the apparent contradiction between the simultaneous heaving pressure and soil moisture tension in a freezing soil. He proposed that the heaving force comes from the unfrozen water films that separate the soil particles from the ice surface. According to Kaplar, these thin water films carry and transmit the intergranular effective stress, acting as miniature hydraulic jacks forcing the overburden upwards. This process creates suction in the water films, and water flows upwards to the freezing front in response to the pressure gradient. Kaplar used the analogy of a suction-type water pump to further explain this process.

Numerical models became very popular beginning in the 1970's, perhaps as a result of the development of computer support. One such model is called the "hydrodynamic" model of frost heaving. It is considered a phenomenological or global model as it addresses the process of frost heaving as a whole, rather than focusing on the details of an individual ice lens formation. Harlan (1973), Taylor and Luthin (1976, 1978), and Guymon et al. (1980, 1981) presented one-dimensional finite difference or finite element models that coupled heat and moisture flow through a rigid porous medium. These authors recognized the presence of a frozen fringe within the soil, and its reduced permeability as important factors in determining frost heave (Smith 1985). Some of the above authors indicated that the generalized hydrodynamic model was sensitive to hydraulic parameters and boundaries conditions, and none of these numerical models incorporated overburden pressure (Nixon 1987). Additional papers that discuss this type of modeling include: Guymon and Luthin (1974); Kinosita (1975); Aguirre-Puente and Fremond (1976); Outcalt (1976, 1979); Sheppard et al. (1978); Dudek and Holden (1979); Jame and Norum (1980); Hromadka (1980); Ryokai (1985); and Cary (1987).

Radd and Oertle (1973) investigated the effects of pressure upon frost heaving. Their experiments demonstrated that ice lenses can grow at temperatures below the freezing point and at large pressures. Arvidson and Morgenstern (1977) coined the phrase "shut-off pressure" to describe the pressure necessary to stop frost heaving. The shut-off pressure depends on the soil type, the stress history, and the freezing temperature. Takashi et al. (1978) referred to the shut-off pressure as the "critical effective stress," and Konrad (1993) indicated that shut-off pressures as high as 1200 kPa may be necessary to effectively eliminate frost heaving.

Sheeran and Yong (1975) and Yong et al. (1979) discussed how salt content affects the double layer and unfrozen water content in a freezing soil. Chamberlain (1983) also addressed frost heave of saline soils, indicating that the salt content can reduce lens size and segregation

water content by as much as 50 percent. Akimov et al. (1983) discussed the thermochemical characteristics of unfrozen water, and investigated the effects of salinity on the unfrozen water content. Grant et al. (1999) measured the unfrozen water content of soils saturated with different sodium chloride concentrations, using an NMR apparatus. Grant (2000) used thermodynamic principles to explain the effects of salt in freezing soils.

Iwata (1983) and Kuroda (1985) used thermodynamic principles, including chemical potential, to explain the presence of unfrozen water in a frozen soil. Anderson (1989) indicated that the moisture movement driving the frost heave process can be related to the chemical potential and soil suction. Torrance and Schellekens (2003) summarized the possible chemical factors that contribute to the presence of unfrozen water and moisture flow during frost heave, and Marion (1995) discussed the soil chemical properties that are influential in a freezing environment.

Tice et al. (1978, 1982) presented the NMR method as a viable technique to measure unfrozen water content. Oliphant et al. (1983) used an NMR device to investigate moisture migration in response to a temperature gradient. Tice and Oliphant (1984) refined the NMR technique by correcting for the effect of magnetic particles in the soil, and Tice et al. (1989) presented unfrozen water content data for silt obtained using the NMR technique. Kujala (1989) used an NMR apparatus to investigate the unfrozen water content in several different natural soils, and presented an empirical formula used to approximate unfrozen water content. Patterson and Smith (1981) presented time domain reflectometry as a nondestructive technique for measuring unfrozen water content, and Fukuda and Huang (1991) measured unfrozen water content in frozen soils using ultrasonic velocities.

Anderson et al. (1973) measured unfrozen water content on undisturbed frozen soil samples, and found that the unfrozen water content increased as the soil thawed and consolidated into a more compact solid. Savel'ev (1978) presented a qualitative model that described the layers of bound and unbound water that are present between the mineral surface and the ice surface in a freezing soil. Chamberlain and Gow (1979) discussed the effects of freezing and thawing on fine-grained soils, determining that it greatly affects the structure of consolidated clay slurries. The overall permeability increases due to the formation of vertical shrinkage cracks. Efimov et al. (1981) investigated the effects of multiple freeze-thaw cycles on the unfrozen water content. Pusch (1979) demonstrated that unfrozen water content is a function of clay microstructure through experiments on two illitic clays. He found that the unfrozen water

content was higher in the dispersed fresh water clay than in the salt water clay. When the samples were remolded, the unfrozen water contents of both soils were similar and higher than in their undisturbed states, due to higher bulk densities.

Konrad (1989, 1990b) found that unfrozen water content increased with consolidation in a clayey soil. He suggested that the increase in unfrozen water content is due to the rearrangement of the clay particles, which creates an increase in capillary water with an accompanying decrease in void ratio. Doré et al. (1998) postulated that overconsolidating a silty soil changes the intergranular structure, leading to a higher unfrozen water content and hydraulic conductivity. This results in an increase in the soil's frost susceptibility.

Miller (1973, 1976), Miller et al. (1975), and Horiguchi and Miller (1980) conducted experiments using an ice sandwich permeameter, which measured the unfrozen water content and hydraulic conductivity of the tested soil. These experiments provided evidence of the regelation process, in which ice moves down a temperature gradient by continual freezing and thawing. Miller et al. (1975) presented a theoretical model of coupled heat and mass transport in frozen soils based on the permeameter work. Mageau (1978) observed that moisture moves in response to a temperature gradient through unfrozen water films. He concluded that regelation does occur as a result of a temperature gradient, but that it has a small effect on the heave rate, as movement through regelation occurs very slowly. Philip (1980) modeled the regelation of ice, indicating that it is a possible source of ice movement during frost heaving, and Williams (1983) presented a summary of moisture transport mechanisms including regelation. Wood and Williams (1985) used an ice sandwich permeameter to measure regelation in frozen soils, and Wood (1990) stated that irreversible thermodynamics are necessary to describe the regelation flow phenomenon.

Miller (1972, 1977, 1978) presented the basis for a new theoretical frost heave model suitable for non-colloidal soils. He indicated that the capillary theory is inadequate to fully describe the formation of an ice lens, renaming the process described by the capillary theory as "primary frost heaving." In primary frost heaving, the freezing front coincides with the forming ice lens. This rarely occurs in natural systems, with the exception of hoar frost forming on the ground surface. Miller suggested that the ice lenses that form within the soil do so during "secondary frost heaving," in which ice lenses form at some distance behind the freezing front. He used Beskow's term, the "frozen fringe," to describe this zone between the actively forming

ice lens and the freezing front. The presence of the frozen fringe was verified experimentally by Berg et al. (1980) and Ingersoll and Berg (1981), among others.

According to the secondary heave model, water and ice coexist below the freezing point within the frozen fringe. Miller postulated that there is a temperature-induced pressure gradient within the pore ice that is in contact with the unfrozen water films. Based on the generalized Clausius-Clapeyron and Kelvin equations, Miller suggested that as the temperature decreases, the ice pressure increases until it equals the overburden pressure. Once the ice pressure equals the overburden pressure, the effective stress between the soil particles becomes zero, and a new ice lens forms. Miller presented a stress partition function to describe this process:

$$\sigma_n = \chi(\psi)u + [1 - \chi(\psi)]u_i \tag{1.4}$$

where σ_n is the neutral stress, u is the pore water pressure, u_i is the pore ice pressure, and $\chi(\psi)$ is the stress partition function (Miller 1978). The stress partition function is a function of the unfrozen water content within the frozen fringe, which is dependent on the temperature gradient. Loch and Miller (1975) presented frost heave testing results in which the maximum heaving pressures exceeded those predicted by the capillary theory by as much as six times. They verified the presence of the frozen fringe, and compared it to the desiccated zone in a drying soil. Miller and Koslow (1980) demonstrated how the secondary heave model predicted the relationship between the rate of heave and the surface load with a specific thermal and ground water regime under an assumed quasi-steady state condition.

Loch and Kay (1978) evaluated the capillary theory, the hydrodynamic theory, and the secondary heave theory, based on their own laboratory tests. The capillary theory did not predict the true location of ice lenses, which formed up to 0.4 cm behind the freezing front. According to Loch and Kay, both the hydrodynamic and secondary heave theories were inadequate because they did not incorporate the effects of overburden pressure. Using a dual energy gamma scanning system, Loch and Kay measured water expulsion and intake during freezing tests. They stated that none of the three models accounted for water expulsion during freezing, and thereby failed to predict the relative magnitude of water intake.

Takagi (1979, 1980) presented the "adsorption force theory." This theory is based on the premise that the unfrozen water films are composed of "special water" that can support solid-like stresses. Takagi proposed that the suction potential at the freezing front is generated as the external layers of the unfrozen film water surrounding the solid particles freeze and the film tries

to recover its initial thickness. The freezing of the film water creates segregation freezing, which forms ice lenses, and the solid-like stresses in the adsorbed water layer are the source of the heaving pressure. Hopke (1980) presented a similar frost heave model, which also assumed an anisotropy within the pressure of the unfrozen water films.

Miller responded to Takagi's theory with "The Adsorbed Film Controversy (Miller 1980)." He used the analogy of the earth as a giant soil particle in order to describe how the water films are made of ordinary water that is under the same pressure as the ice. He also discussed how the diffuse electric double layer should not be discounted in the frost heaving process. Accordingly, the secondary heave model incorporates the double layer concept by addressing adsorption forces in the context of unfrozen films, surface tension, and interfacial curvature in order to predict the penetration of ice into soil pores. Black (1989) reiterated Miller's arguments, indicating that the differing thickness of the water film around a soil particle is responsible for the apparent anomaly in water pressure.

Gilpin (1980) presented a comprehensive frost heave model that produced similar results to those obtained in the laboratory. Gilpin's model was based on the behavior of water at the water-soil interface and certain limiting factors in frost heaving, which are the rate of heat conducted away from the freezing front, and the hydraulic resistances of the frozen fringe near the ice lens and within the unfrozen soil. Gilpin recognized the presence of attractive forces at the mineral surface, which have been described at various times as ionic forces, surface adsorption effects, and induced dipole alignments. However, Gilpin stated that the origin of these forces is not important for the purpose of his model.

O'Neill and Miller (1982, 1985) revised the secondary heave model and presented the governing equations for what is now known as the "rigid ice model." The authors stated that water is preferentially attracted to the mineral surface by adsorption forces. O'Neill and Miller did not explain the origin of these adsorption forces but noted their importance, stating that these forces are an integral part of the rigid ice model. Due to the surface forces, a film of unfrozen water surrounds a mineral grain at sub-freezing temperatures, separating the grain from ice. If a temperature gradient were imposed on this system, the water film would thin on the cold side of the particle as the unfrozen water begins to freeze. Water would move from the warm side of the soil particle to the cold side via the adsorption forces, allowing the unfrozen water film to remain symmetric about the mineral grain. Assuming that the mineral grain was part of a stationary network of soil particles, the ice instead would move down the temperature gradient by the same

regelation process described above. The rigid ice model is similar to the secondary heave model, relying on the Kelvin and Clausius-Clapeyron equations, thermodynamics, and the stress partition function to predict when a new ice lens will form. O'Neill and Miller indicated that this finite element model produces results similar to those seen in the laboratory; however, the authors acknowledged that the model was not perfect, especially when predicting water and heat flow through the frozen fringe. Miller (1983) indicated that the rigid ice model differs from Gilpin's model in the assumption that the ice moves by regelation.

The secondary heave model, or alternately the rigid ice model, is the most comprehensive frost heave model as it predicts all of the characteristics of frost heave, including the high heaving pressures measured in the laboratory (Fowler and Noon 1993). Conversely, it also may be the most difficult model to use and to extend to more intricate frost heave scenarios due to its complexity (Smith 1985, Fowler and Noon 1993, Krantz and Adams 1996). Konrad and Duquennoi (1993) and Konrad (1993) questioned the correctness of using the stress partition function, noting that the existence of a particle separation pressure had not been confirmed experimentally. Krantz and Adams (1996) indicated that the O'Neill and Miller model is subject to numerical convergence problems.

Several authors presented variations upon the secondary heave model. Some authors also did experimental testing to verify Miller's theory and suggested improvements. Papers written in these areas include: Takagi (1982); Holden (1983); Holden et al. (1985); Comparini (1988); Ishizaki and Nishio (1988); Piper et al. (1988); Padilla and Villeneuve (1990, 1992); Sheng and Chen (1991); Sheng and Knutsson (1993); Fowler and Noon (1993); Sheng et al. (1994, 1995); Ketcham and Black (1995); Yang (1997); Gorelik et al. (1998); and Harris and Davies (1998). Krantz and Adams (1996) presented a model that improved upon the rigid ice model. Their improvements included the incorporation of scaling and asymptotic analysis to provide a more realistic regelation mechanism. Peterson and Krantz (1998) used this improved model to simulate differential frost heaving.

While advancements were being made in theoretical frost heave models, others were developing empirical methods to predict frost heave amounts. Takashi et al. (1978) discussed the effects of varying overburden pressure and freezing rate on frost heave. The authors presented an empirical formula that relates the frost heave ratio, ξ, to the overburden pressure and freezing rate:

$$\xi = \xi_o + 100\left(\sigma_o/\sigma\right)\cdot\left(1+\sqrt{U_o/U}\right) \tag{1.5}$$

where σ is the applied overburden pressure, U is the freezing rate, and ξ_o, σ_o, and U_o are soil constants. The frost heave ratio is defined as

$$\xi = \frac{\Delta H_f}{H_l}\cdot 100 \tag{1.6}$$

where ΔH_f is the frost heave amount at the end of the freezing test, and H_l is the sample length prior to freezing. This approach now is known as the Takashi method, and the Japan Geotechnical Society incorporated this approach into their standard test methods for the frost prediction of soils (Japan Geotechnical Society 2003). Takashi et al. (1982) refined the laboratory procedures used in conjunction with the Takashi method, and Ratkje (1982) and Ratkje et al. (1982) calculated the hydraulic conductivity of frozen soils based on Takashi's data. Miyata and Akagawa (1991) experimentally demonstrated that the main factors affecting the frost heave ratio are overburden pressure, the temperature gradient in the frozen fringe, and the freezing rate.

Konrad and Morgenstern (1980, 1981, 1982, 1983) presented a different empirical approach to the prediction of frost heave. These authors indicated that the formation of ice lenses depends on applied pressure, the freezing rate, and the soil suction and permeability within the frozen fringe. They assumed that the Clausius-Clapeyron equation was valid at the base of an ice lens, that water flow is continuous across the frozen fringe accumulating at the base of the last ice lens, and that the temperature profile across the frozen fringe is linear. Water from unfrozen soil migrates to the freezing front through unfrozen water films in response to a temperature-induced suction gradient. As the temperature decreases, the water films decrease in thickness, which results in a reduced permeability across the frozen fringe. Konrad and Morgenstern suggested that, during the formation of the final ice lens in a step-freezing test, the water intake flux, V_o, is proportional to the temperature gradient in the frozen fringe, or

$$V_o = SP_o\, gradT \tag{1.7}$$

where $gradT$ is the temperature gradient in the frozen fringe, and SP_o is the proportionality constant termed the "segregation potential." The authors indicated that this approach works for transient freezing situations, as well as those in which a quasi-equilibrium is established during

the formation of the last ice lens. Konrad and Morgenstern acknowledged that the unfrozen water content is dependent on surface adsorption effects that are related to the soil specific surface area, mineralogy and grain size distribution, and the type of exchangeable cations present; however, the authors do not address this area further in their phenomenological approach.

Konrad (1987, 1990) suggested improvements of freezing tests in order to better calculate the segregation potential of a soil, and discussed how the method could be applied to frost heave prediction of saline soils. He indicated that the segregation potential could be calculated both from step-freezing tests, in which the top temperature is "stepped" to a negative temperature at the beginning of the test and the bottom temperature is held at an above-freezing value, and from ramped-freezing tests, in which both top and bottom temperatures are "ramped" down simultaneously through the test (Konrad 1988). Other researchers further refined the segregation potential method for use in certain modeling applications and general laboratory use, including: Akagawa et al. (1985); Jessberger and Jagow (1989); Saarelainen (1989); Shen and Konrad (1993); Svec and Chang (1993); Konrad and Nixon (1994); and Ito et al. (1998).

Rieke (1982) and Rieke et al. (1983) identified the specific surface area as a critical soil property in frost heaving, and used the segregation potential method to investigate the relationship between frost heaving and specific surface area. Nixon (1991) presented an outgrowth of the segregation potential method called the "discrete ice lens theory," stating that the segregation potential approach does not predict the pore-water expulsion that is observed during the early portion of freezing tests. Krantz and Adams (1996) indicated that the segregation potential approach may not be fully predictive, as the segregation potential constant is an unknown function of several boundary conditions.

Researchers continued to develop coupled heat and mass transfer numerical models, incorporating elements of previously established models and methods. Papers describing these numerical models include: Fukuda and Nakagawa (1985); Mu and Ladanyi (1987); Konrad and Duquennoi (1993); Newman and Wilson (1997); Førland et al. (1988); Lewis and Sze (1988); Ryokai et al. (1988); Miyata (1988); Alonso et al. (1989); Schellekens (1997); and Hermansson (2000, 2002).

Chen and Wang (1988, 1991, 1991b) presented an empirical frost heave model that includes the effects of initial water content, initial dry unit weight, frost penetration rate, water level, and the plasticity and salinity of the soil. Xu et al. (1999) summarized years of frost heave

testing that investigated the mechanism of frost heave and salt expansion of soils, and presented empirical formulae that were derived from these numerous tests. Michalowski and Voller (1991) and Michalowski (1993) presented a global frost heaving model that relies on a porosity-growth rate function rather than on ice lens formation. Dash (1989) discussed thermomolecular pressure in surface melting and applied it to the frost heaving phenomenon, and Rempel et al. (2004) incorporated surface melting in a continuum model based on integral force balances.

Miyata (1998) and Miyata and Akagawa (1997, 1998) indicated that the Clausius-Clapeyron equation typically used in frost heave analysis poorly predicts the amount of freezing expansion because it relies on a static condition. These authors introduced a revised version of the generalized Clausius-Clapeyron equation that accounts for the dynamic nature of water movement in the freezing soil. Miyata and Akagawa experimentally confirmed the validity of the equation, and developed a new pore water pressure gage to measure unfrozen water pressure at the ice lens forming front.

With the advent of more comprehensive theoretical models and predictive empirical approaches, frost heave tests became more sophisticated and precise. Penner and Goodrich (1981), Penner (1982), Yoneyama et al. (1983), and Akagawa (1988, 1988b, 1990) investigated frost susceptible soils and the frost heave phenomenon through the use of x-ray photography. After refining the x-ray method to study the frozen fringe, Akagawa (1990) indicated that the rigid ice model is based on assumptions that still remain to be proven by precise experiments. Additional refinements in frost heave testing methods and apparatus were made by: Akagawa (1983); Chen et al. (1983); Mageau and Sherman (1983); Yong et al. (1984); Ishizaki and Nishio (1985); McCabe and Kettle (1985, 1985b); Ohrai and Yamamoto (1985); Penner (1986); Johnson et al. (1986); Chamberlain (1987); Yamamoto et al. (1988); Svec (1989); and Hazen et al. (1993).

To summarize, Taber and Beskow were the progenitors of frost heave research. They laid down the foundation of this study area by comprehensively describing the frost heave phenomenon. The investigations that have been conducted over the years hence can be divided into several broad categories, namely: 1) theory, 2) laboratory and field experimentation, and 3) numerical modeling. In addition to these three categories, supporting investigations into the nature of water have been made, which include water structure, viscosity, and the hydraulic conductivity and unfrozen water content of freezing soils. The majority of the proposed frost heave theories are based on the physics and thermodynamics of the process. The major theories

are generally vague on soil properties, although several state the importance of "mineral surface effects" or "adsorption forces" upon the unfrozen water films in a freezing soil. The numerical models rely upon both theoretically derived equations and experimentally measured parameters to successfully predict and quantify frost heave. Copious laboratory experiments have yielded several empirical equations and frost heave criteria. Nearly every variable in the soil freezing process has been the subject of scores of laboratory experiments. One experimental topic, however, that has received a dearth of attention is the influence of mineral surface effects upon frost heaving. Only a few individuals conducted research in this area, with much of the experimental work done close to 50 years ago. The antiquity of the previous surface chemistry research, coupled with the dependence of frost heave theories and numerical models on soil properties, makes the subject of cation effects on the frost susceptibility of soils important and rich for further discoveries.

1.3 Research Objectives

A few individuals investigated cation effects on the frost susceptibility of soil, including Grim (1952, 1958), Lambe (1953), and Nersesova (1961). Their experiments were conducted nearly 50 years ago with rudimentary frost heave testing apparatus that had poor temperature control and low repeatability. Furthermore, much of the previous experimental testing was conducted either on homogenous soils composed solely of one clay mineral, or on artificial "soils," made from a manufactured blend of grain sizes and minerals.

The purpose of the research presented in this dissertation is to investigate the adsorbed cation effects on the frost susceptibility of natural heterogeneous soils (see Figure 1.1 for a graphical representation of the organization of this dissertation). A comprehensive suite of laboratory experiments were conducted on five natural soils (see Table 1.1 for a summary of soil tests conducted for this research). Although more complicated than homogeneous soils and artificial blends, natural heterogeneous soils were chosen for testing and analysis because results obtained from these soils will represent actual field conditions more closely than those from artificial soils. Four of the soils were sampled from disparate regions within the state of Alaska, which have histories of frost heaving problems. Thus, this dissertation also serves as a repository for a comprehensive description of the frost susceptibility, chemical properties, and mineralogy of four naturally occurring Alaskan soils.

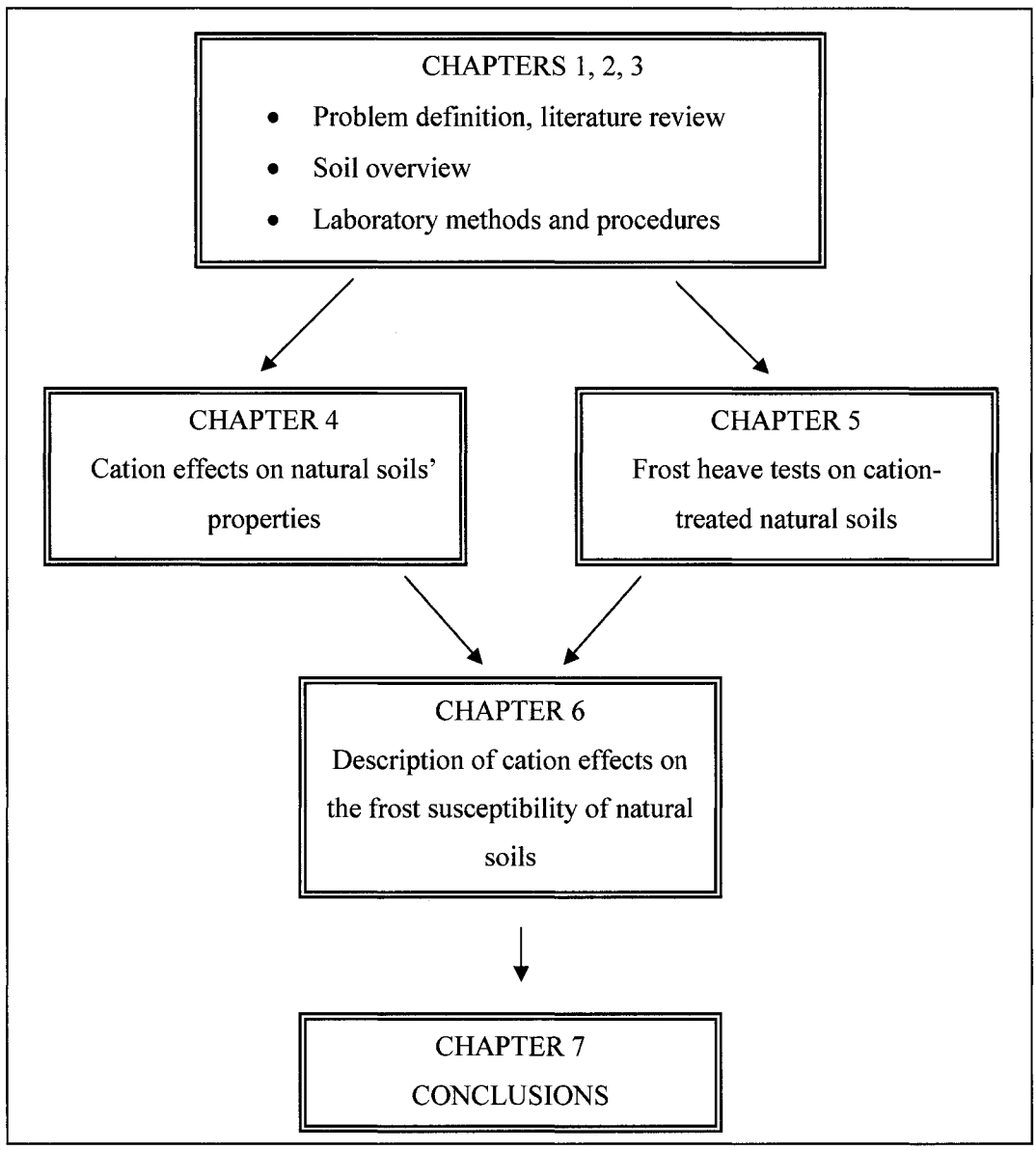

Figure 1.1: Flowchart detailing the organization of this dissertation

Table 1.1: Comprehensive summary of soil testing conducted from 2003 through 2006. The numbers within the table indicate the number of tests performed per soil, including those of the associated cation-treated samples (unless otherwise noted).

Test	Soil				
	CR	DEA	FS	HS	HV
Sieve analysis	2	2	2	2	2
Hydrometer analysis	8	8	6	8	6
Atterberg limits	2	2	2	2	2
USCS classification	2	2	2	2	2
Organic content	2	2	2	2	2
Specific gravity	2	2	2	2	2
pH*	1	1	1	1	1
Electroconductivity*	1	1	1	1	1
Soluble cations	1	1	1	1	1
Cation exchange capacity	1	1	1	1	1
Specific surface area	1	1	1	1	1
XRD analysis	2	2	2	2	2
SMC curve	1	1	1	1	1
Zeta potential	5	5	3	5	3
Unfrozen water content	5	5	3	5	3
Frost heave tests	6	6	4	10	6

* These numbers reflect tests made to the BSLN samples only, and do not include measurements made on the associated cation-treated samples.

Chapter 2 contains descriptions of these natural soils, including their engineering index properties, chemical properties, clay content and mineralogy, and gradation. To determine the soils' inherent frost susceptibilities, a laboratory system including a state-of-the-art frost heave testing apparatus was developed, which produces highly repeatable and accurate results. For all freezing tests conducted, the same freezing method, temperature gradient, freezing rate, and overburden pressure were applied, thereby reducing the changing variable to the soil properties. The exchangeable cations of the five natural soils were varied systematically. Chapter 3 contains a detailed description of all laboratory methods and procedures used in this research, including the cation soil treatments, determination of soil-moisture characteristic curves, zeta potential measurements, unfrozen water content measurements, and frost heave testing procedures.

The testing results that describe the adsorbed cation effects on the five natural soils' properties are presented in Chapter 4. Chapter 4 also includes an analysis of the soil-moisture characteristic curves as related to the unfrozen water content. Frost heave test results from all cation-treated samples are presented in Chapter 5. The results presented in Chapters 4 and 5 are combined in a statistical analysis, which is presented as Chapter 6, in order to quantitatively describe the adsorbed cation effects on the frost susceptibility of natural soils. Finally, Chapter 7 contains the summary and conclusions, as well as suggestions for future research.

CHAPTER 2: SOIL DEPOSITIONAL HISTORIES, CHEMICAL PROPERTIES AND MINERALOGY

2.1 Depositional Histories and Sample Locations

Natural soils were chosen over artificial blends for frost heave testing and analysis. Although more complicated due to inhomogeneity in physical and chemical characteristics, the results obtained from tests on natural soils better reflect realistic frost heave processes and are more applicable to field predictions. Four different soils were collected from various locations throughout Alaska: Copper River silty clay (CR) from near Glennallen, DeArmoun sandy loam (DEA) from Anchorage, Fairbanks silt (FS) from Fairbanks, and Happy Valley silt loam (HV) from the North Slope of Alaska (see Figure 2.1).

Additionally, a quantity of Hanover silt loam (HS) was acquired from the U.S. Army Cold Regions Research and Engineering Laboratory (CRREL) in Hanover, New Hampshire. This soil was selected for testing as it has been a quasi-standard in many frost heave experiments run at CRREL. The exact sample location, and thus the depositional history, of the HS soil is not available, as the individual who sampled the soil no longer works at CRREL (D. Cole, personal communication, October 2006). The index properties, mineralogy, and other soil properties, as well as the sampled locations of the four Alaskan soils, are discussed in detail in the following sections. Appendix B contains maps and photographs of each sampled location.

2.1.1 Copper River Silty Clay (CR)

The Copper River Lowland is a broad, smooth plain located in the southeastern portion of Interior Alaska (Wahrhaftig 1965). At various times throughout the Pleistocene Epoch, the glaciers in the surrounding mountains coalesced and blocked the drainage of the Copper River to the south. During these times, the Copper River Lowland would fill with water, creating the large proglacial Lake Atna. The most recent occurrence of Lake Atna was during the Last Glacial Maximum (i.e., 20,000 yr BP), when the lake covered more than 5,200 km^2 of the lowland (Ferrians, Jr. et al. 1983).

The lacustrine deposits in the lowland consist of typical laminated lake sediments, as well as nonsorted deposits, referred to as glaciolacustrine diamicton deposits, with ice-rafted sediments throughout. Thus, the deposits mostly consist of silty clay and clayey silt with

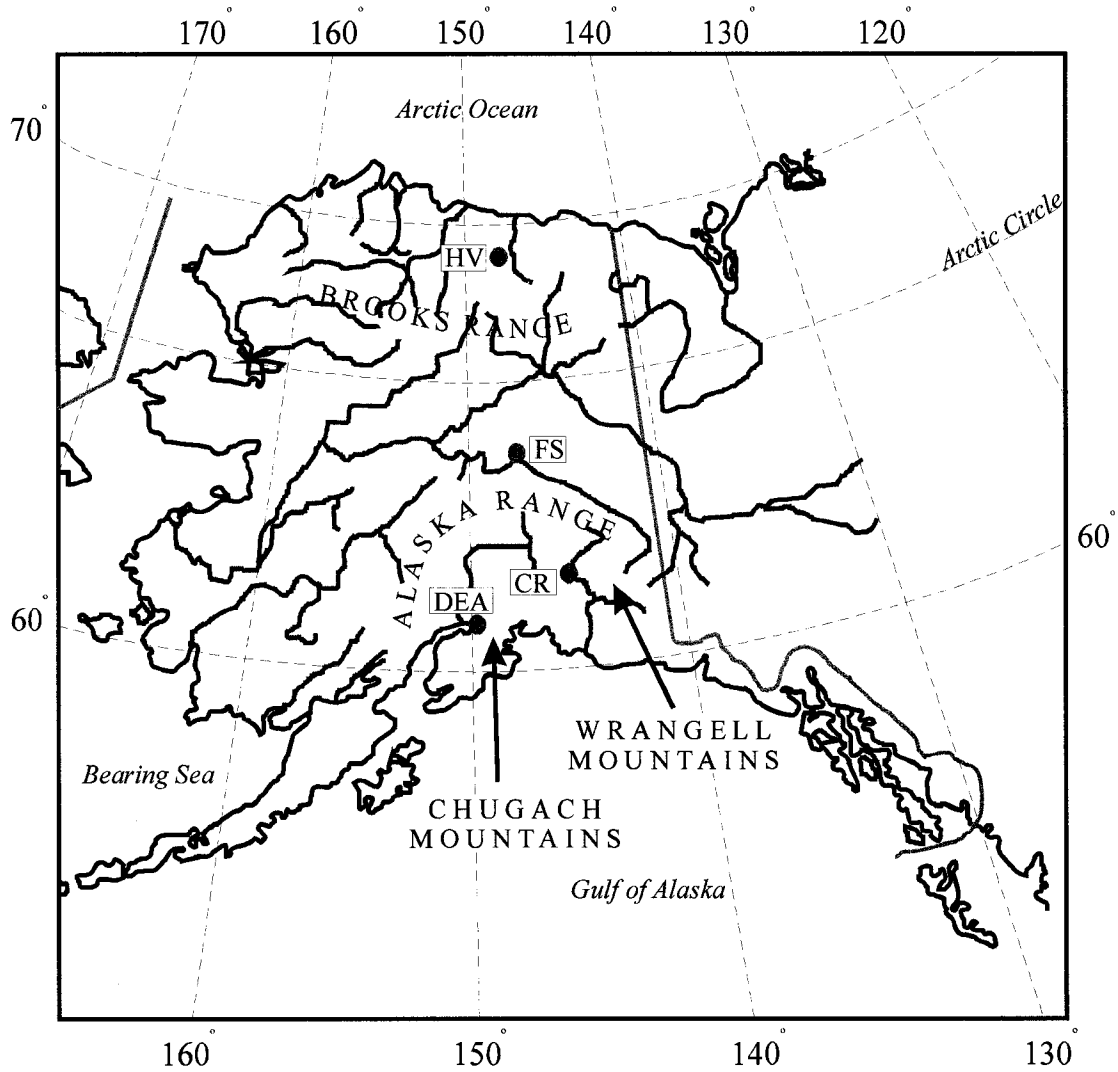

Figure 2.1: Generalized map of Alaska, showing soil sample locations. Major rivers are shown in blue, and the political state boundaries are shown in gray. The four sample locations are shown as red dots.

pervasively scattered sand and gravel. Radiocarbon dating of the organic material at the top horizon of the lacustrine deposits indicates that Lake Atna drained around 9,400 ± 300 yr BP (Ferrians, Jr. et al. 1983). After the glacial lake drained, the major river drainages began down-cutting into the glaciolacustrine sediments, creating exposures over 60-m high in some places.

The local roadways and airport within this area have experienced severe frost heave damage due to the presence of the underlying silty clay (Ledbetter 1959). Samples of the Copper River silty clay (CR) were taken from within the Richardson Highway right-of-way near Mile Post 113, and immediately west of the Copper River (N62.08311°, W145.44100°). The uniformly gray silty clay was sampled directly below the surficial organic mat, and contained sparse, small rootlets that were removed upon sampling.

2.1.2 DeArmoun Sandy Loam (DEA)

The Anchorage area is a lowland immediately adjacent to the Chugach Mountains to the east and bounded by the Knik Arm and the Turnagain Arm of Cook Inlet to the north, west, and south. These geographic features have played a major role in the formation of the area's soils. Throughout the Pleistocene Epoch, glaciers from the Chugach Mountains and other mountains surrounding the area repeatedly advanced into Cook Inlet. During the interglacial periods, the Anchorage area was subjected to marine and fluvial processes, making a complex sedimentary record (Updike and Schmoll 1985). The last major glacial advance occurred during the Late Pleistocene, the record of which is preserved by a series of lateral moraines along the flanks of the Chugach Mountains (Schmoll et al. 1999).

DeArmoun Road, located in south Anchorage, has experienced distress due to frost heaving (D. Hemstreet, personal communication, March 2003). The DeArmoun Road deposit is a diamicton described as an "inlet-modified morainal landform (Schmoll et al. 1999)," indicating that it has a glacioestuarine origin. The sample site was located at the corner of DeArmoun and Von Scheben Roads (N61.10148°, W149.75522°). Samples of the DeArmoun sandy loam were collected from the ditch immediately adjacent to the roadway embankment. The brown sandy loam contained pockets of gray and brown mottled silty clayey soil.

2.1.3 Fairbanks Silt (FS)

Unlike the Copper River Lowland and the greater Anchorage area, the Fairbanks area was not covered by glaciers or glacial lakes during the Pleistocene. Instead, the area received silty aeolian deposits, called loess. The loess sedimentary record in the Fairbanks area indicates

that deposition began in the Pliocene Epoch and continued through the Pleistocene (Westgate et al. 1990). Some minor loess deposition continues today, when strong winds travel over the Alaska Range and transport glacial outwash material to the north. The Tanana River, immediately to the south of the Fairbanks area, provides a local source of loess. The thickness of the loess varies depending on location. As it is easily eroded, the loess is often less than one meter thick on the crests of hills where it typically overlies bedrock (Lindholm et al. 1957). In valley bottoms, transported and reworked loess deposits range from 3 to 90-m thick (Péwé 1955). Many papers written on the subject of frost heaving refer to this loess as Fairbanks silt.

A road cut near the intersection of Fiddle Way and Isberg Road (N64.79715°, W148.04402°) was chosen as the sample location of Fairbanks silt (FS). Fiddle Way, located between Chena Ridge Loop and Cripple Creek Road, is a gravel-surfaced road that demonstrates frost heaving and related distress during the winter months. During sample collection, however, it was noted that the roadway embankment rests directly on highly weathered schist bedrock, which is responsible for the frost heave damage, rather than on FS. The FS soil in the road cut consisted of brown silt with some rootlets and minor mottling.

2.1.4 Happy Valley Silt Loam (HV)

The Happy Valley area is located along the Sagavanirktok River north of the Brooks Range. This area was glaciated during the mid-Pleistocene by glaciers originating in the Brooks Range about 40 km to the south (Brown and Kreig 1983). The Happy Valley area is the type locality for the Sagavanirktok River Glaciation (Detterman et al. 1958). The Sagavanirktok moraines have a subdued, rounded topography due to weathering and slope processes. The down-slope movement of surficial soil and the presence of permafrost have resulted in the formation and preservation of an organic-rich silt loam that typically covers the glacial till (Brown and Kreig 1983).

The Happy Valley silt loam (HV) was sampled roughly 100 m west of the Dalton Highway at Mile 334.5 (N69.15667°, W148.83683°). The brown organic-rich silt loam was removed from below the organic mat.

2.2 Engineering Index Properties and "Baseline" Sample Preparation

Two separate samples of each soil were tested by the Alaska Department of Transportation and Public Facilities Northern Region Materials Laboratory (AK DOT&PF NRML). This laboratory is certified by the AASHTO Materials Reference Laboratory (AMRL),

and the tests performed were according to standard AASHTO and ASTM procedures (see Table 2.1).

Table 2.2 contains a summary of the soil classifications and engineering properties as determined by the AK DOT&PF NRML. The USDA soil classifications were added as an additional means of characterizing each soil. For some tests such as fine specific gravity, the values differed between the duplicate samples. For these cases, each value is shown in Table 2.2.

The CR samples were the only soil samples to demonstrate a plastic index; all other soils tested were non-plastic. The HV samples had liquid limits of 34 and 38, respectively. Also, this soil was highly organic, with demonstrated organic contents of 7.9 percent and 8.4 percent, respectively. The tested organic contents for the CR samples were 3.9 percent and 4.1 percent, respectively, although visual observations did not indicate the presence of organic material. As clay minerals can contain a large amount of structural water, the organic-by-ignition test may lead to a "false-positive" as the water content is removed from the sample and as the minerals undergo irreversible structural changes. This false organic content often is demonstrated by bedrock samples, and is a product of the testing procedure (D. Stanley, personal communication, February 2005; S. Meierotto, personal communication, February 2005). Thus, the CR soil was not considered as an organic soil.

The grain size distributions for the five natural soils are presented in Figure 2.2. The DEA and HS are well-graded soils, whereas FS is poorly-graded consisting of uniform, coarse silt grains. Both HV and CR contain a higher percentage of clay-sized particles than the other soils.

Rieke et al. (1983) indicated that the silt- and clay-sized fractions of natural soil are the most critical in the frost heaving process. In order to produce the most conservative frost heave estimates, as well as eliminate the additional variable of a wide spread in grain size distributions, each natural soil was sieved following the procedure implemented by Rieke et al. (1983). These samples, consisting of particles smaller than 0.075 mm, are referred to as the "Baseline" (BSLN) samples.

Figure 2.3 contains the grain size distributions of the prepared BSLN samples. The FS and HS samples demonstrate similar poorly-graded distributions, with HS containing slightly more clay-sized particles than FS. The DEA sample demonstrates a well-graded distribution, even in the grains smaller than 0.075 mm. The CR and HV samples demonstrate similar

Table 2.1: List of standard laboratory test methods

Test Name	Test Number	
	AASHTO[a]	ASTM[b]
Sieve Analysis of Fine and Coarse Aggregates	T27 / T11	C126 / C117
Particle Size Analysis of Soils	T88	D422
Determining the Liquid Limit of Soils	T89	D4318
Determining the Plastic Limit and Plasticity Index of Soils	T90	D4318
Classification of Soils and Soil-Aggregate Mixtures for Highway Construction Purposes	M145-91	D3282
Organic Content of Soils by Ignition	T267	D2974
Specific Gravity of Soils	T100	D854

[a] Standard Specifications for Transportation Materials and Methods of Sampling and Testing: AASHTO, 24th Ed., 2004, Part 1 Specifications, Part 2 Tests.

[b] Annual Book of ASTM Standards, 2004.

Table 2.2: Summary of soil classification and engineering index properties

Soil	Soil Classification				Liquid Limit	Plastic Index	Fine Specific Gravity	Organic Content (%)
	USDA	USCS	AASHTO	AK DOT&PF Textural				
CR	Silty clay	ML, CL	A-6(12), A-6(15)	Slightly organic silty clay	38, 39	11, 14	2.65, 2.73	3.9, 4.1
DEA	Sandy loam	SM	A-4(0)	Slightly organic gravelly sandy silt	NV	NP	2.56, 2.71	1.5, 2.0
FS	Silt	ML	A-4(0)	Slightly organic silt	NV	NP	2.63, 2.66	1.3, 1.5
HS	Silt loam	ML	A-4(0)	Sandy silt	NV	NP	2.68, 2.76	0.9
HV	Silt loam	ML	A-4(2), A-4(3)	Organic silt	34, 38	NP	2.54	7.9, 8.4

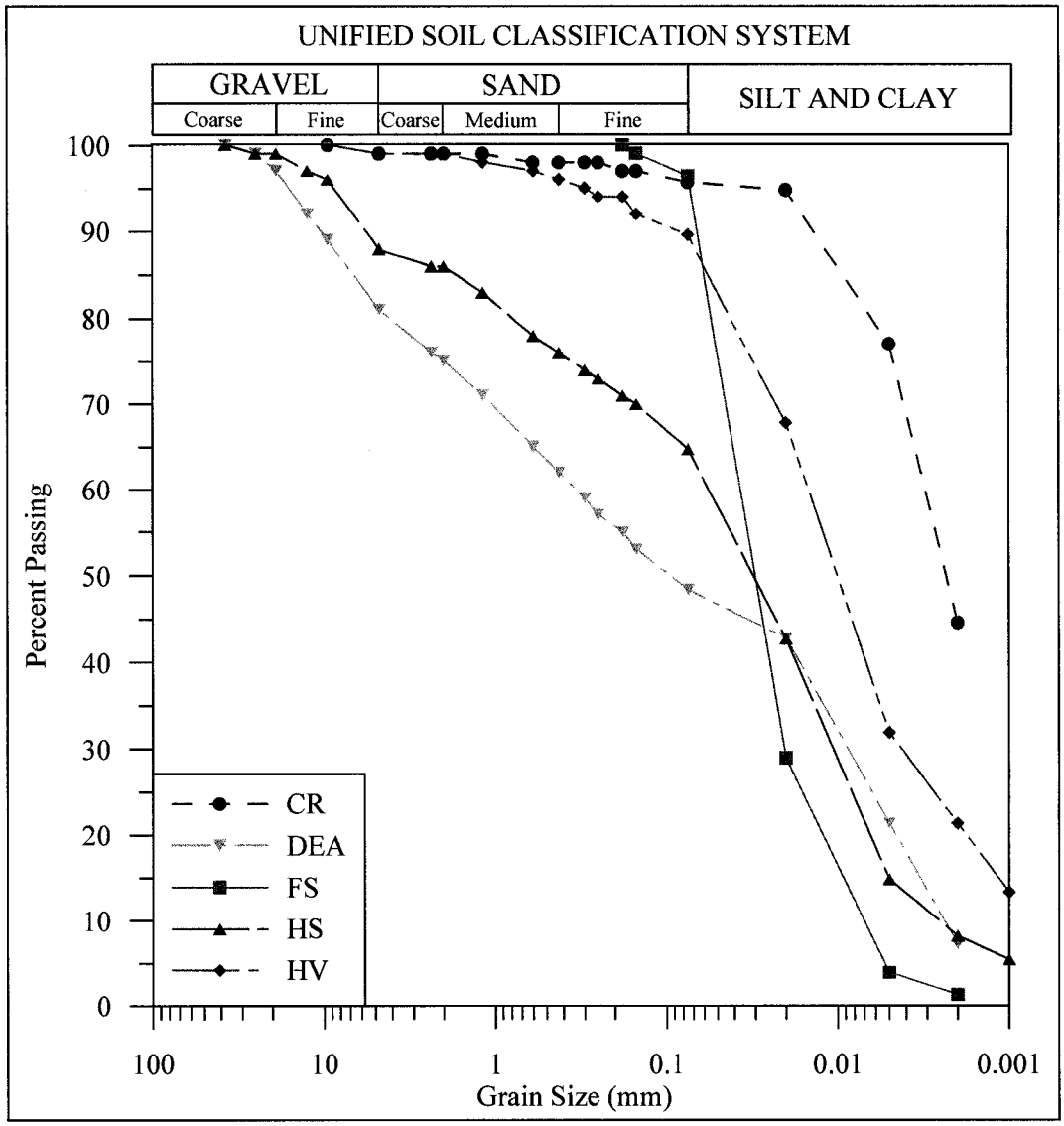

Figure 2.2: Grain size distributions for the five natural soils

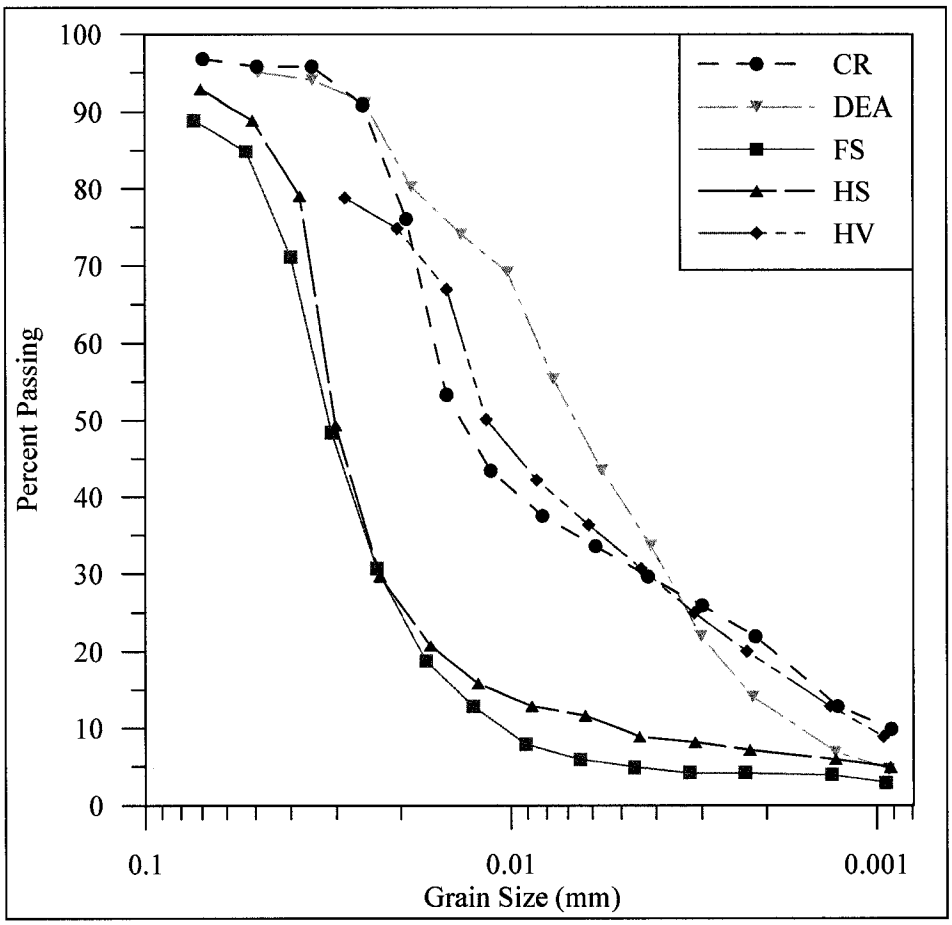

Figure 2.3: Grain size distributions for the BSLN soil samples

distributions to each other, as each contains more clay-sized particles than the other BSLN samples.

All organic matter was removed from the BSLN samples, in order to focus only on the mineral particles and their effects. For most of the soil samples, this consisted of removing rootlets during the initial sieving process. The HV sample required additional preparation, however, due to its high organic content. The organic matter was removed from the HV soil with hydrogen peroxide, following the standard procedure outlined by the Soil Science Society of America (Kunze and Dixon 1986). A portion of the sieved HV soil with its original organic content was retained, however, and used in frost heave testing in order to compare to the HV soil without organics. The organic HV sample is referred to as HV ORG.

2.3 Soil Chemistry

Soil surface area measurements, chemical characterization, and qualitative x-ray diffraction (XRD) analyses on the BSLN soil samples were conducted by Washington State University (WSU) in Pullman, Washington. The surface area measurements were conducted using a Micromeritics ASAP 2010 Surface Area analyzer. This apparatus utilizes the nitrogen gas sorption technique and the Brunauer, Emmett, and Teller (BET) equation to determine the number of adsorbate molecules in a monolayer on the soil particles, from which the specific surface area is calculated (Kunze and Dixon 1986).

WSU technicians prepared saturated extracts of soil solution using the method outlined by Rhoades (1996). This method is not standardized, as the method varies slightly from soil to soil (J. Boyle, personal communication, November 2006). To prepare the soil slurry, enough water is added to a 100 g soil sample for the soil to reach saturation. In this method, saturation is defined as the point at which the soil slurry begins to slide off of a metal spatula. The soil slurry is allowed to equilibrate overnight. The soil is then centrifuged, and the soil solution is decanted and filtered to remove particulates.

The cation exchange capacity (CEC) and concentration of soluble cations from the saturated extracts were measured using a Varian Spectra 220 FS Atomic Absorption Spectrometer and a method outlined by Sumner and Miller (1996). WSU technicians measured the pH and electroconductivity of the saturated extracts using a Beckman Phi 45 pH meter with combination electrode, and a method outlined by Rhoades (1996). Table 2.3 contains the results of these analyses.

Table 2.3: Summary of chemical characterization and specific surface area measurements of BSLN samples

Soil	pH	Electroconductivity (dS/m)	Soluble Cations (mmol/kg)					Cation Exchange Capacity (mmol/kg)	Specific Surface Area (m^2/g)
			Ca^{2+}	Mg^{2+}	Na^{+}	K^{+}	sum		
CR	6.76	1.89	10.00	3.98	3.29	0.10	17.37	287.0	16.04 ± 0.35
DEA	6.79	0.77	1.33	0.59	1.24	0.02	3.18	90.1	5.41 ± 0.10
FS	7.10	0.28	0.96	0.17	0.24	0.05	1.42	112.5	6.54 ± 0.18
HS	7.05	1.05	5.16	0.24	0.96	0.03	6.39	101.3	9.25 ± 0.21
HV	4.68	0.90	4.48	1.28	0.81	0.03	6.60	136.4	8.44 ± 0.14

2.4 XRD Analysis and Soil Mineralogy

WSU technicians conducted the qualitative XRD analysis using copper Kα radiation, with a graphite monochrometer and a theta compensating slit (refer to Appendix C for a general overview of the principles of XRD and mineral identification techniques). The XRD samples were prepared using a preferred orientation method. In order to determine the presence of various clay minerals, several sample preparations were analyzed, which included magnesium (Mg^{2+})-saturated air-dried, Mg^{2+}-saturated glycerol solvated, potassium (K^{+})-saturated air-dried, K^{+}-saturated heated to 550°C, and K^{+}-saturated intercalated with dimethyl sulfoxide (DMSO) vapor. Figures 2.4 and 2.5 contain the XRD charts for the CR sample and treatments, respectively. The XRD charts of the remaining soil samples and treatments are included in Appendix D.

The most conspicuous feature of each diffraction pattern is the sharp peak at approximately ~26.7° 2θ. This is the 3.34 Å (101) peak of quartz. Further observation identifies the smaller quartz peak at about 20.9° 2θ. While the (101) peaks are generally sharp, they have some broadening toward their bases, which may indicate the presence of a finer-grained clay with a coincident reflection peak or imperfection of the quartz crystal structures.

Working from left to right, each soil pattern has a series of peaks at roughly ~6.3°, ~12.5°, ~18.9°, ~25.3°, and ~31.7° 2θ. These peaks may represent the (00*l*) basal plane reflections of chlorite and/or kaolinite. Other diagnostic techniques are necessary to separately identify these minerals.

The series of peaks at ~8.8°, ~17.8°, ~26.7°, ~36.0°, and ~45.3° 2θ represent the (00*l*) basal plane reflections of illite and/or muscovite. Generally, these peaks are broad, possibly indicating that the mineral has a small particle size or poor crystallinity. This suggests that the mineral is illite, rather than muscovite. Doing a "best fit" to the different (θ0*l*) reflections yields the following d-spacing for the illite/muscovite peak: 9.97 Å for CR, 9.99 Å for DEA, 9.98 Å for FS, 10.07 Å for HS, and 10.00 Å for HV. Since these basal spacings are slightly higher than the d-spacing of muscovite, they may indicate the presence of illite. However, these d-spacings were calculated using an average Kα wavelength, and the peaks were obtained from patterns that had a resolution of 0.05° 2θ, both of which may contribute to errors in the above calculations. Although the presence of illite is strongly suspected, a definitive answer to this question can not

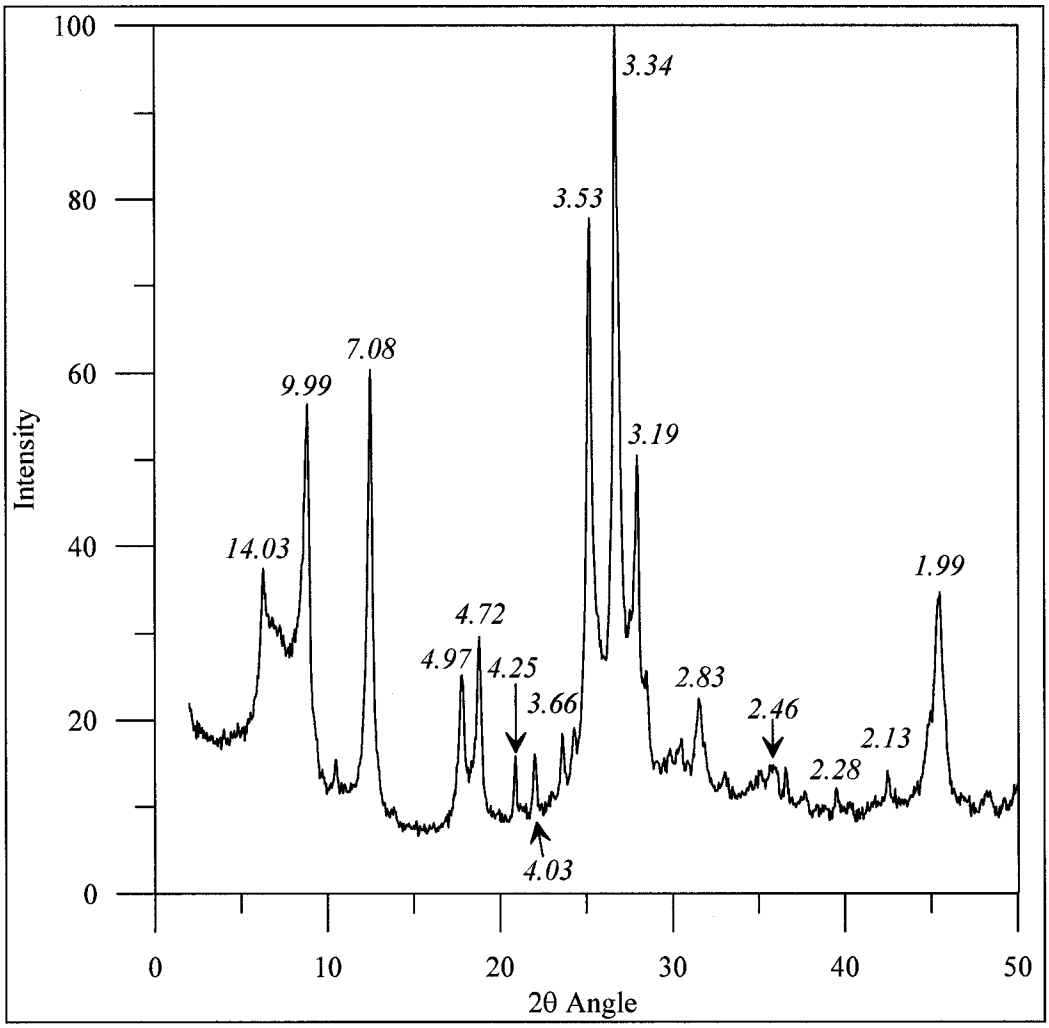

Figure 2.4: Full-range XRD pattern for CR. Annotation above or near each major peak gives the d-spacing in Angstroms.

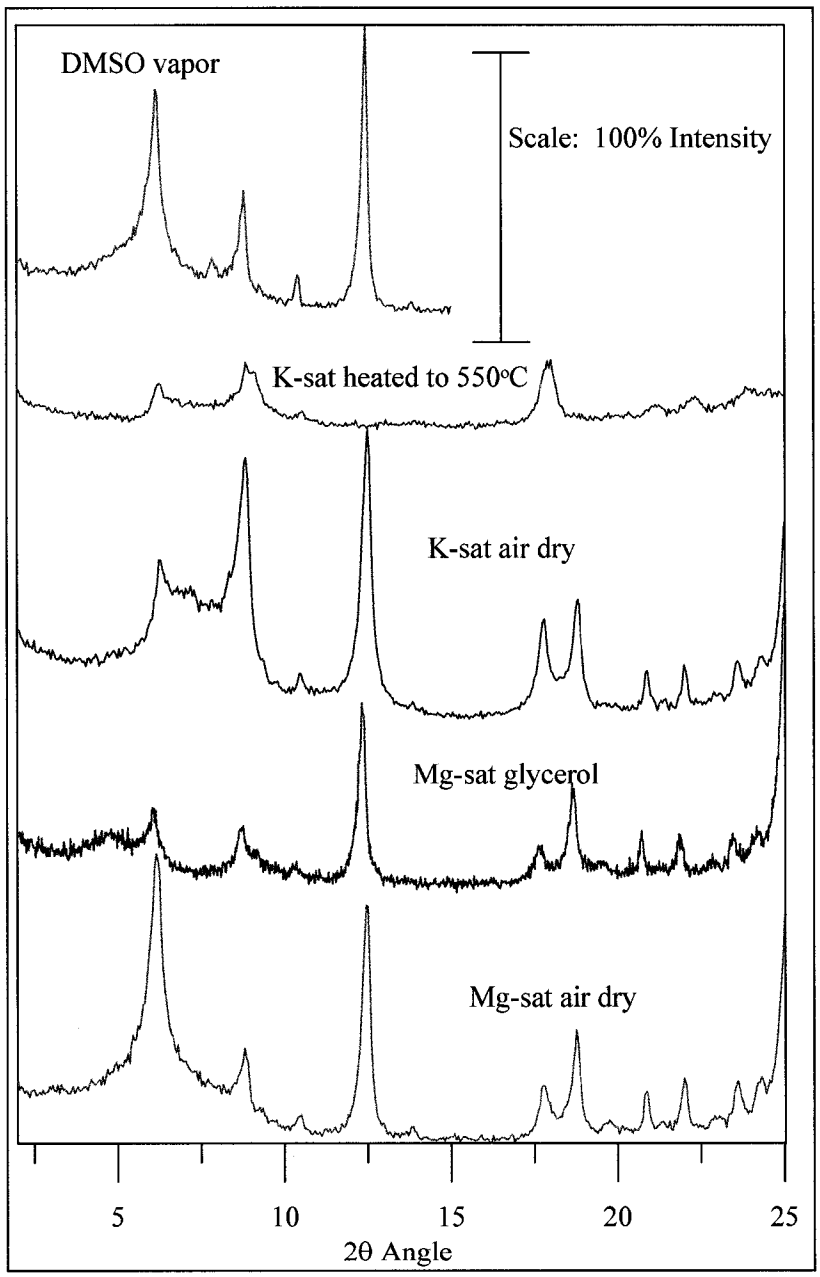

Figure 2.5: XRD patterns of the various treatments on CR soil

come from this level of XRD analysis. Additionally, all of the samples except for HV demonstrate peaks in the range of ~22.02° 2θ, which may indicate the presence of feldspar.

Based on these overall observations, each soil contains quartz, illite/muscovite, chlorite and/or kaolinite. Each soil may also contain smectite, as smectite's peaks would closely match those of chlorite and illite/muscovite. Additional analysis must be made to determine the presence of smectite. All soils, except for possibly HV, also contain a minor amount of feldspar. The FS pattern is different from the others because of the broad, fuzzy hump that appears in the middle of the pattern. This feature is indicative of amorphous material, indicating either that FS contains amorphous material, or that the XRD instrument picked up the glass slide because the slide did not contain enough sample material.

In order to determine the presence of kaolinite, the K^+-saturated air-dried patterns are compared against the DMSO patterns. These patterns are presented in Figure 2.5 and in Appendix D, and have been normalized after removing the background intensity. With the addition of DMSO, all soils demonstrate the shift of the (001) reflection to roughly 7.89° 2θ. The peak at the original location (i.e., 2θ = 12.65°) remains, indicating that chlorite is also present in the soils. The presence of kaolinite can be further supported by the collapse of the (001) and (002) peaks at 12.65° and ~25° 2θ when the samples are heated to 550°C.

In order to establish the presence of smectite, a comparison must be made between the Mg^{2+}-saturated air-dried patterns and the Mg^{2+}-saturated, glycerol-solvated patterns. The DEA soil does not demonstrate any peak shift in the glycerol-solvated pattern. The CR, FS, and HV soils demonstrate a general peak shift to smaller 2θ values and the development of broad peak at ~4.9° 2θ. This peak shift may indicate the presence of smectite, or mixed-layer illite/smectite. The glycerol-solvated pattern for HS demonstrates a general peak shift to slightly larger 2θ values, possibly indicating the presence of mixed-layer chlorite/smectite.

To summarize, the analysis of the qualitative XRD results indicates that all of the BSLN soils contain chlorite, illite/muscovite, quartz, and (with the possible exception of HV) feldspar. The analysis also indicates that CR, FS, and HV contain some portion of smectite or mixed-layer illite/smectite, while HS contains mixed-layer chlorite/smectite. The DEA sample does not contain any form of smectite. After this initial analysis and in light of concurrent frost heaving test results, further semi-quantitative XRD analysis was deemed necessary. K/T GeoServices, Inc. in Argyle, Texas, a laboratory that specializes in XRD analysis, conducted the semi-quantitative XRD analysis. The analysis was conducted using a Rigaku automated powder

diffractometer, a copper x-ray source, and a scintillation x-ray detector. The XRD samples were prepared using a powder mount method, in which the individual mineral grains are randomly oriented. A complete description of the sample preparation and analytical procedures, as provided by K/T GeoServices, Inc., is included in Appendix D.

The results of the semi-quantitative XRD analysis are contained in Table 2.4 (for the complete set of XRD curves from the semi-quantitative analysis, see Appendix D). K/T GeoServices technicians stress that the detection limits of XRD are on the order of one to five weight percent, with the detection limits varying for each different mineral. Additionally, the percentage of a mineral present is dependent on the percentages of the other minerals in the sample. Thus, if errors occur in reporting one mineral, all the remaining minerals may be over- or underestimated. For these reasons, the results presented in Table 2.4 may not represent exact amounts, but instead should be used for only semi-quantitative comparison.

The results contained in Table 2.4 match those of the qualitative analysis fairly well, indicating that all BSLN samples contain quartz, illite/mica, kaolinite, and chlorite, as well as other non-clay mineral species. The semi-quantitative analysis indicated that the CR soil contains mixed-layer chlorite/smectite rather than mixed-layer illite/smectite. The HS soil also contains mixed-layer chlorite/smectite, whereas the FS and HV soils contain mixed-layer illite/smectite. As indicated by the qualitative XRD analysis, the DEA sample is unique, as it does not contain any form of smectite. Summing the weight percents in Table 2.4 indicates the following total percentages of phyllosilicates in the BSLN samples: CR 23.7 percent, DEA 8.9 percent, FS 9.6 percent, HS 20.8 percent, and HV 18.7 percent.

2.5 Overview of Clay Mineral Surface Chemistry

Soils typically are composed of a mixture of grain sizes, with the larger particles providing the inactive framework of the soil and with the finer particles, such as clays, providing the active portion of the soil (Taylor and Ashcroft 1972). Early in the history of frost heave research, individuals recognized that the type of clay minerals present within the soil is critical to its frost susceptibility (Grim 1952; Linell and Kaplar 1959; Lambe et al. 1969; among others). Furthermore, it was discovered that the exchangeable cations present within the soil affect the grain size distribution, the water content, and the frost susceptibility. Thus, an understanding of the typical clay minerals found in soil and their surface chemistry characteristics is essential to

Table 2.4: Summary of semi-quantitative XRD mineral analysis of BSLN samples

Summary Mineralogy (Weight Percent)	CR	DEA	FS	HS	HV
Quartz	19%	41%	32%	35%	67%
K-Feldspar	1.2%	1.4%	2.1%	2.6%	0.5%
Plagioclase	47%	44%	45%	36%	13%
Amphibole	5.9%	3.7%	3.7%	4.3%	0.5%
Calcite	0.8%	0%	2.3%	1.0%	0%
Dolomite	0%	0%	2.5%	0%	0%
Pyrite	2.3%	0.9%	2.7%	1.1%	0.2%
R-O M-L I/S*	0%	0%	1.5%	0%	0%
R-O M-L C/S**	7.2%	0%	0%	1.8%	0%
O M-L I/S***	0%	0%	0%	0%	6.7%
Illite & Mica	5.6%	3.2%	4.7%	12%	7.4%
Kaolinite	1.2%	0.7%	1.0%	1.0%	1.1%
Chlorite	9.7%	5.0%	2.4%	6.0%	3.5%
TOTAL	100%	100%	100%	100%	100%
Phyllosilicate Mineralogy (Relative Abundance)					
R-O M-L I/S*	0%	0%	15%	0%	0%
R-O M-L C/S**	30%	0%	0%	9.0%	0%
O M-L I/S***	0%	0%	0%	0%	36%
Illite & Mica	24%	36%	49%	57%	39%
Kaolinite	5.1%	7.9%	11%	4.9%	5.7%
Chlorite	41%	56%	25%	29%	19%
Total	100%	100%	100%	100%	100%
%S in M-L I/S****	50	0	90	40	15

* Randomly Ordered Mixed-Layer Illite/Smectite

** Randomly Ordered Mixed-Layer Chlorite/Smectite

*** Ordered Mixed-Layer Illite/Smectite

**** Percent Smectite in Mixed-Layer Illite/Smectite

understanding the frost heave process. The overview of clay mineral surface chemistry presented here also will provide the foundation from which to interpret the current research's experimental results.

A general overview of several clay minerals and their structures is presented in Appendix C. Each of these minerals demonstrates some amount of isomorphous substitution, which results in an overall negative surface charge, or negative potential (Y_o). The negative potential is balanced by a swarm of hydrated cations about the mineral surface. The cation swarm has structure, as the closest cations to the mineral surface form a tightly adsorbed layer called the Stern layer (Taylor and Ashcroft 1972) (see Figure 2.6). The negative potential of the mineral surface is reduced by the presence of the cations within the Stern layer according to Helmholtz double layer theory. The remaining negative potential is balanced by the less structured portion of the cation swarm, called the Gouy-Chapman diffuse double layer (Taylor and Ashcroft 1972). The cation swarm, inclusive of all internal structure, is referred to as the diffuse double layer, the electric double layer, or simply as the double layer in clay mineral literature.

The negative potential at the Stern layer, represented as Y_δ in Figure 2.6, is manifested as the zeta (ζ) potential, which can be quantified by placing a dilute soil slurry into an electric field (see Section 3.3 for a description of this procedure). The negatively-charged soil particles will migrate toward the positive pole, while the remaining cation swarm in the fluid will migrate toward the negative pole. The ζ potential is the negative potential formed at the shearing surface of the soil particle (Greenland and Hayes 1978). The ζ potential depends on the type of cations adsorbed within the Stern layer. Thus, changing the adsorbed cations on the mineral surface affects the measured ζ potential and the overall double layer thickness.

The ζ potential is critical when discussing clay minerals, since it describes in part the type of soil structure the clay minerals will form (Cornell University 1951, Lambe 1953, Heagler, Jr. 1964). The presence of divalent cations in the Stern layer better neutralizes the mineral surface charge than monovalent cations, resulting in a lower ζ potential, a thinner diffuse layer, and a thinner layer of oriented water at the mineral's surface (Grim 1958). The presence of either Ca^{2+} or Mg^{2+} in the Stern layer will produce a well-defined, oriented water layer about four water molecules thick (Grim 1958). Clay particles with low ζ potentials are able to approach each other and form edge-to-face electrostatic bonding, resulting in a

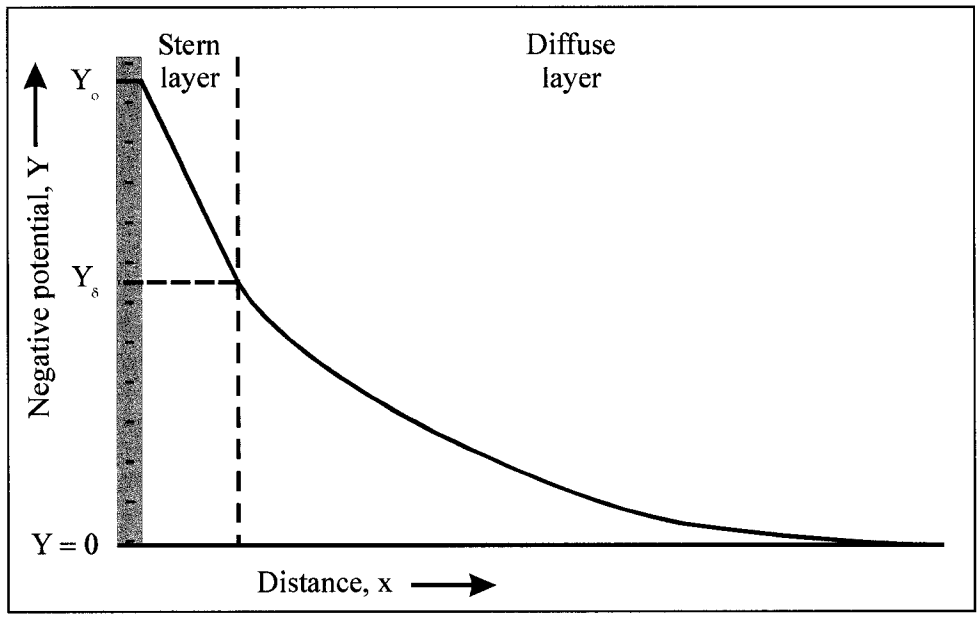

Figure 2.6: Schematic representation of the electric double layer, including the Stern and diffuse layers. The shaded gray rectangle represents the mineral surface carrying an overall negative charge. (Adapted from Taylor and Ashcroft (1972))

flocculated structure (Hillel 1980, Heagler, Jr. 1964). A clay having a flocculated, or aggregated, structure will have a higher permeability.

Conversely, monovalent cations in the Stern layer cause a higher ζ potential, a thicker diffuse layer, and a thicker adsorbed water layer. The presence of Na^+ in the Stern layer will result in an adsorbed water layer that is tens of water molecules thick (Grim 1958). Unlike the Na^+ ion, K^+ may cause structural collapse within the clay mineral, resulting in thin oriented water layers (Grim 1958). Clay minerals containing monovalent cations in the Stern layer orient themselves in positions of minimum energy due to the net repulsive force (Heagler, Jr. 1964), forming a dispersed soil structure. The dispersed structure gives these clays very low permeabilities. Thus, the type of cation adsorbed onto the clay mineral surface will determine its state of dispersion or aggregation and degree of permeability (Cornell University 1951). Consolidation experiments also indicated that clays having higher ζ potentials retain more water at a given load than do clays with low ζ potentials (Cornell University 1951). Additionally, the type of cation adsorbed onto a clay mineral surface will affect the movement of water through adsorbed water films at water contents below saturation (Kemper 1960).

Some research has been done to explain the effects of cation exchange on the ζ potential, microaggregate formation, unfrozen water content, and frost susceptibility of various clay minerals. Kaolinite demonstrates the largest frost susceptibility of the clay minerals (Grim 1952, Lambe 1953, Rieke et al. 1983, Czurda and Schababerle 1988). Czurda and Schababerle (1988) determined that kaolinite has thin water films, but that the water in these films is more mobile than that in other clays, which perhaps gives it its high frost susceptibility. Grim (1952) indicated that the characteristics of kaolinite are less affected by exchanging the adsorbed cations than other clay minerals, due to its small specific surface area and low cation exchange capacity. Nersesova and Tsytovich (1963) found this to be true, as they demonstrated that the unfrozen water content curves of Na^+- and Ca^{2+}-treated kaolinite were nearly identical. Nersesova (1961) also found this to be true, as exchanging the cations in a kaolinite-rich soil did not greatly affect its microaggregate formation. However, when the kaolinite soil was frozen, the Ca^{2+}-treated sample heaved approximately 52 mm through the course of the test, whereas the Na^+- and K^+-treated samples heaved only approximately 9 mm and 5 mm, respectively (Nersesova 1961). Thus, the frost susceptibility of kaolinite depends less on microaggregate formation and more on the nature of the adsorbed water, which is effected by the exchangeable cations. Nersesova

(1961) attributed the reduction in frost susceptibility to the effect of the exchangeable cations on the surface energy of the soil.

The smectite clays, unlike kaolinite, are highly dependent on the type of exchangeable cation present. This is attributed to the high specific surface areas and cation exchange capacities of these clays, which include the mineral montmorillonite. When smectite is treated with Na^+, it is highly hydratable, with a large diffuse double layer and large amounts of oriented, adsorbed water (Lambe 1953, Odom 1984). The water will enter in between the unit layers, making the smectite mineral swell (see Figure C.2). The water is held tightly at the surface, but becomes more mobile with distance away from the surface. Thus, even with a large water content, smectite will contain essentially no mobile water (Grim 1952). Czurda and Schababerle (1988) reiterated this, stating that although the water films are thicker in a Na^+-treated montmorillonite, the water's mobility is greatly restricted. Grim (1952) indicated that when K^+ is adsorbed onto montmorillonite, the clay demonstrates very little water adsorption with a definite configuration, thereby possessing more "mobile" water. Research at Cornell University (1951) in this area suggested that some permanent fixation of the K^+ ion may occur within the montmorillonite crystal structure. Nersesova and Tsytovich's (1963) research indicated that the unfrozen water content of Na^+-treated montmorillonite was greater than that of the Ca^{2+}-treated sample by approximately 60 percent at -0.2°C.

Through her experiments on microaggregate formation, Nersesova (1961) found that the structure of a soil rich in montmorillonite was highly dependent on the exchangeable cation. Treating the montmorillonite-rich soil with cations increased the overall grain size in the following order: $Na^+ < K^+ < Ca^{2+}$. The cation treatments demonstrated nearly identical trends in increasing frost susceptibility, with the Na^+- and K^+-treated samples heaving approximately 8 and 7 mm, respectively, while the Ca^{2+}-treated sample heaved approximately 38 mm. Lambe (1953) discovered a similar trend in the relationship between cation treatment and the frost susceptibility of montmorillonite soil. From Lambe's experiments, the frost susceptibility of the cation-treated soils increased in the following order: $Na^+ < Ca^{2+} < Mg^{2+}$. Nersesova (1961) attributed this trend in frost susceptibility to the formation of larger microaggregates at the expense of the colloidal clay particles. Lambe (1953) made a similar explanation for this dramatic change in frost susceptibility. He stated that a coarse-grained soil would become less frost susceptible by effectively removing the fine grains through aggregation. A fat clay,

however, would be made more frost susceptible when the clays were aggregated, due to an increase in its permeability.

Lambe (1953) and Grim (1952) each discovered that illite and chlorite have frost susceptibilities in between those of kaolinite and montmorillonite. Grim (1952, 1958) attributed this to the intermediate amount of oriented water on these minerals' surfaces. Illite possesses thicker adsorbed water films than kaolinite; however, the adsorbed water is not held as rigidly as in montmorillonite. Kazda (1979) obtained similar results from NMR experiments with kaolinite, illite, and montmorillonite. Grim (1952) postulated that a mixed-layer illite/smectite would be highly frost susceptible. From the above discussion, it follows that a mixed-layer chlorite/smectite also would be highly frost susceptible.

CHAPTER 3: LABORATORY METHODS AND PROCEDURES

3.1 Soil-Moisture Characteristic Curves

How much water, or moisture, a soil retains at increasingly negative pressures, or suctions, is a function of soil density, pore size, texture, and mineralogy. The soil-moisture characteristic (SMC) curve is a graphical representation of the function between volumetric water content and matric suction, also called matric potential (ψ_m) (Hillel 1980). The SMC function, also referred to as the retention function, demonstrates hysteresis due to the difference in how the soil pores fill and empty. The two hysteretic portions of the SMC curve are called the main wetting curve (MWC) and the main drying curve (MDC), and which curve is measured depends on the type of analysis conducted (Klute 1986). Since the freezing process of soils can be compared to the drying process, only the MDC curves were measured for each of the five BSLN soils. Different laboratory methods must be used to determine the SMC over the extreme range of matric suctions a drying soil experiences. The methods used are presented below according to the range of negative pressures for which they are suitable. The results from all three methods are combined to create a complete SMC curve.

All of the BSLN soil samples tested were remolded, or disturbed, samples. Samples were prepared by adding small quantities (e.g. 20 mL) of distilled, deionized water to the soil sample and thoroughly mixing with a metal spatula. This process was repeated until the soil was moist enough to form a ball when squeezed in the palm of the hand, leaving some moisture on the skin. A standard brass ring (54 mm ID x 30 mm cylinder) was placed on a metal plate, and soil was added to the ring in lifts approximately 10-mm thick. After soil was added to the ring, it was tamped in place using a wooden dowel. When the amount of soil nearly filled the ring, a second ring was added to the top of the first, and excess soil was added and tamped into the second ring. A thin knife was used to slice between the first and second rings, thereby removing all excess soil and leaving a uniformly filled brass ring with two uniform surfaces. Soil samples in standard brass rings packed in this manner were used for the low-range and mid-range matric suction tests.

3.1.1 Low-Range Matric Suctions

The hanging water column apparatus (Vomocil 1969) can be used in the laboratory to determine the SMC for suctions less than 20 kPa, or approximately 2 m of pressure head.

Vomocil listed excessive evaporation loss of the draining soil water as one source of error inherent in this method. Since fine-grained soils, such as silt and clay, require longer time to reach equilibrium than coarse-grained soils, the evaporation error is greater. Indeed, with the standard hanging water column apparatus, a compromise must be made between attaining equilibrium and avoiding excessive evaporation loss.

In cold locations, low relative humidity (RH) may cause excessive evaporation in the laboratory setting. For example, during the winter in Fairbanks, Alaska, it is not unusual for temperatures to reach -40°C. After the cold air is heated to 20°C in the buildings without the addition of moisture in the ventilation systems, the RH can be as low as 2 percent. In this extremely dry condition, the saturation deficit in the laboratory environment can reach 2.29 kPa (Fritschen and Gay 1979). Unless modifications are made to the hanging water column apparatus, the evaporation driven by such a tremendous saturation deficit would cause severely erroneous results.

A schematic of the modified hanging water column apparatus used to measure the SMC curves for the BSLN soils is shown in Figure 3.1. An undisturbed soil sample in a standard brass ring was placed in a Tempe cell (A) (Reginato and van Bavel 1962) equipped with a 0.5 bar (~5 m negative pressure head) porous plate. This apparatus took the place of the Büchner funnel with porous plate described by Vomocil (1969). Tygon tubing (6 mm ID) connected the drainage tube (B) of the Tempe cell to glass tubing (6 mm ID) (C) serving as a manometer.

Modifications to reduce evaporation consisted of three items. First, a 23 gauge hypodermic needle inserted through a rubber stopper (D) was located in the top of the manometer. The small passageway through the needle reduced evaporation while allowing for air pressure equilibrium. Second, a water-filled vinyl tube (19 mm ID) (E) stoppered at both ends, surrounded the connecting Tygon tubing. This "water jacket" retarded evaporation through the inner tubing walls. Short lengths of Tygon tubing remained exposed at either end of the water jacket to facilitate assembly of the apparatus. Third, the Tempe cell and a small beaker of water (F) were placed inside a plastic container with removable lid (G) to retard evaporation from the air connection port (H). A second hypodermic needle (I) was inserted through the lid of the plastic container to allow air pressure equilibrium throughout the test.

Rather than lowering the water reservoir as suggested by Vomocil (1969), the platform (J) on which the Tempe cell rested was raised in increments during the test, while the manometer

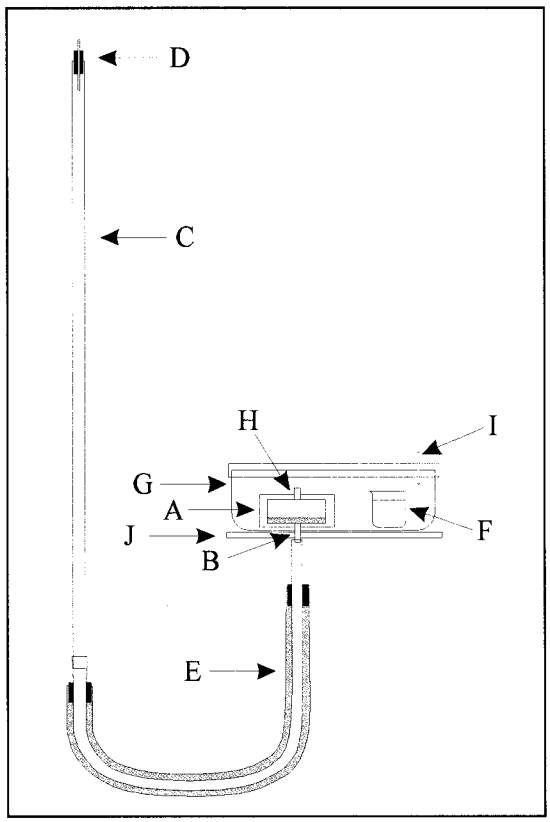

Figure 3.1: Schematic of the modified hanging water column apparatus. (A) Tempe cell, (B) drainage tube, (C) manometer, (D) hypodermic needle in rubber stopper, (E) water-filled vinyl tube, (F) beaker with water, (G) plastic container with tight fitting lid, (H) air connection port, (I) hypodermic needle in lid of plastic container, (J) raising platform.

remained fixed. After equilibrium was reached, the elevation of the soil bottom inside the Tempe cell and the meniscus in the manometer were recorded. The difference in elevation of these two readings is the matric potential, ψ_m.

This process was repeated until the platform was at the top of the apparatus. The inner brass ring containing the soil sample was removed from the Tempe cell, and the final gravimetric soil moisture content, w_f, was determined using standard Soil Science Society of America procedures (Gardner 1986). The gravimetric soil moisture content at each platform setting, w_i, was calculated by:

$$w_i = w_f + \frac{V_f - V_i}{M_d - M_r} \cdot \rho_w \tag{3.1}$$

where V_f is the final water volume calculated from the final manometer reading, V_i is the water volume calculated from the manometer reading at each platform setting, M_d is the final dry mass of the sample plus ring and weighing dish, M_r is the tare mass of the ring and weighing dish, and ρ_w is the density of the wetting fluid, which was distilled, deionized water in this case. The volumetric moisture content at each platform setting, θ_i, was calculated by:

$$\theta_i = w_i\left(\frac{\rho_b}{\rho_w}\right) \tag{3.2}$$

where ρ_b is the dry bulk density of the sample. From these calculations, the θ_i at each corresponding matric suction was determined. This procedure was followed on duplicate samples for each of the BSLN soils for matric suctions between 0 m and 1.75 m.

3.1.2 Mid-Range Matric Suctions

Values for soil-moisture at matric suctions between 20 kPa and 1.5 x 10^3 kPa, or approximately 2 m and 150 m of negative pressure head, respectively, were determined using a pressure plate extractor and accompanying laboratory system. With this system, standard brass rings containing saturated soil samples were placed inside the extractor on a saturated ceramic plate, also called a pressure plate cell. The pressure within the extractor was increased to a specified amount, and the soils were allowed to reach the corresponding equilibrium moisture contents. The amount of time necessary for a soil to reach equilibrium depended on the soil

texture and mineralogy. For example, a silty soil only took a few hours to equilibrate, whereas a clayey soil required up to a month. Once equilibrium was obtained, the soil samples were removed from the pressure vessel, and their gravimetric moisture contents were determined for the given pressure, or matric suction, applied. The pressure within the vessel was increased to a higher value, and the process was repeated. Care was taken to ensure that the ceramic plate in use had a higher bubbling pressure than that applied in the extractor. Additionally, wet towels were applied to the surface of the soil samples to prevent evaporation during the test.

Each of the five BSLN samples were tested in this fashion, using pressure plate extractors, pressure plate cells, and a compressed air manifold available from Soilmoisture Equipment Corporation. Duplicate samples were run for each pressure. The moisture retained by the soils was measured at approximately 4 m, 15 m, 30 m, 60 m, and 100 m pressure head. Each sample was also tested at a higher pressure that ranged between 125 m and 140 m, depending on how the entire laboratory system equilibrated when the pressure was applied.

3.1.3 High-Range Matric Suctions

The vapor sorption method was required for matric suctions higher than 1.5×10^3 kPa, or approximately 150 m of negative pressure head. In this method, the RH inside a sealed glass desiccator was controlled by a saturated solution poured into the bottom of the desiccator. The soil samples (~1 g), contained in clean, dry vials, were placed on a shelf above the saturated solution in the desiccator. The caps were removed from the vials, and the soil samples were allowed to reach equilibrium with the vapor of the environment. Equilibrium was determined by carefully capping each vial and repeatedly weighing the individual samples. Care was taken to keep the vials free of dust and fingerprints, as measurements needed to be made to the nearest 0.0001 g. Once equilibrium was obtained, the final moisture content of each sample was determined.

In a separate process, the electrical conductivity (EC) of each soil was determined by measuring the EC of fluid extracted from a soil paste (Durnford and Lorentz, unpublished laboratory manual, 1993). The EC of the sample was calculated by:

$$EC_{sample} = \frac{w_{paste}}{w_{sample}} \cdot EC_{paste} \tag{3.3}$$

where w_{paste} and w_{sample} are the moisture contents of the paste and the sample, respectively. The osmotic pressure, or osmotic potential (ψ_o) of the soil paste was determined from a chart relating osmotic pressure to electrical conductivity, such as that available from the USDA (US Salinity Staff 1954). The total potential, ψ_t, of each sample was calculated using:

$$\psi_t = -\frac{RT}{M_w g}\ln(RH) \tag{3.4}$$

where R is the ideal gas constant, T is the absolute temperature, M_w is the gram molecular weight of water vapor, g is gravitational acceleration, and RH is the relative humidity of the vapor (Durnford and Lorentz, unpublished laboratory manual 1993). The matric potential, ψ_m, is the difference between the total potential and the osmotic potential, or:

$$\psi_m = \psi_t - \psi_o \tag{3.5}$$

Duplicate samples for each BSLN soil were tested using the vapor sorption method. The five compounds with different RH used were: sodium hydroxide (NaOH), calcium chloride ($CaCl_2 \cdot 6H_2O$), potassium carbonate ($K_2CO_3 \cdot 2H_2O$), sodium chloride (NaCl), and potassium dichromate ($K_2Cr_2O_7$). The RH of each compound at 20°C is listed in Table 3.1 (Winston and Bates 1960).

3.2 Cation Soil Treatments

In order to investigate the effects of surface chemistry on frost heaving, cation treatments were applied to each BSLN soil. Four different salts, magnesium chloride ($MgCl_2$), calcium chloride ($CaCl_2$), sodium chloride (NaCl), and potassium chloride (KCl), were used for the various treatments. All four cation treatments were prepared using the CR, DEA, and HS soils. Only two cation treatments were prepared for each of the FS and HV soils. Table 3.2 contains a summary of the cation treatments prepared.

For each cation treatment, a 1M solution of the salt was prepared using distilled, deionized water. Approximately 100 g of soil was added to a plastic jar and one liter of the solution was pored over the soil. The jar was sealed and vigorously shaken by hand. Then, the soil/salt slurry was allowed to sit overnight, to ensure complete saturation of the soil. Three jars of the soil/salt slurry were prepared at one time. After sitting overnight, the jars were placed on top of a mechanical shaker and were shaken for at least a 12-hour period.

Table 3.1: Relative humidity values over saturated solutions

Compound	Relative Humidity at 20°C
NaOH	5.5
$CaCl_2 \cdot 6H_2O$	32.5
$K_2CO_3 \cdot 2H_2O$	44.0
NaCl	76.0
$K_2Cr_2O_7$	98.0

Table 3.2: Summary of prepared cation treatments

Soil	Cation Treatments			
CR	Ca^{2+}	Mg^{2+}	Na^+	K^+
DEA	Ca^{2+}	Mg^{2+}	Na^+	K^+
FS	---	Mg^{2+}	Na^+	---
HS	Ca^{2+}	Mg^{2+}	Na^+	K^+
HV	Ca^{2+}	---	Na^+	---

After completion of the shaking and cation exchange, the soil/salt slurry was poured into glass, Büchner filter funnels (600 mL) that were inserted into Erlenmeyer flasks (1000 mL). Vacuum was applied to the funnels, causing the solution to drain into the flasks. Once the solution completely drained from the soil, the soil was removed from the funnel and again placed into the plastic jars for rinsing. Distilled, deionized water was added to the soil, and it was shaken overnight. The soil solution was poured into the Büchner filter funnels, vacuum was applied, and the soil was allowed to drain again. After the first two rinses, the electroconductivity of the soil fluid was measured using a hand-held conductivity meter. The chlorine content of the soil fluid was determined with a chlorine test kit that utilized the direct reading titrator method. The rinsing process was repeated until the electroconductivity reached an asymptotic value, which typically ranged from 40 μS to 200 μS depending on the type of soil and cation treatment. The chlorine content after the complete rinsing was typically between 8 ppm and 20 ppm, also depending on the soil and cation treatment.

For each preparation described above, approximately 300 g of soil was prepared. This overall process then was repeated four times for each cation, in order to produce enough soil for frost heave testing. After the initial sieving to prepare the BSLN samples, not enough quantity of some BSLN soils existed to prepare each of the individual cation treatments separately. For these soils, the same soil portion was used repeatedly. In these cases, the Ca^{2+} and Mg^{2+} samples were prepared first, because of their high relative selectivity.

In practice, the silty soils required a few weeks to prepare. The clayey soils, however, required up to two months to prepare enough soil for frost heave testing. Soils saturated with Na^{+} and K^{+} required longer periods of time to prepare than their counterparts, as these soils were very slow to drain through the filter funnels.

3.2.1 Grain Size Distributions

The effect of each cation treatment on the soil's grain size distribution was investigated using hydrometer analysis. The hydrometer analysis was conducted using a standard procedure (Das 1997), with one exception. For each BSLN sample and each of the cation treatments listed in Table 3.2, the hydrometer tests were run without the use of a deflocculant such as sodium hexametaphosphate. Adding sodium hexametaphosphate to the soil slurry effectively replaces the adsorbed cations with the sodium ion, thereby eliminating the effects of the cation soil treatments (Hillel 1980). Instead, for these hydrometer tests, each prepared soil slurry was

vigorously shaken by hand before being added to the graduated cylinder. In this way, the effective grain size, or microaggregate, distribution of each soil treatment can be determined.

3.3 Zeta Potential Measurements

The colloidal clay particles in a soil carry a negative surface charge and, when placed into an electric field, will migrate towards the positive pole (Taylor and Ashcroft 1972). This movement is termed electrophoresis, and the particles' electrokinetic velocity, v_e, that results from electrophoresis is defined as:

$$v_e = \frac{D^* \zeta E'}{4\pi\mu} \tag{3.6}$$

where D^* and μ are the dielectric constant and viscosity of the fluid, respectively, E' is the applied electric field, and ζ is the electrokinetic potential, or ζ potential (Taylor and Ashcroft 1972). The ζ potential of a colloid can be determined by first measuring the electrophoretic mobility of the particles, which is the product of the applied electric field and the electrokinetic velocity, and then applying Equation 3.6.

The ζ potential of the BSLN samples and each of the cation soil treatments was determined using a Zeta-Meter. The Zeta-Meter consists of a DC power supply, a clear plastic electrophoresis cell, platinum-iridium cathode and anode, two illuminators for viewing the sample, and a Zeiss 1/b stereoscopic microscope (Zeta-Meter, Inc. 1975) (see Figure 3.2). The microscope is equipped with an "ocular micrometer," which provides a calibrated distance over which the particles can be timed. Using the 8X objective, one full scale division of the micrometer is 120 μm.

To begin the sample preparation, 0.5 g of each soil sample was placed into a scintillation vial, which was filled with distilled, deionized water. After the soil was completely saturated, the vial was shaken vigorously in order to suspend most of the soil particles. A small portion of the suspension was taken from the vial and mixed with additional distilled, deionized water to create a dilute slurry for ζ potential measurements. The amount of suspension removed and diluted was not exact; instead, these samples were prepared "by eye," having the concentration necessary to provide adequate particle tracking under the Zeta-Meter microscope (Zeta-Meter, Inc. 1975). The dilute solution was pored into the electrophoresis cell and the anode and cathode were inserted. Care was taken to remove all air bubbles, as the presence of air can greatly affect

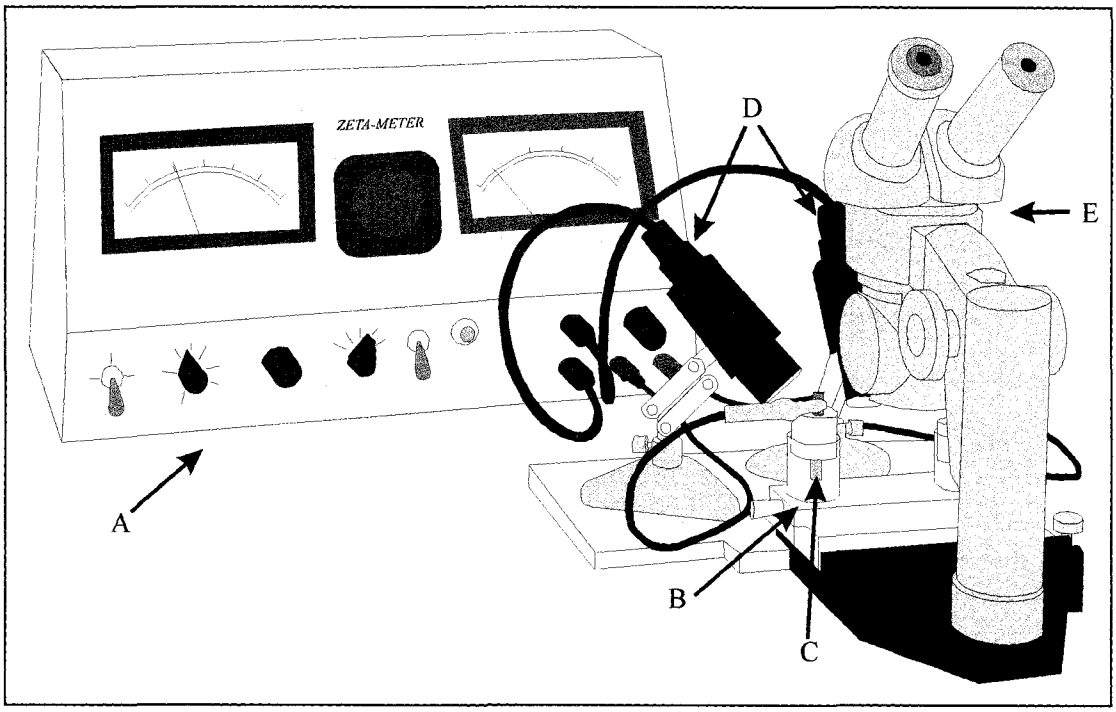

Figure 3.2: Schematic of the Zeta-Meter apparatus. (A) DC power supply, (B) clear plastic electrophoresis cell, (C) platinum-iridium anode (the cathode is out of view behind the microscope), (D) two illuminators, (E) Zeiss 1/b stereoscopic microscope. (Adapted from Zeta-Meter, Inc. (1975))

the ζ potential calculations. The electrophoresis cell was positioned under the microscope, the anode and cathode were connected to the DC power supply, and 300 V was applied to the cell for approximately one minute before the illuminator was powered on.

Corrections were made to the position of the electrophoresis cell once the illuminator was powered on. Particle tracking began immediately, as the heat from the illuminator will accumulate in the cell, causing erroneous ζ potential measurements. The time necessary for a particle to travel one full scale division was recorded, and 50 particles were tracked in this manner. The dilute solution was replaced after 15 to 25 particles were tracked. This ensured that the heat added by the illuminator had a minimal effect on the ζ potential measurement. Once all 50 particles were tracked, the time measurements and charts available in the Zeta-Meter manual (1975) were used to calculate the ζ potential of the soil.

3.4 Unfrozen Water Content Measurements Using Nuclear Magnetic Resonance (NMR)

The nuclear magnetic resonance (NMR) method utilizes the magnetic properties of atomic nuclei. Many nuclei act as magnetic dipoles as they possess a charge and they spin, which produces angular momentum and a magnetic field. When a nuclear magnetic dipole is placed into an external magnetic field, the nucleus aligns itself within the field.

The Fourier-transformation NMR method involves stimulating nuclei, or "spins," with radio-frequency (RF) electromagnetic radiation and observing the signals the nuclei emit as they return to their equilibrium conditions (Atkins and de Paula 2002). For the discussion that follows, this equilibrium magnetization, or primary magnetic field, is called M_o, and it is designated as the z-direction in an x-y-z coordinate system.

An NMR device typically has a coil that both transmits the RF radiation and detects the signal from the nuclei. The RF transmitter applies a second magnetic field in the form of RF electromagnetic radiation in a short pulse. This pulse causes the nuclei to realign to 90° or 180° from the z-direction. If a 90° pulse is applied, then the spins are oriented in the xy-plane. Immediately after the pulse, the spins begin to lose energy and return to their equilibrium positions. This is called spin relaxation. The signal received in the detector coil decreases exponentially. This signal is the free-induction decay (FID). Software programs that may accompany NMR instruments usually use Fourier-transformation mathematics to process the signal from the time domain to the frequency domain. This generates an NMR spectrum.

After a pulse ends, the spins begin to return to their equilibrium positions of M_o with a time constant called the longitudinal relaxation time, T_1 (Atkins and de Paula 2002). As the spins lose energy, the NMR detector coil sees the energy as a signal, but some of the energy is lost to the "lattice" or the surroundings. Thus, another name for the T_1 constant is the spin-lattice relaxation time. This time is short for liquids and much longer for solids.

Immediately after a 90° pulse, the spins are aligned in the xy-plane. They begin to move away randomly from this alignment, becoming out of phase with each other. This occurs exponentially with a time constant called the transverse relaxation time, T_2 (Atkins and de Paula 2002). In this case, the nuclei are exchanging energy with each other. Thus, T_2 is also called spin-spin relaxation time. Solids typically have short T_2 times, whereas those for liquids are longer.

Tice et al. (1982) demonstrated that the NMR technique is suitable and highly accurate for determining the unfrozen water content in a frozen soil. They compared their NMR results with physical desorption data, and obtained excellent agreement between the two techniques. Tice and Oliphant (1984) indicated that the NMR technique is hampered slightly by the presence of magnetic soil particles, which have the effect of reducing the signal strength.

The unfrozen water contents of all BSLN and cation treatment samples were determined using the NMR technique at Hokkaido University in Sapporo, Japan. Due to shipping constraints, only a small portion of each soil/soil treatment was available for testing. Dr. Akagawa and Dr. Iwahana of Hokkaido University, and Dr. Huang of the University of Alaska Fairbanks, performed the NMR measurements.

For these tests, a small quantity of soil was saturated to have a gravimetric water content of approximately 60 percent. The sample was placed under vacuum and de-aired for about eight hours, and during the de-airing, the soil grains settled. Because the quantity of soil was small and because it was difficult to fully consolidate, precipitation of soil grains was used in lieu of consolidation. The "settled" soil was sampled with a small metal cylinder. The soil and cylinder were immersed into liquid nitrogen and frozen for about 10 minutes. This "quick-freeze" ensured that ice lenses did not grow, thereby resulting in a uniform soil texture. The sample was then placed into a freezer to warm up to -30°C. Once warmed, the cylinder was removed from the freezer, and the soil plug it contained was removed and pushed into a Teflon tube. The Teflon tube was placed into a sample holder in a temperature bath, and allowed to equilibrate to -20°C. Once equilibrated, the Teflon tube containing the sample was removed from the

temperature bath and placed into the NMR apparatus. An FID reading was made, which took about 5 seconds, and the tube was returned to the temperature bath. Once the NMR apparatus was reset for a new reading, the tube was placed again into the NMR apparatus and a T_2 measurement was made. The tube then was returned to the temperature bath, in which the temperature was raised. This process was repeated for all the desired temperatures. NMR measurements were made at the following temperatures: -0.2°C, -0.5°C, -1°C, -2°C, -3°C, -4°C, -5°C, -7.5°C, -10°C, -15°C, and -20°C. Once all of the warming temperatures were made, the process was reversed, and cooling measurements were made over the same temperature increments. After the process was completed, the sample was warmed to above freezing, and FID and T_2 measurements were made at 10°C. The moisture content of the soil was determined at the above-freezing temperature, and the unfrozen water content, w_U, at each sub-freezing temperature was calculated by:

$$w_U = \frac{w_{10^oC} \cdot x_T}{x_{10^oC}} \tag{3.7}$$

where w_{10^oC} is the measured gravimetric water content at 10°C, x_{10^oC} is the NMR signal amplitude at 10°C, and x_T is the NMR signal amplitude at the corresponding sub-freezing temperature. Thus, all w_U values reported are gravimetric water contents. All NMR signals used in calculations presented here represent FID peak times.

3.5 Frost Heave Testing

Frost heave testing has been conducted in laboratories worldwide for over 80 years. As such, the types of frost heave testing apparatus, while sharing similar elements, are numerous and varied. The laboratory system and frost heave test cell used in this research is state-of-the-art and can accommodate a variety of freezing methods. The frost heave test cell was developed by Dr. Akagawa of Hokkaido University, Sapporo, Japan, based on his lengthy experience in the area of frost heave testing. The laboratory procedure was designed in order to yield reproducible results with a high level of repeatability.

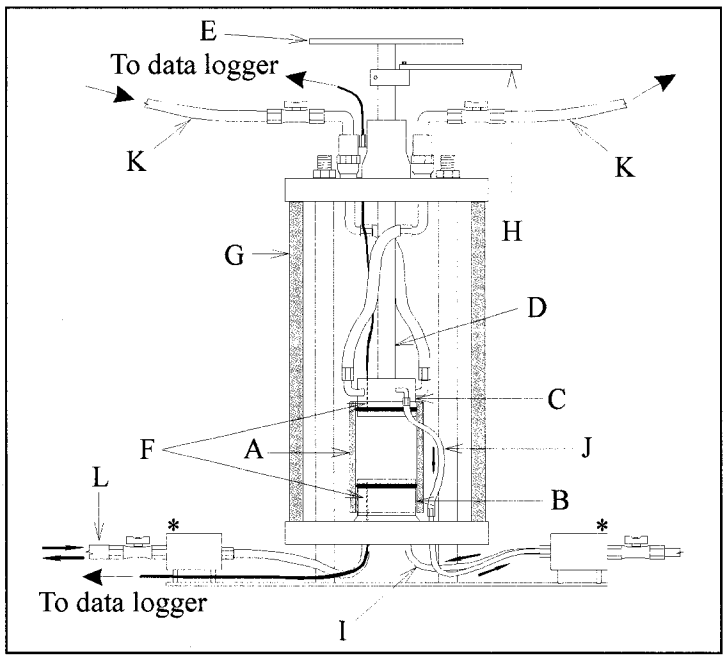

Figure 3.3: Frost heave test cell schematic. A) inner cylinder; B) lower pedestal; C) upper pedestal; D) vertical rod; E) circular overburden plate; F) platinum RTDs; G) outer cylinder; H) horizontal arm (arrow indicates direction of laser measurement); I) pore water intake; J) pore water drain; K) upper pedestal circulating fluid inlet and outlet; L) lower pedestal circulating fluid inlet and outlet; (*) indicate banks of valves, only the first two of which are shown in the schematic.

3.5.1 Laboratory Equipment

The laboratory system consists of a frost heave test cell, a modified refrigerator, and various equipment necessary for measuring heave, water intake, and soil temperature. The frame of the frost heave test cell is of stainless steel construction (see Figure 3.3). An acrylic cylinder (A) (60 mm inside diameter (ID), 7.5 mm nominal wall thickness, 145 mm length) of optical quality contains the soil sample. The cylinder is positioned inside the frost heave test cell between the lower pedestal (B) that is affixed to the base of the apparatus, and the upper pedestal (C), which can move vertically as a piston. The pedestal surfaces in direct contact with the soil sample are porous metal, which allow the passage of pore water and allow efficient heat exchange between the soil sample and the cooling fluid circulating through channels within the pedestals. A vertical rod (D) attaches to the upper pedestal and passes through a bearing in the upper frame of the test apparatus. O-rings lubricated with silicon grease fit in grooves in both the upper and lower pedestals, providing a water-tight seal when the inner cylinder is in place. The soil needs only to overcome the frictional resistance of the lower pedestal o-ring, as the upper o-ring is "frozen" in place with the heaving soil.

Overburden pressure can be applied by placing weights onto a circular plate (E) affixed to the top of the vertical rod. The weight of the upper pedestal, rod, and plate, and the frictional resistance of the O-ring, provide a minimum of 9.1 kPa, which the freezing soil must overcome to heave upwards. This minimum pressure is present in all tests. Platinum resistance temperature detectors (RTD) (F) inserted within each pedestal measure the respective pedestal temperature. Each RTD is accurate to within ±0.01°C.

A larger, removable acrylic cylinder (G) (168 mm ID, 15.5 mm nominal wall thickness, 387 mm length) surrounds the inner cylinder and pedestals, creating a dead air space within the annulus. The optical quality of both concentric acrylic cylinders allows for visual observation of any ice lensing that may develop during the course of the frost heave test. Some convection may occur between the acrylic cylinders, due to temperature differences between the upper and lower pedestals. In one experiment conducted with a similar device by Dr. Akagawa, the horizontal temperature gradient was measured with temperature sensors embedded along the vertical axis of the soil sample, and along the inner wall of the acrylic cell. The horizontal temperature difference measured at the 0°C isotherm was essentially zero (S. Akagawa, personal communication, March 2005). Since ice lensing occurs at the freezing front (i.e., approximately

the 0°C isotherm), it is at this temperature for which the horizontal thermal stability is most critical. Because the measured temperature difference was small, the tests are considered to be strongly one-dimensional. If visual observation of the soil freezing is not required, the inner cylinder can be wrapped with a closed-cell foam insulation blanket to reduce the effect of convection. Such a blanket, with an approximate R-value of 0.46 $m^2 \cdot °C \cdot W^{-1}$, was added for the most of the tests presented here.

A Keyence LK-081 laser supported from a magnetic base measures the vertical distance to a horizontal arm (H), affixed with a set-screw along the vertical rod (see Figure 3.3 for laser measurement orientation). Thus, the laser measures heave as the upper pedestal assembly moves upwards during the test. The horizontal arm may require periodic adjustment to accommodate the laser's range (65 - 95 mm). This laser model has a 3 μm resolution.

The porous metal plates in the upper and lower pedestals allow the flow of water to or from the soil sample. This feature, along with separate cooling systems, accommodates bi-directional freezing. For the series of tests presented here, freezing occurred top-down, with pore water supplied to the sample bottom (I). A double-walled burette serves as the pore water reservoir. Water intake is measured using a Validyne DP-10 differential pressure transducer (DPT) that measures the difference between the pressure at the base of the water column in the burette and the air pressure. Measurements of water intake are accurate to 0.05 mm. The burette is filled via a reservoir of de-aired water.

The circulating fluid is cooled and circulated via two PolyScience Model 1167 programmable circulating baths, one for each pedestal. A 50% water / 50% ethylene glycol solution is used in each bath, and circulated at a rate of 24 L/min. The baths' programming capacity allows for a nearly endless combination of temperature gradients and freezing rates to be applied to the sample, as well as different freezing test methods (e.g., ramped freezing, step-freezing, etc.). All tests presented here used the ramped freezing method, in which a constant freezing rate is approached in the sample.

The test cell and laser are housed within a modified refrigerator. The compressor of the commercial-sized, glass-door refrigerator runs continuously. To control the temperature, heat is supplied via three banks of four 100-W light bulbs. Two banks are on continuously, and a PID (proportional, integral, derivative) control logic device controls the third bank's operation. The refrigerator temperature maintains 1.5°C ± 0.5°C. A sheet of aluminum-coated insulation shields the frost heave cell from the radiative effects of the light bulbs, and a fan circulates the air,

creating better thermal stability within the refrigerator. These refrigerator modifications reduce temperature fluctuations experienced in larger cold rooms due to human traffic and defrost cycles (Mageau and Sherman 1983). The refrigerator is turned off and given a minimum of 24 hours to defrost between frost heave tests. The glass door is a handy feature that allows visual observations of the apparatus without opening the door and disturbing the thermal stability of the frost heave test. The frost heave test cell and laser sit on a steel table within the refrigerator. The legs of the steel table penetrate through the refrigerator and rest on the floor of the laboratory, thereby reducing noise in the laser measurement due to vibrations in the refrigerator.

All wires and tubing are routed through a portal in the wall of the refrigerator. The tubing for the circulating fluid is heavily insulated, which limits the temperature rise from the circulating bath to the upper pedestal to 0.1°C, and to the lower pedestal to 0.06°C. These temperature differences are consistent over time, and can be accounted for when programming the baths.

3.5.2 Soil Sample Preparation

The following sample preparation eliminated many natural variations present in undisturbed samples and increased the repeatability of tests. The soil was soaked in distilled, deionized water for several days to ensure uniform saturation. The saturated soil was mixed into a slurry with a water content greater than the liquid limit of the soil. This facilitated a more uniform particle distribution throughout the sample. The slurry was poured into a consolidation cell, and a vacuum was applied for a minimum of two hours to de-air the soil. Once the air in the slurry was removed, 200 kPa of pressure was applied to the soil. Although consolidation at this pressure caused the soil to be over-consolidated, it was the minimum pressure that allowed post-consolidation handling of the less cohesive silts. Consolidation took from two days to a week, depending on the soil type, and was considered complete when the downward movement of the piston in the consolidation cell was 0.025 mm or less per 24-hour period. Three aluminum tubes (58 mm ID, 1.5 mm nominal wall thickness, 150 mm length) with one beveled edge used for cutting, were used to sample the soil. The tubes were wrapped in plastic and stored upright inside an air-tight container until used for testing.

3.5.3 Laboratory Testing Procedure

The Japan Geotechnical Society (2003) has established standard test methods for the frost heave prediction of soils. The following procedure was adapted from those test methods.

Prior to testing, any bubbles present in the pore water line were purged and the pore-water was de-aired using a vacuum pump. The burette was filled with de-aired water to a level that was equal to the base of the soil sample. The pore water valve on the frost heave apparatus was opened to purge any remaining air and to allow a layer of water to form on the top of the lower pedestal, thereby ensuring good hydraulic contact with the soil sample.

Silicon grease was applied to the inside of the inner acrylic cylinder and to the o-rings on the upper and lower pedestals. Prior to testing, each sample was trimmed to roughly 55 mm in length. To do this, a solid stainless-steel push rod (57.7 mm OD, 160 mm length) was inserted into the aluminum tube from the end with the beveled edge. A portion of the sample was removed and the soil surface was smoothed. The push rod was removed and the process was repeated from the other end. At this time, the sample was measured and trimmed to approximately 55 mm. The sample was inserted carefully into the acrylic cylinder by mating the beveled edge of the aluminum tube to one end of the cylinder and sliding the aluminum tube down on the push rod. Because of this sampling technique, all soils tested were "upside down" once placed into the frost heave apparatus. In other words, if consolidated in the consolidation cell, the sample was turned 180° from its original orientation when placed into the acrylic cylinder.

The cylinder containing the soil was quickly placed on the lower pedestal. The upper pedestal was lowered until contact was made with the sample. Any excess water in the sample drained via the upper porous metal plate. The pore water valve was opened, and the soil was allowed to completely saturate for a period of several hours.

Once saturated, the pore water valve was closed, and the horizontal arm was adjusted for consolidation measurements. Once a baseline measurement was made via the data logger (Agilent 34970A Data Acquisition / Switch Unit, with two HP34901A 20-Channel Multiplexers), 100 kPa of overburden pressure was applied. The laser measurements were recorded and this second period of consolidation was considered complete when no further movement was recorded. The soil in the cell was photographed with a scale to determine pre-freeze height, which was determined to the nearest millimeter. The insulation was wrapped around the inner cylinder, the overburden pressure was removed, the rest of the apparatus was assembled, and the horizontal arm was adjusted for heave measurements. The refrigerator and the circulating baths were turned on, and all were allowed to come to thermal equilibrium, which took about 8 hours.

Prior to beginning the freezing test, the data logger program was initiated and the baths were programmed with the appropriate information. In order to account for the temperature rise between the baths and the frost heave cell, the bath programs were "buffered." For example, the beginning temperature for the upper pedestal was -0.4°C, as was the ending temperature for the bottom pedestal. The 0.4°C buffer ensured that once ice was nucleated within the soil, it did not melt due to above-freezing temperatures during the test.

One of the upper pedestal valves was closed and the respective bath was set to -10°C, in order to induce a "thermal shock" and initiate freezing in the sample. When the set temperature was reached, the upper pedestal valve was opened, and the upper pedestal temperature was closely monitored. When the soil began to freeze, there was a temperature rise associated with latent heat, and this rise was readily apparent in the upper pedestal temperature. Once freezing commenced, the programs were started on both baths. The ice nucleation temperature in the soils was typically between -3 to -4°C.

Once the test was started, daily observations were required to ensure enough water was in the burette, and that the horizontal arm was within the laser's range. Depending on the soil and the testing regime, the burette was filled several times, and the horizontal arm was lowered.

The freezing test was complete when the freezing front passed below the bottom of the sample. Once this occurred, water intake and heave dropped dramatically, although heave continued at a very low rate.

The upper and lower pedestal temperatures were set to 0.5°C in order to destroy the bond between the soil and the porous metal plate. The refrigerator was turned off for defrosting, the apparatus was disassembled, and the acrylic cylinder containing the frozen soil was removed from the apparatus. The soil was removed from the cylinder, wrapped in plastic, labeled, and immediately stored in a freezer for later observations.

CHAPTER 4: SMC RESULTS AND CATION EFFECTS ON SOIL PROPERTIES

4.1 Soil-Moisture Characteristic Curves

The soil-moisture characteristic (SMC) curve data for the five BSLN soils are presented in Figure 4.1. Each individual symbol represents one data point obtained from one of the three methods discussed in Chapter 3, including the results for replicate samples at a given matric potential (ψ_m).

Generally, there is good agreement between replicate samples. The most notable exceptions are the deviations between the replicate samples for CR and HS from the low-range matric suction method. At low ψ_m, the pore-size distribution and capillary effects determine how much water a soil retains (Hillel 1980). Thus, the SMC at low ψ_m is considerably dependent on soil compaction. The differences between the replicate samples are attributed to differences in levels of compaction between individual samples, and Table 4.1 contains a summary of the dry bulk densities of samples prepared in the standard brass rings. The low-range replicates with the lower dry bulk densities demonstrated volumetric water contents that produced smoother curves when joined with the mid-range suction data. As the resulting smoother curves are more typical of those seen in the soil physics literature, the points having the lower dry bulk densities were used in the curve-fitting for the CR and HS soils. While this variation of dry bulk density caused noticeable differences in the data at low ψ_m, the agreement between replicates is much better at higher ψ_m. This is because the soil water retention at these higher suctions depends much less on the soil compaction, and more on the soil adsorption characteristics, structure, and specific surface area (Hillel 1980).

The values for the volumetric water content of all BSLN samples at the highest ψ_m tested were higher than the volumetric water content measured at the immediately lower ψ_m. These points were obtained using the vapor sorption method, and specifically, with sodium hydroxide. The apparent shift to higher water contents is attributed to an error in the preparation of the sodium hydroxide solution. The solution was not completely saturated based on visual observation, as there was some concern about its etching the glass desiccator. Because the solution was not completely saturated, there was an unknown increase in its relative humidity,

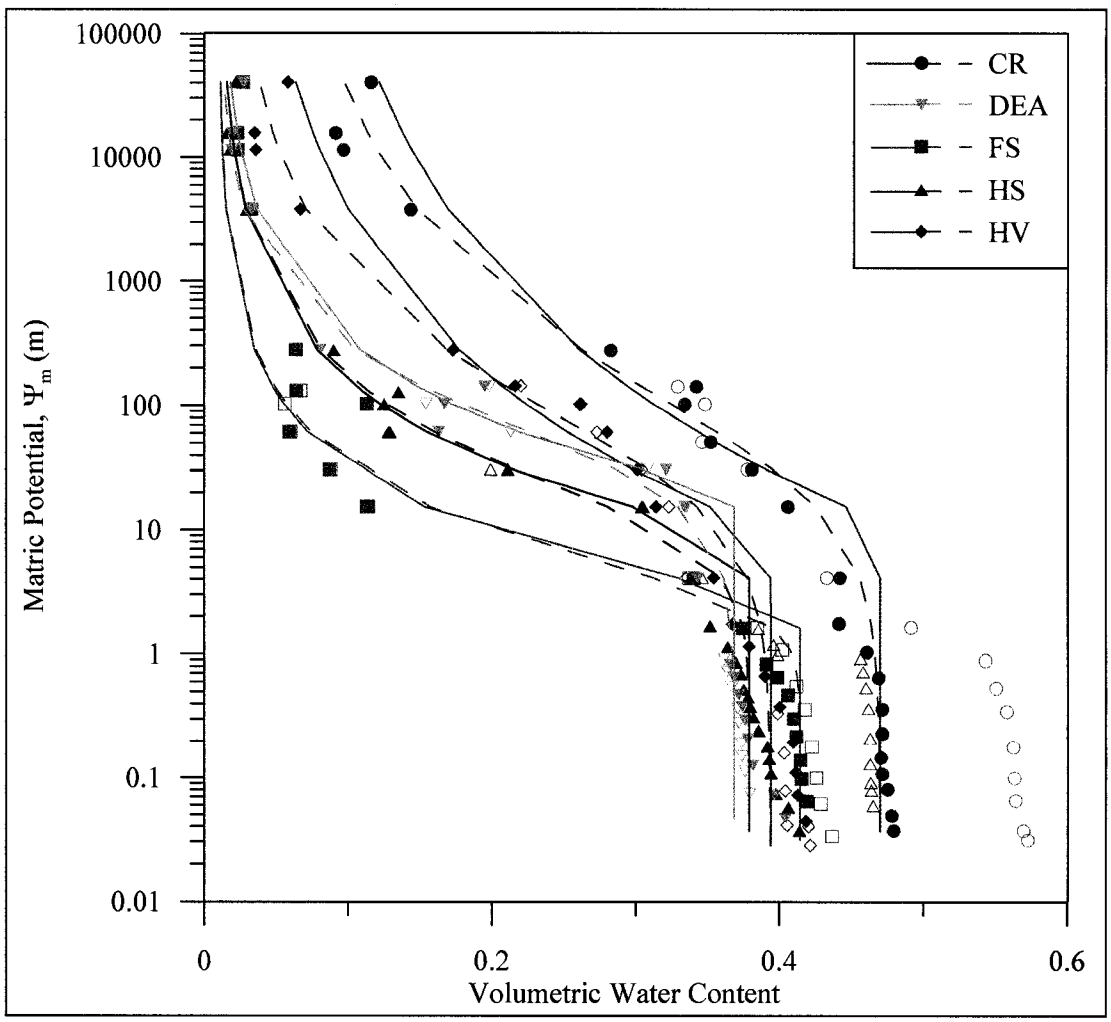

Figure 4.1: Soil-moisture characteristic (SMC) curves. Individual measurements of moisture content at various ψ_m are shown as individual symbols. Where the duplicate measurements differed from each other, the second measurement is shown as an open symbol. SMC curves fitted using the Brooks-Corey equation are shown as solid lines, and SMC curves fitted using the van Genuchten equation are shown as dashed lines. The color for a given soil is consistent for all symbols and lines (e.g. CR is green).

Table 4.1: Summary of BSLN samples' dry bulk densities. The dry bulk density for each replicate from the low-range matric suction tests is given, and the range of dry bulk densities for the mid-range matric suction tests represents 12 samples of each soil.

Soil	Dry Bulk Density ($\times 10^3$ kg/m^3)	
	Low-Range	Mid-Range
CR	1.30, 1.38	1.31 – 1.50
DEA	1.65, 1.65	1.59 – 1.70
FS	1.46, 1.46	1.33 – 1.49
HS	1.58, 1.62	1.58 – 1.64
HV	1.48, 1.52	1.50 – 1.61

causing an error in the data. These points at the highest ψ_m were included in the curve-fitting process; however, their values were weighted at 50 percent reliability.

The "RETC (Version 6.0) Code for Quantifying the Hydraulic Functions of Unsaturated Soils" was used to fit curves to the data points. This program was written by van Genuchten et al. (1991) and is available for free use from the U.S. Salinity Laboratory. The RETC Code provides several different combinations of parametric models as curve-fitting options. Curve fitting was done utilizing both the Brooks-Corey and the van Genuchten equations. The Brooks-Corey equation approximates the volumetric water content, θ, as:

$$\theta = \begin{cases} \theta_r + (\theta_s - \theta_r)(\alpha h)^{-\lambda} & (\alpha h > 1) \\ \theta_s & (\alpha h \le 1) \end{cases} \tag{4.1}$$

where θ_s and θ_r are the saturated and residual volumetric water contents, respectively, α is an empirical parameter, h is the matric suction (ψ_m), and λ is a pore-size distribution index (van Genuchten et al. 1991). The inverse of α is termed the air entry pressure or bubbling pressure. The Brooks-Corey equation produces fairly accurate results for coarse-grained soils, but is less accurate for fine-grained soils due to the lack of a well-defined air entry pressure (van Genuchten et al. 1991). A dimensionless form of Equation 4.1 is:

$$S_e = \begin{cases} (\alpha h)^{-\lambda} & (\alpha h > 1) \\ 1 & (\alpha h \le 1) \end{cases} \tag{4.2}$$

where:

$$S_e = \frac{\theta - \theta_r}{1 - \theta_r} \tag{4.3}$$

Brooks and Corey (1966) call S_e the effective saturation. The van Genuchten equation is defined as:

$$S_e = \frac{1}{\left[1 + (\alpha h)^n\right]^m} \tag{4.4}$$

where α, m, and n are empirical curve-fitting parameters (van Genuchten et al. 1991).

SMC curves fitted using Equations 4.2 and 4.4 are shown in Figure 4.1. With the exception of the CR and HS low-range replicates noted above, all replicate points were included in the curve-fitting process. The Brooks-Corey curves are shown as solid lines, while the

respective van Genuchten curves are shown as dashed lines in the same color for a given soil. The Brooks-Corey curves typically show a vertical segment followed by a sharp break. This break represents the air entry pressure, at which point the largest of the soil pores begin to drain. This break is less defined for the CR and HV soils, indicating the difficulty with which the Brooks-Corey equation predicts the air entry pressure for fine-grained soils. The van Genuchten curves, on the other hand, represent these regions of the SMC curves as smooth functions. The two different sets of curves match each other fairly well through the mid-range ψ_m. For the CR and HV soils, the curves deviate from each other at the high-range ψ_m, with the van Genuchten curves providing a better correlation to the measured data points.

The general forms of the curves presented in Figure 4.1 are typical of the types of soil they represent. For example, the FS SMC curve has a relatively low air entry pressure, which is typical of a silty soil. From this point, the water content decreases rapidly with a small rise in ψ_m, and the soil quickly reaches the θ_r value. At the other extreme, the CR SMC curve is typical for a clayey soil, having an indistinct air-entry pressure, retaining more moisture than the silty soil for any given ψ_m, and slowly reaching the θ_r value. The SMC curves for the DEA, HS, and HV soils fall in between these two end members.

The curves were fitted for each set of data by first selecting the θ_r and forcing the program to use this value. The values for θ_r were determined graphically, using the method presented by Brooks and Corey (1964). The RETC Code using the forced θ_r value was run to approximate θ_s. The initial θ_s approximation was adjusted until the highest coefficient of determination (r^2) was obtained.

Table 4.2 contains a summary of the soil-retention parameters input into and produced by the RETC Code, as well as the r^2 values for each analysis. The values for θ_s, θ_r, and λ were compared to those measured by Rawls et al. (1982), who assembled such values from 1,323 soils from the literature. The comparison indicated that the CR values match those typical of a silty clay, and the DEA values match those typical of a sandy loam. The HV values are typical for a silt loam, with the exception of θ_s, which is lower than the given range. This deviation may be due to the dry bulk density of the HV soil after compaction. The HS values do not fall

Table 4.2: Summary of soil-retention parameters

Soil	θ_s	θ_r	Brooks-Corey			van Genuchten			
			α	λ	r^2	α	m	n	r^2
CR	0.470	0.050	0.085	0.217	0.955	0.029	1.005	0.307	0.979
DEA	0.369	0.010	0.049	0.498	0.968	0.043	2.185	0.238	0.971
FS	0.415	0.010	0.365	0.605	0.987	0.351	2.610	0.230	0.988
HS	0.379	0.010	0.108	0.496	0.984	0.078	1.421	0.383	0.986
HV	0.394	0.020	0.103	0.258	0.949	0.027	1.005	0.428	0.974

within the range typical of a silt loam, but more closely match sandy loam values. Rawls et al. (1982) do not give values for silt; however, the FS values in Table 4.2 lie within the typical range of a sandy loam.

4.2 Cation Effects on Unfrozen Water Content

Plots of unfrozen water content, w_U, versus temperature for each BSLN soil and the corresponding cation soil treatments are presented in Figures 4.2 through 4.6. The w_U presented in these figures are the gravimetric unfrozen water contents, as determined using the method presented in Section 3.4. In order to simplify the comparison of w_U among the cation treatments and among the various soils, the w_U at -0.2°C are summarized in Table 4.3. These values were chosen because -0.2°C is close to the freezing point in soils.

A comparison of the w_U for the BSLN soils indicates that FS has the lowest overall w_U, followed by DEA and HS, respectively. The low FS w_U may partly be due to its high magnetic mineral content, which lowers the NMR signal strength (S. Akagawa, personal communication, September 2006). The clayey HV and CR soils have more than twice the w_U than the aforementioned silty soils.

Analysis of each soil individually reveals some interesting features. For the CR soil, the Na^+-treated sample's w_U is nearly twice that of the remaining treatments, which are all very close to one another. The w_U of the DEA BSLN and corresponding cation treatments are quite similar to each other through the complete range of temperatures. The FS samples arranged in decreasing order of w_U are Mg^{2+} > Na^+ > BSLN. For the HS soil, the w_U of the BSLN and Ca^{2+}- and Mg^{2+}-treated soils are very close to one another, while the K^+-treated sample's w_U is nearly twice as large. The HS Na^+-treated sample demonstrated a w_U intermediate to the two extremes. The HV samples arranged in decreasing order of w_U are Na^+ > BSLN > Ca^{2+}.

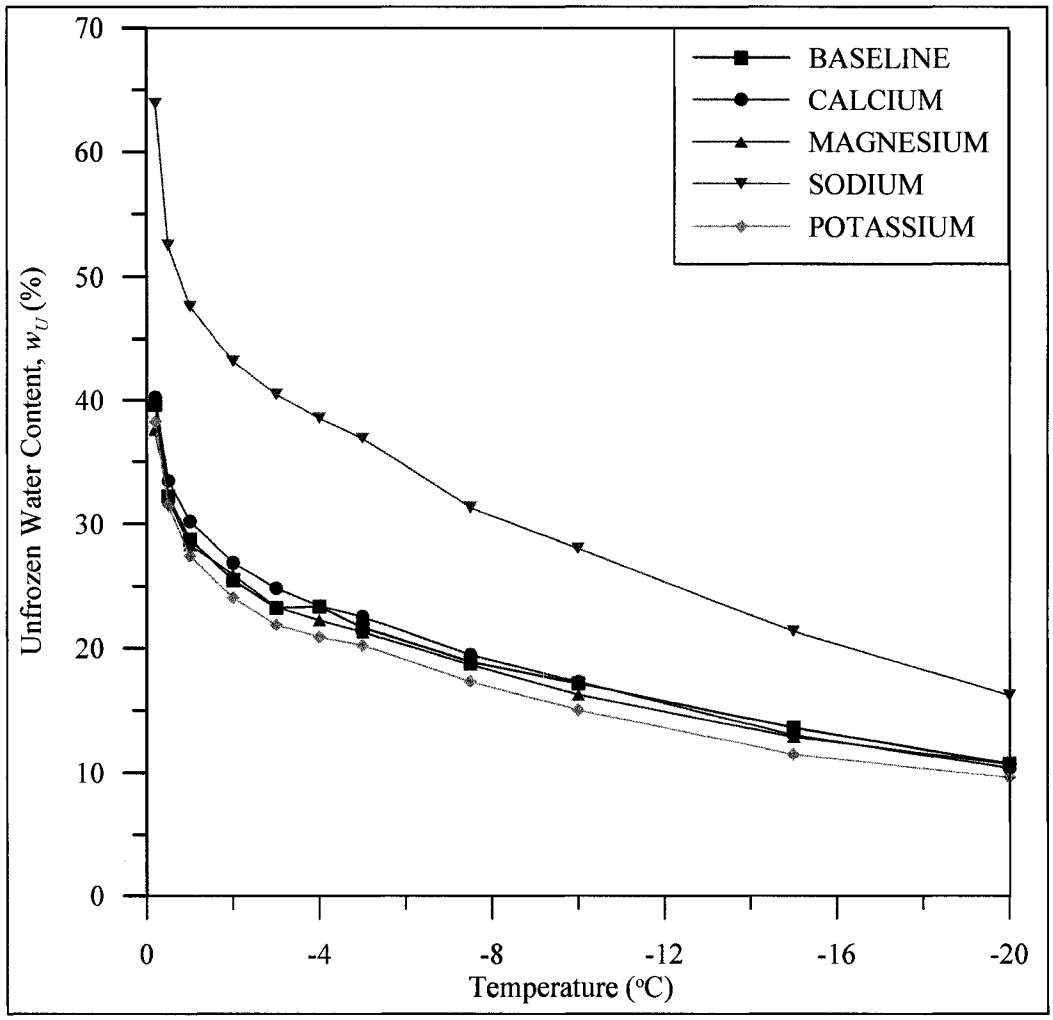

Figure 4.2: Unfrozen water content, w_U, versus temperature for CR BSLN and corresponding cation treatments

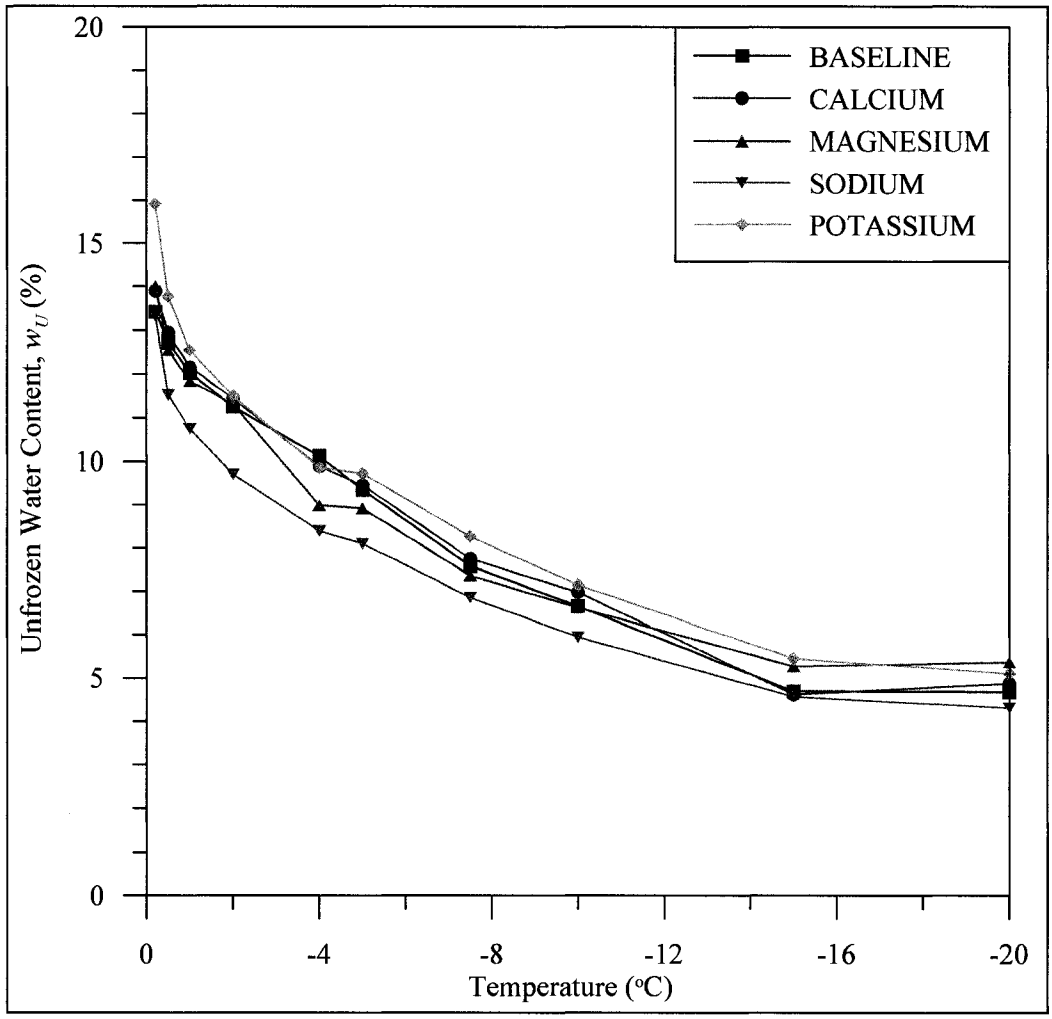

Figure 4.3: Unfrozen water content, w_U, versus temperature for DEA BSLN and corresponding cation treatments

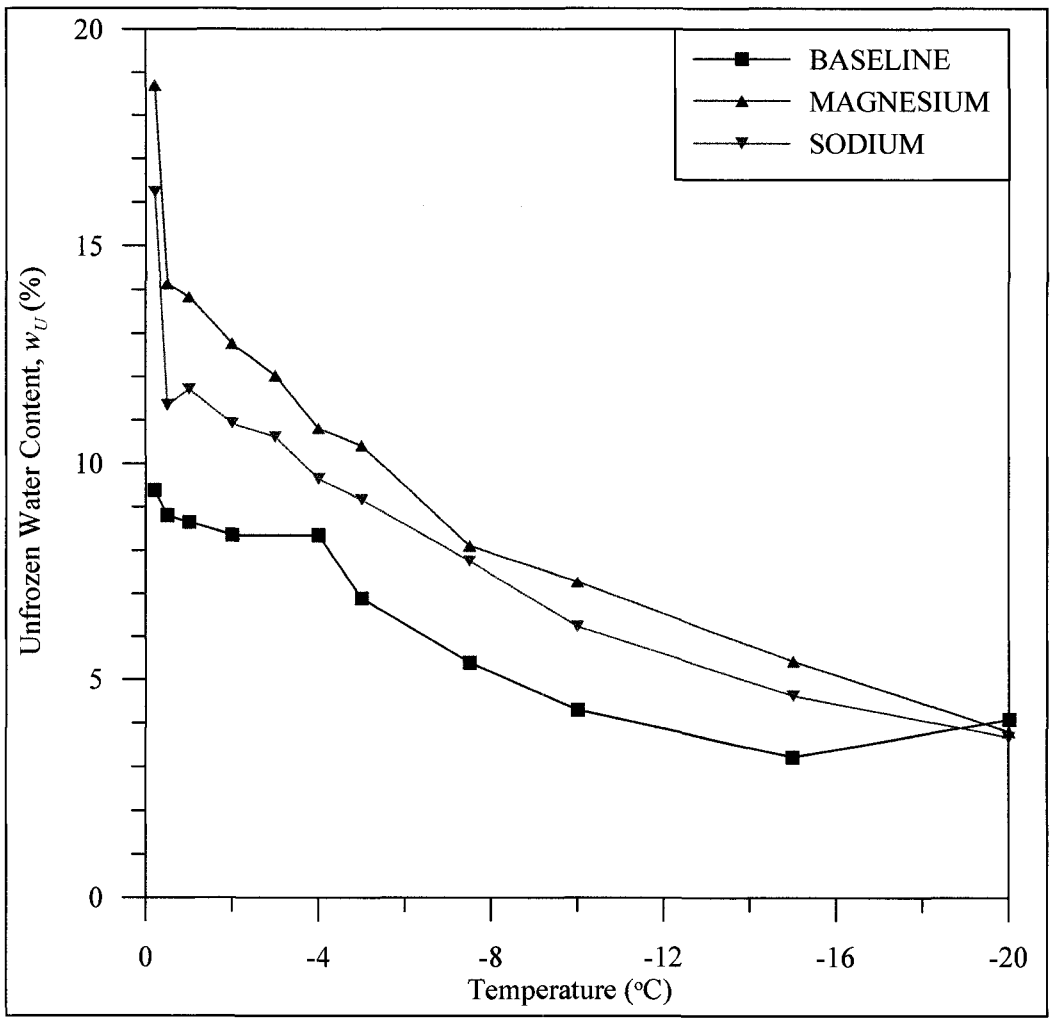

Figure 4.4: Unfrozen water content, w_U, versus temperature for FS BSLN and corresponding cation treatments

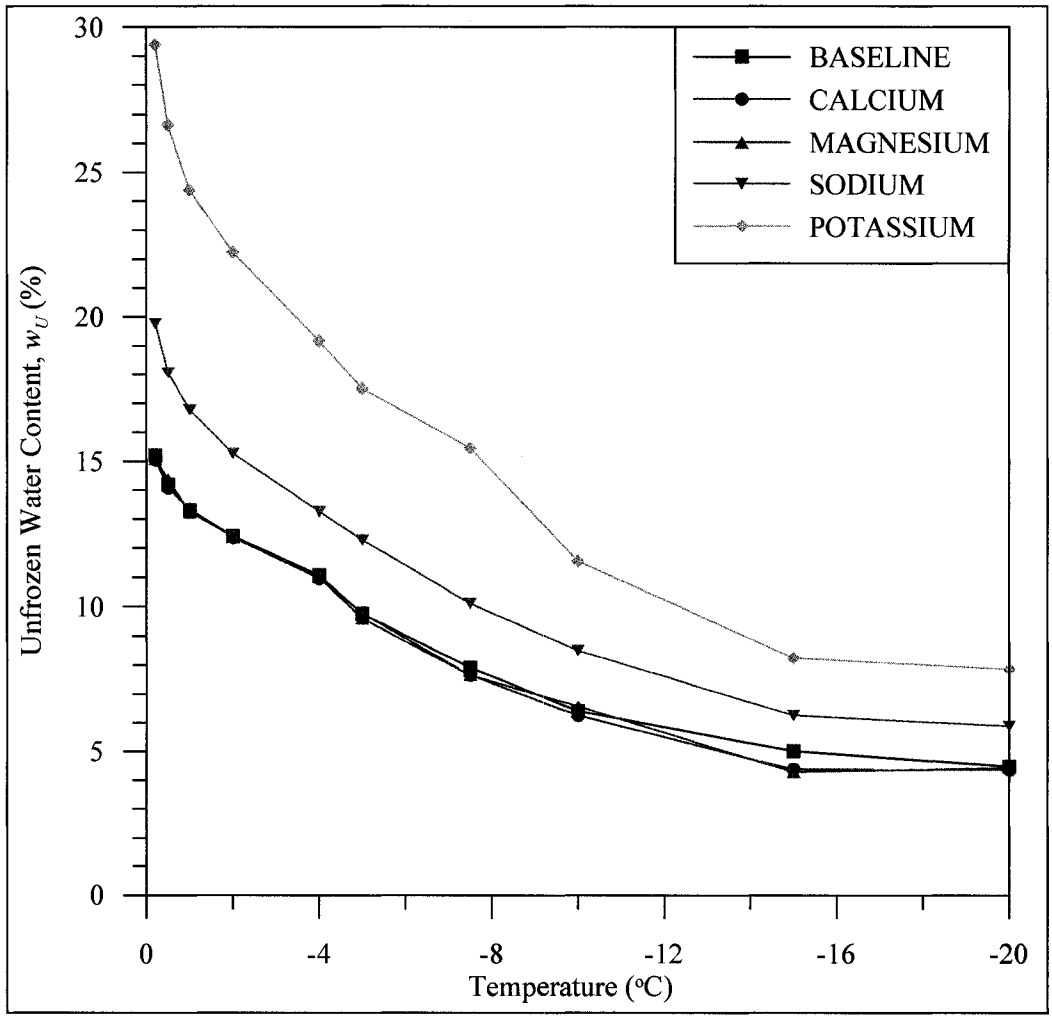

Figure 4.5: Unfrozen water content, w_U, versus temperature for HS BSLN and corresponding cation treatments

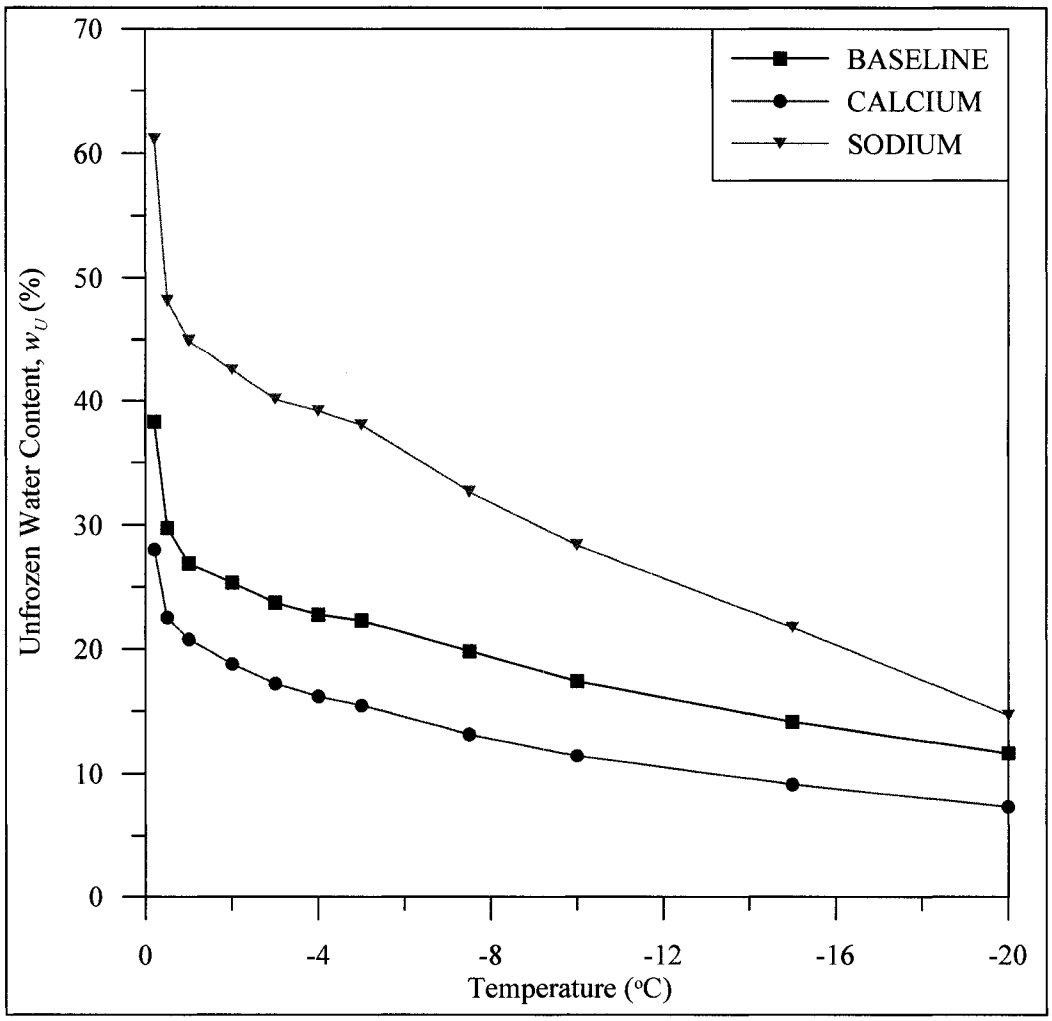

Figure 4.6: Unfrozen water content, w_U, versus temperature for HV BSLN and corresponding cation treatments

Table 4.3: Summary of unfrozen water contents, w_U , at -0.2°C

Soil	Unfrozen water content, w_U (%)				
	BSLN	Ca^{2+}	Mg^{2+}	Na^{+}	K^{+}
CR	39.6	37.6	40.2	63.9	38.2
DEA	13.4	13.9	14.0	13.3	15.9
FS	9.4	---	18.7	16.2	---
HS	15.2	15.0	15.1	19.8	29.4
HV	38.3	28.0	---	61.1	---

4.3 Correlation between Unfrozen Water Content and Soil-Moisture Characteristic Curves

The soil-moisture characteristic (SMC) and unfrozen water content (w_U) data obtained from each BSLN soil indicate that these five soils demonstrate a wide range of water retention properties. The CR and HV soils, with their high clay contents, retain more water at high matric potentials (ψ_m), than do the silty DEA, FS, and HV soils (see Figure 4.1). Townend et al. (2001) indicate that the water retention by clays at high ψ_m is attributed to adsorption by the individual particles, rather than capillary effects. Likewise, CR and HV contain more than twice the w_U at -0.2°C than DEA, FS, and HV (see Table 4.3).

Miller (1963) and Koopmans and Miller (1966), as well as others, have suggested that the soil-moisture characteristic (SMC) curve should have an analogous function called the soil freezing characteristic (SFC) curve. The SMC describes the soil water content as a function of matric potential (ψ_m), which is equivalent to the quantity $(\Delta P_a - \Delta P_w)$, where ΔP_a is the gauge pressure of the soil atmosphere, and ΔP_w is equivalent to the gauge pressure of the soil water (Koopmans and Miller 1966). These authors postulated that the SFC should describe the soil water content as a function of freezing temperature. As the SMC can be separated into two hysteretic portions called the main wetting curve and the main drying curve, the SFC should have two analogous hysteretic portions, namely a warming curve and a cooling curve, respectively. For all analysis and discussion that follows, only the main drying curve of the SMC and the cooling curve of the SFC are considered.

The pressure in a freezing soil system is related to the temperature by the Clausius-Clapeyron equation, one form of which is presented in Chapter 1 as Equation 1.2. If it is assumed that ΔP_w is equal to 0 and that the solute concentration is negligible, Equation 1.2 may be reduced to:

$$\Delta P_a / (-\Delta T) = 1110\ kPa/^{o}C \tag{4.5}$$

where $-\Delta T$ is the deviation from the freezing point (Koopmans and Miller 1966).

For soils in which adsorption forces dominate over capillary forces (i.e., colloidal soils), Koopmans and Miller (1966) suggested that corresponding points on the SMC and SFC curves are related to each other by:

$$(\Delta P_a - \Delta P_w) = (\Delta P_i - \Delta P_w) \tag{4.6}$$

where ΔP_i is the gauge pressure of ice. Because the water content at these corresponding points is equal, a plot of pressure (kPa) from the SMC curve versus temperature (°C) from the SFC curve will produce a straight line, with a slope of 1110 kPa/°C, as indicated by Equation 4.5. This plot will be referred to in what follows as the SMC-SFC relation, for brevity.

When plotting the SMC-SFC relation for a colloidal Na^+-saturated bentonite, Koopmans and Miller observed that the slope deviated from the 1110 kPa/°C derived from the Clausius-Clapeyron equation. They attributed this deviation in slope and shift in intercept to the presence of solutes formed from the hydrolysis and decomposition of the clay, indicating that solutes would reduce the slope (Koopmans and Miller 1966). To adjust for the solute effect, Koopmans and Miller "corrected" their points for the freezing point depression, which adjusted their measured slope from 1070 kPa/°C to 1150 kPa/°C, a deviation of only 40 kPa/°C from the theoretically-derived slope. Additionally, Koopmans and Miller adjusted their data to account for the shift in the intercept of their regression line from the origin.

The SMC data from the five BSLN soils were compared against w_U data from the NMR analysis using the method presented by Koopmans and Miller (1966), and the SMC-SFC relations are presented in Figure 4.7. The temperature plotted along the x-axis in Figure 4.7 is equivalent to the ΔT in Equation 4.5. All of the BSLN soils were treated as colloids following the relationship given in Equation 4.6.

For each of the BSLN SMC-SFC relations, a linear regression analysis was performed using the least squares method. The slopes of the resulting trend lines (with the corresponding BSLN soil listed in parentheses) are: 152 kPa/°C (FS), 928 kPa/°C (HV), 1040 kPa/°C (HS), 1365 kPa/°C (DEA), and 3455 kPa/°C (CR). These slopes deviate from the theoretically-derived slope by as much as 2345 kPa/°C, and the slopes for CR and DEA are higher than the theoretically-derived slope. The intercept of each trend line varied from the origin by as much as 3152 kPa. Additionally, the data points for each BSLN soil shown in Figure 4.7 demonstrate deviation from linear trends, resulting in coefficients of determination (r^2) that range from 0.82 to 0.95.

Based on the comparison of these results with those of Koopmans and Miller (1966), it is apparent that the relationships presented as Equations 4.5 and 4.6 do not describe these soils. The range of measurements made by Koopmans and Miller (1966) were limited to 400 kPa for

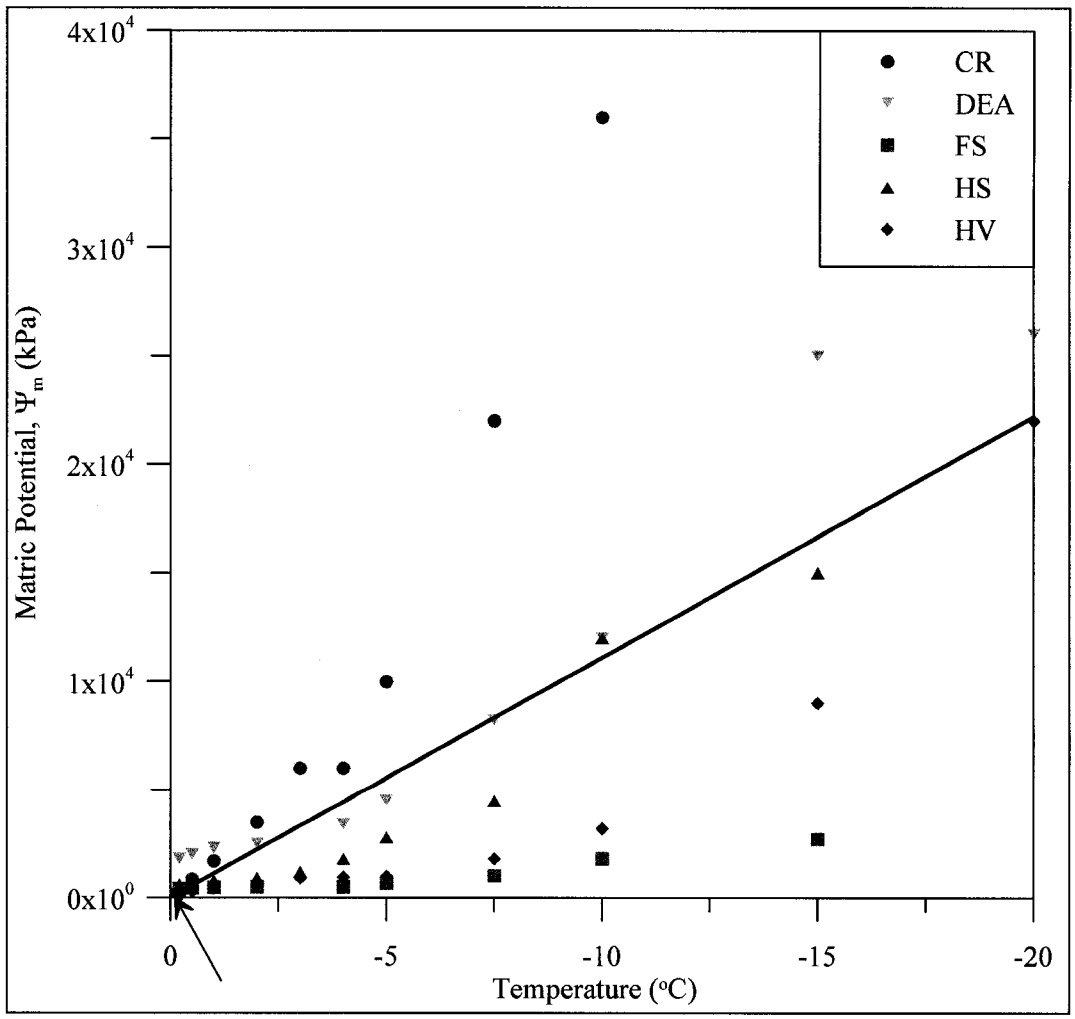

Figure 4.7: SMC-SFC relations for the BSLN soils using the Koopmans and Miller method. The solid line shown represents the theoretical relationship of pressure versus temperature, with a slope of 1110 kPa/°C. The range of data presented by Koopmans and Miller (1966) is represented by a black rectangle near the origin, as indicated by the arrow.

the SMC data and -0.15°C for the SFC data (represented by a black rectangle near the origin in Figure 4.7). Thus, the range of data presented here is orders of magnitude larger than that of Koopmans and Miller's research. Additionally, Koopmans and Miller created a unique apparatus that served both as a dilatometer and a pressure plate. Thus, the same samples were used for both SMC and SFC measurement. Black and Tice (1989) performed similar analysis of the SMC and SFC for a sandy loam. These authors indicated that a SMC-SFC relation can be established only if the soil samples have the same complete initial saturation and bulk densities. The BSLN samples used for the NMR measurements were not consolidated because of the small sample size (i.e., approximately 50 g). Thus, it is assumed that the dry bulk densities of the SMC samples, given in Table 4.1, were much larger than those of the w_U samples. As mentioned in Section 4.1, the SMC is more dependent on the dry bulk density for low ψ_m than for high ψ_m. Since both Koopmans and Miller (1966) and Black and Tice (1989) conducted their suites of experiments for extremely low ψ_m, their concern about the dry bulk density is warranted. However, the discrepancies between the dry bulk densities of the BSLN SMC and SFC samples may be unimportant for the large range of data presented here.

The ψ_m and temperature data were analyzed to find a better relationship between these two variables. Analysis indicates that a closer correlation exists between the square root of ψ_m and temperature for the range of data presented here. The revised SMC-SFC relations, which represent $\sqrt{\psi_m}$ ($kPa^{1/2}$) versus temperature (°C), are presented in Figure 4.8. A linear regression analysis was performed using the least squares method for each of the revised SMC-SFC relations, producing correlations ranging from 0.95 to 0.99. The deviation of the intercepts of the resulting trend lines from the origin, which is as high as 39.13 $kPa^{1/2}$, is attributed to solutes in the soil water and to the variation in dry bulk density of the SMC low ψ_m tests. The slopes of the resulting trend lines (with the corresponding BSLN soil listed in parentheses) are: 2.19 $kPa^{1/2}$/°C (FS), 6.26 $kPa^{1/2}$/°C (HV), 6.73 $kPa^{1/2}$/°C (DEA), 7.27 $kPa^{1/2}$/°C (HS), and 16.89 $kPa^{1/2}$/°C (CR). Further analysis indicates that these slopes have a high correlation to the ζ potential, demonstrating a coefficient of determination of 0.93.

This analysis indicates that the relationship given as Equation 4.6 does not adequately describe natural colloidal soils for the ranges of ψ_m and temperatures presented here. When

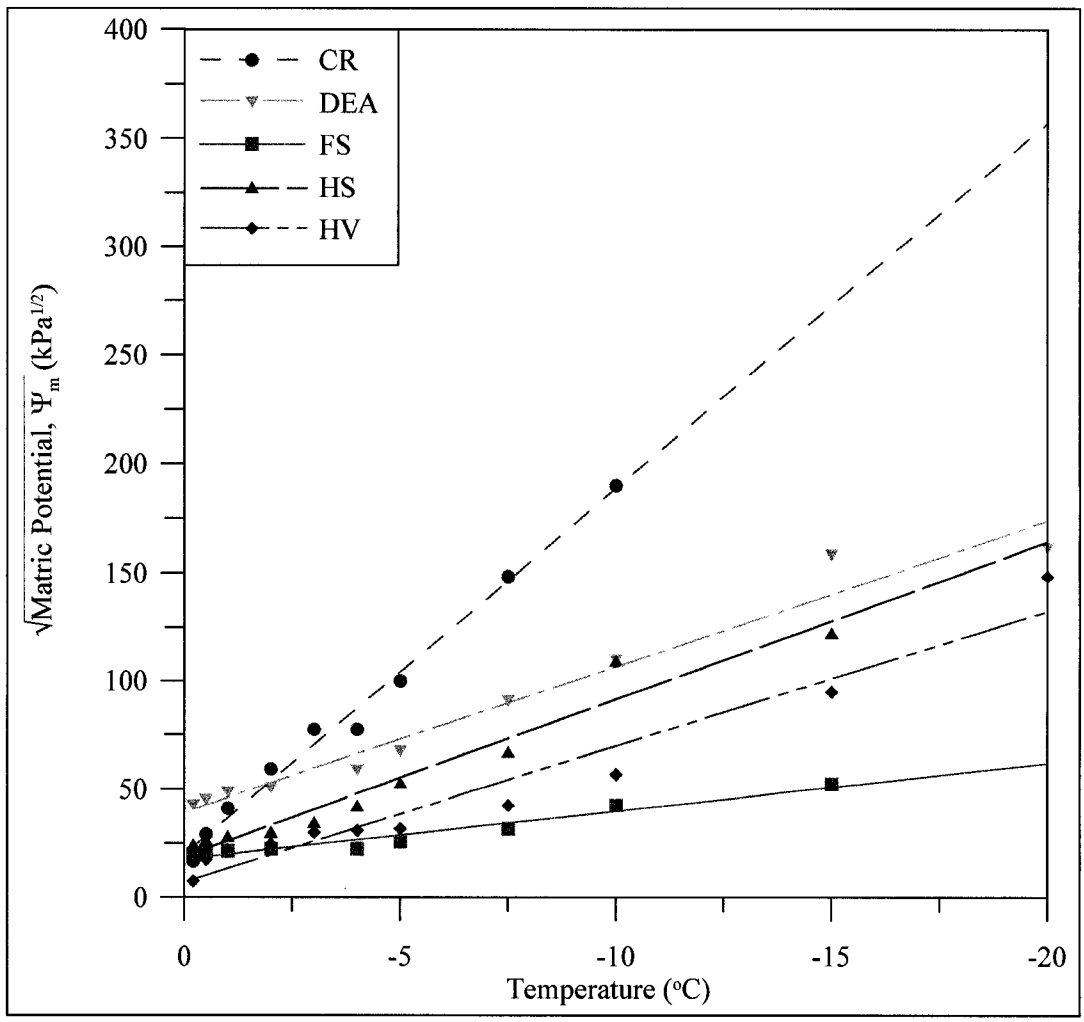

Figure 4.8: Revised SMC-SFC relations for the BSLN soils. Linear regression trend lines are shown for each BSLN soil.

deriving Equation 4.6, Koopmans and Miller (1966) assumed that ΔP_w is equal to 0. In his derivation of the Clausius-Clapeyron equation, Loch (1978) indicated that the "total potential," p_w (which is equivalent to Koopmans and Miller's ΔP_w), of soil water is defined as

$$p_w = p - \pi \tag{4.7}$$

where p is the hydrostatic pressure and π is the osmotic pressure. Loch stated that the π term included the effects of adsorbed cations and solute ions. From the overview of clay mineral surface chemistry presented in Section 2.5, it is apparent that π is highly significant for colloidal soils and should not be ignored.

The results of this analysis suggest that corresponding points on the SMC and SFC curves for the BSLN soils are related by

$$\sqrt{\left(\Delta P_a - \Delta P_w\right)} = \eta \cdot \Delta T \tag{4.8}$$

where $\left(\Delta P_a - \Delta P_w\right)$ is equal to ψ_m, and ΔT is defined as

$$\Delta T = \frac{-\left(\overline{V}_i \Delta P_i - \overline{V} \Delta P_w\right) \cdot T_o}{L_{fs}} \tag{4.9}$$

which is obtained by solving for ΔT in the Clausius-Clapeyron equation (see Section 1.2 for a description of the terms in Equation 4.9). The coefficient η in Equation 4.8 is equivalent to the slope of a plot of $\sqrt{\psi_m}$ ($kPa^{1/2}$) versus temperature (°C).

4.4 Cation Effects on Grain Size Distributions

The grain size distributions for the aggregated BSLN and cation-treated soil samples are presented in Figures 4.9 through 4.13. For DEA and FS, the grain size distributions for the various cation treatments are similar for the smallest particles. With increasing grain size (i.e., greater than 0.008 mm for DEA and 0.03 mm for FS), however, the different treatments cause differences in the grain size distributions. For the coarser particles, the treatments listed in order of increasing grain size are $Na^+ < Mg^{2+} < K^+ <$ BSLN $\approx Ca^{2+}$ for DEA, and $Na^+ \approx Mg^{2+} <$ BSLN for FS. The various treatments yield similar grain size distributions for the HS soil, with the exception of the K^+-treated sample. This sample demonstrated a much finer overall grain size distribution than the other HS samples. The cation treatments resulted in significantly different grain size distributions for the CR and HV soils. Listed in order of increasing grain size, the treatments for the CR soil are $K^+ \approx Na^+ < Ca^{2+} < Mg^{2+}$, where the overall distribution for the

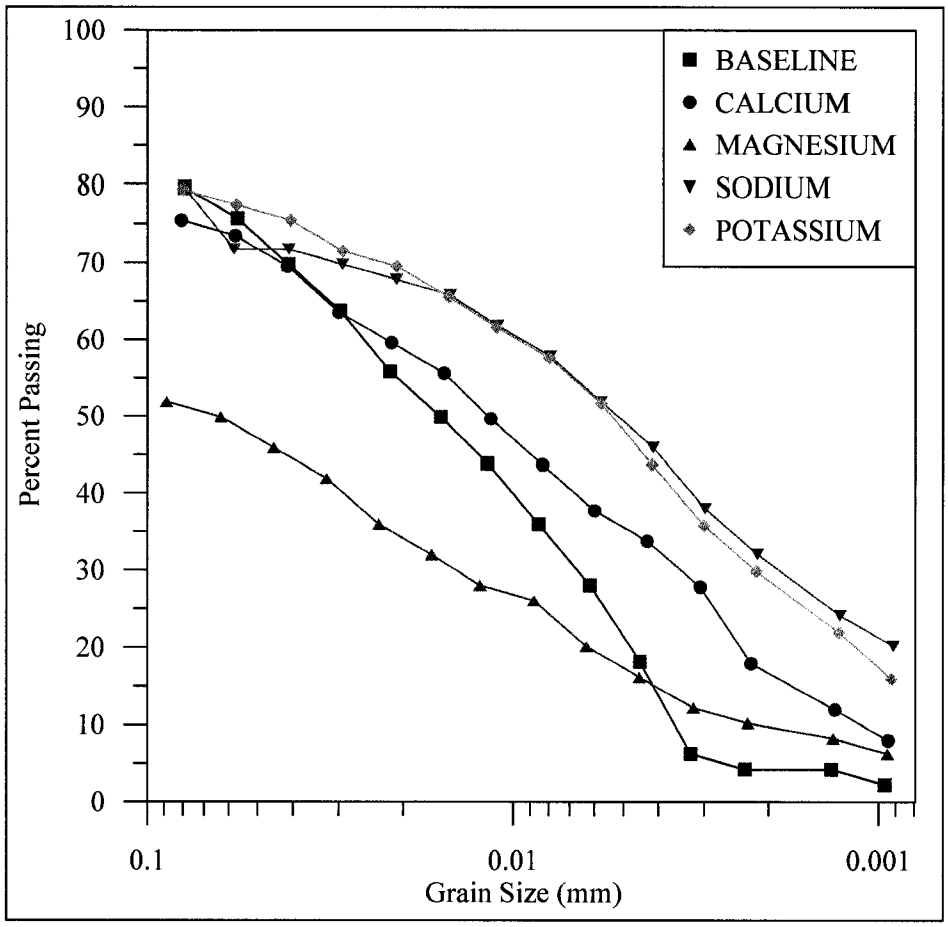

Figure 4.9: Grain size distributions for the aggregated CR BSLN and corresponding cation treatments

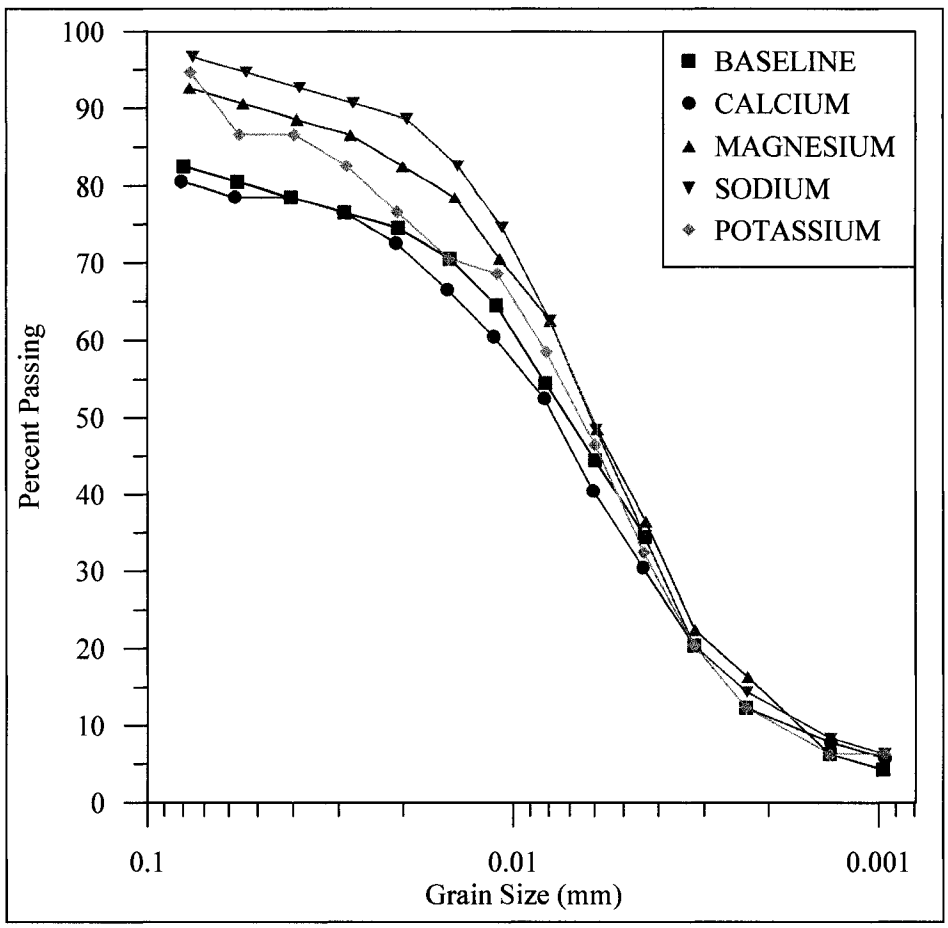

Figure 4.10: Grain size distributions for the aggregated DEA BSLN and corresponding cation treatments

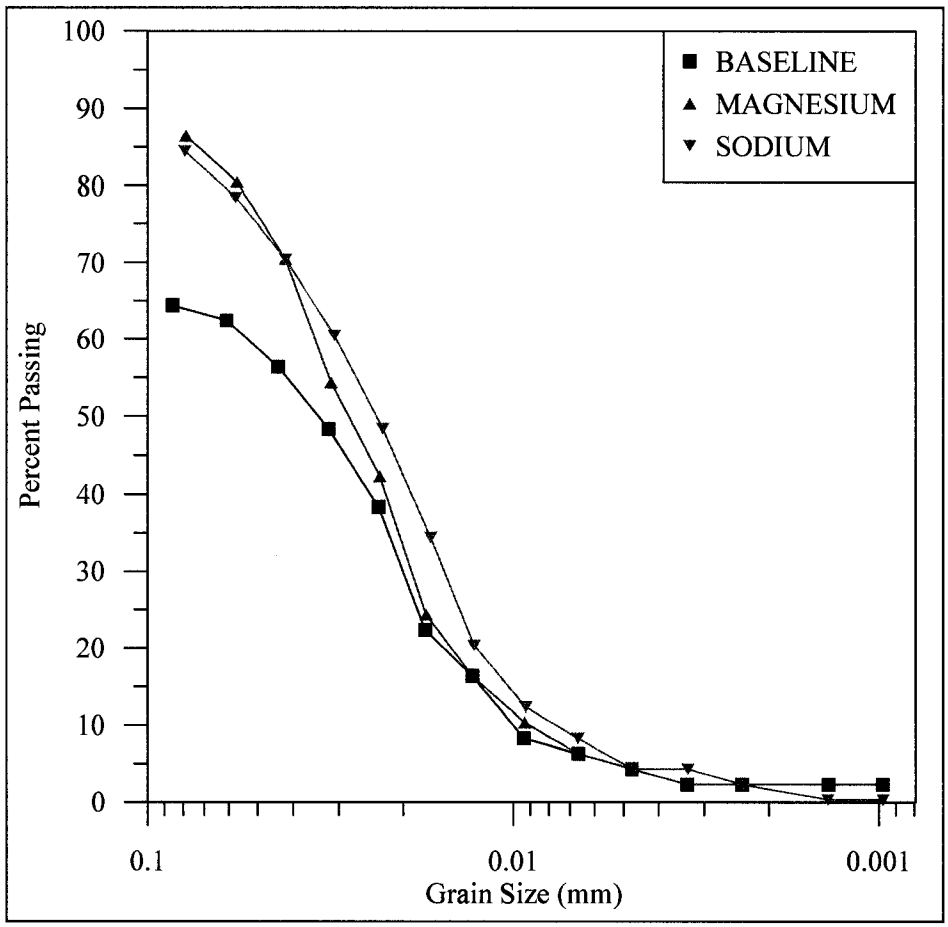

Figure 4.11: Grain size distributions for the aggregated FS BSLN and corresponding cation treatments

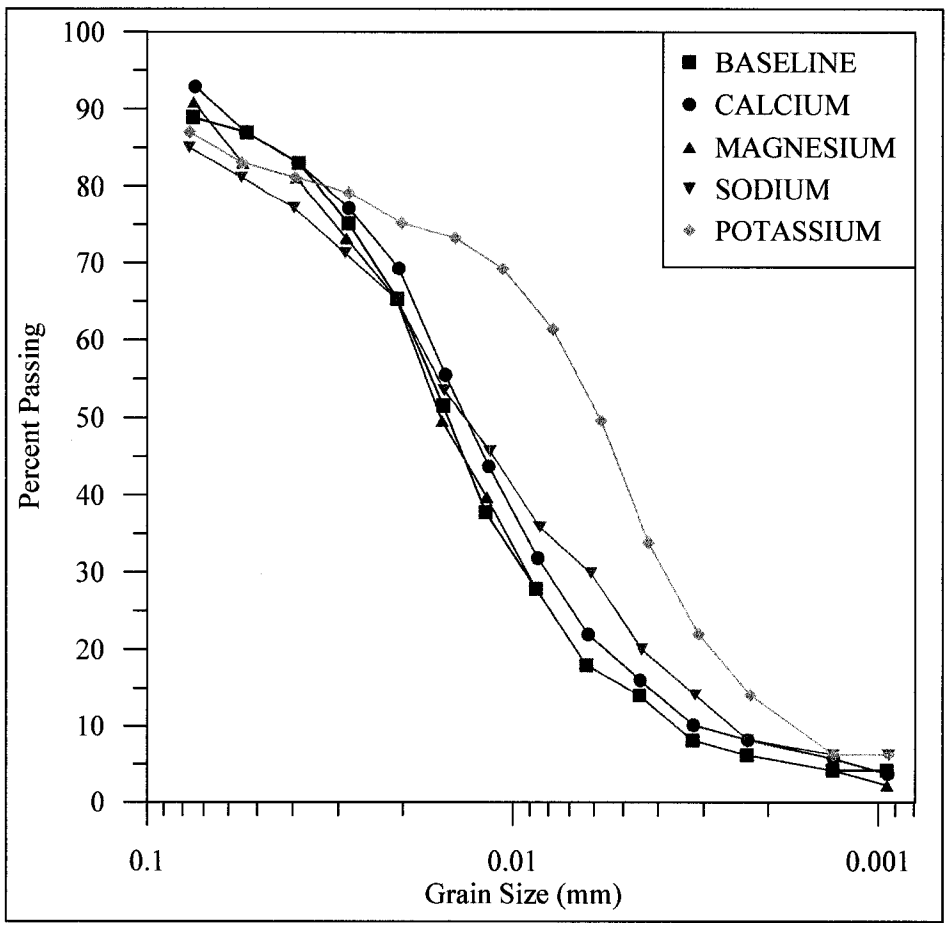

Figure 4.12: Grain size distributions for the aggregated HS BSLN and corresponding cation treatments

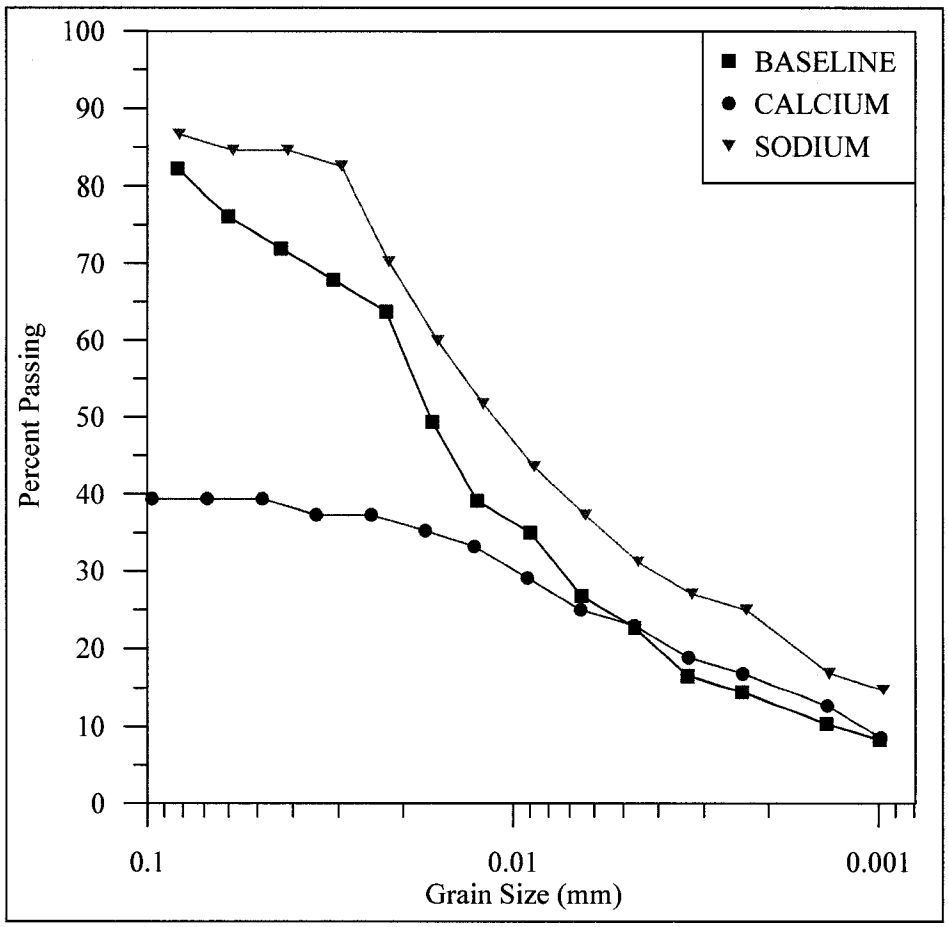

Figure 4.13: Grain size distributions for the aggregated HV BSLN and corresponding cation treatments

Mg^{2+}-treated sample is significantly larger than the other treatments. The grain size distribution for the CR BSLN sample varies from all of the other treatments, unsystematically crossing several of the other distribution curves. For HV, the treatments listed in order of increasing grain size are Na^{+} < BSLN < Ca^{2+}, for which the trend in cation treatment order is similar to CR. The grain size distribution for the HV Ca^{2+}-treated sample is significantly larger than the other grain size distributions.

Some of the variation in the grain size distributions may be due to inadequate dispersion of the soils to their basic aggregated states. In other words, vigorously shaking the sample slurries by hand may not have been sufficient to reduce the larger chunks of soil to individual aggregates of a few mineral grains. This may be especially true for the clayey CR and HV soils. With that caveat being made, there is a notable trend in the effects of the cation treatments. For all of the soils, the Na^{+}- and/or K^{+}-treated samples demonstrated the smallest overall grain size distributions. For most of the soils, the Ca^{2+}- and/or Mg^{2+}-treated samples demonstrated the largest overall grain size distributions.

4.5 Cation Effects on Zeta Potential

As a fine-grained soil may contain several different types of clay minerals, its measured ζ potential will form a wide particle-charge distribution curve, demonstrating the range of ζ potential for all clay minerals present (Riddick 1968). To determine the median ζ potential value for the bulk soil, the following procedure, which is outlined by Riddick (1968), was employed. The times recorded during the tracking of fifty particles were rounded to the nearest tenth of a second. The recorded times were tallied and converted to the corresponding ζ potentials. The tallied ζ potential values were summed to determine cumulative percent. A graph of ζ potential versus the cumulative percent of the fifty particles tracked, which is the particle-charge distribution curve described by Riddick (1968), was used to determine the median ζ potential and range.

Figures 4.14 through 4.18 contain graphs of the ζ potential curves for each BSLN soil and the corresponding cation treatments, and the median ζ potentials for all of the samples are summarized in Table 4.4. There are noticeable trends in the ζ potential data. For example, the median ζ potential values for the BSLN, Ca^{2+}, and Mg^{2+} samples are similar to each other, with

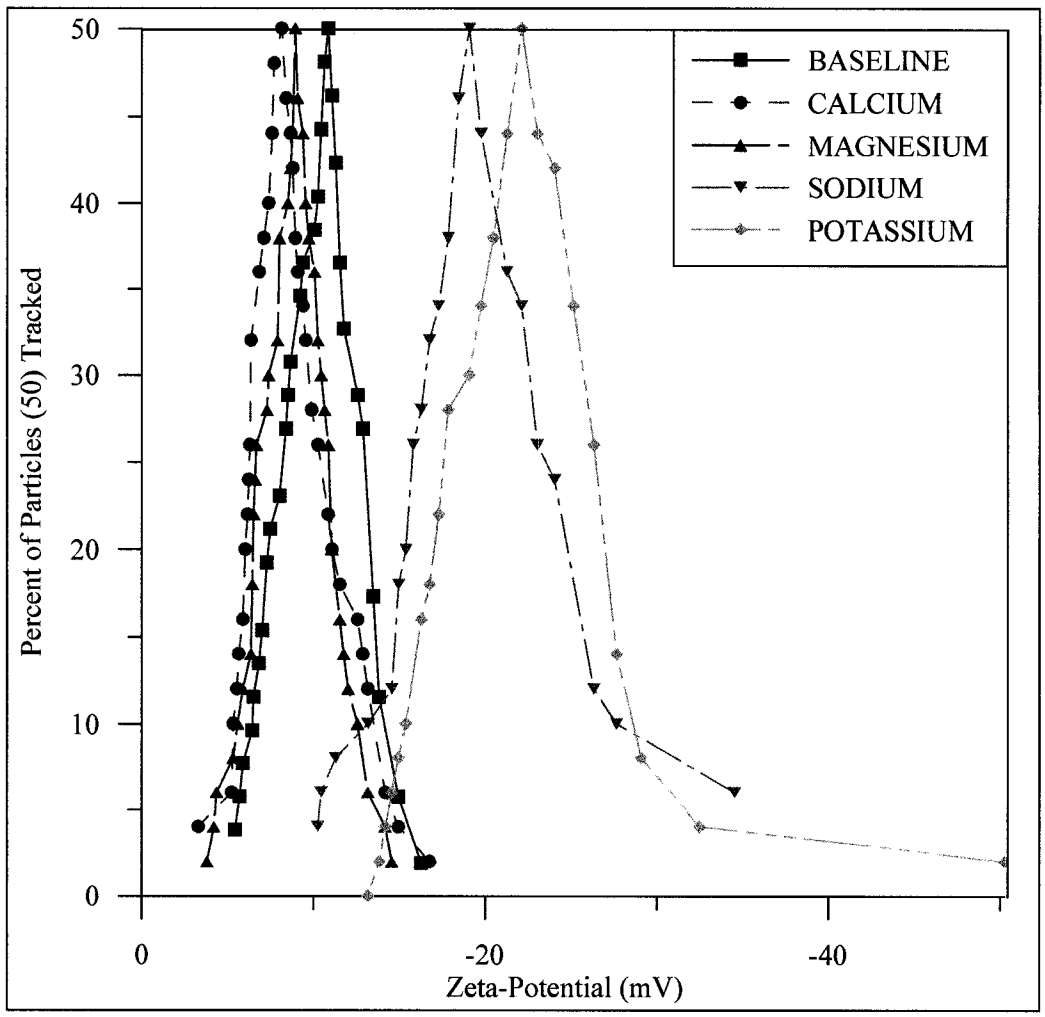

Figure 4.14: ζ potential distribution curves for CR BSLN and corresponding cation treatments

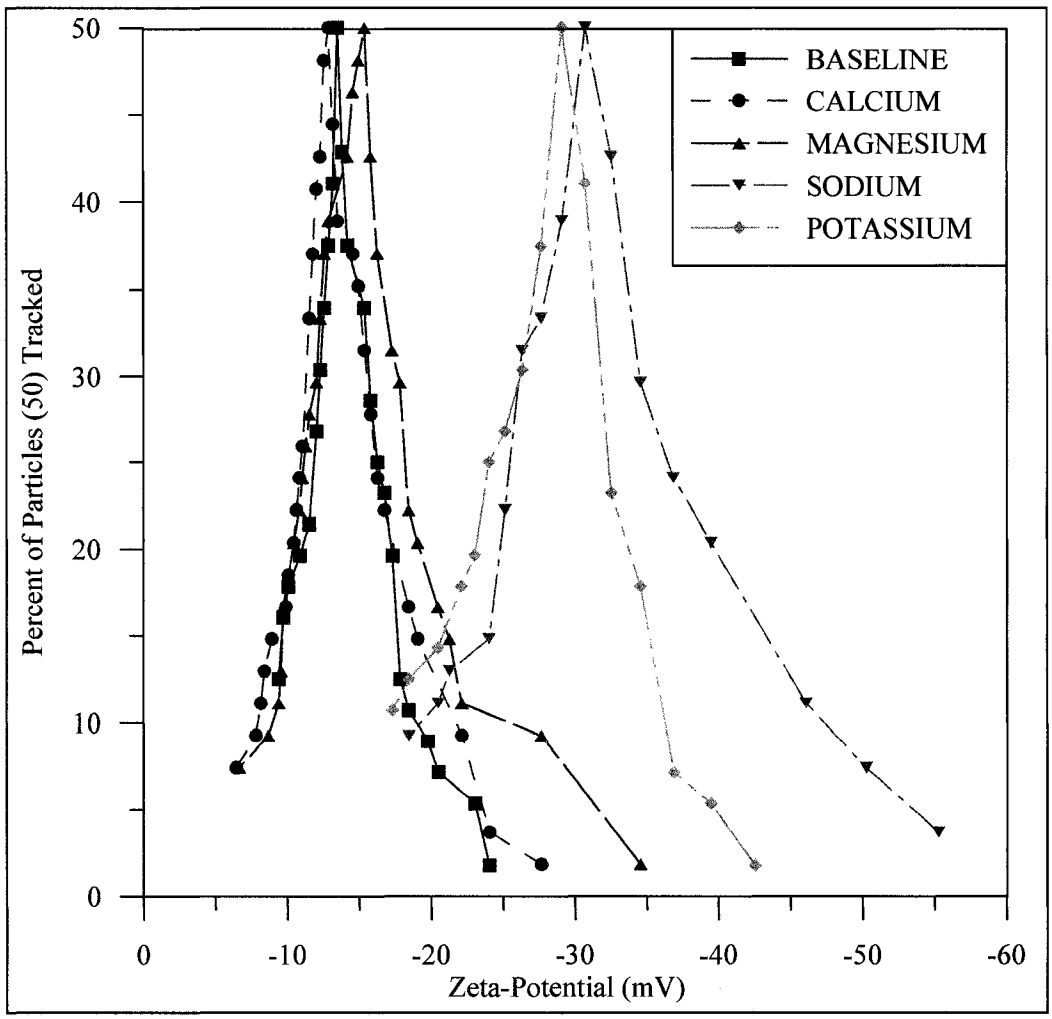

Figure 4.15: ζ potential distribution curves for DEA BSLN and corresponding cation treatments

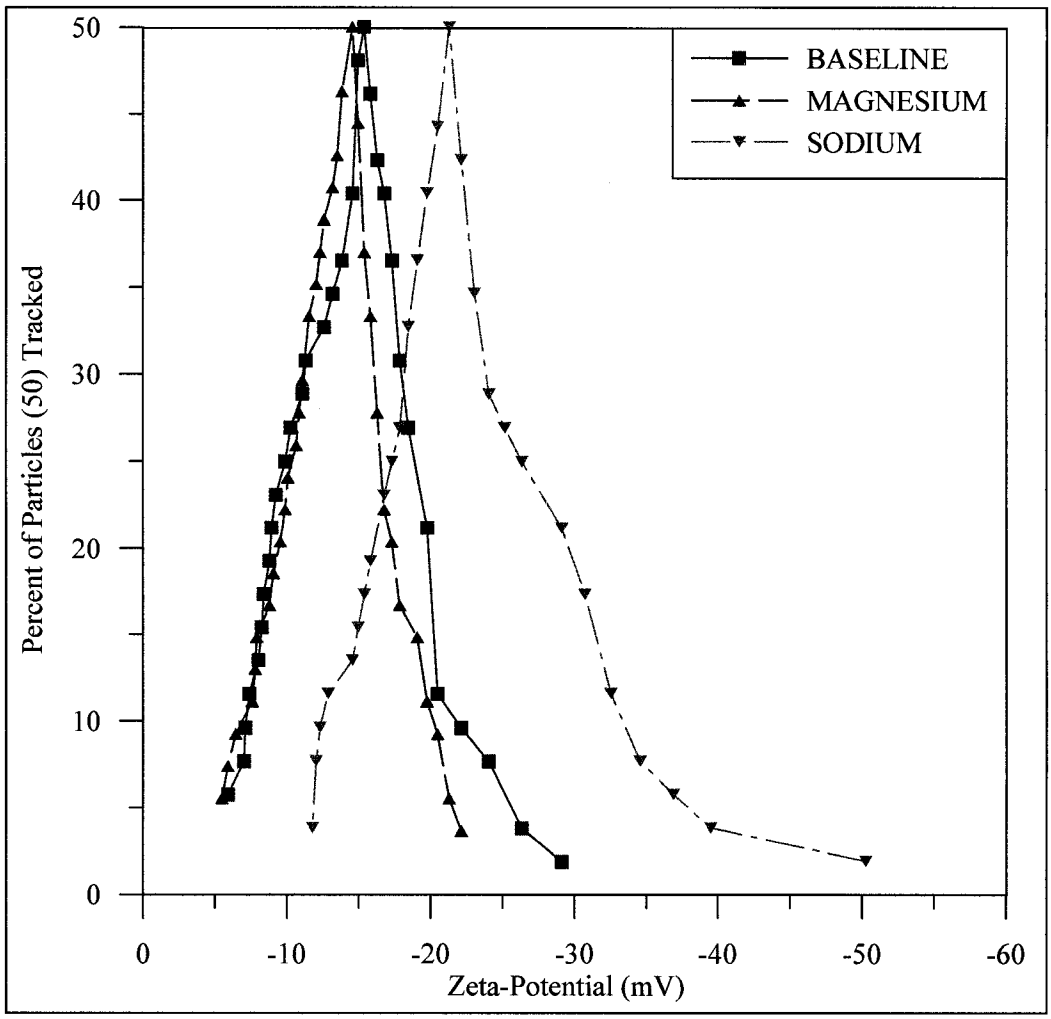

Figure 4.16: ζ potential distribution curves for FS BSLN and corresponding cation treatments

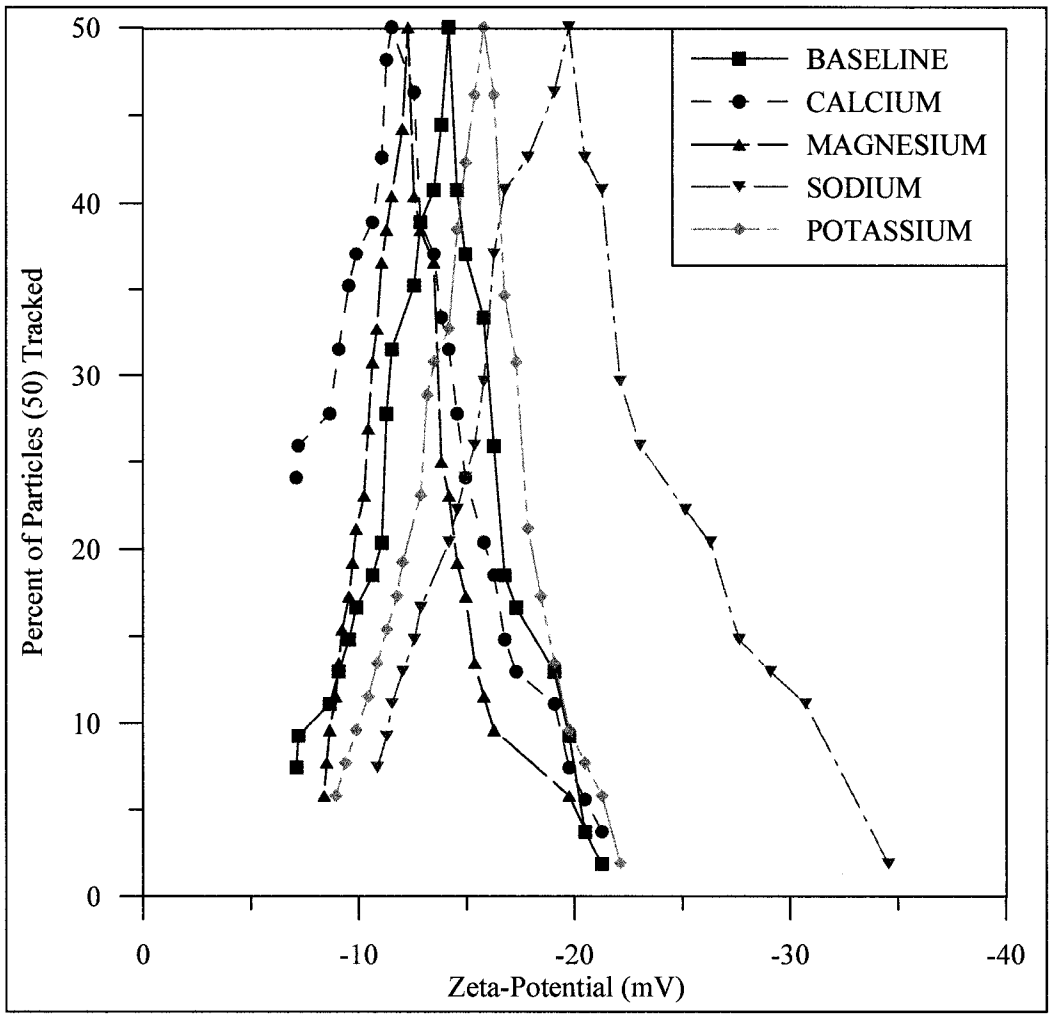

Figure 4.17: ζ potential distribution curves for HS BSLN and corresponding cation treatments

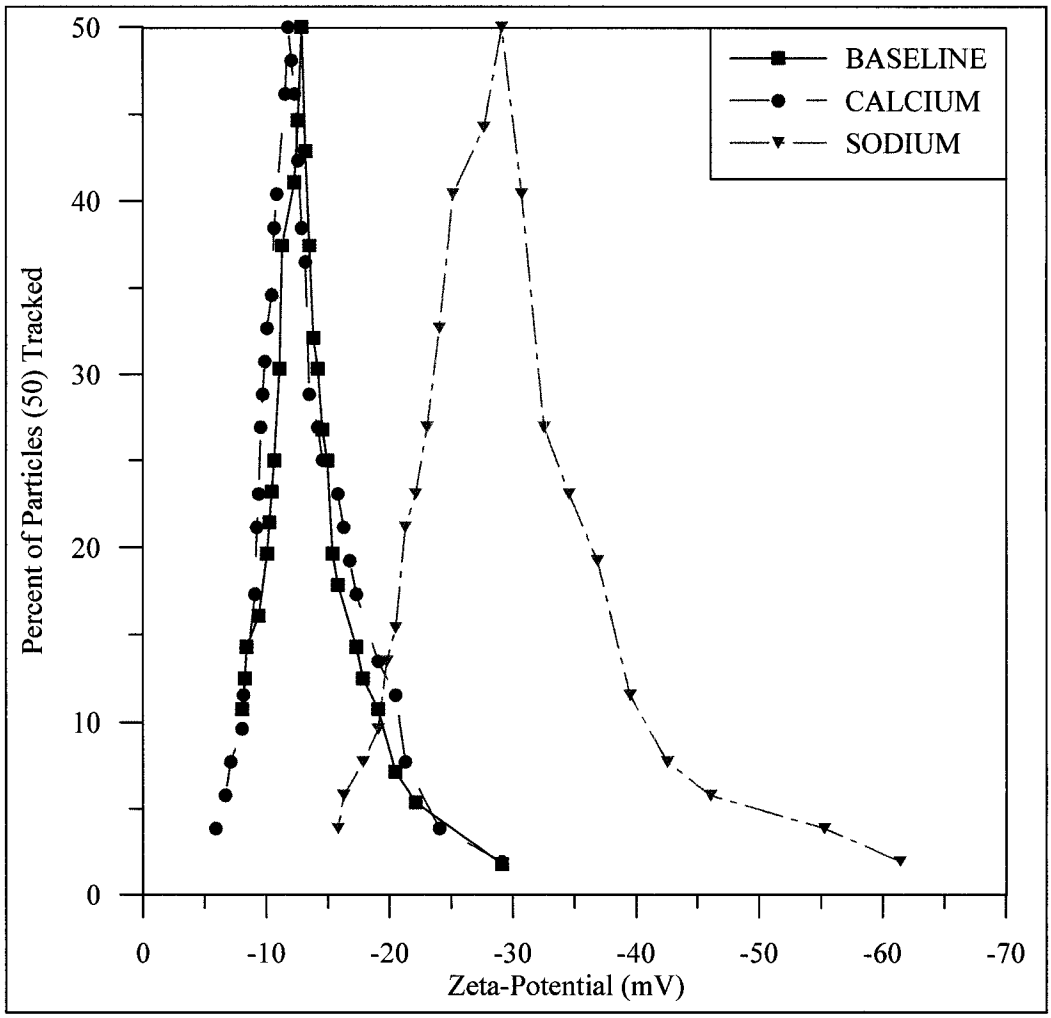

Figure 4.18: ζ potential distribution curves for HV BSLN and corresponding cation treatments

Table 4.4: Summary of ζ potential median values

Soil	ζ potential (mV)				
	BSLN	Ca^{2+}	Mg^{2+}	Na^{+}	K^{+}
CR	-10.84	-8.13	-8.92	-19.06	-22.11
DEA	-13.48	-12.86	-15.36	-30.71	-29.09
FS	-15.36	---	-14.55	-21.26	---
HS	-14.17	-11.76	-12.28	-19.74	-15.79
HV	-12.86	-11.76	---	-29.09	---

the ζ potential for Ca^{2+} being less negative than that for Mg^{2+}. The ζ potential for the BSLN sample is typically more negative than those for the divalent treatments, with the exception of the DEA BSLN sample. The ranges in ζ potential for the BSLN, Ca^{2+}, and Mg^{2+} samples are small, which results in narrow peaks at the median ζ potential. Conversely, the ranges for the Na^{+} and K^{+} samples are larger, resulting in wider curves. The median ζ potential values for the monovalent treatments are similar to each other and distinctly more negative than the BSLN and divalent treatments for a given soil. This distinct grouping is less prevalent for HS, although the general trend in the median ζ potential values is still present. The ζ potential values summarized in Table 4.4 are typical for clay minerals (S. Lin, personal communication, October 2006).

CHAPTER 5: FROST HEAVE TEST RESULTS

5.1 General Results, BSLN Repeatability and Comparison

The CR-A frost heave test will be used as an example to describe the features typical of the frost heave test results. The CR-A raw data are shown in Figure 5.1. The top and bottom pedestal temperatures are shown in dark blue and red, respectively. A portion of the thermal shock at the beginning of the test is represented by the negative spike in the top pedestal temperature at the extreme left of the graph. The full negative value of the thermal shock is not represented on the graph due to the five minute recording interval. The top and bottom pedestal temperatures ramp down uniformly through the length of the test, and level out at 115 hours, indicating the end of the temperature bath program. Some minor variation in the top pedestal temperature near the end of the test is evident as noise in the temperature curve. This represents temperature variation due to the increased viscosity of the fluid in the corresponding temperature bath. Once this problem with the equipment was diagnosed, the fluid was replaced.

The amount of heave is shown in green, and water intake is shown in sky blue. The water intake was calculated by dividing the volume of water measured by the cross-sectional area (i.e., 2.83×10^3 mm^2) of the inner cylinder containing the soil sample. During the beginning of some of the frost heave tests, a 1-mm to 2-mm thick layer of ice formed above the top surface of the soil sample. Correspondingly, in these tests, the heave measurements were initially negative, indicating the initial consolidation of the soil at the onset of freezing. The end of consolidation and beginning of heave was identified as the most negative heave value measured, which typically was on the order of a fraction of a millimeter. The proceeding data were adjusted to zero at this point. The total amount of consolidation during freezing for these frost heave tests was not measured since this requires additional specialized equipment and procedures, such as using x-ray photography to measure the displacement of lead spheres embedded within the soil sample.

In Figure 5.1, the water intake deviates an increasing amount from the measured heave throughout the test, and abruptly levels off at 105 hours, indicating the freezing of the lower porous plate. Soil heave continues after that time, but at a decreasing rate. This indicates that segregated ice continues to form in the sample, despite the closed-system caused by the freezing of the pore water intake line. Additionally for this test, there is a deviation of about nine percent between the measured heave and the water intake, which corresponds to the expansion upon

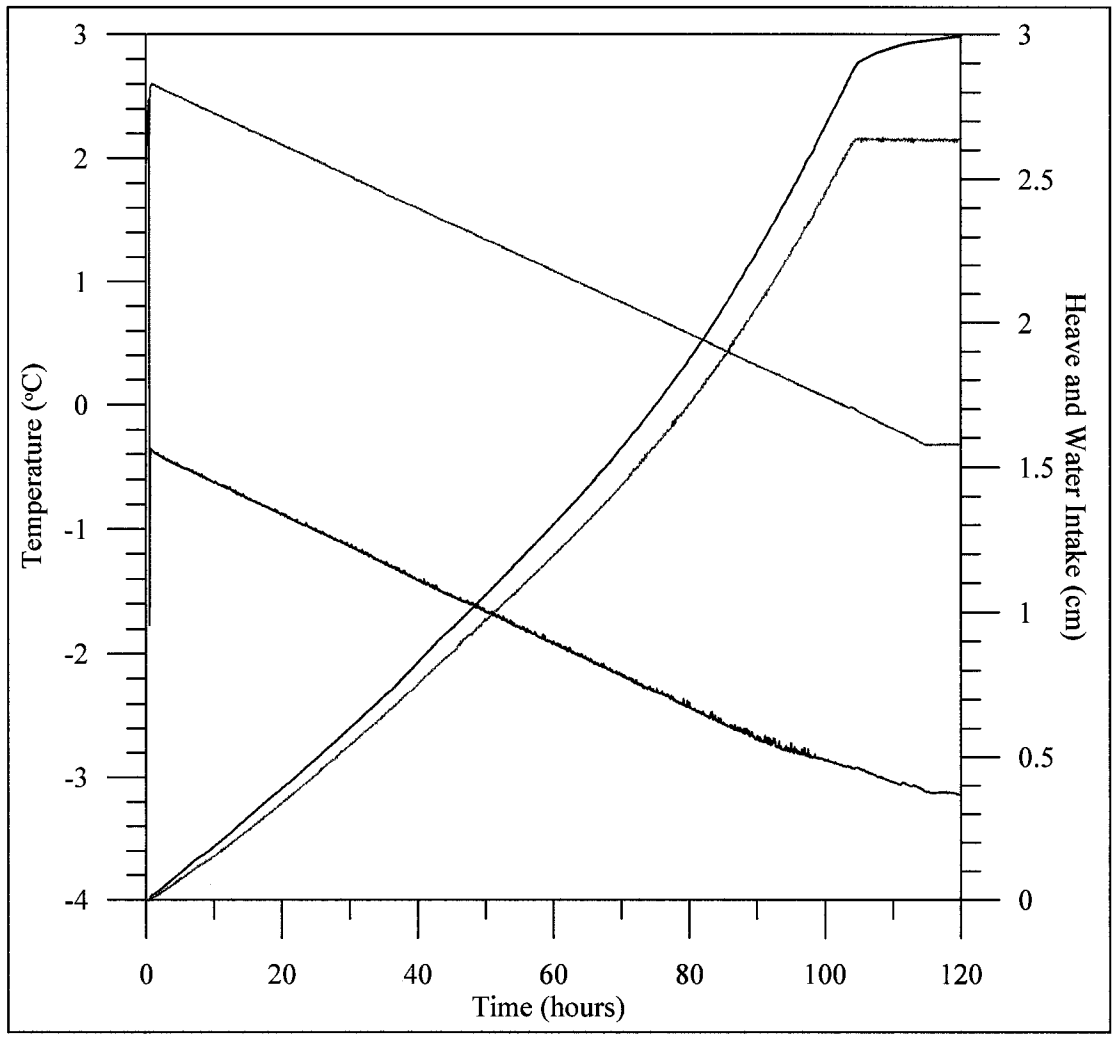

Figure 5.1: Raw data for CR-A frost heave test. The top and bottom pedestal temperatures (°C) are shown in dark blue and red, respectively. The amount of heave (cm) is shown in green, and the amount of water intake (cm) is shown in sky blue.

freezing of the initial water content within the soil pores. For some tests, the deviation between the measured heave and the water intake is greater than nine percent, perhaps indicating that some of the samples had initial water contents that were greater than saturation. The soil is completely frozen prior to the end of the bath program. This overestimate in the bath program length was made deliberately to ensure that the complete soil length would be frozen by the end of the test. The same trend is present in all of the test results. The raw data from each frost heave test are presented graphically in Appendix E.

The frost heave test results presented graphically are in terms of percent heave, which is defined as:

$$Percent\_Heave = \frac{\Delta H}{H_l} \cdot 100 \tag{5.1}$$

where ΔH is the frost heave amount measured from the beginning of the test, and H_l is the sample length just before freezing. The total amount of frost heave experienced by each sample is presented as the frost heave ratio (ξ), which is defined as:

$$\xi = \frac{\Delta H_f}{H_l} \cdot 100 \tag{5.2}$$

where ΔH_f is the frost heave amount at the end of the freezing test, and H_l is the sample length just before freezing. Each test was considered at an end when the bottom pedestal temperature reached 0°C, with the exception of the CR Ca^{2+} frost heave test, which was completely frozen before the bottom pedestal bath program reached 0°C. This was due to an overestimation of the sample length, resulting in an error in the bath program. For this test, the end was defined as the point when the water intake stopped abruptly.

In order to determine the repeatability of the frost heave testing apparatus, replicate samples of each of the BSLN soils were tested. Additionally, replicate samples of HV ORG were tested, in order to compare this soil's frost heave susceptibility to HV. The results of the repeatability tests for the BSLN samples and the HV ORG samples are shown in Figures 5.2 through 5.7. For most of the soils, the overall concave shapes of the heave versus time curves (shown as (a) in Figures 5.2 through 5.7) are similar for the early portions of the tests, deviating slightly from each other afterward. The DEA samples are the exception to this, as the two curves deviated from each other at the beginning of the tests, deviating less towards the end of the tests. The HV ORG replicate curves are nearly an exact match.

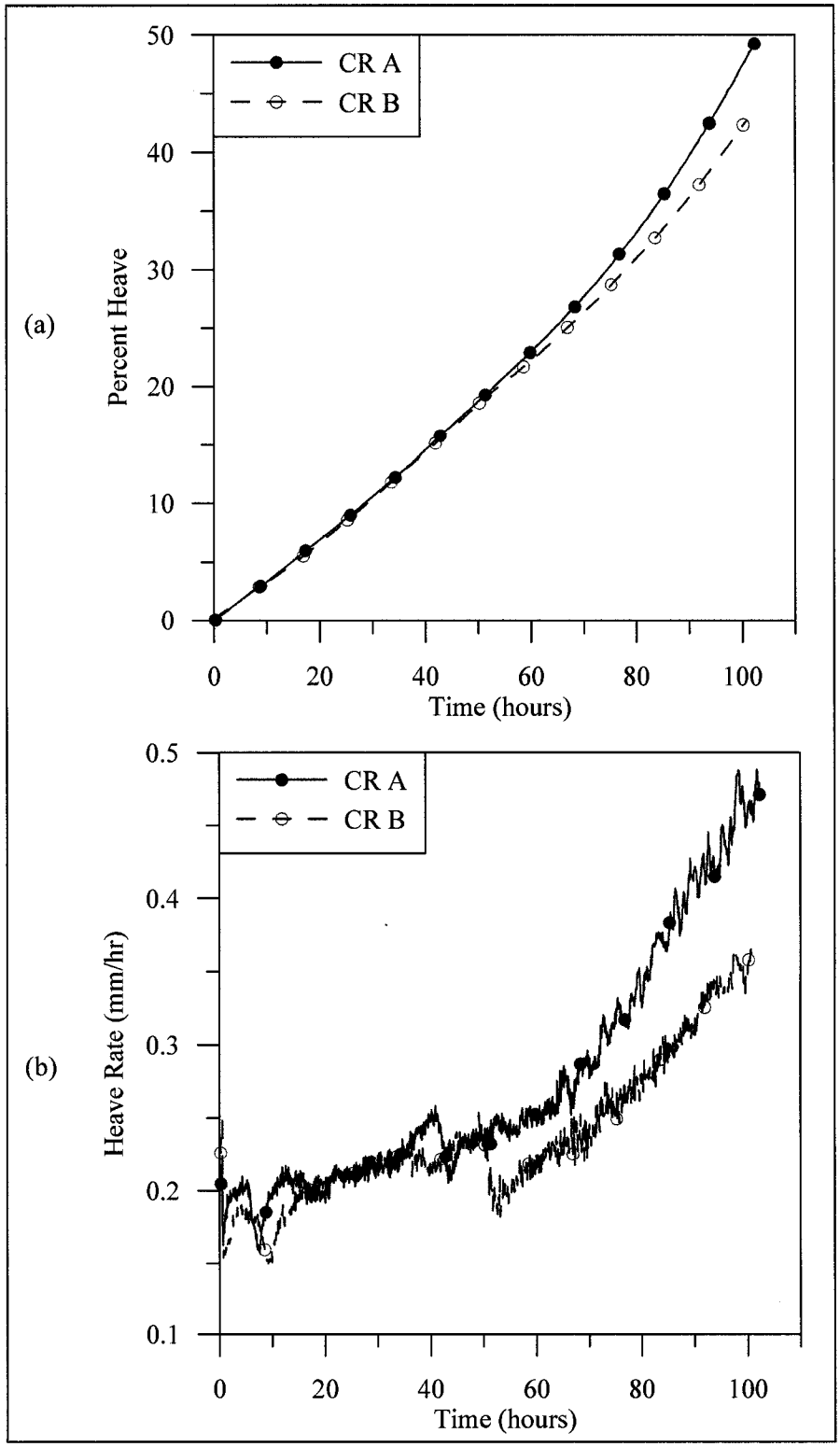

Figure 5.2: CR BSLN repeatability test results. (a) percent heave, and (b) heave rate.

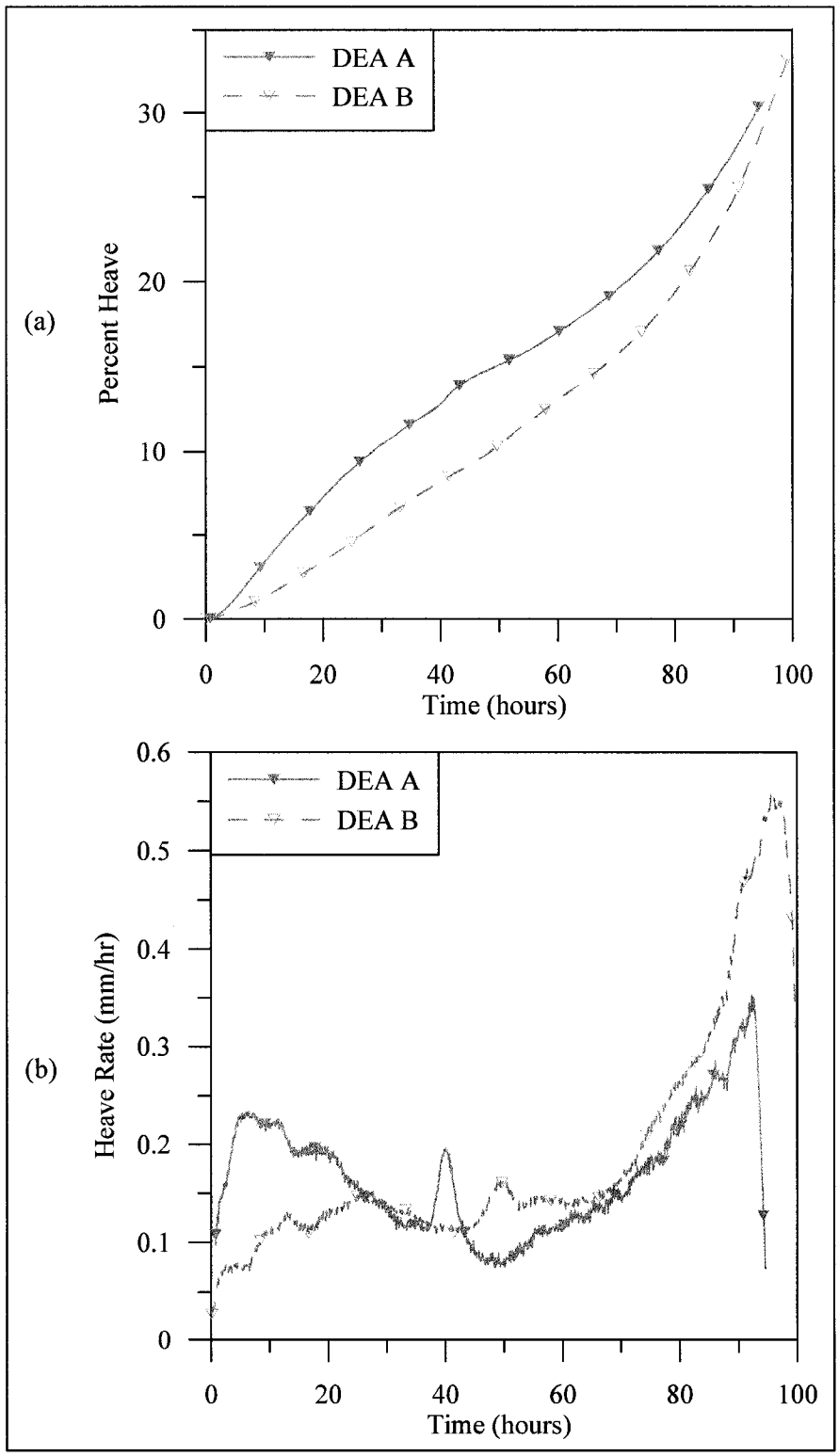

Figure 5.3: DEA BSLN repeatability test results. (a) percent heave, and (b) heave rate.

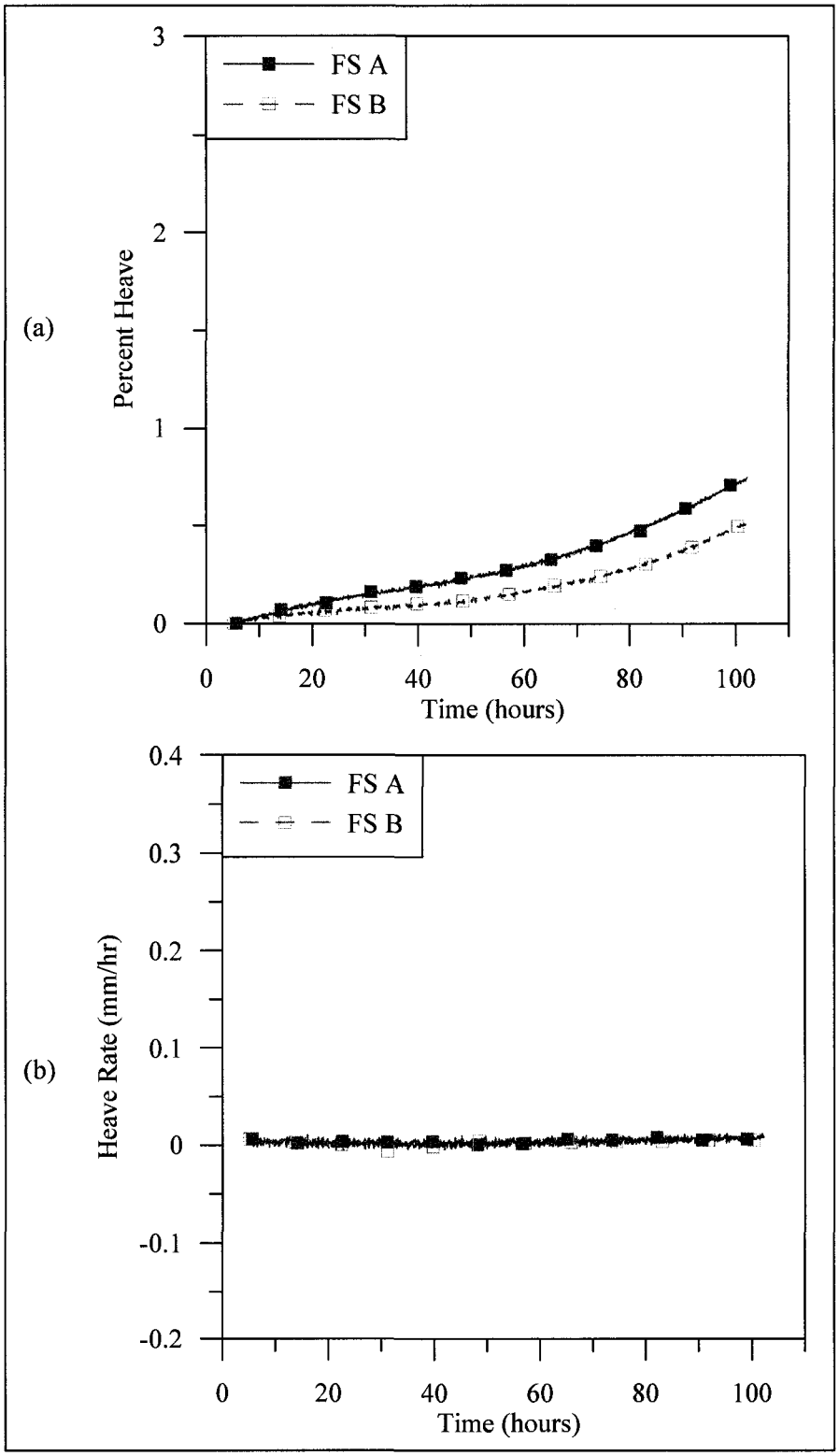

Figure 5.4: FS BSLN repeatability test results. (a) percent heave, and (b) heave rate.

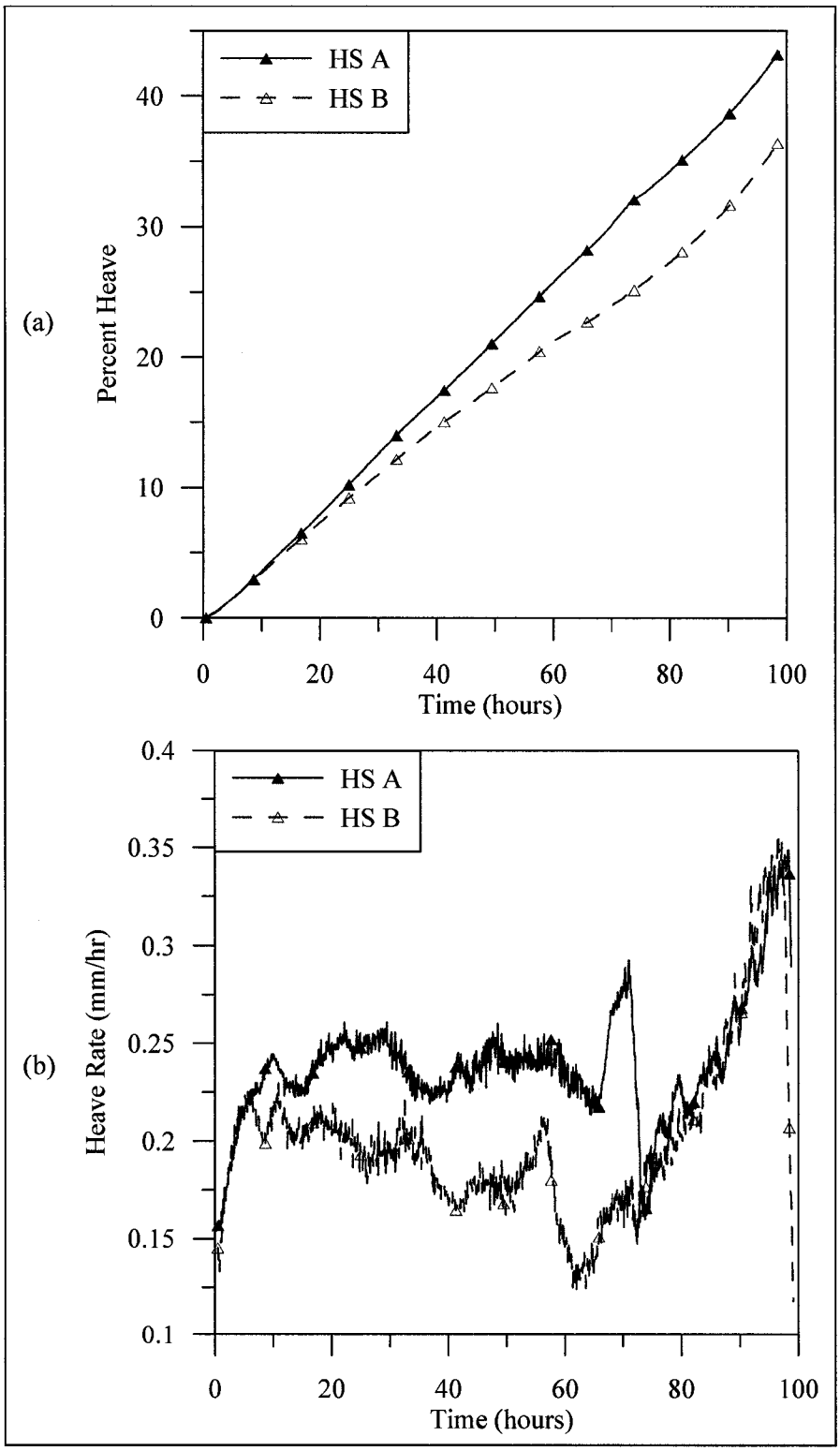

Figure 5.5: HS BSLN repeatability test results. (a) percent heave, and (b) heave rate.

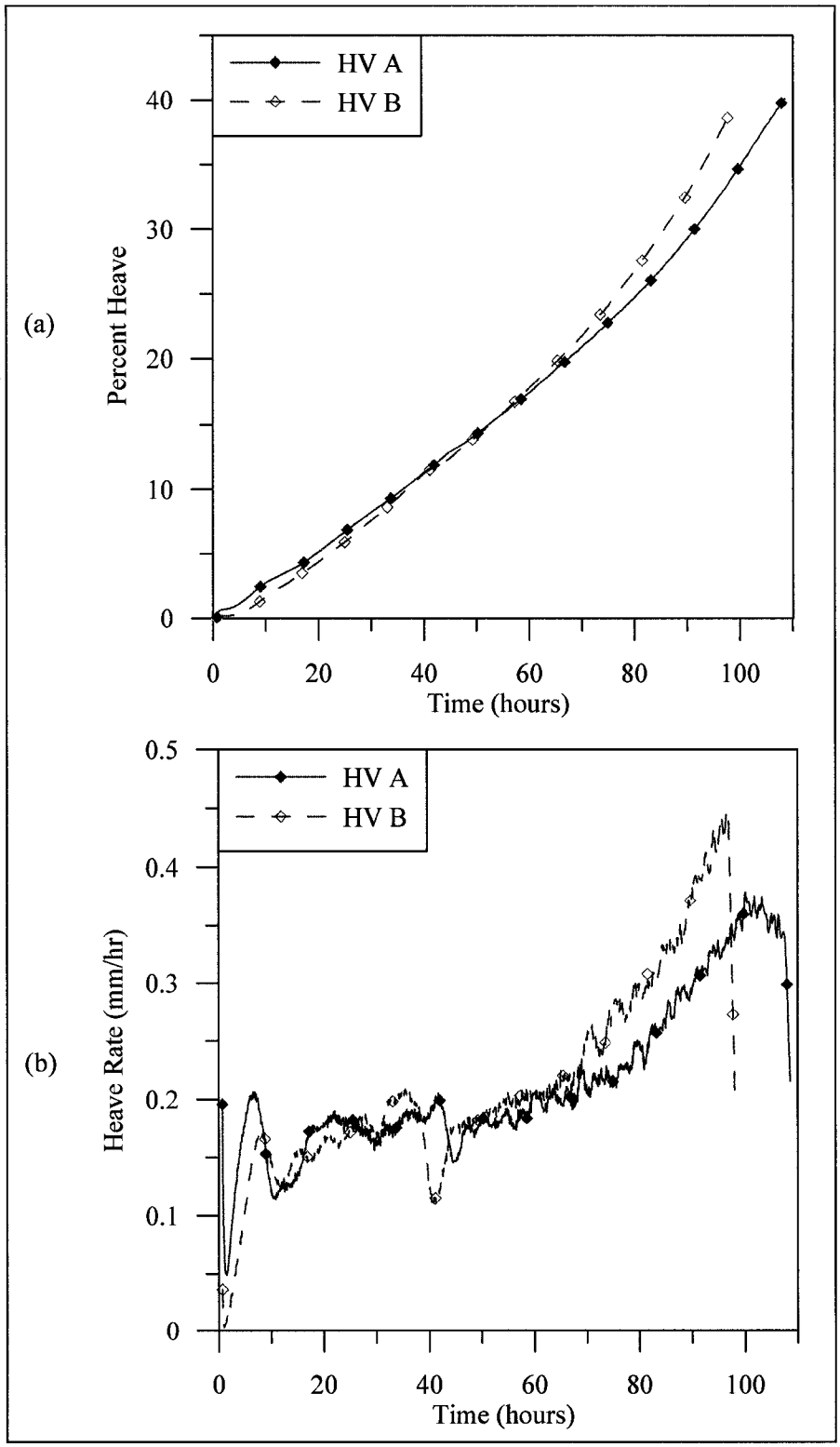

Figure 5.6: HV BSLN repeatability test results. (a) percent heave, and (b) heave rate.

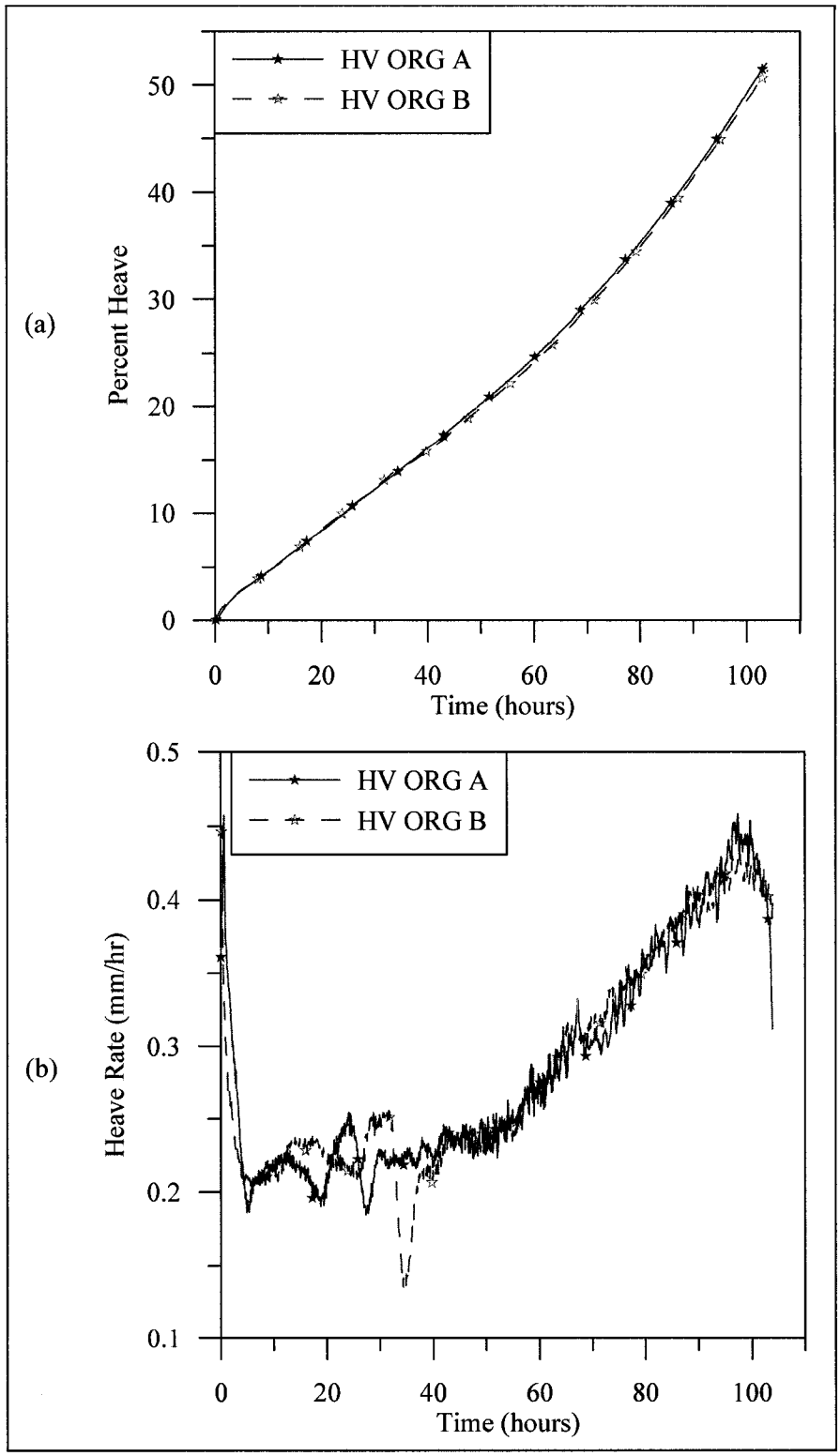

Figure 5.7: HV ORG repeatability test results. (a) percent heave, and (b) heave rate.

The ξ for each replicate pair are summarized in Table 5.1. The difference between replicates varies from 0.2 percent to 6.7 percent. These differences are attributed to errors in the initial soil length measurement and to small textural variations between soil samples. As discussed in Chapter 3, the soil is measured to the nearest millimeter once it is placed inside the inner cylinder. This can introduce as much as 1 percent error in ξ. Despite attempts to remove variations from the samples with the slurry method described in Chapter 3, textural differences may be inherent in each soil sample. Finally, since only one frost heave apparatus is available for testing, the replicate samples must remain in the air-tight container for up to two weeks before they are tested. During this time, changes in the moisture content of the samples may occur. All of these factors may contribute to the differences in ξ.

The heave rate (HR) versus time curves are shown as (b) Figures 5.2 through 5.7. The HR curves were smoothed using a two-hour running average. For each test, typically the HR rose quickly to an "average rate" for at least 50 hours. After this time, the HR rose in a linear fashion until the end of the freezing test. The average HR values for the beginning of each test, which were determined graphically, and the maximum HR values at the end of each test are summarized in Table 5.1. Some HR curves contain anomalous spikes, which may be due to differences in soil texture at certain horizons in the soil samples. The HR ramping to a maximum value in the last portion of each test is attributed to soil stratification and to the increasing shortening of the unfrozen portion of the soil sample with time. Despite fastidious attempts to ensure a uniform slurry and consolidated soil, some stratification may have occurred during the consolidation period. Since each sample is placed "upside down" from its natural orientation, the fine-grained particles would be at the bottom of the sample within the frost heave cell. As the freezing front penetrates the lower portions of the sample, the fine-grained particles may increase the HR. Additionally, during the later stages of the test, there is less soil volume between the freezing front and the moisture source within the lower porous plate, which results in a higher "effective permeability" and an increase in HR. The HR ramping occurs earlier, around 50 to 60 hours, for the clayey soils such as CR, HV, and HV ORG, and later at around 65 to 70 hours for the silty soils such as DEA and HS. FS is an exception to these trends, as this soil demonstrated negligible heave.

The difference between ξ for the replicates was less than 7 percent, and the difference between the average HR and the maximum HR for replicates was less than 0.05 mm/hr and

Table 5.1: Summary of frost heave ratios (ξ) and heave rates (HR) from BSLN and HV ORG repeatability tests

Sample	ξ (%)		Avg. HR (mm/hr)		Max. HR (mm/hr)	
	A	B	A	B	A	B
CR BSLN	49.2	42.7	0.22	0.22	0.49	0.37
DEA BSLN	30.6	33.7	0.15	0.13	0.35	0.56
FS BSLN	0.7	0.5	0.00	0.00	0.00	0.00
HS BSLN	43.4	36.7	0.23	0.18	0.35	0.35
HV BSLN	40.1	38.9	0.17	0.16	0.38	0.45
HV ORG	52.0	51.3	0.23	0.23	0.45	0.45

0.21 mm/hr, respectively. These results indicate that the frost heave apparatus and testing procedure produce highly repeatable results, allowing analysis of the trends in the data, rather than wondering if the trends are artifacts of the equipment. In the following analyses, the replicate with the highest ξ is used for comparison.

A comparison between the HV BSLN and HV ORG frost heave tests is shown in Figure 5.8. The difference between the ξ for the HV BSLN and HV ORG tests is 12.0 percent. Since the difference between the ξ for the HV replicates is 1.2 percent and that between the HV ORG replicates is 0.7 percent, the overall ξ difference between HV and HV ORG is significant. The same soil, removed of its colloidal organic content, becomes less frost susceptible, as indicated by Linell and Kaplar (1959).

A comparison of the BSLN frost heave test results is shown in Figure 5.9, and photographs of each of these samples after testing are shown in Figure 5.10. The ξ for these BSLN tests are summarized in Table 5.2. Most noticeable about Figure 5.9 is FS, which had a ξ of 0.7 percent. Throughout the FS freezing tests, water was observed to be expulsed from the samples. The fact that coarse-grained soils expulse water upon freezing and do not demonstrate frost heaving has been noted many times in the frost heaving literature. While FS is classified as silt, the soil is coarse silt and is poorly-graded. This combination causes FS to be non-frost susceptible. Several researchers have used "Fairbanks silt" in frost heave tests, including Hoekstra (1966), Berg et al. (1980), and Ingersoll and Berg (1981). The latter authors indicated their preference for this soil due to its high frost susceptibility. While the soil sampled for these previous experiments did not come from the same location as the FS sample, it is assumed that all "Fairbanks silt" samples are of the same initial origin, i.e. loess. The loess in the greater Fairbanks area, however, has been reworked in places. The redeposition of the loess onto lower slopes and into valley bottoms may have caused a breakdown of the grains, creating a more well-graded soil. Also, the addition of organic matter into the reworked soil fragments will increase its frost susceptibility, as indicated by the HV versus HV ORG comparison.

For the remaining BSLN samples, CR has the highest ξ, followed by HS, HV, and DEA, respectively. The trend of percent heave versus time presented in Figure 5.9 for these soils is generally linear, although there is a curvature in the later portions of each test that corresponds to the increase in HR. Again, the increase in HR is attributed to the shortening of the soil sample with time and thus an increase in the "effective permeability."

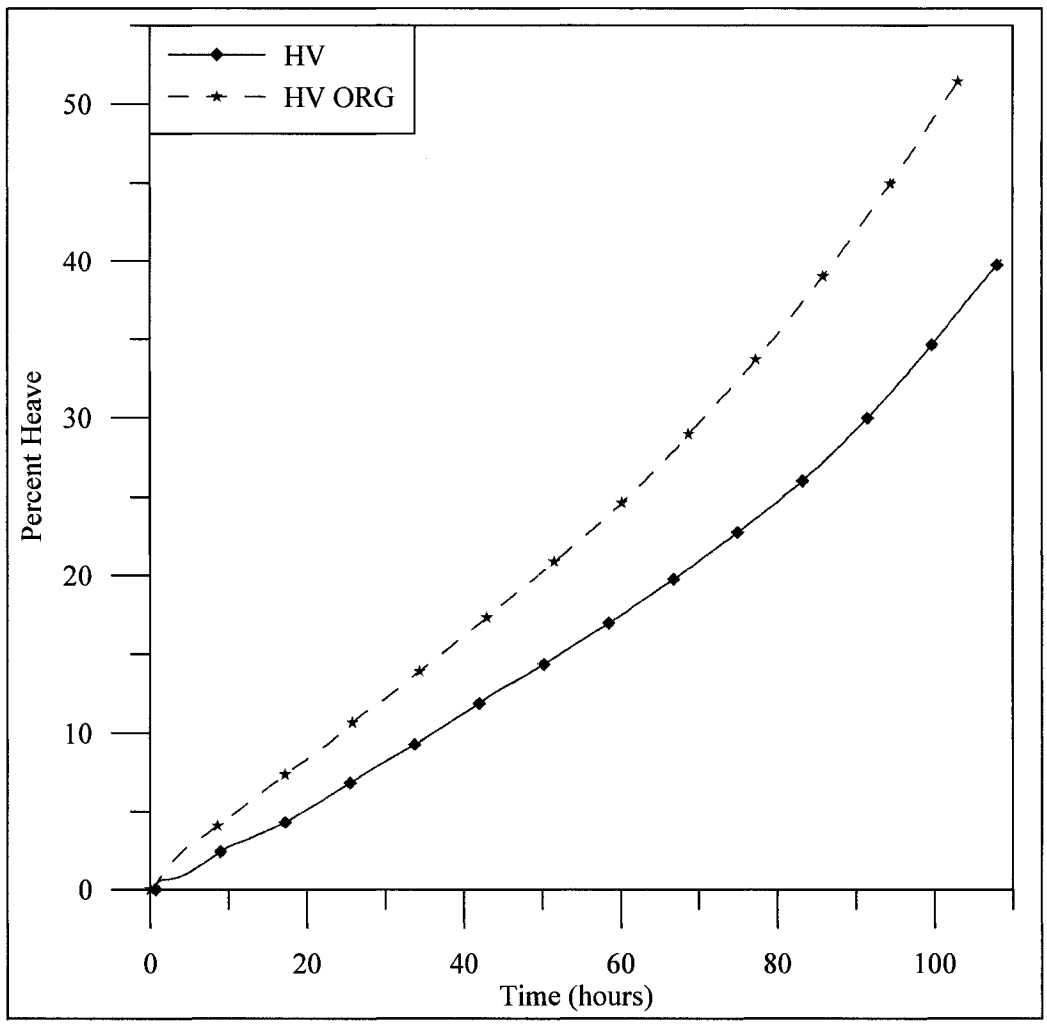

Figure 5.8: Comparison of HV and HV ORG frost heave tests

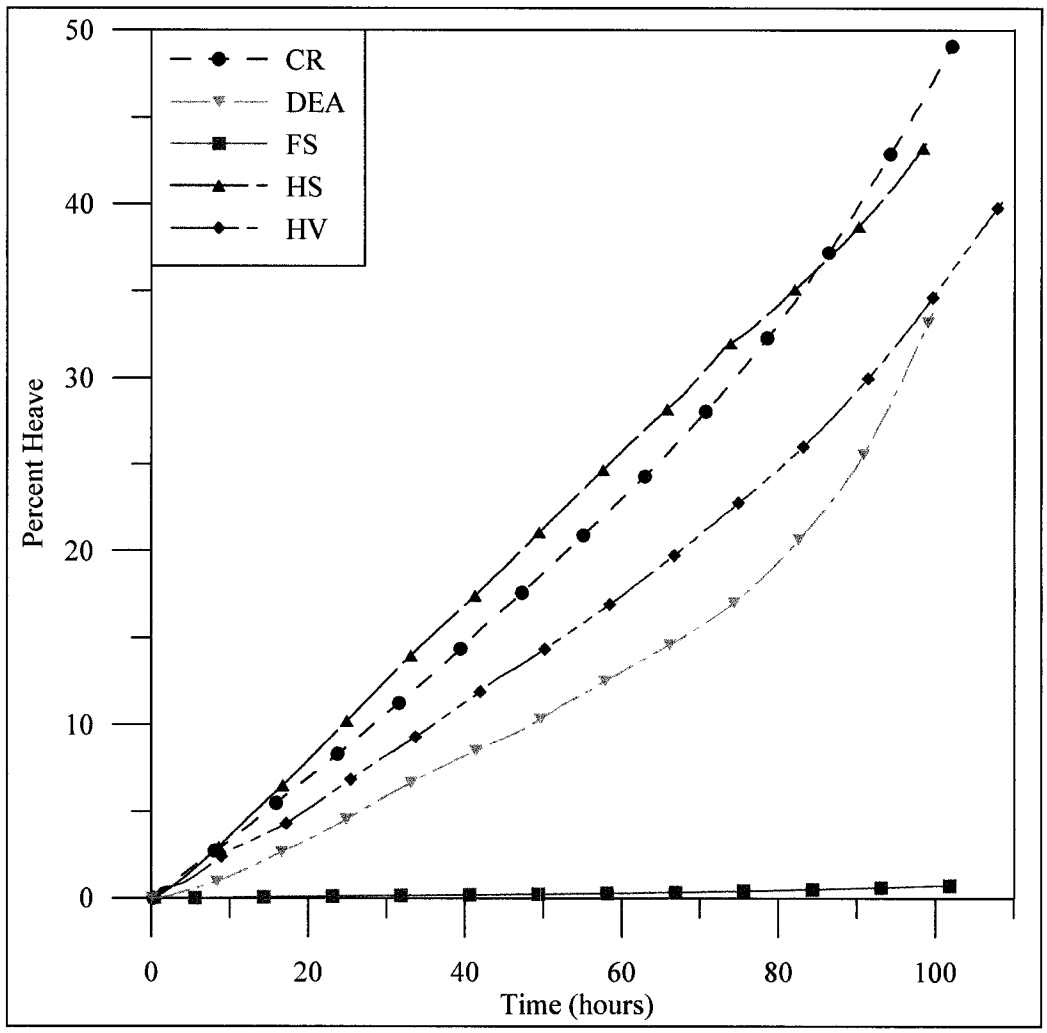

Figure 5.9: Comparison of BSLN frost heave tests

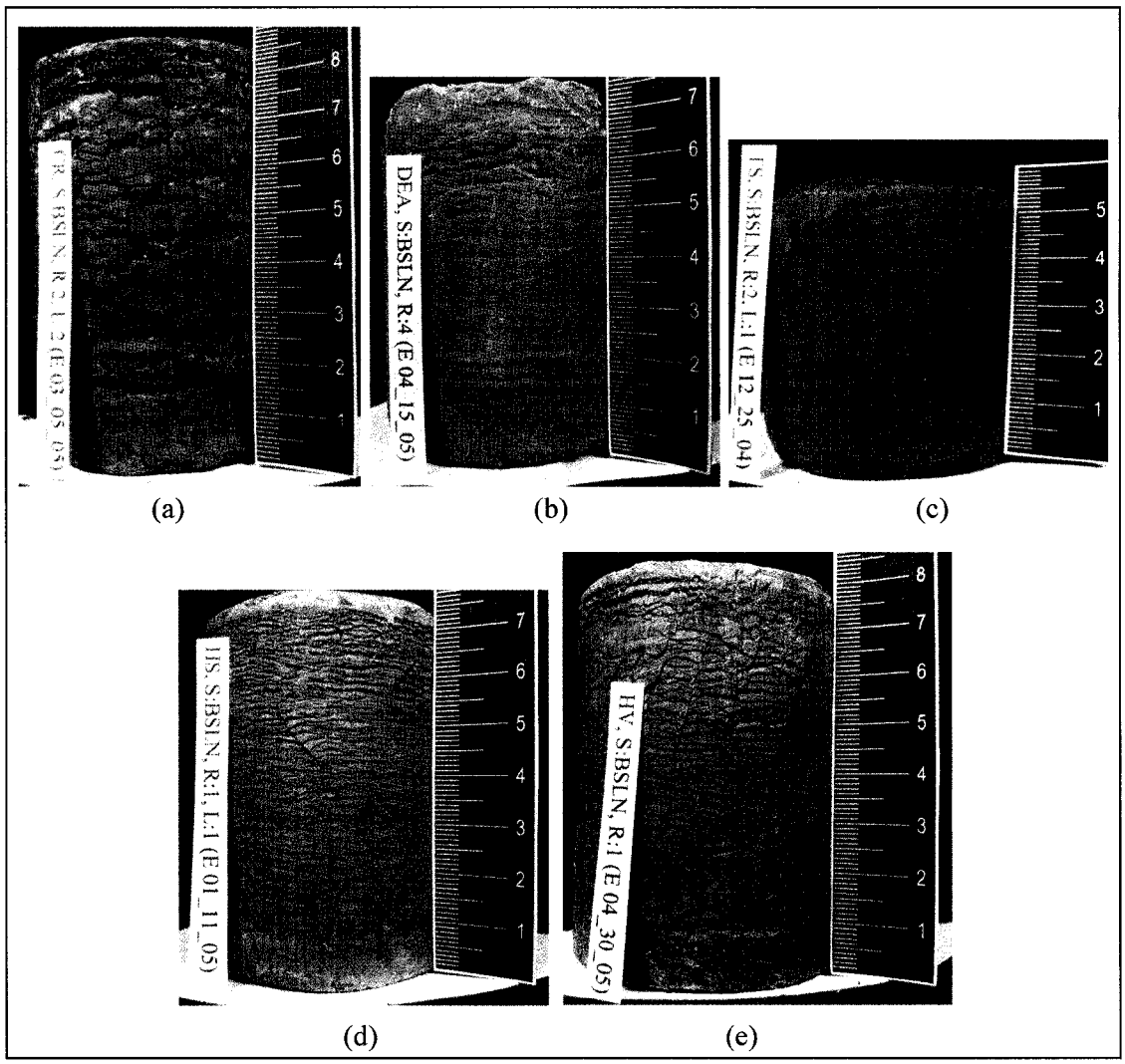

Figure 5.10: Photographs of BSLN frost heave test samples. The different BSLN soils shown (with their initial lengths indicated in parentheses) are: (a) CR (57 mm), (b) DEA (55 mm), (c) FS (57 mm), (d) HS (54 mm), and (e) HV (58 mm).

Table 5.2: Summary of frost heave ratios (ξ) for the BSLN samples

Soil	ξ (%)
CR	49.2
DEA	33.7
FS	0.7
HS	43.4
HV	40.1

The DEA and HS samples developed micro-lenticular ice lenses oriented parallel to each other and perpendicular to the heat flow direction (see Figures 5.10(b) and (d), respectively). The CR sample developed larger ice lenses up to 3-mm thick with a greater overall spacing (see Figure 5.10(a)). Vertical ice structures are also present in the photograph. These larger ice lenses and vertical structures are typical of frozen clay. Based on visual observations, the vertical cracks form ahead of the freezing front as the unfrozen soil is desiccated by movement of water to the freezing front. Water provided to the sample from the double-walled burette fills the cracks and freezes as the freezing front moves downwards through the sample. The HV sample appears to be a hybrid between the two cases discussed above (see Figure 5.10(e)). This frozen soil contains small, parallel ice lenses, with narrow vertical cracks running nearly continuously throughout the sample. These features indicate that the soil possesses properties that are intermediate between a silty soil and a clayey soil. Finally, the FS sample contained no visible ice, appearing nearly the same frozen as prior to freezing (see Figure 5.10(c)).

In Figures 5.10(a), (b), (d), and (e), the bottom 10 to 15 mm of each soil sample contain fewer ice lenses than the rest of the sample. This is attributed to the "buffering" of the temperature bath programs, as described in Chapter 3. Since the bath corresponding to the bottom pedestal is programmed to be ramped down to -0.4°C, there is a zone of soil that experiences freezing from both directions. Thus, the upper portion of the soil sample images are more indicative of the true behavior under one-directional freezing, and the bottom 15 mm should be ignored. This testing problem can be solved in the future by placing 15 mm of fine sand directly above the bottom pedestal and below the soil sample (S. Akagawa, personal communication, June 2005).

5.2 HS Cation Treatment Repeatability

In order to determine both the repeatability of and significant differences among the cation treatments, replicate samples of each of the HS cation treatments were tested. The percent heave and HR results of the HS cation treatment replicates are shown in Figures 5.11 through 5.14. Similar trends are present in these data as in the BSLN results, containing both an "average" HR in the beginning portion of the tests, followed by ramping to a maximum value. The average HR values for the beginning of each test and the maximum HR values at the end of each test are summarized in Table 5.3. Of note in these tests, is that the Ca^{2+}- and Mg^{2+}-treated samples demonstrated an initial very high peak in HR at the beginning of the tests. After this

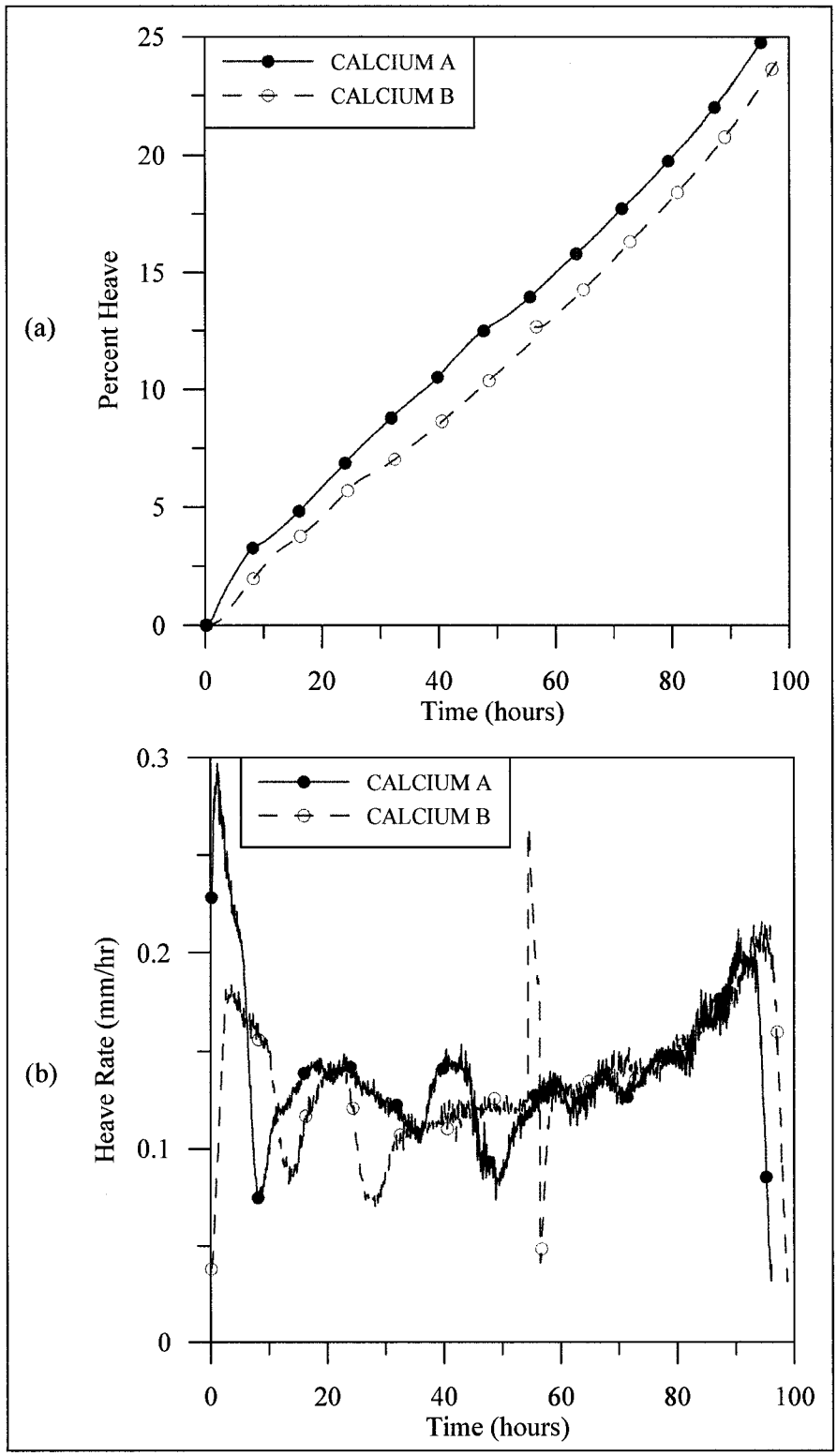

Figure 5.11: HS Ca^{2+} repeatability test results. (a) percent heave, and (b) heave rate.

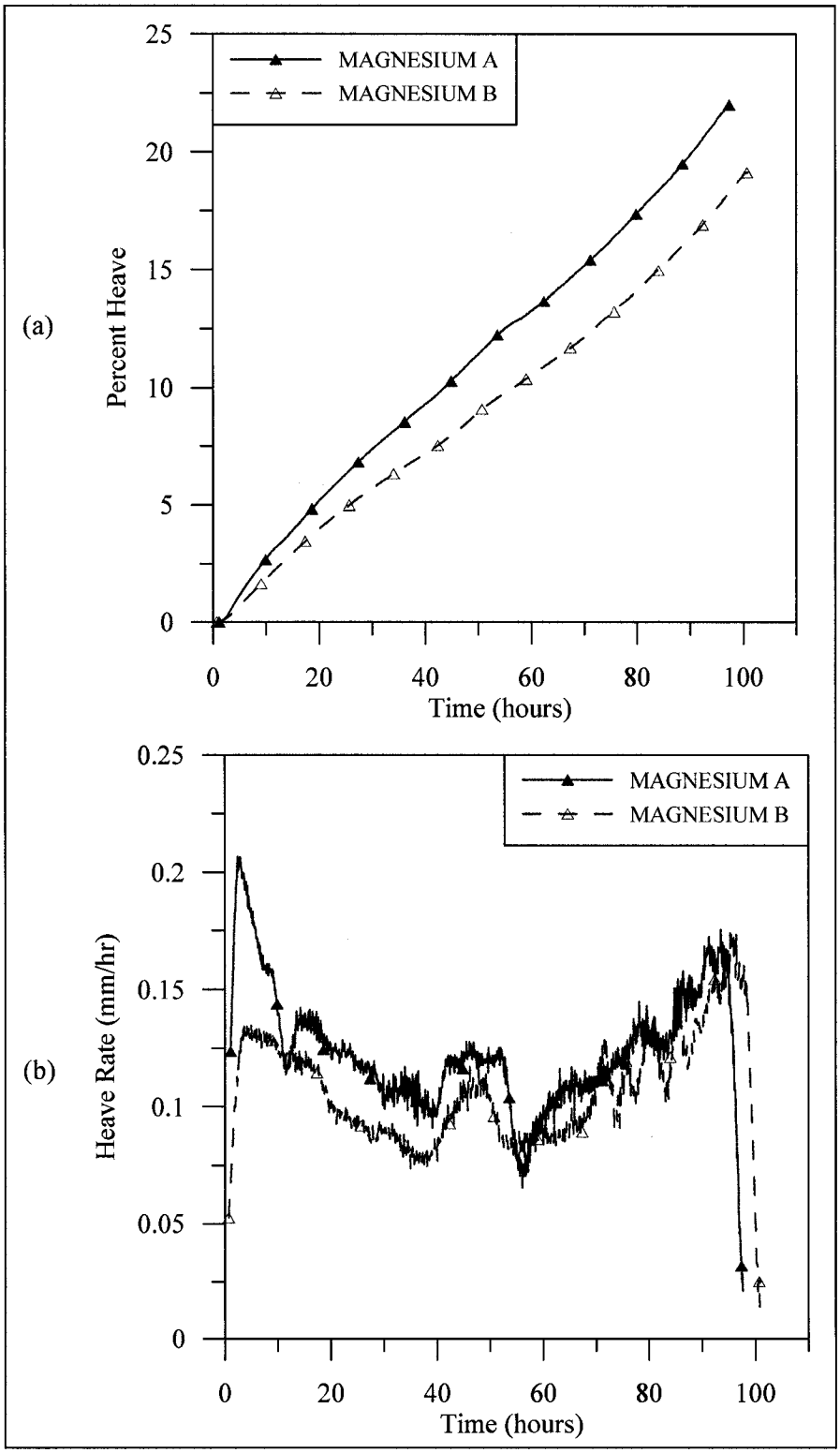

Figure 5.12: HS Mg^{2+} repeatability test results. (a) percent heave, and (b) heave rate.

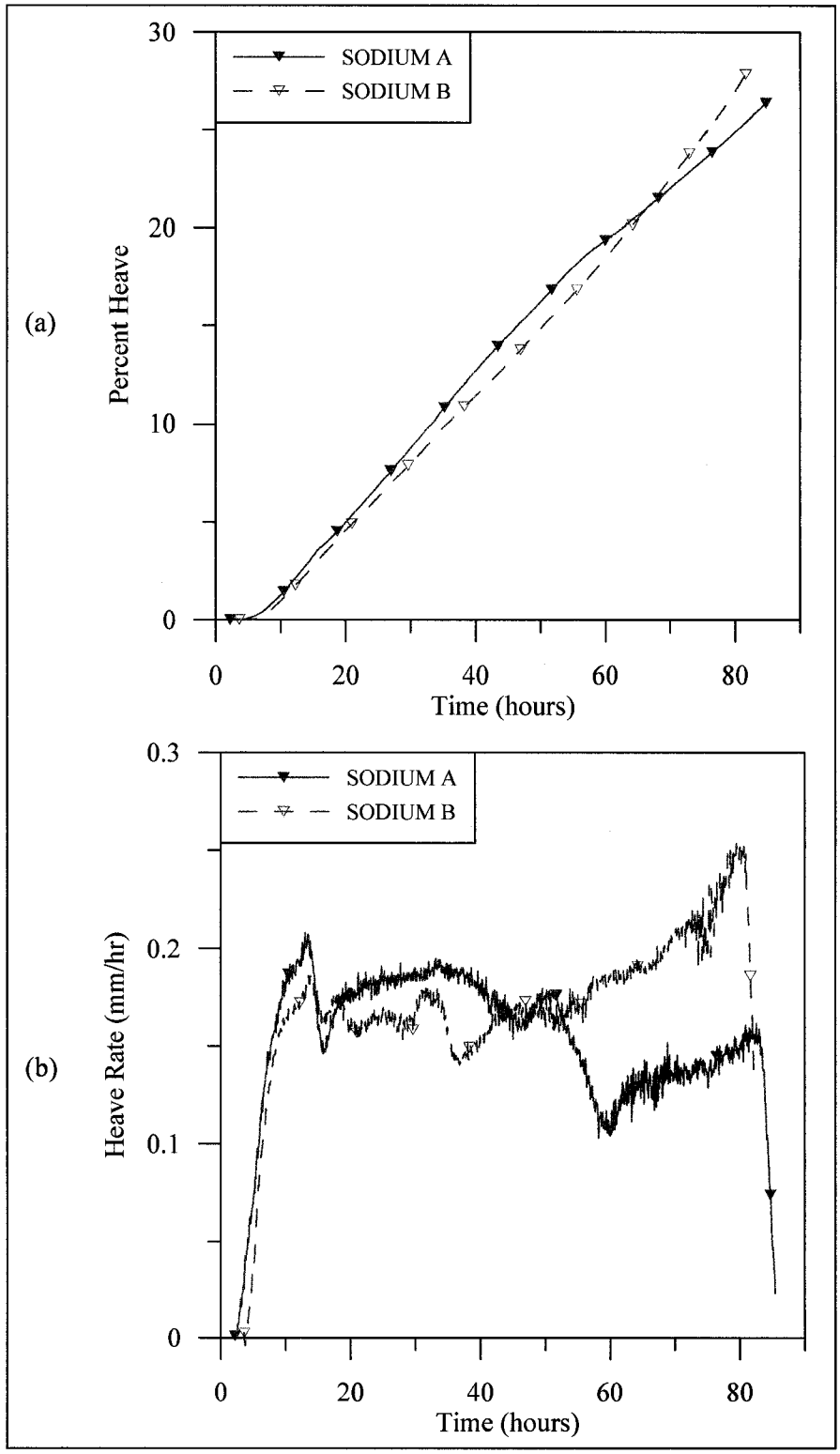

Figure 5.13: HS Na^+ repeatability test results. (a) percent heave, and (b) heave rate.

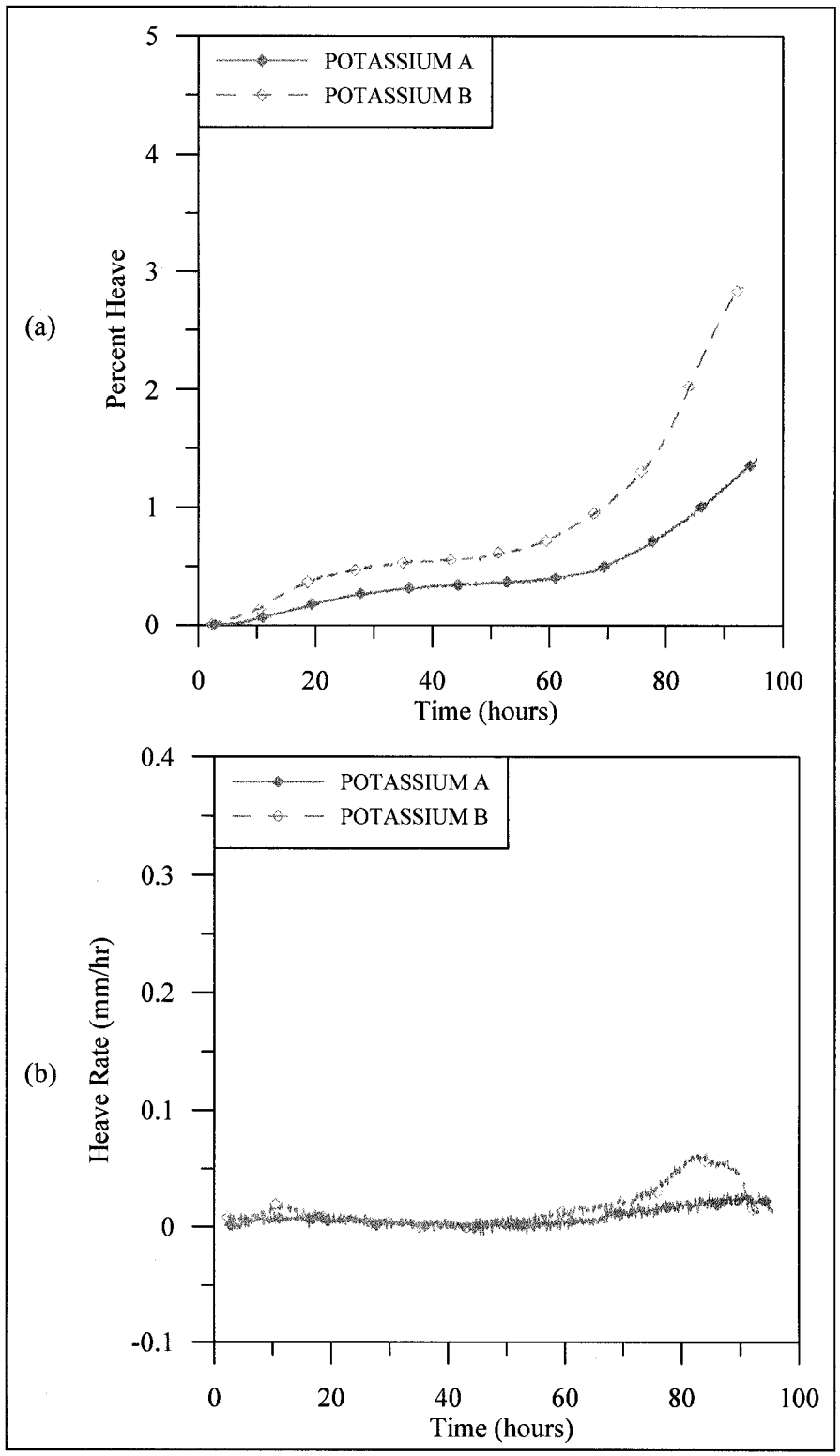

Figure 5.14: HS K^+ repeatability test results. (a) percent heave, and (b) heave rate.

Table 5.3: Summary of frost heave ratios (ξ) and heave rates (HR) from HS cation treatment repeatability tests

Sample	ξ (%)		Avg. HR (mm/hr)		Max. HR (mm/hr)	
	A	B	A	B	A	B
HS Ca^{2+}	25.0	24.2	0.13	0.12	0.21	0.21
HS Mg^{2+}	22.0	19.1	0.12	0.10	0.17	0.17
HS Na^{+}	26.6	28.1	0.17	0.16	0.16	0.25
HS K^{+}	1.4	2.9	<0.01	<0.01	0.03	0.06

peak, the HR dropped off until the ramping at the end of the test. For Na^+ B, the "maximum" HR value at the end of the ramping is actually a misnomer, since it is less than the average HR during the beginning portion of the test (see Table 5.3). The Na^+ and K^+ replicates did not demonstrate heaving for up to 3.5 hours after the given test began. This is attributed to the initial consolidation of the soil by the segregating ice. This causes an effective lowering of the overall ξ, as indicated by Penner (1959), Williams (1963), and Yamamoto et al. (1988), among others. Finally, the HR data for the Ca^{2+}-B test contains anomalous spikes around 55 hours into the test (see Figure 5.11(b)). These spikes are the result of filling the double-walled burette incorrectly, and inadvertently introducing pressure into the water system. The problem was corrected later in the test; however, a related spike in percent heave is also evident in Figure 5.11(a).

The ξ, and average and maximum HR values for each replicate pair are summarized in Table 5.3. The difference in ξ between replicates varies from 0.8 percent to 2.9 percent, and the differences in average HR are 0.02 mm/hr or less. These differences are considered insignificant, allowing comparison among the cation treatments to occur without questioning the reliability of the data.

5.3 Cation Treatment Comparison for Each BSLN Soil

During the first cation treatment preparations, it was noted that the soils saturated with Na^+ and K^+ drained slowly during the chloride rinsing process. The soils that demonstrated this the most were CR, HS, and HV. Additionally, these soils were difficult to load in the consolidation cell. If the pressure was added too quickly to the soil slurry, the slurry would "blow out" of the orifice from which the pore water drained. As such, the procedure was modified to slowly load these soils. For the most extreme cases, the soil slurry was placed into the consolidation cell, and allowed to sit for 24 hours before any pressure was added. After 24 hours, pressure was added incrementally up to the maximum value of 200 kPa. At the end of the consolidation period, the top of the soil in the consolidation cell was soft, while the bottom portion was firm. Since each of these samples was turned end for end when placed into the acrylic cylinder, the top of the sample appeared to be more consolidated consisting of coarser grains, than the bottom portion. Additionally, these three soils demonstrated sporadic adjustments to the pressure applied during the second consolidation in the frost heave apparatus. Due to this procedure modification, some of the soil slurries stratified, which was noted once the

samples were placed into the acrylic cylinder. The HS K^+-treated sample contained the most stratification. Most of these soils also demonstrated a delay in heaving after the thermal shock, which is attributed to the consolidation of the soil immediately below the newly forming segregated ice.

At the other extreme, the DEA and FS soil slurries began to settle and "self-consolidate" immediately after placement in the consolidation cell. Alterations of the consolidation procedure for these soils included elimination of the de-airing period and immediately applying pressure to the slurry.

The results of CR BSLN and cation treatment tests are presented in Figure 5.15, and photographs of each test are presented in Figure 5.16. When preparing the various CR cation treatments, it was noticed that the Ca^{2+}-treated soil drained more quickly than did the Mg^{2+}-treated soil. As mentioned previously, the Na^+- and K^+-treated soils both drained slowly, with the Na^+-treated sample requiring seven weeks to prepare. The Na^+-treated sample was very soft when placed into the acrylic cylinder prior to freezing.

The results in Figure 5.15 indicate that the Ca^{2+}-treated sample demonstrated the most heave, followed by BSLN, K^+, Mg^{2+}, and Na^+ in order of their decreasing frost heave ratios. The photographs of the various treatments in Figure 5.16 all demonstrate the large horizontal ice lenses and vertical cracks that are typical of frost heave manifestation in clay. Although the samples had differing initial lengths (see the caption for Figure 5.16), the relative amount of heave among the five samples is indicated by the number of ice lenses present and their thicknesses. The effects of soil desiccation also can be seen especially well in Figures 5.16(a), (c) and (d). The exterior of these samples, when viewed against the dark background, is not uniform, but exhibits localized areas of concavity especially in areas of ice lenses. For all of the CR samples, the soil pulled away from the walls of the acrylic cylinder as it froze due to the freezing-driven desiccation.

The results of the DEA BSLN and cation treatment tests are presented in Figure 5.17, with corresponding photographs of the post-freeze samples in Figure 5.18. The Na^+- and K^+-treated slurries behaved unlike any of the other soils when consolidated. The coarse grains settled to the bottom of the consolidation cell almost immediately. The upper, fine-grained portion proceeded to consolidate, but remained soft. When the aluminum tubes were pushed into the consolidated soil, they were unable to penetrate the lower, coarse-grained portion, even when 500 kPa of pressure was applied to the consolidation cell piston above the aluminum tubes.

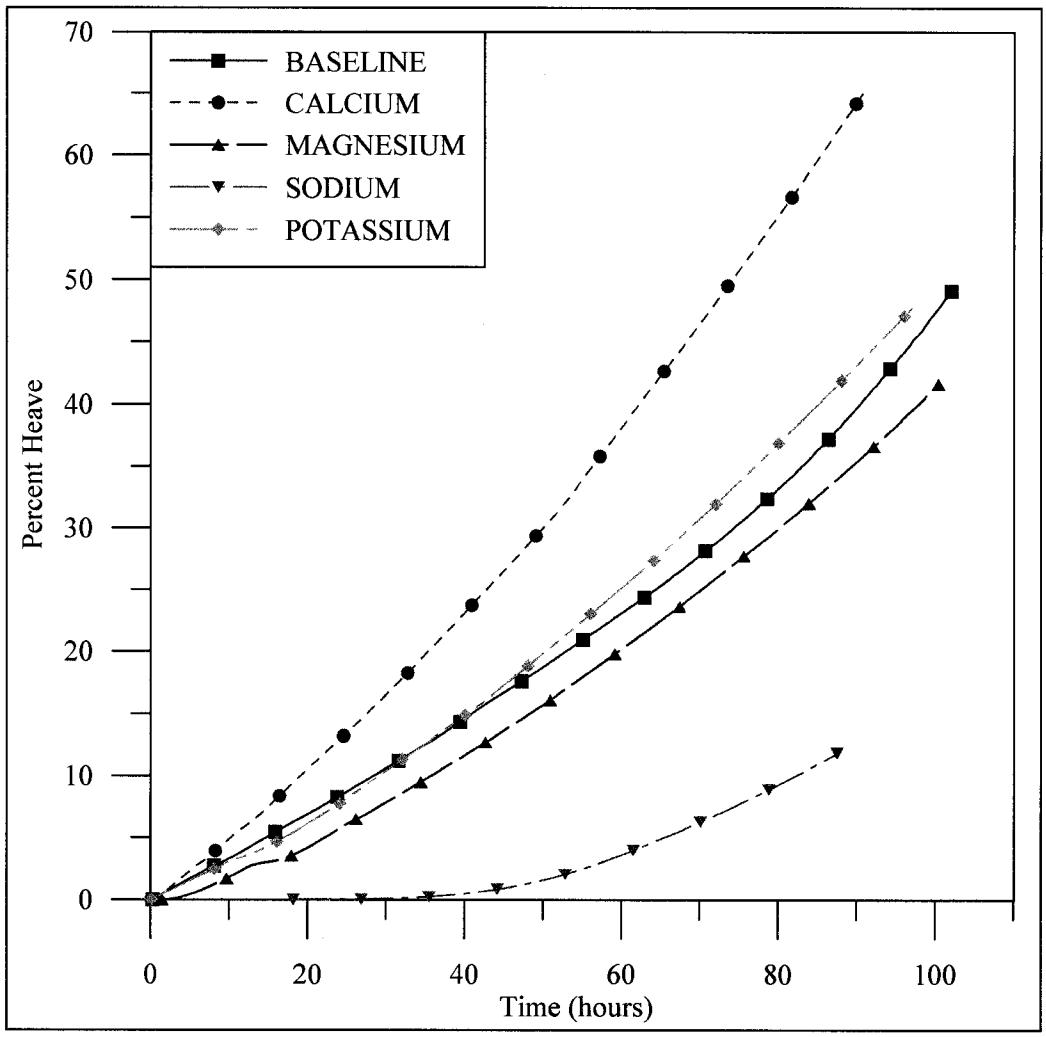

Figure 5.15: CR BSLN and cation treatment frost heave results

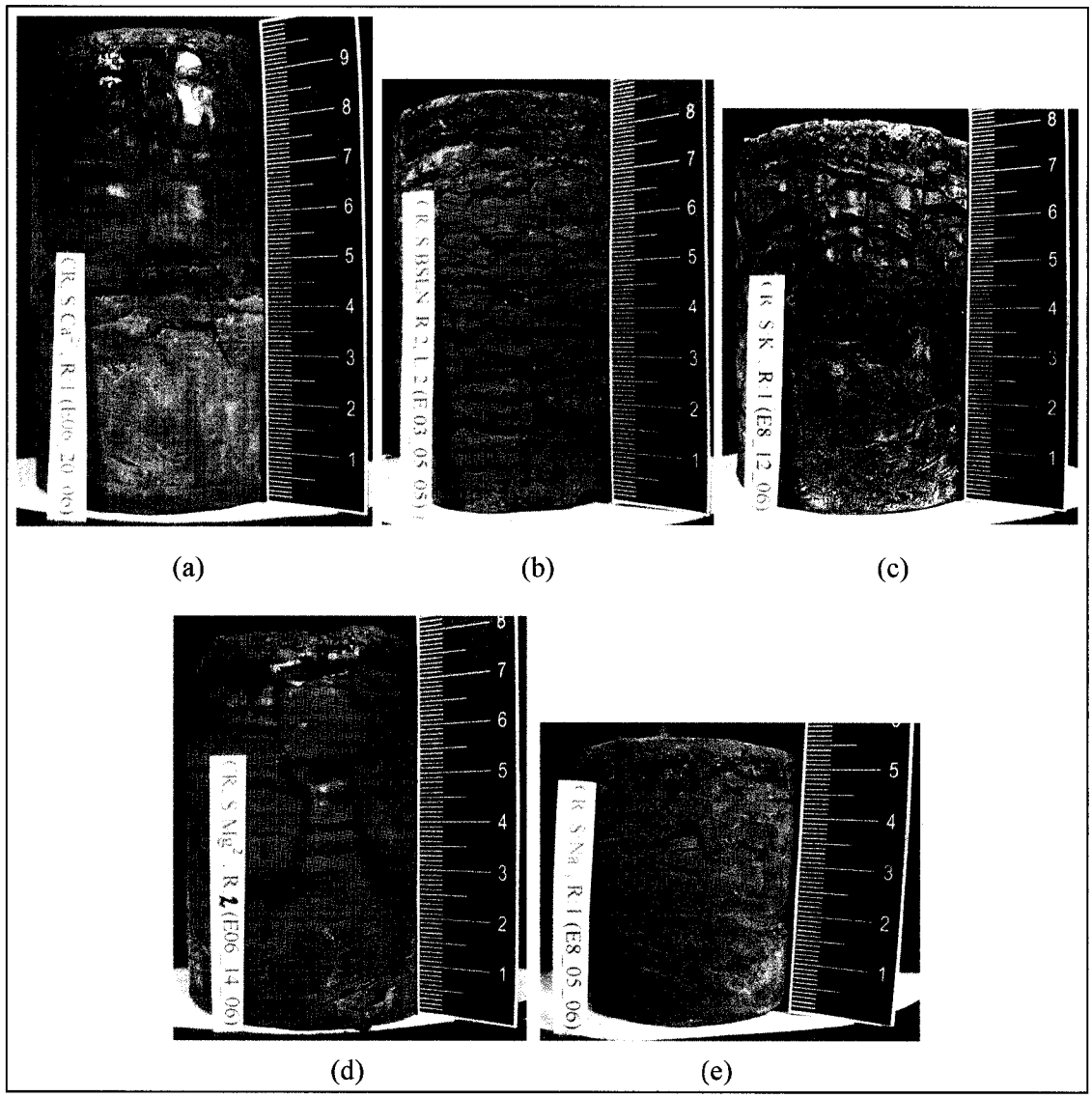

Figure 5.16: Photographs of CR BSLN and cation treatment frost heave test samples. The CR BSLN and different cation treatments shown (with their initial lengths indicated in parentheses) in order of decreasing frost heave ratio are: (a) Ca^{2+} (58 mm), (b) BSLN (57 mm), (c) K^{+} (54 mm), (d) Mg^{2+} (56 mm), and (e) Na^{+} (49 mm).

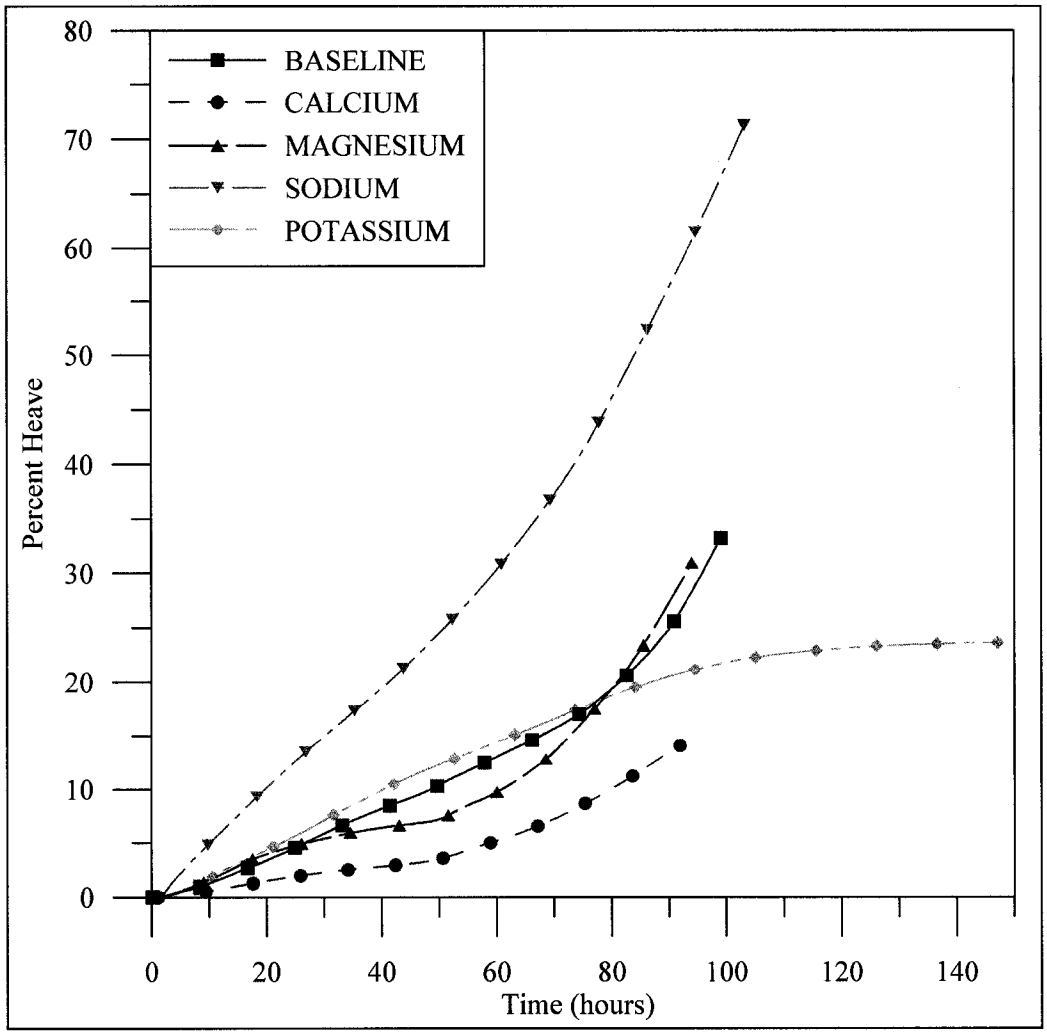

Figure 5.17: DEA BSLN and cation treatment frost heave results

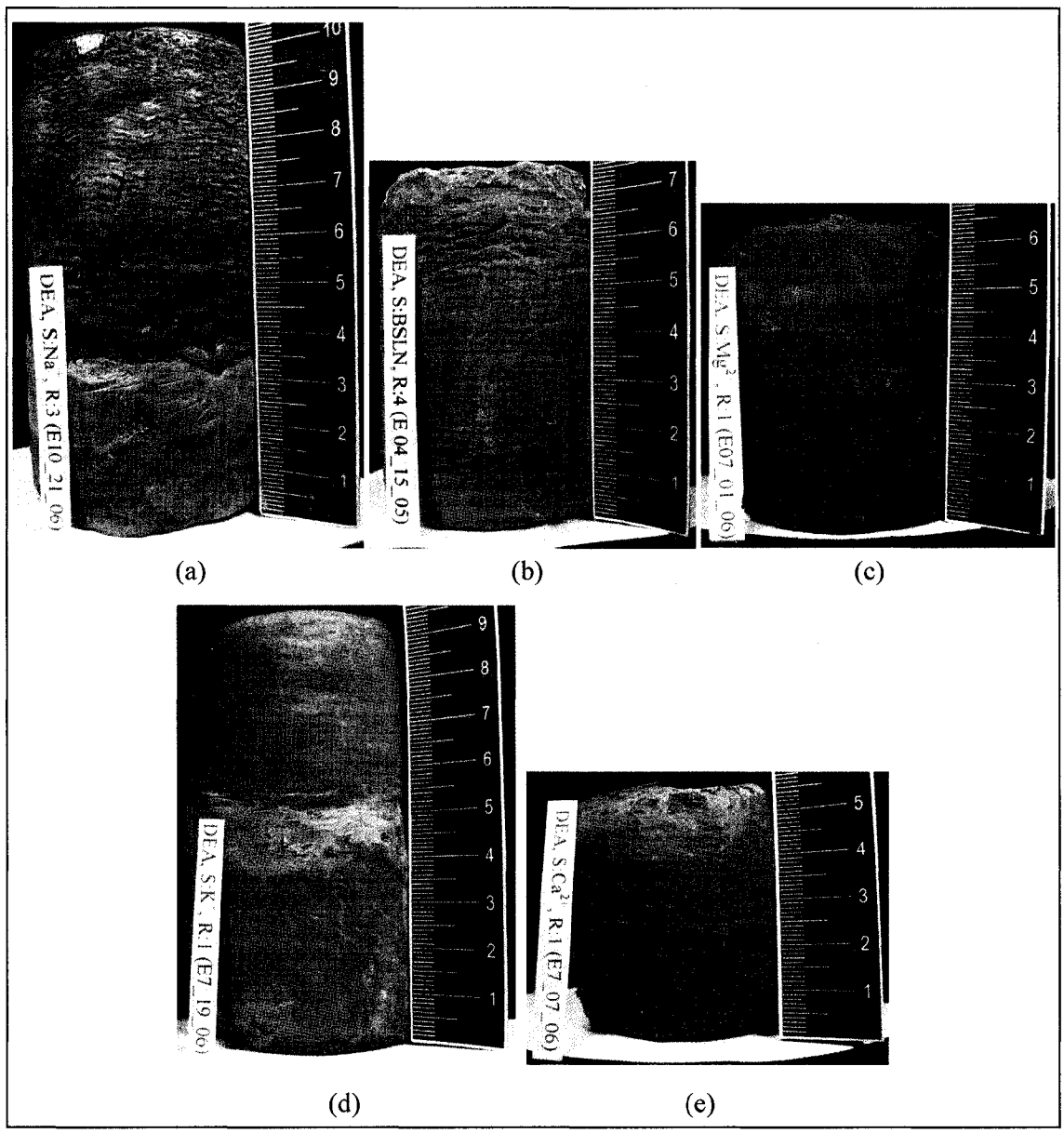

Figure 5.18: Photographs of DEA BSLN and cation treatment frost heave test samples. The DEA BSLN and different cation treatments presented (with their initial lengths) in order of decreasing frost heave ratios: (a) Na^+ (57 mm), (b) BSLN (55 mm), (c) Mg^{2+} (53 mm), (d) K^+ (82 mm), (e) Ca^{2+} (52 mm). The upper three to five mm of the Ca^{2+}- and Mg^{2+}-treated samples thawed and were lost while removing the samples from the acrylic cylinder. These photographs show the remaining sample lengths.

Because samples procured from the upper, fine-grained portion were not long enough for a frost heave test, the DEA Na^+ and K^+ slurries were both consolidated within the frost heave cell. Thus, the results of the DEA Na^+ and K^+ frost heave tests differ from all other tests, as they were frozen "right-side up." Within the acrylic cylinder, the same pattern occurred, as the coarse grains immediately settled to the bottom. The upper, fine-grained portion remained soft at the end of the consolidation period. The initial length of the DEA K^+-treated sample was longer than those of the other samples, due to difficulty in gauging how much slurry was necessary within the acrylic cylinder to procure the appropriate sample length. After the K^+ frost heave test was completed, the bottom portion of the sample was hard, dry, and difficult to remove from the frost heave apparatus. During the first DEA Na^+ frost heave test, an 83-mm thick ice lens formed at the surface of the sample (see Figure 5.19). This massive ice lens contained isolated soil masses. The soil below the ice lens in the cylinder did not segregate and appeared to be desiccated at the end of the test. The DEA Na^+-treated sample was difficult to remove from the frost heave apparatus, due to its longer initial length and massive ice lens. The ice lens was extricated and preserved intact. The soil, however, was unable to be removed intact. To remove the soil, it was necessary to apply air pressure to the bottom of the soil through the lower porous plate, and slice off portions of the sample as it was forced up and out of the acrylic cylinder. A slice of the soil that was below the ice lens is shown on the left in Figure 5.19. Because the bulk of the Na^+-treated sample did not form segregated ice lenses, this frost heave test was considered as an anomaly. A second frost heave test of the DEA Na^+-treated soil was run, and these results are included in Figures 5.17 and 5.18.

The DEA Mg^{2+}- and Ca^{2+}-treated samples could not be removed from the acrylic cylinder before the upper few millimeters of soil thawed and were lost. Thus, the photographs in Figure 5.18 show the samples in their shortened states after testing.

The DEA Na^+-treated sample demonstrated the greatest amount of heave, followed by BSLN, Mg^{2+}, K^+, and Ca^{2+}, in order of their decreasing frost heave ratios. The BSLN, Mg^{2+}, and Ca^{2+} curves shown in Figure 5.17 have a concave appearance, whereas the K^+ curve is convex. This difference in shape is attributed to the orientations of the samples and the corresponding stratification. For example, as the BSLN, Mg^{2+}-, and Ca^{2+}-treated samples were oriented in the standard "upside down" fashion, the HR increased as the freezing front intercepted the fine-grained particles in the lower portion of the sample. This trend is also apparent in Figure

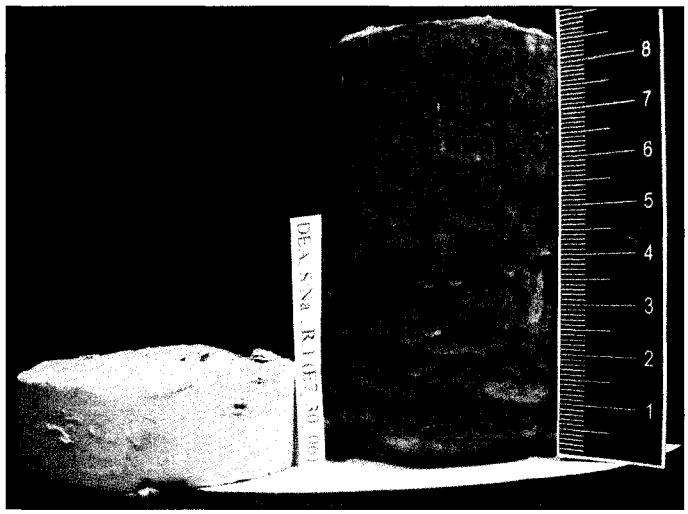

Figure 5.19: Photograph of the first DEA Na^+-treated frost heave test sample. An ~83-mm thick ice lens (shown on the right) formed at the surface of the sample. The soil below the massive ice lens did not segregate and appeared to be desiccated at the end of the test. A portion of the desiccated soil is shown on the left.

5.18(c), in which ice lenses are apparent in the lower portion of the sample but not in the upper portion. Since the K^+-treated sample was highly stratified in the "right side up" orientation, the HR decreased as the coarse-grained particles in the lower portions of the sample were intercepted by the freezing front. These trends are not as apparent for the Na^+-treated sample, which demonstrated an unprecedented amount of heave. The stratification of the DEA Na^+- and K^+-treated samples is highly apparent in Figures 5.18(a) and (d). In these photographs, the bottom portion of each sample has a larger diameter than the upper portion, and is massive, containing no ice lenses. The upper portion of the sample pulled away from the walls of the acrylic cylinder, much like the CR tests; however, the bottom portion remained consolidated tightly against the cylinder wall throughout the test.

The results of the FS BSLN and cation treatment tests are presented in Figure 5.20, with corresponding photographs of the post-freeze samples in Figure 5.21. Following Nersesova's (1961) statement that the addition of certain cations could turn a non-frost susceptible soil into a frost susceptible one, the FS soil was treated with Mg^{2+} and Na^+. The data in Figure 5.20 indicate that neither of the cation treatments applied increased the frost susceptibility of FS. In fact, they both had the opposite effect, with a decrease in the ξ for the Mg^{2+}- and Na^+-treated samples. The Na^+-treated sample experienced consolidation for the first 83 hours of the test, at which point the sample demonstrated a slight upward movement. The photographs in Figure 5.21 show the samples after freezing; however, no evidence of freezing is visible within the samples.

The results of the HS BSLN and cation treatment tests are presented in Figure 5.22, with corresponding photographs of the post-freeze samples in Figure 5.23. As mentioned earlier, the Na^+-treated sample drained very slowly during the chloride rinsing process, the initial consolidation, and during the second consolidation within the frost heave cell. The K^+-treated sample, which also drained slowly, demonstrated a noticeable change in texture. This sample became slippery and soft when wet, like a clay. Stratification was apparent in the K^+-treated sample when it was placed into the acrylic cylinder.

For the HS series, the BSLN soil demonstrated the greatest amount of heave, followed by Na^+, Ca^{2+}, Mg^{2+}, and K^+. The K^+-treated sample expulsed water during the frost heave test. Visual inspection of the post-freezing photograph of the K^+-treated sample does not indicate any evidence of ice lensing (see Figure 5.23(e)). The remaining samples in Figure 5.23 show no signs of desiccation or stratification.

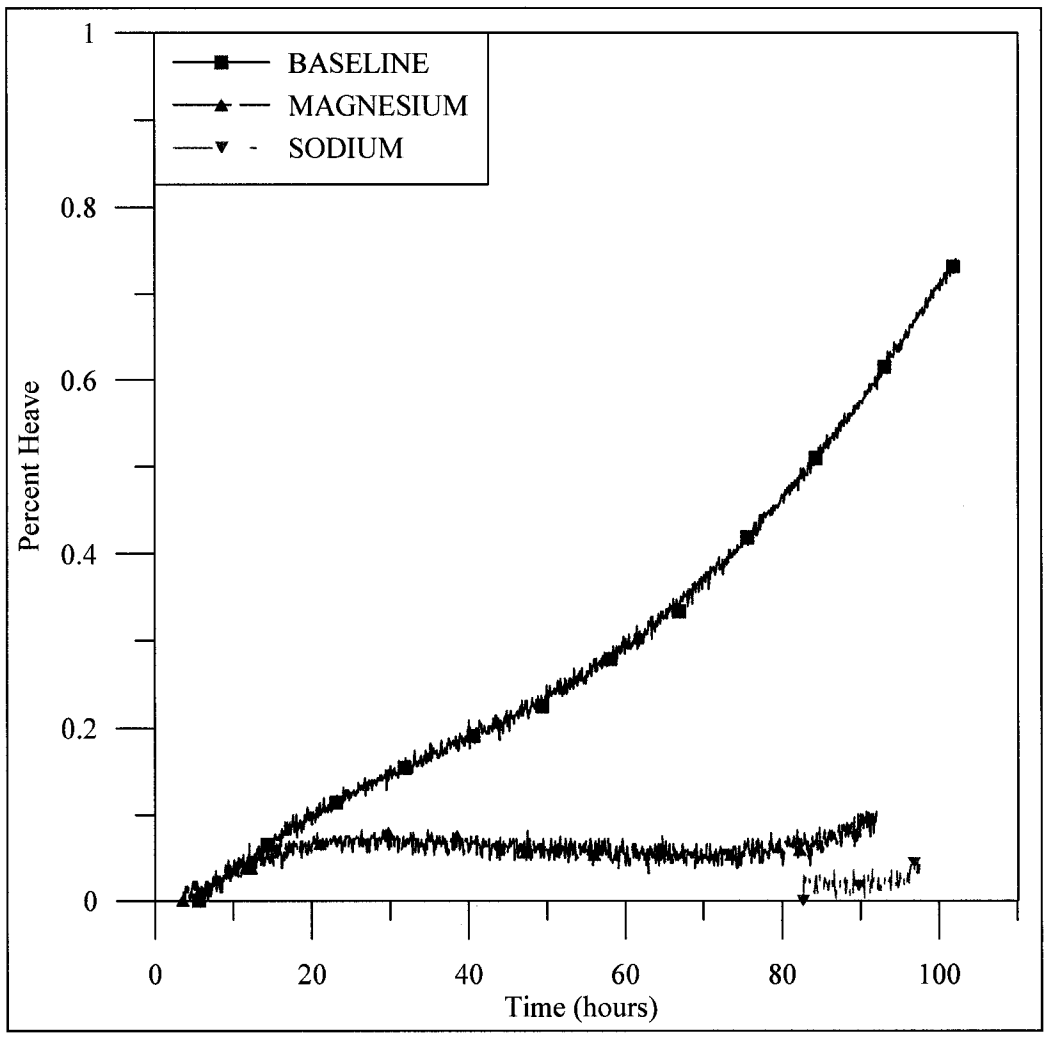

Figure 5.20: FS BSLN and cation treatment frost heave results

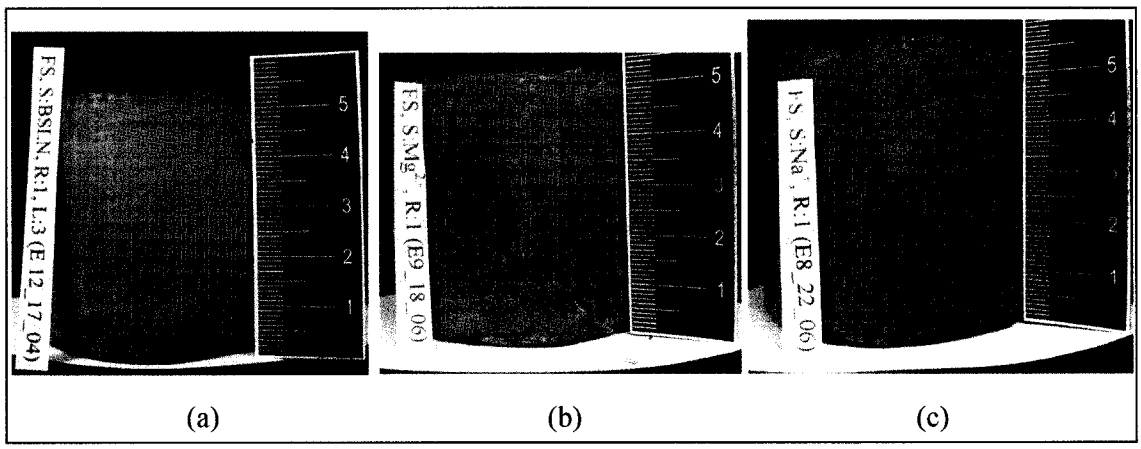

Figure 5.21: Photographs of FS BSLN and cation treatment frost heave test samples. The FS BSLN and different cation treatments shown (with their initial lengths in parentheses) in order of decreasing frost heave ratios are: (a) BSLN (57 mm), (b) Mg^{2+} (52 mm), and (c) Na^{+} (55 mm).

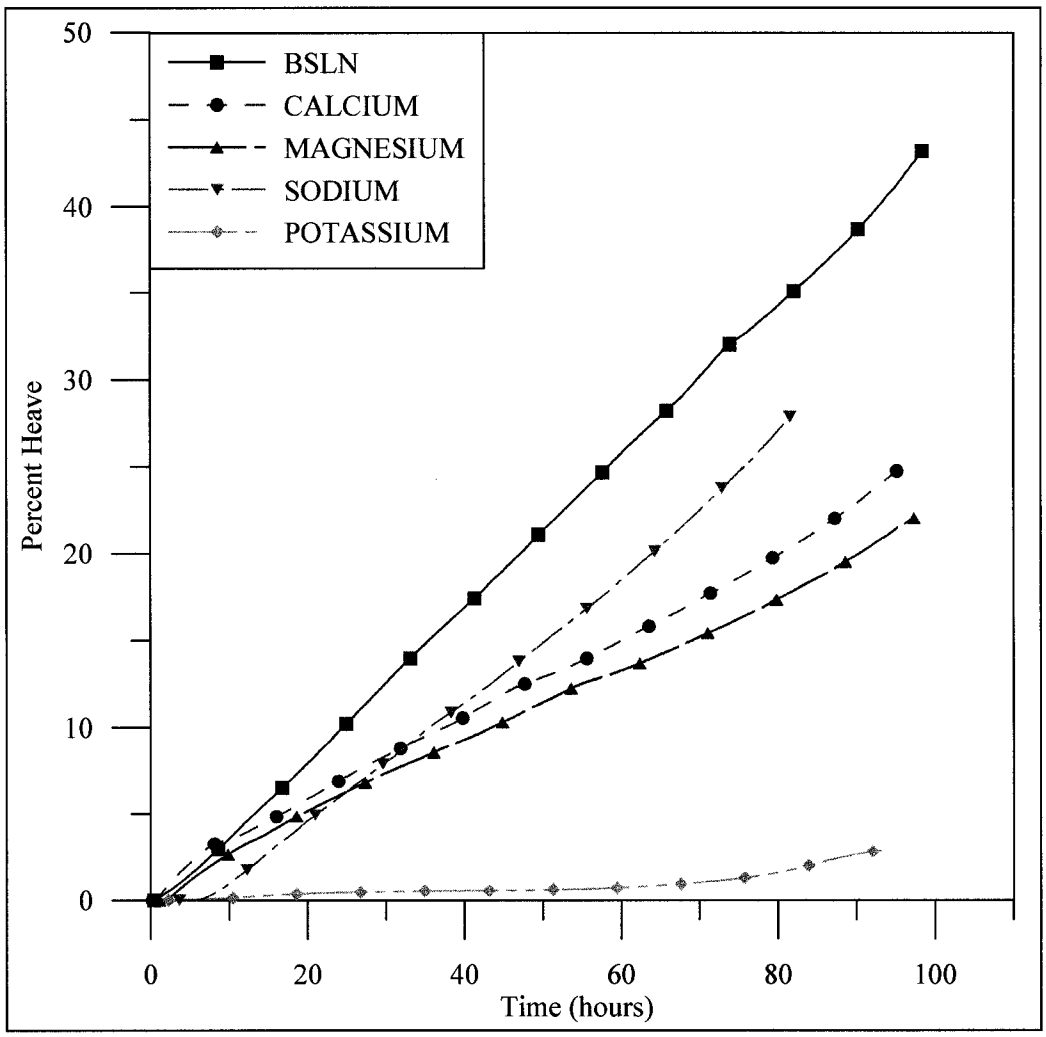

Figure 5.22: HS BSLN and cation treatment frost heave results

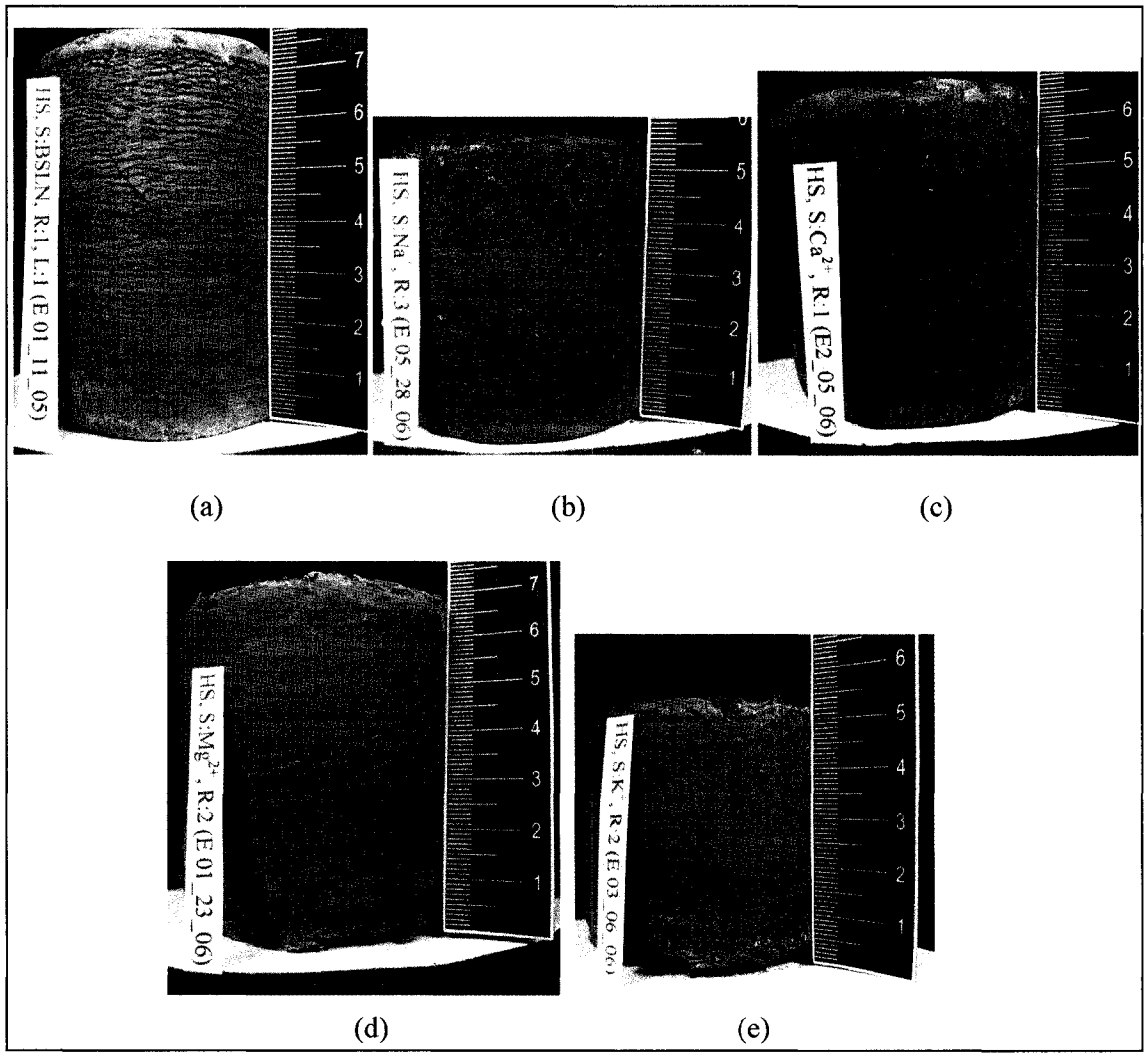

Figure 5.23: Photographs of HS BSLN and cation treatment frost heave test samples. The HS BSLN and different cation treatments shown (with their initial lengths in parentheses) in order of decreasing frost heave ratios are: (a) BSLN (54 mm), (b) Na^{+} (48 mm), (c) Ca^{2+} (54 mm), (d) Mg^{2+} (55 mm), (e) K^{+} (53 mm).

The results of the HV BSLN and cation treatment tests are presented in Figure 5.24, with corresponding photographs of the post-freeze samples in Figure 5.25. Only two cation treatments, Ca^{2+} and Na^{+}, were prepared from this soil. For the HV soil, the BSLN sample demonstrated the most heave, followed by the Ca^{2+}- and Na^{+}-treated samples, respectively. The ice lenses that formed within the Ca^{2+}-treated sample were much smaller than those in the BSLN sample, and were concentrated in the upper portion of the sample. In the Na^{+}-treated sample, ice lenses formed only within the upper 13 mm of the sample. Both the Ca^{2+}- and Na^{+}-treated samples demonstrated some soil desiccation.

A summary of the ξ for all of the BSLN soils and corresponding cation treatments is presented in Table 5.4.

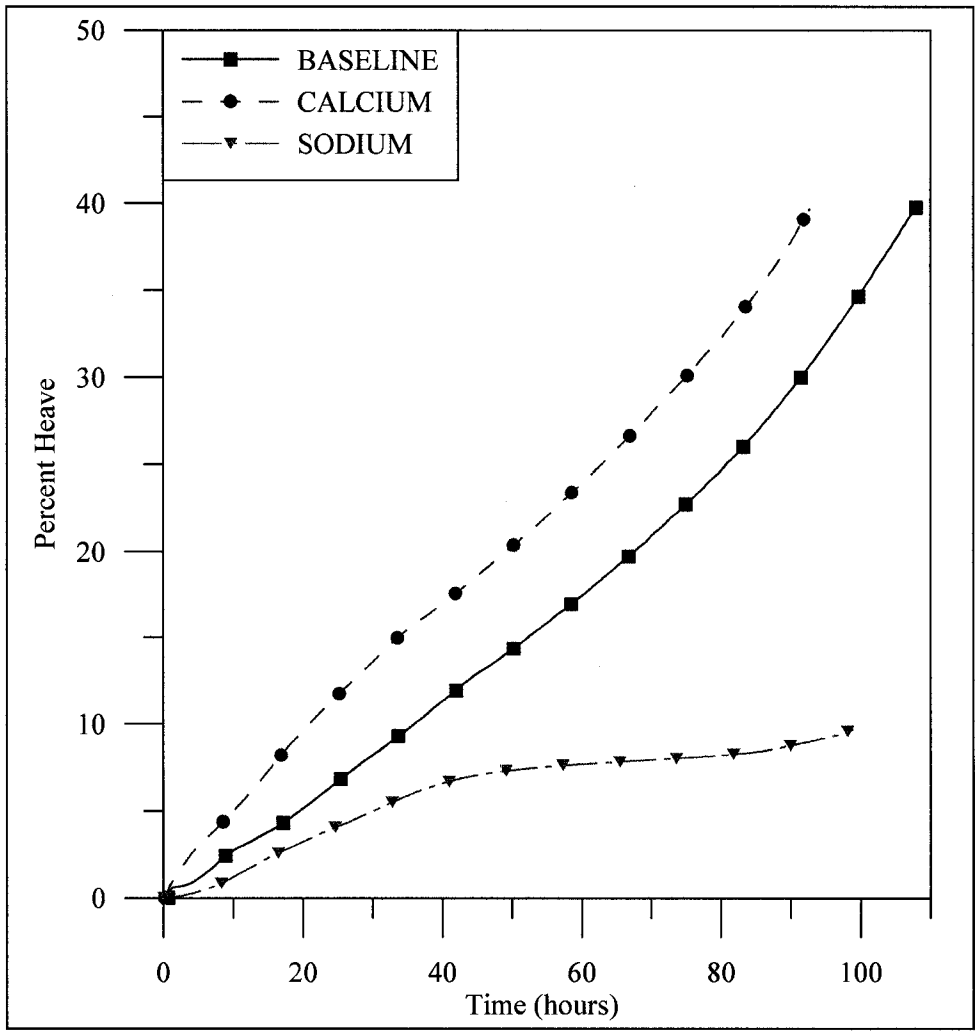

Figure 5.24: HV BSLN and cation treatment frost heave results

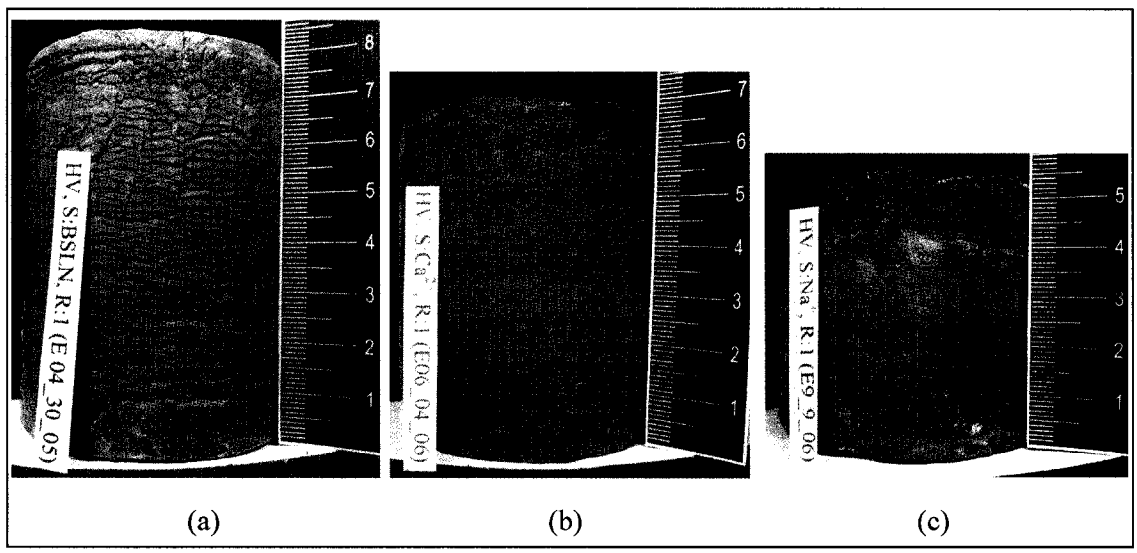

Figure 5.25: Photographs of HV BSLN and cation treatment frost heave test samples. The HV BSLN and different cation treatments presented (with their initial lengths) in order of decreasing frost heave ratio: (a) BSLN (58 mm), (b) Ca^{2+} (53 mm), (c) Na^{+} (55 mm).

Table 5.4: Summary of the frost heave ratios (ξ) of the BSLN soils and corresponding cation treatments

Soil	ξ (%)				
	BSLN	Ca^{2+}	Mg^{2+}	Na^{+}	K^{+}
CR	49.2	65.0	41.6	12.0	47.7
DEA	33.7	14.2	30.9	71.9	23.6
FS	0.7	---	0.1	<0.1	---
HS	43.4	25.0	22.0	28.1	2.9
HV	40.1	39.6	---	9.7	---

CHAPTER 6: ANALYSIS OF CATION EFFECTS ON FROST HEAVING

6.1 Analysis of BSLN Soils' Frost Susceptibilities

As indicated by the results presented in Chapter 5, the five untreated BSLN soils demonstrated a wide range of frost susceptibilities. In order to determine the most important parameters for frost heaving in these untreated soils, a multiple linear regression analysis was performed on the relevant BSLN soil properties and experimental results. Figure 6.1 contains a graphical summary of some of the experimental results. The grain size distributions for the aggregated BSLN samples are presented in Figure 6.1(a). The percent of particles smaller than 2 μm (i.e., clay-sized particles) of each aggregated BSLN soil was determined from these grain size distributions, and will be referred to as C, for brevity. The w_U versus temperature curves for the BSLN samples are presented as Figure 6.1(c). Finally, the revised SMC-SFC relations and comparison of BSLN soils frost heave tests are reproduced as Figures 6.1(b) and (d), respectively. As presented in Section 4.3, the slope of each plot of $\sqrt{\psi_m}$ versus temperature in Figure 6.1(b) is defined as η. Table 6.1 contains a summary of the numerical data used in the multiple linear regression analysis. Most of the data have been reproduced from other sections of this manuscript, with the exception of C, which were calculated from the grain size distributions presented in Figure 6.1(a). The values for smectite, kaolinite, and chlorite are the weight percent of each mineral relative to the bulk sample, with the percent smectite value representing any form of interlayered smectite. The percent of illite/muscovite was not included in this analysis, as a distinction between the illite content and the muscovite content can not be made solely from the XRD analysis (see Appendix C). All statistical analysis was performed using the JMP Statistical Discovery Software Version 3.

The small sample size represented by the BSLN soils limited the number of variables in the multiple linear regression analysis to three. Results from various regressions performed indicate that the three variables demonstrating the highest coefficient of multiple determination (R^2) are ζ potential, cation exchange capacity (CEC), and specific surface area; however, CEC and specific surface area are highly correlated to each other, as the CEC is partially a function of the surface area. The combination of ζ potential, η, and C demonstrated the next highest R^2. While the ζ potential and η are moderately correlated to each other, this model was selected because the three parameters better describe a wider range of soil properties. A summary of the

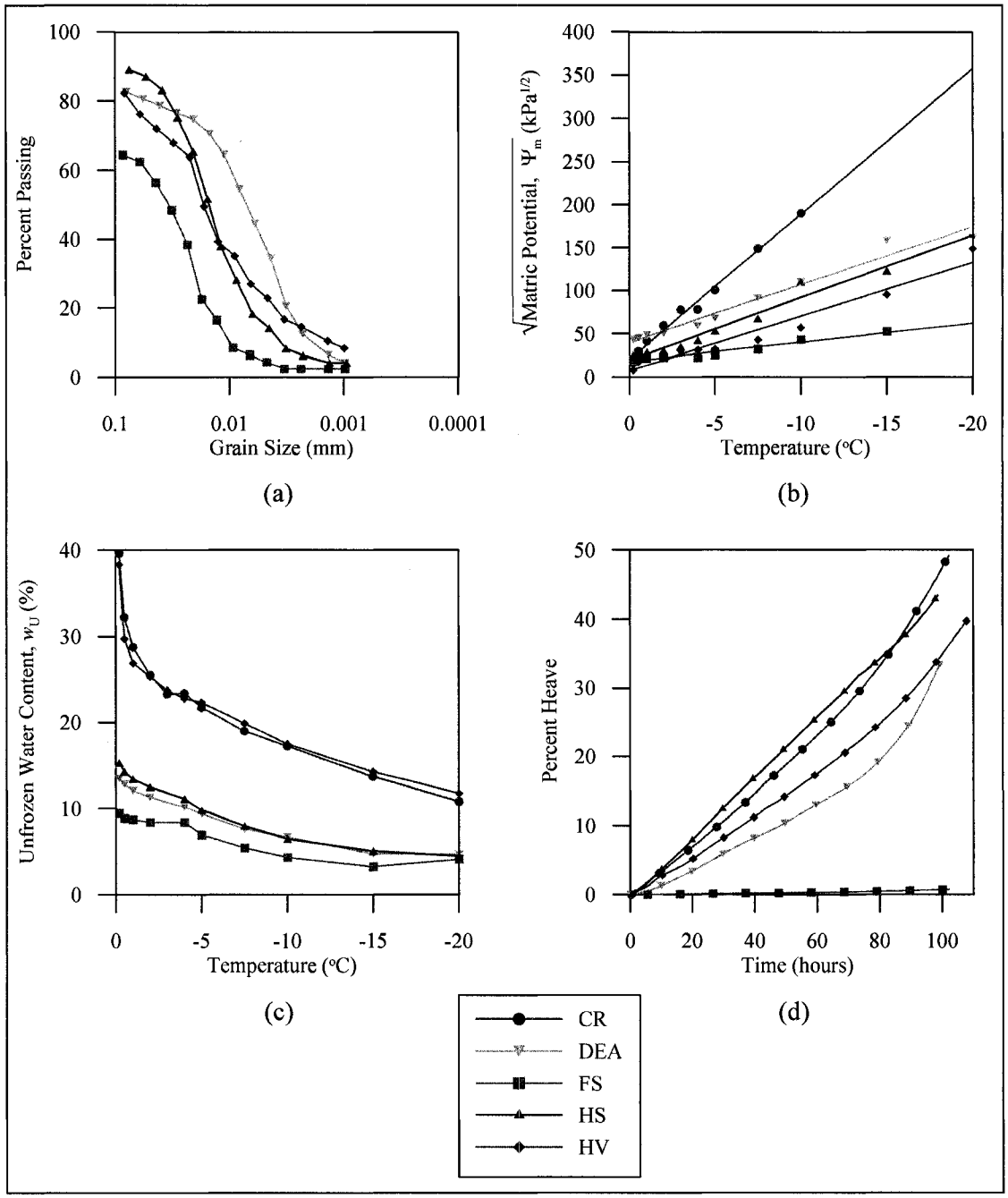

Figure 6.1: Summary of selected BSLN experimental results. The different graphs presented are: (a) grain size distributions for the aggregated BSLN samples; (b) revised SMC-SFC relations (also shown as Figure 4.8); (c) unfrozen water content, w_U, versus temperature; and (d) comparison of BSLN soils frost heave tests (also shown as Figure 5.9).

Table 6.1: Summary of selected BSLN soil properties and experimental results

Soil	Cation Exchange Capacity (mmol/kg)	Specific Surface Area (m^2/g)	C (%)	Smectite* (%)	Kaolinite (%)	Chlorite (%)	w_U at -0.2°C (%)	η ($kPa^{1/2}/°C$)	ζ potential (mV)	ξ (%)
CR	287.0	16.04	4	7.2	1.2	9.7	39.6	16.89	-10.84	49.2
DEA	90.1	5.41	11	0	0.7	5.0	13.4	6.73	-13.48	33.7
FS	112.5	6.54	2	1.5	1.0	2.4	9.4	2.19	-15.36	0.7
HS	101.3	9.25	6	1.8	1.0	6.0	15.2	7.27	-14.17	43.4
HV	136.4	8.44	13	6.7	1.1	3.5	38.3	6.26	-12.86	40.1

* Interlayered smectite

multiple regression output, including a plot of the measured frost heave ratios (ξ) against predicted ξ, is presented in Figure 6.2. The predicted ξ were determined using the resulting equation from the multiple linear regression analysis, which is:

$$\xi = -283.56 - 16.95(\zeta) + 7.93(\eta) + 3.94(C) \quad (6.1)$$

The statistical model results presented in Figure 6.2 indicate that the coefficient of multiple determination for these selected parameters is 0.92. Despite this high value, the analysis of variance (ANOVA) results indicate that this statistical model is not significant (i.e., Pr > F = 0.36). This may be partly due to the small sample size, and use of Equation 6.1 must be tempered by that knowledge. The small sample size precluded the inclusion of more variables that also may affect the soils' ξ.

Despite the apparent lack of significance in the statistical analysis, the frost susceptibility of these natural soils appears to be most correlated to ζ potential, η, and C. Further multiple linear regression analyses of these three parameters indicate that ζ potential and η both are highly correlated to the percentages of smectite, kaolinite, and chlorite present in the soil (see Figures 6.3 and 6.4 for the multiple regression summaries and plots). The relationship of ξ to smectite, kaolinite, and chlorite is presented as a ternary diagram in Figure 6.5. The color contours in this diagram indicate that, for the BSLN soils with their original adsorbed cations, ξ is most sensitive to chlorite content. To summarize, the results of this analysis indicate that for these five BSLN soils, frost heaving is most dependent on adsorbed cations (i.e., ζ potential), water retention properties and unfrozen water content (i.e., η), amount of microaggregates smaller than 2 μm (i.e., C), and the clay content, especially the chlorite content, as represented by ζ potential and η.

It is felt that the demonstrated frost heave behavior of each BSLN soil can be explained qualitatively using the results of the regression analysis and the information presented in Section 2.5. Each of the five BSLN soils contains a mixture of silt- and clay-sized particles that is considered to be frost susceptible by many criteria based solely on grain size distributions; however FS demonstrated an extremely small ξ. FS, which was sampled from an aeolian loess deposit, demonstrated the largest overall grain size distribution, with only two percent of particles smaller than 2 μm (i.e., $C = 2$). FS also contains 9.6 percent clay minerals, including mixed-layer illite/smectite, kaolinite, and chlorite, all of which have moderate to high frost

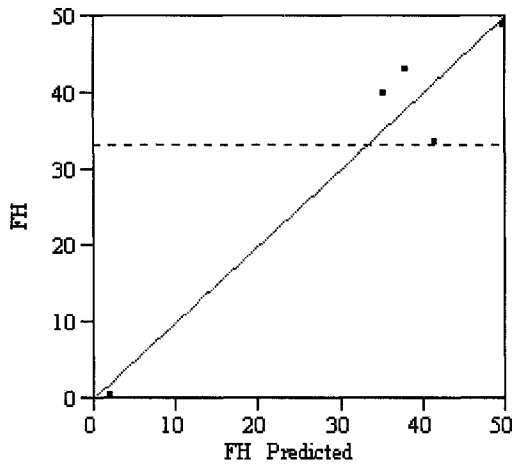

Regression Statistics	
R^2	0.92
R^2 Adjusted	0.68
RMSE	10.89
Mean of Response	33.42
Observations	5

ANOVA

	DF	*SS*	*MS*	*F-value*	*Pr > F*
Regression	3	1345.37	448.65	3.78	0.36
Residual	1	118.54	118.54		
Total	4	1463.91			

	Parameter Estimate	*Standard Error*	*t-value*	*P-value*
Intercept	-283.56	252.23	-1.12	0.46
ζ potential	-16.95	15.29	-1.11	0.47
η	7.93	4.68	1.69	0.34
C	3.94	2.03	1.94	0.30

Figure 6.2: Multiple regression summary output for BSLN soils. Included is a plot of measured frost heave ratios (ξ) against predicted ξ taken from the JMP program output.

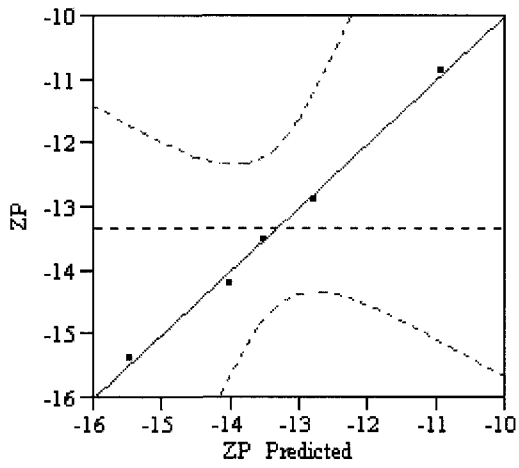

Regression Statistics	
R^2	0.99
R^2 Adjusted	0.98
RMSE	0.22
Mean of Response	-13.34
Observations	5

ANOVA

	DF	*SS*	*MS*	*F-value*	*Pr > F*
Regression	3	11.22	3.74	78.31	0.08
Residual	1	0.05	0.05		
Total	4	11.27			

	Parameter Estimate	*Standard Error*	*t-value*	*P-value*
Intercept	-10.93	0.98	-11.17	0.06
% smectite	0.56	0.07	8.33	0.08
% kaolinite	-6.25	1.14	-5.47	0.12
% chlorite	0.36	0.04	8.29	0.08

Figure 6.3: Multiple regression summary output and plot from ζ potential analysis. The plot was taken from the JMP program output, with the dashed red lines representing 95% confidence intervals.

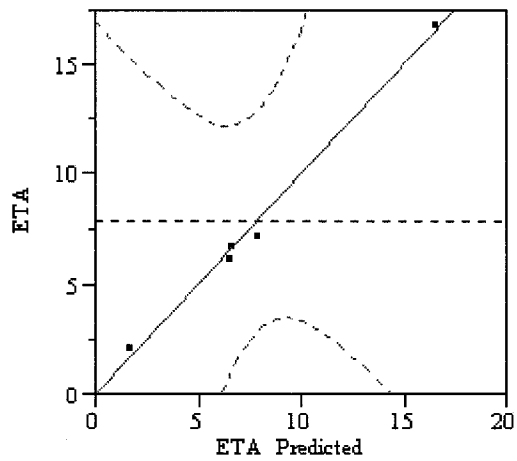

Regression Statistics	
R^2	0.99
R^2 Adjusted	0.97
RMSE	0.88
Mean of Response	7.87
Observations	5

ANOVA

	DF	*SS*	*MS*	*F-value*	*Pr > F*
Regression	3	117.11	39.04	50.79	0.10
Residual	1	0.77	0.77		
Total	4	117.87			

	Parameter Estimate	*Standard Error*	*t-value*	*P-value*
Intercept	2.07	3.92	0.53	0.69
% smectite	0.67	0.27	2.50	0.24
% kaolinite	-5.33	4.58	-1.16	0.45
% chlorite	1.65	0.17	9.53	0.07

Figure 6.4: Multiple regression summary output and plot from η analysis. The plot was taken from the JMP program output, with the dashed red lines representing 95% confidence intervals.

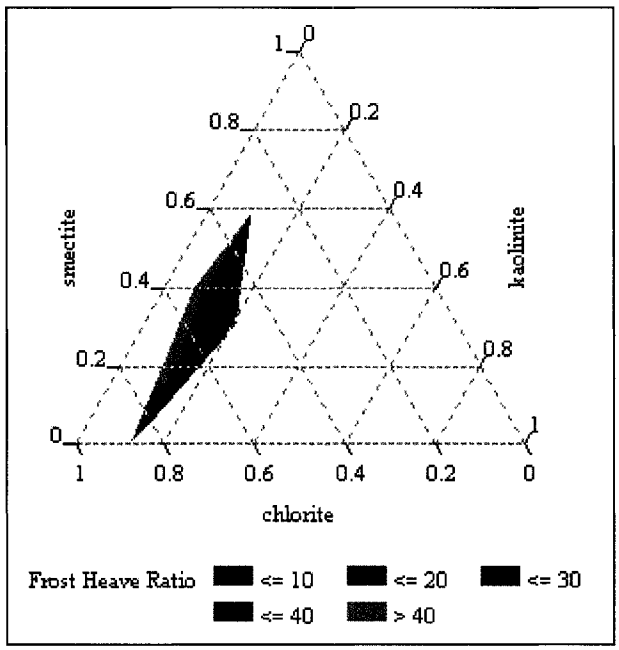

Figure 6.5: Ternary diagram of smectite, kaolinite, and chlorite, with ξ from the BSLN samples as the response variable. The indices on each side of the diagram represent normalized clay content values.

susceptibilities. Despite its clay content, the overall poorly-graded and coarse grain size distribution gives FS low moisture retention properties and a low w_U, which is manifested as a small value for η. The small η, combined with a small C, causes FS to be essentially non-frost susceptible, as demonstrated by its extremely small ξ.

The remaining four BSLN soils have well-graded grain size distributions and some clay content, which gives each a significant ξ. Of all the clay minerals, smectite (including mixed-layer illite/smectite and mixed-layer chlorite/smectite) strongly influences the chemical properties in a given soil because of its high specific surface area. It follows that a soil with a high clay content, and more specifically, with a high smectite content, will have a large value for η. In other words, such a soil will retain water at very high matric potentials, and have a large unfrozen water content at very low temperatures. Soils with high smectite contents are dependent on ζ potential, as this partly determines the structure of the soil and the thickness of the unfrozen water films, and the ζ potential is dependent on the composition of the adsorbed cations. The results of the soluble cation concentration analysis of the BSLN soils presented in Table 2.3 indicate that Ca^{2+} cations are the predominantly adsorbed cation in each of the BSLN soils. Each soil contains some amount of Mg^{2+} and Na^{+}, and very small amounts of K^{+}. It should be noted, however, that this analysis did not account for the presence of trivalent cations that may also be adsorbed by the BSLN soils.

As indicated by the XRD data summarized in Table 6.1, CR has the largest smectite, kaolinite, and chlorite content of the five BSLN soils, resulting in a large η. The predominance of Ca^{2+} as the adsorbed cation causes CR to have a low ζ potential, resulting in the formation of clay microaggregates with thin, relatively mobile unfrozen water films, and an overall high permeability. This combination of clay composition and surface chemistry properties results in CR demonstrating the highest ξ (see Figure 5.10 for a photographs of the post-freeze BSLN samples).

The ξ for the DEA, HS, and HV soils are intermediate to the CR and FS end members. This can be explained by the ζ potential and η, which are also intermediate to those of CR and FS. The HS and HV soils each contain smectite, kaolinite, and chlorite. Although DEA contains no smectite, it does contain an appreciable amount of chlorite, which may have a strong influence on ξ, as indicated by the ternary diagram in Figure 6.5.

6.2 Analysis of Cation Effects on Soil Properties and Frost Heaving

Visual observations of the testing results presented in Chapters 4 and 5 suggest possible trends in the behavior of the cation-treated samples. The results from the grain size distribution analysis (see Section 4.4), ζ potential measurements (see Section 4.5), w_U measurements (see Section 4.2), and frost heave testing (see Section 5.3) were analyzed using statistical methods to further identify trends in behavior. Table 6.2 contains a summary of the numerical data used in the analysis, most of which have been reproduced from other sections of this manuscript. The exceptions to this are the values for C, which were calculated from the grain size distributions presented in Figures 4.9 through 4.13. Values for cation exchange capacity (CEC) and specific surface area were also included in the analysis, and are reported for each BSLN soil in Table 6.1.

Scatter plots of each combination of variables having unique values for each cation-treated sample are presented in Figure 6.6. Linear and second-order polynomial functions were fit to the data in each plot; these trend lines with their coefficients of determination (r^2) are shown in Figure 6.6, if r^2 is greater than 0.1. The trend lines of ζ potential, w_U, and C versus measured ξ indicate that each of these variables may have a nonlinear relationship to ξ (see Figures 6.6(a), (b), and (c), respectively). The plots of w_U and C versus ζ potential do not demonstrate any significant correlation (see Figures 6.6(d) and (e), respectively). The plot of w_U versus C demonstrates a linear trend, with a coefficient of determination of approximately 0.5.

Comparisons of percentages of smectite, kaolinite, and chlorite to measured ξ are presented in Figure 6.7. These graphs include the results from all of the cation-treated samples, as well as the BSLN samples. The FS samples, although containing a moderate amount of smectite and kaolinite, as well as some chlorite, maintain a conspicuous position near the x-axis. The CR samples contain the largest amount of each of the three clays; however, the demonstrated ξ for CR cover a wide range. The DEA, HS, and HV soils typically contain moderate amounts of all three clays. One exception to this is DEA, which contains no smectite, as seen in Figure 6.7(a). Despite this lack of smectite, one of the DEA samples (i.e., the Na^+-treated sample) demonstrated the highest ξ of all samples. The lack of consistent trends in the frost heave behavior of the cation-treated samples as seen in Figure 6.7 indicates that clay content by itself is not sufficient to explain the frost heave behavior of these soils.

Table 6.2: Summary of selected soil properties and experimental results for all BSLN and cation-treated samples

Treatment	ζ potential (mV)	w_U at -0.2°C (%)	C (%)	Total clay (%)	Smectite (%)	Kaolinite (%)	Chlorite (%)	ξ (%)
CR BSLN	-10.84	39.6	4	23.7	7.2	1.2	9.7	49.2
CR Ca^{2+}	-8.13	37.6	17	23.7	7.2	1.2	9.7	65.0
CR Mg^{2+}	-8.92	40.2	10	23.7	7.2	1.2	9.7	41.6
CR Na^{+}	-19.06	63.9	31	23.7	7.2	1.2	9.7	12.0
CR K^{+}	-22.11	38.2	29	23.7	7.2	1.2	9.7	47.7
DEA BSLN	-13.48	13.4	11	8.9	0	5.0	0.7	33.7
DEA Ca^{2+}	-12.86	13.9	11	8.9	0	5.0	0.7	14.2
DEA Mg^{2+}	-15.36	14.0	14	8.9	0	5.0	0.7	30.9
DEA Na^{+}	-30.71	13.3	13	8.9	0	5.0	0.7	71.9
DEA K^{+}	-29.09	15.9	11	8.9	0	5.0	0.7	23.6
FS BSLN	-15.36	9.4	2	9.6	1.5	2.4	1.0	0.7
FS Mg^{2+}	-14.55	18.7	2	9.6	1.5	2.4	1.0	0.1
FS Na^{+}	-21.26	16.2	2	9.6	1.5	2.4	1.0	0.04
HS BSLN	-14.17	15.2	6	20.8	1.8	6.0	1.0	43.4
HS Ca^{2+}	-11.76	15.0	8	20.8	1.8	6.0	1.0	25.0
HS Mg^{2+}	-12.28	15.1	6	20.8	1.8	6.0	1.0	22.0
HS Na^{+}	-19.74	19.8	8	20.8	1.8	6.0	1.0	28.1
HS K^{+}	-15.79	29.4	12	20.8	1.8	6.0	1.0	2.9
HV BSLN	-12.86	38.3	13	18.7	6.7	3.5	1.1	40.1
HV Ca^{2+}	-11.76	28.0	17	18.7	6.7	3.5	1.1	39.6
HV Na^{+}	-29.09	61.1	23	18.7	6.7	3.5	1.1	9.7

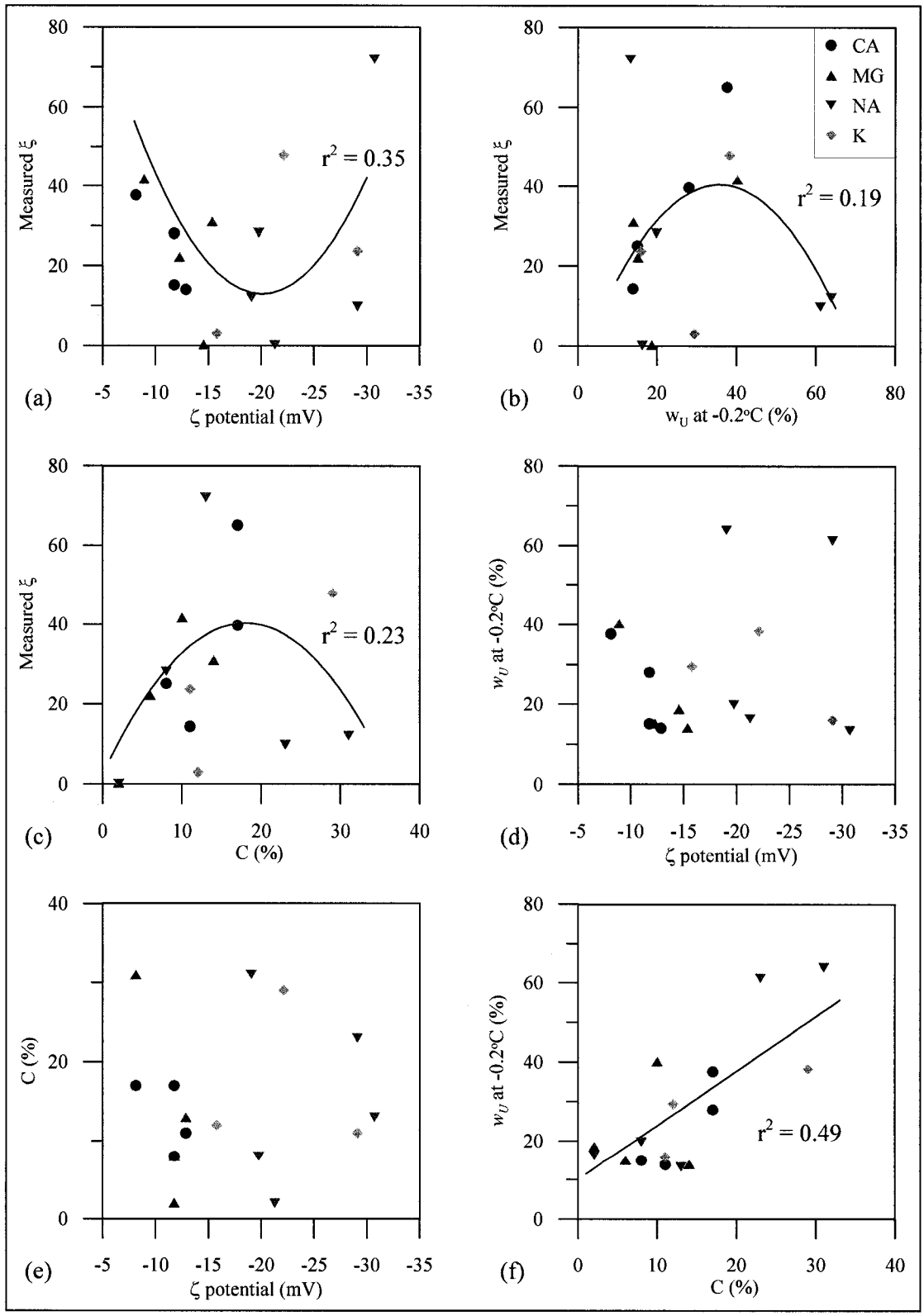

Figure 6.6: Scatter plots of measured experimental variables

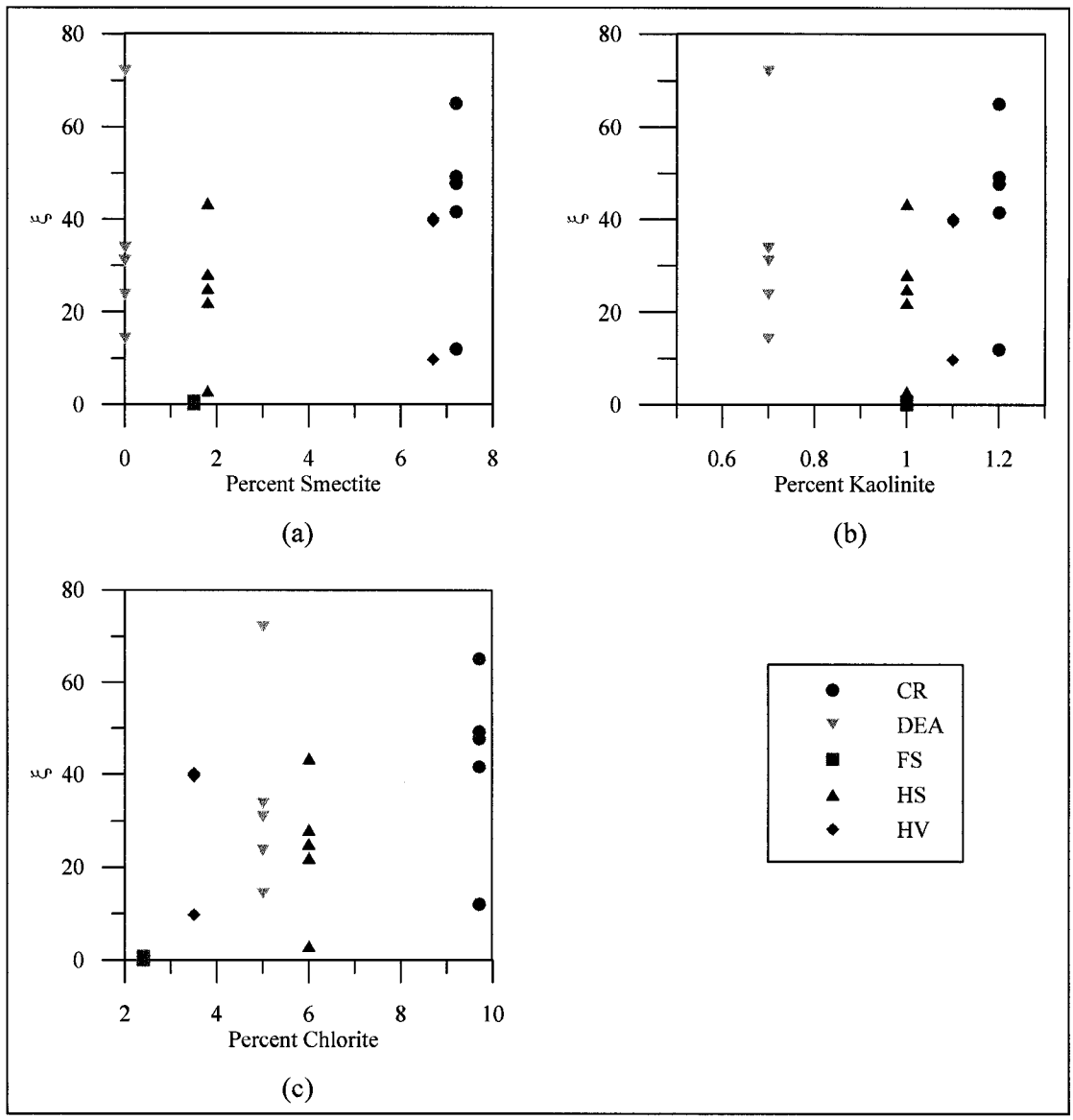

Figure 6.7: Comparison of measured ξ versus amounts of smectite, kaolinite, and chlorite. The measured ξ for all tests versus percentages of smectite, kaolinite, and chlorite are shown in (a), (b), and (c), respectively.

Figure 6.8 contains ternary diagrams of smectite, kaolinite, and chlorite for each of the four different cation treatments. For each diagram, the color contours represent the response of ξ to amounts of these three clays. The diagrams indicate that, for all of the cation treatments, ξ is most sensitive to chlorite content. In addition to this correlation to chlorite, the diagram for Na^+ treatments (see Figure 6.8(c)) indicates a secondary correlation to smectite.

Multiple linear regression analyses were performed for each group of cation treatments. The small size of these groups (i.e., five samples for Na^+, four samples for both Ca^{2+} and Mg^{2+}, and three samples for K^+) limited the number of variables in the regression analyses to between one and three. Combinations of all variables summarized in Table 6.2, a well as CEC and specific surface area, were investigated in order to determine the set of variables that most explains the frost heave behavior for each cation treatment. Additionally, regressions were run on the cross products of ζ potential and w_U, since the trend lines in Figure 6.6 indicate non-linear relationships for these variables. Summaries of the regression output for each cation treatment, including plots of the measured frost heave ratios (ξ) against predicted ξ, are presented as Figures 6.9 through 6.12. For the Ca^{2+}-treated samples, ξ is highly correlated to w_U and to the cross of ζ potential with itself, with a demonstrated R^2 of 0.99 (see Figure 6.9). The resulting empirical relationship for the four Ca^{2+}-treated samples is:

$$\xi = 36.72 - 0.22(\zeta)^2 + 1.16(w_U) \tag{6.2}$$

For the Mg^{2+}-treated samples, ξ is highly correlated to the percent of chlorite and to the cross of ζ potential with itself, with a demonstrated R^2 of 0.99 (see Figure 6.10). The resulting empirical relationship for the four Mg^{2+}-treated samples is:

$$\xi = -70.24 + 0.22(\zeta)^2 + 9.72(\%Cl) \tag{6.3}$$

where $\%Cl$ is the weight percent of chlorite relative to the bulk sample. For the Na^+-treated samples, ξ is highly correlated to the percent of chlorite, w_U, and to the cross of ζ potential with itself, with a demonstrated R^2 of 0.99 (see Figure 6.11). The resulting empirical relationship for the five Na^+-treated samples is:

$$\xi = -45.2 + 0.09(\zeta)^2 - 0.9(w_U) + 8.52(\%Cl) \tag{6.4}$$

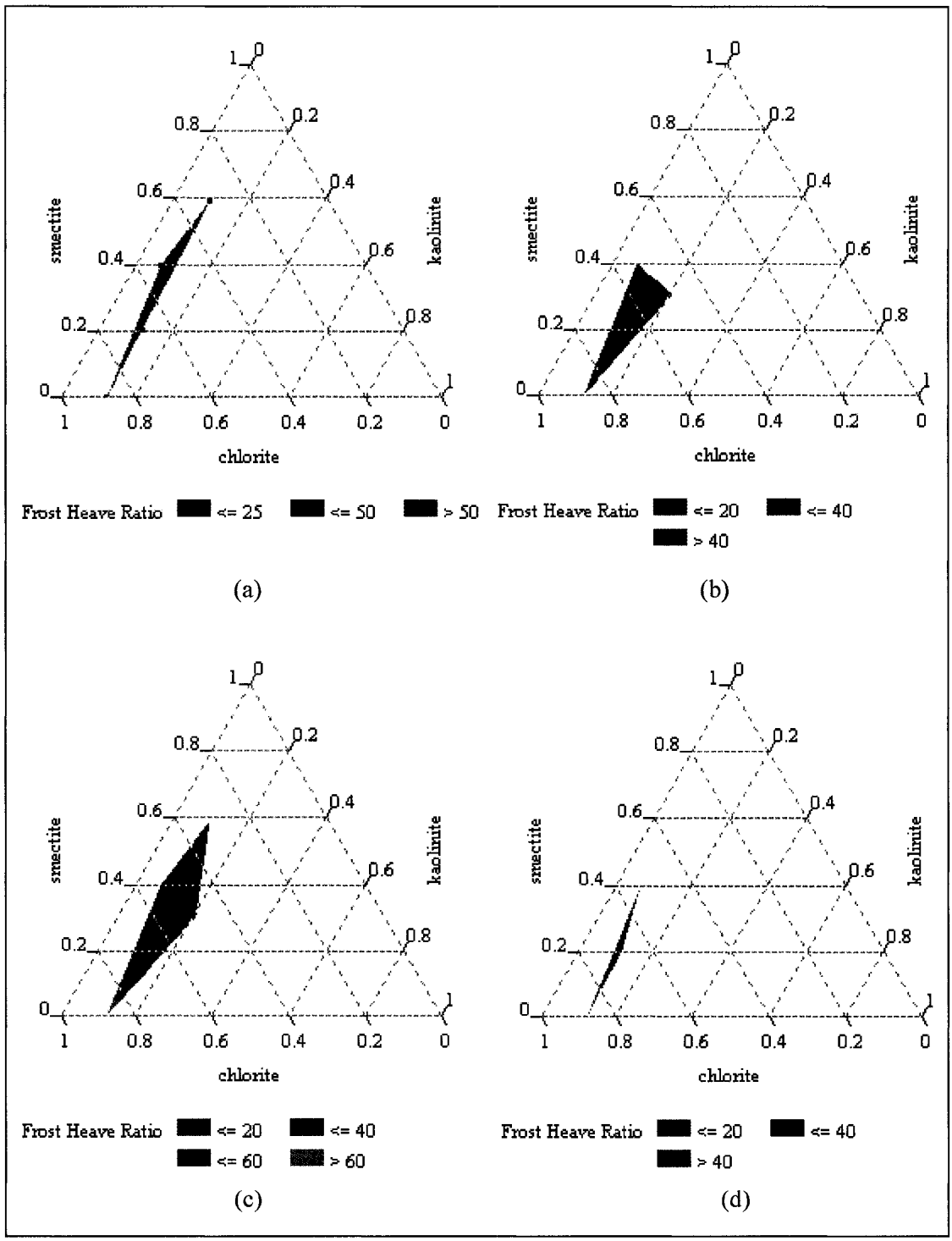

Figure 6.8: Ternary diagrams of smectite, kaolinite, and chlorite, with ξ as the response variable. The four plots represent results from the four different cation treatment groups: (a) Ca^{2+}, (b) Mg^{2+}, (c) Na^{+}, and (d) K^{+}. The indices on each side of the diagram represent normalized clay content values.

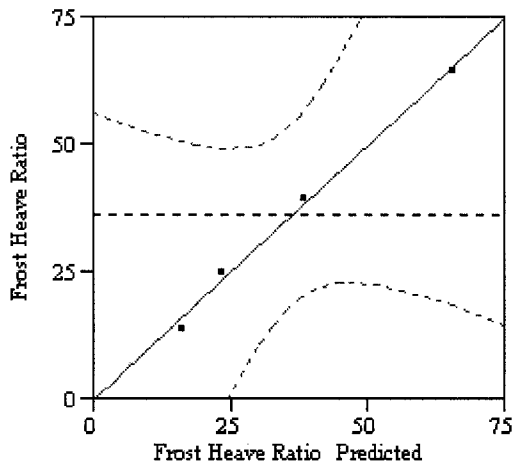

Regression Statistics	
R^2	0.99
R^2 Adjusted	0.98
RMSE	2.81
Mean of Response	35.95
Observations	4

ANOVA

	DF	*SS*	*MS*	*F-value*	*Pr > F*
Regression	2	1442.27	721.14	91.10	0.07
Residual	1	7.92	7.92		
Total	3	1450.19			

	Parameter Estimate	*Standard Error*	*t-value*	*P-value*
Intercept	36.72	17.03	2.16	0.28
$\zeta \cdot \zeta$	-0.22	0.08	-2.74	0.22
w_U	1.16	0.30	3.81	0.16

Figure 6.9: Multiple regression summary output and plot from Ca^{2+} treatment analysis. The plot was taken from the JMP program output, with the dashed red lines representing 95% confidence intervals.

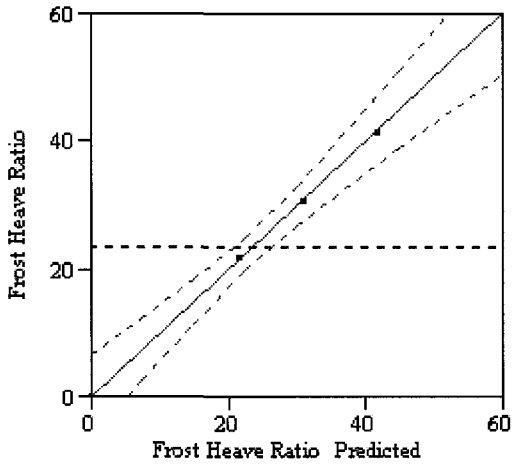

Regression Statistics	
R^2	0.99
R^2 Adjusted	0.99
RMSE	0.40
Mean of Response	23.65
Observations	4

ANOVA

	DF	*SS*	*MS*	*F-value*	*Pr > F*
Regression	2	931.93	465.97	2957.55	0.01
Residual	1	0.16	0.16		
Total	3	932.09			

	Parameter Estimate	*Standard Error*	*t-value*	*P-value*
Intercept	-70.24	1.96	-35.89	0.02
$\zeta \cdot \zeta$	0.22	0.006	33.52	0.02
Chlorite (%)	9.72	0.15	63.32	0.01

Figure 6.10: Multiple regression summary output and plot from Mg^{2+} treatment analysis. The plot was taken from the JMP program output, with the dashed red lines representing 95% confidence intervals.

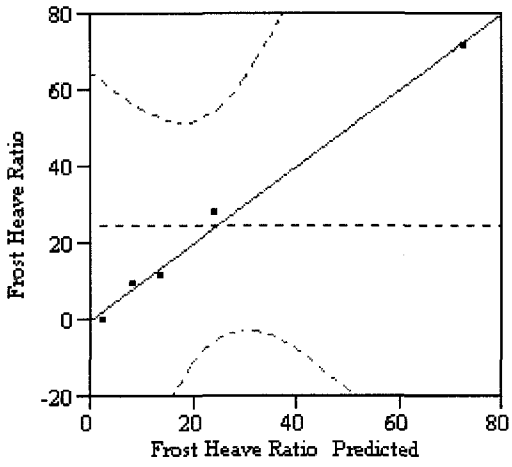

Regression Statistics	
R^2	0.99
R^2 Adjusted	0.97
RMSE	5.25
Mean of Response	24.35
Observations	5

ANOVA

	DF	*SS*	*MS*	*F-value*	*Pr > F*
Regression	3	3205.61	1068.54	38.75	0.12
Residual	1	27.57	27.57		
Total	4	3233.19			

	Parameter Estimate	*Standard Error*	*t-value*	*P-value*
Intercept	-45.20	10.26	-4.41	0.14
$\zeta \cdot \zeta$	0.09	0.01	8.66	0.07
w_U	-0.90	0.12	-7.61	0.08
Chlorite (%)	8.52	1.17	7.27	0.09

Figure 6.11: Multiple regression summary output and plot from Na^+ treatment analysis. The plot was taken from the JMP program output, with the dashed red lines representing 95% confidence intervals.

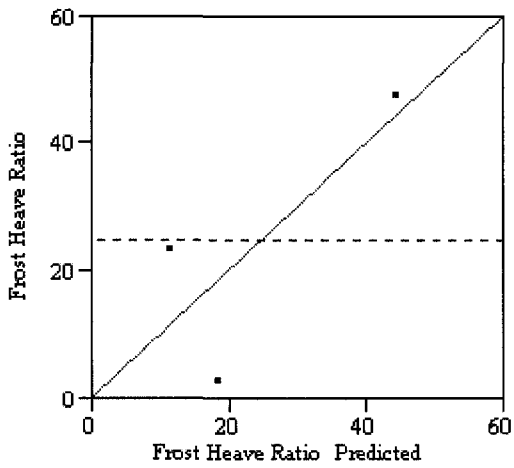

Regression Statistics	
R^2	0.60
R^2 Adjusted	0.20
RMSE	20.02
Mean of Response	24.73
Observations	3

ANOVA

	DF	*SS*	*MS*	*F-value*	*Pr > F*
Regression	1	604.81	604.81	1.51	0.43
Residual	1	400.64	400.64		
Total	2	1005.45			

	Parameter Estimate	*Standard Error*	*t-value*	*P-value*
Intercept	-23.73	41.10	-0.58	0.67
Chlorite (%)	7.02	5.72	1.23	0.43

Figure 6.12: Multiple regression summary output and plot from K^+ treatment analysis

Finally, the results of the statistical analysis for the K^+-treated samples are presented in Figure 6.12. The best statistical model indicates that ξ is correlated to the percent of chlorite; however, the R^2 for this model is 0.6, indicating that this model is marginally significant. Additionally, the small sample size for K^+ treatments makes this group of treatments a poor candidate for statistical analysis.

Multiple linear regression analyses were performed on the entire group of BSLN and cation-treated samples, using the data presented in Table 6.2 along with the CEC and specific surface area, in order to determine if a combination of variables exists that may explain the frost heave behavior for all of these soils and treatments. In Table 6.2, the values for percent total clay represent the percentage of clay minerals relative to the bulk sample of each soil as determined by the semi-quantitative XRD analysis. The values for smectite, kaolinite, and chlorite are the weight percent of each mineral relative to the bulk sample, with the percent smectite value representing any form of interlayered smectite. The percentage of illite/muscovite was not included in this analysis, as a distinction between the illite content and muscovite content can not be made solely from XRD analysis (see Appendix C).

Analysis of the regression results indicated that C, the total amount of clay present in the soil, CEC, and specific surface area were not significant variables. Further multiple regression analyses were conducted using only the ζ potential, w_U, and the amount of smectite, kaolinite, and chlorite in the soil. Additionally, regressions were run on the cross products of ζ potential and w_U, since the trend lines in Figure 6.6 indicate non-linear relationships for these variables. The results from the most significant statistical model, which demonstrated a coefficient of multiple determination (R^2) of 0.73, are presented in Figure 6.13. This relatively high R^2 indicates that much of the variation in measured ξ may be described by ζ potential crossed by itself, w_U, and the amount of smectite, kaolinite, and chlorite in the soil. Additionally, the analysis of variance results indicate that this statistical model is significant, as do the P-values for each variable used in the regression. The predicted ξ included in the plot in Figure 6.13 were determined using the resulting equation from the multiple linear regression analysis, which is:

$$\xi = 94.9 + 0.03(\zeta)^2 - 1.65(w_U) + 13.07(\%Sm) - 102.5(\%Ka) + 4.78(\%Cl) \quad (6.5)$$

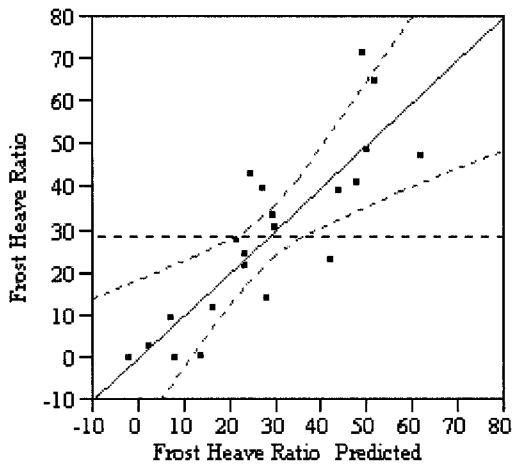

Regression Statistics	
R^2	0.73
R^2 Adjusted	0.64
RMSE	12.49
Mean of Response	28.64
Observations	21

ANOVA

	DF	*SS*	*MS*	*F-value*	*Pr > F*
Regression	5	6308.61	1261.72	8.08	<0.001
Residual	15	2341.69	156.11		
Total	20	8650.30			

	Parameter Estimate	*Standard Error*	*t-value*	*P-value*
Intercept	94.90	30.58	3.10	0.007
$\zeta \cdot \zeta$	0.03	0.01	1.91	0.08
w_U	-1.65	0.39	-4.18	<0.001
Smectite (%)	13.07	2.77	4.71	<0.001
Kaolinite (%)	-102.50	33.85	-3.03	0.009
Chlorite (%)	4.78	1.32	3.61	0.003

Figure 6.13: Multiple regression summary output for all BSLN and cation-treated samples. The plot was taken from the JMP program output, with the dashed red lines representing 95% confidence intervals.

where $\%Sm$, $\%Ka$, and $\%Cl$ are the weight percents of smectite, kaolinite, and chlorite, respectively, relative to the bulk sample. The parameters in Equation 6.5 listed in order of decreasing significance, as determined by the P-values, are w_U and smectite, chlorite, the cross product of ζ potential, and kaolinite. The use of Equation 6.5 in predicting ξ must be tempered by the knowledge that the equation was determined from 21 samples derived from five very different soils.

To summarize, the results of this analysis indicate that for the entire group of samples tested for this research, frost heaving is most dependent on adsorbed cations (i.e., ζ potential), w_U, and the amount of smectite, kaolinite, and chlorite present in the soil. The results of the statistical analysis of the individual cation treatments indicate that the frost susceptibility of: 1) Ca^{2+}-saturated soil is most dependent on ζ potential and w_U; 2) Mg^{2+}-saturated soil is most dependent on ζ potential and amount of chlorite; and 3) Na^{+}-saturated soil is most dependent on ζ potential, w_U, and the amount of chlorite. These results generally are consistent with the BSLN analysis results presented in Section 6.1. For the BSLN samples, however, the additional variable η was available for the statistical analysis. Because η describes a soil's water retention properties at increasing ψ_m and decreasing temperatures, it may be of essential importance in quantifying ξ. Thus, it is suggested that future research include the determination of soil-moisture characteristic curves for each of the cation-treated samples used in this study. The veracity of the empirical equations developed from the analysis presented in this chapter should be confirmed, and refinements made, by similar testing conducted on additional disparate soils. Finally, the activity of each of the cation-treated soils should be determined and included in future multiple linear regression analysis.

CHAPTER 7: CONCLUSIONS

7.1 Executive Summary

Rigorous frost heaving research began over 80 years ago. The resulting voluminous body of research can be divided into three broad categories, namely theory, laboratory and field experiments, and numerical modeling. Of the copious laboratory experiments conducted, the investigation of mineral surface effects on frost heaving has received little attention. The few individuals who conducted research in this area did so nearly 50 years ago with rudimentary frost heave testing apparatus that had poor temperature control and low repeatability. Furthermore, much of the previous testing was conducted on homogenous soils or artificial blends that have limited applicability to actual field conditions.

The purpose of the research presented in this dissertation is to investigate the adsorbed cation effects on the frost susceptibility of natural heterogeneous soils through experimental testing. A comprehensive suite of laboratory experiments was conducted on five natural heterogeneous soils. The exchangeable cations of each soil were varied systematically, with Ca^{2+}-, Mg^{2+}-, Na^{+}-, and K^{+}-treated samples prepared from the natural soils. Experimental testing conducted for this research included measurements of engineering index properties, chemical properties, clay content and mineralogy, soil-moisture characteristic (SMC) curves, unfrozen water content (w_U), zeta (ζ) potential, and frost heave testing.

To determine the soils' inherent frost susceptibilities, frost heave tests were conducted using a state-of-the-art laboratory system. The system consists of: a modified refrigerator; a frost heave test cell; a laser for measuring heave; a differential pressure transducer for measuring water intake; and platinum resistance temperature detectors for measuring pedestal temperatures. The modified refrigerator maintains the specified temperature ±0.5°C during the full length of the test, which typically is not possible for larger cold rooms. The frost heave testing apparatus and associated testing procedure produce highly repeatable results, as indicated by the low variability of frost heave ratios (ξ) (i.e., less than 7 percent) and average heave rates (i.e., less than 0.05 mm/hr) of tested replicates. This high level of repeatability allows for a more sophisticated analysis of demonstrated trends in the data.

A comparison of the SMC and w_U data obtained for each of the five soils allowed the development of soil-moisture characteristic-soil freezing characteristic (SMC-SFC) relations over an unprecedented range of measurements. The results indicate that corresponding points on

the SMC and SFC curves for the BSLN soils are related by

$$\sqrt{(\Delta P_a - \Delta P_w)} = \eta \cdot \Delta T \tag{4.8}$$

where $(\Delta P_a - \Delta P_w)$ is equal to the matric potential (ψ_m), and ΔT is the difference in temperature from the melting point in °C, which can be derived from the Clausius-Clapeyron equation. The coefficient η in Equation 4.8 is equivalent to the slope of a plot of $\sqrt{\psi_m}$ versus temperature.

The five untreated BSLN soils demonstrated significantly different ξ, ranging from 0.7 percent to 49.2 percent. The results of a multiple linear regression analysis of the BSLN experimental data indicate that the predicted ξ can be determined by:

$$\xi = -283.56 - 16.95(\zeta) + 7.93(\eta) + 3.94(C) \tag{6.1}$$

where C is the percent of particles smaller than 2 μm. Further regression analyses indicate that ζ potential and η are highly correlated to the percentages of smectite, kaolinite, and chlorite present in the soil. To summarize, the statistical analysis indicates that the frost susceptibility of the five BSLN soils is most dependent on adsorbed cations (i.e., ζ potential), water retention properties and unfrozen water content (i.e., η), amount of microaggregates smaller than 2 μm (i.e., C), and the clay content, especially the chlorite content, as represented by ζ potential and η.

The experimental results indicate that changing the predominately adsorbed cation in a natural soil greatly affects the soil's properties and frost susceptibility. The demonstrated ξ for all cation-treated samples appears to be most sensitive to the types and amounts of clay in the soil, especially the amount of chlorite. For the Ca^{2+}, Mg^{2+}, and Na^{+} treatments, the predicted ξ can be determined by the following equations, respectively:

$$\xi_{Ca^{2+}} = 36.72 - 0.22(\zeta)^2 + 1.16(w_U) \tag{6.2}$$

$$\xi_{Mg^{2+}} = -70.24 + 0.22(\zeta)^2 + 9.72(\%Cl) \tag{6.3}$$

$$\xi_{Na^{+}} = -45.2 + 0.09(\zeta)^2 - 0.9(w_U) + 8.52(\%Cl) \tag{6.4}$$

where $\%Cl$ is the weight percent of chlorite relative to the bulk sample. The small K^{+} treatment sample size precludes the development of a similar empirical relationship. Multiple linear regression analyses were performed on the entire group of BSLN and cation-treated samples,

resulting in the following empirical relationship:

$$\xi = 94.9 + 0.03(\zeta)^2 - 1.65(w_U) + 13.07(\%Sm) - 102.5(\%Ka) + 4.78(\%Cl) \quad (6.5)$$

where $\%Sm$, $\%Ka$, and $\%Cl$ are the weight percents of smectite, kaolinite, and chlorite, respectively, relative to the bulk sample.

The results of this statistical analysis indicate that for all untreated and cation-treated samples, frost heaving is most dependent on adsorbed cations (i.e., ζ potential), w_U, and the amount of smectite, kaolinite, and chlorite present in the soil. The results from each cation treatment indicate that the frost susceptibility of: 1) Ca^{2+}-saturated soil is most dependent on ζ potential and w_U; 2) Mg^{2+}-saturated soil is most dependent on ζ potential and amount of chlorite; and 3) Na^{+}-saturated soil is most dependent on ζ potential, w_U, and the amount of chlorite.

7.2 Significant Contributions from this Research

There are several notable contributions from the body of research presented here. First, this dissertation serves as a repository for the results from a comprehensive suite of soil property and frost heave tests on four Alaskan soils and a soil from Hanover, New Hampshire. SMC-SFC relations were developed for these five soils over an unprecedented range of measurements, and yielded a new variable, η, which describes the water retention properties of soil at increasing matric potentials and decreasing temperatures. The ζ potentials of these natural soils were measured and analyzed, as related to frost heaving.

A state-of-the-art laboratory system was developed for frost heave testing, which allowed precise measurements of temperature, water intake, and heave. The soil preparation method and laboratory system ensured a high level of repeatability between frost heave tests on replicate soil samples. The cation effects on the frost susceptibility of heterogeneous soils were measured and analyzed. Previous investigations in this area of research have suggested that the application of certain salt treatments can systematically increase or decrease the frost susceptibility of a given soil. The results of the research presented here indicate that the response of a given soil to a salt treatment may not be as predictable and systematic as previously suggested. Indeed, these results indicate that the cation effects on frost heaving in natural heterogeneous soils are quite complicated and will require much further testing before they are fully understood.

7.3 Suggestions for Future Research

Due to time constraints, SMC curves were not developed for each of the cation-treated samples. The analysis of the entire body of BSLN data indicates that the variable η, which requires SMC data, may be of essential importance in quantifying ξ, as η describes a soil's water retention properties at increasing ψ_m and decreasing temperatures. Thus, it is suggested that future research includes the determination of SMC curves for each of the cation-treated samples used in this study. The veracity of the empirical equations developed from the data presented in this dissertation should be confirmed, and refinements made, by similar testing conducted on additional disparate soils. Electron microscopy should be conducted on each of the BSLN and cation-treated samples, in order to define each sample's soil structure. The soluble cation concentration analysis of the BSLN samples should be expanded to include trivalent cations, such as Al^{3+} and Fe^{3+}. Finally, the activities of each of the cation-treated soils should be determined and included in future multiple linear regression analysis.

The variation in the testing results is attributed to the wide range of natural soils chosen for experimentation. If natural soils were simple systems, it is plausible that the frost heave phenomenon may have been described with the development of the capillary theory in the 1950's. Even testing homogeneous soils and artificial blends yields results that are difficult to correlate to each other (Lambe 1953). This area of research, although challenging to pursue due to the complexity of natural soils and the wide range of disciplines it encompasses, may provide critical elements hitherto missing from frost heave models.

The importance of understanding the adsorbed cation effects on the frost susceptibility of soil is not purely academic. Grim (1952) noted that cation exchange occurs sometimes unexpectedly in soils, perhaps as a result of construction activities or changes in groundwater flow. An example of an anthropogenic change in soil surface chemistry is the application of salt (typically NaCl) to roadway surfaces during the winter to improve driving conditions. Years of this treatment may result in the accumulation of cations within the upper portion of the roadway embankment, and depending on the type of material from which the embankment was constructed, may cause an increase in the embankment material's frost susceptibility. This process may explain the damage seen in a stabilized base course emplaced during a recent highway improvement project in Interior Alaska.

REFERENCES

Aguirre-Puente, J., and Fremond, M. (1976). "Frost and water propagation in porous media." *Proc., Conference on Soil-Water Problems in Cold Regions*, American Geophysical Union, Edmonton, Alberta, Canada, 137-154.

Aguirre-Puente, J., and Gruson, J. (1983). "Measurement of permeabilities of frozen soils." *Proc., Permafrost: Fourth International Conference*, University of Alaska Fairbanks and National Academy of Sciences, Fairbanks, Alaska, 5-9.

Akagawa, S. (1983). "Relation between frost heave and specimen length." *Proc., Permafrost: Fourth International Conference*, University of Alaska Fairbanks and National Academy of Sciences, Fairbanks, Alaska, 1-6.

Akagawa, S. (1988). "Evaluation of the X-ray radiography efficiency for heaving and consolidation observation." *Ground Freezing 88: Proc. of the Fifth International Symposium on Ground Freezing*, Nottingham, England, 23-28.

Akagawa, S. (1988b). "Experimental study of frozen fringe characteristics." *Cold Regions Science and Technology*, 15, 209-223.

Akagawa, S. (1990). *X-ray Photography Method for Experimental Studies of the Frozen Fringe Characteristics of Frozen Soil,* CRREL Special Report 90-5, Hanover.

Akagawa, S., Yamamoto, Y., Hashimoto, S. (1985). "Frost heave characteristics and scale effect of stationary frost heave." *Ground Freezing: Proc. of the Fourth International Symposium on Ground Freezing*, Sapporo-shi, Japan, 137-143.

Akimov, Y. P., Yershov, E. D., Chveryov, V. G. (1983). "The physicochemical nature of the formation of unfrozen water in frozen soils." *Proc., Permafrost: Fourth International Conference*, University of Alaska Fairbanks and National Academy of Sciences, Fairbanks, Alaska, 195-199.

Alonso, E. E., Lloret, A., Gens, A., Battle, F. (1989). "A new approach for the prediction of long term heave." *Proc., Twelfth International Conference on Soil Mechanics and Foundation Engineering*, Rio de Janeiro, Brazil, 571-574.

Ananyan, A. A. (1973). "Nature of water in very fine-grained deposits and its crystallization characteristics." *Proc., Permafrost: Second International Conference, USSR Contribution*, National Research Council of Canada, National Academy of Sciences, Yakutsk, U.S.S.R, 283-286.

Anderson, D. M. (1967). "The interface between ice and silicate surfaces." *Journal of Colloid and Interface Science*, 25, 174-191.

Anderson, D. M. (1989). "Frost heave properties of soils." *Proc., International Symposium on Frost in Geotechnical Engineering*, Saariselka, Finland, 94, 105-125.

Anderson, D. M., and Morgenstern, N. R. (1973). "Physics, chemistry, and mechanics of frozen ground – a review." *Proc., Permafrost: Second International Conference, North American Contribution,* National Research Council of Canada, National Academy of Sciences, Yakutsk, U.S.S.R, 257-288.

Anderson, D. M., and Tice, A. R. (1972). "Predicting unfrozen water contents in frozen soils from surface area measurements." *Highway Research Record*, 393, 12-18.

Anderson, D. M., Tice, A. R., McKim, H. L. (1973). "The unfrozen water and the apparent specific heat capacity of frozen soils." *Proc., Permafrost: Second International Conference, North American Contribution,* National Research Council of Canada, National Academy of Sciences, Yakutsk, U.S.S.R, 289-295.

Arvidson, W. D., and Morgenstern, N. R. (1977). "Water flow induced by soil freezing." *Canadian Geotechnical Journal*, 14(2), 237-245.

Atkins, P., and de Paula, J. (2002). *Physical Chemistry*, 7th Ed, W. H. Freeman and Company, New York.

Berg, R. L. (1975). "Heat and moisture flow in freezing and thawing soils – a field study." *Proc., Conference on Soil-Water Problems in Cold Regions*, American Geophysical Union, Calgary, Alberta, Canada, 148-160.

Berg, R., Ingersoll, J., Guymon, G. (1980). "Frost heave in an instrumented soil column." *Cold Region Science and Technology*, 3(2-3), 211-221.

Beskow, G. (1935). *Soil freezing and frost heaving, with special applications to roads and railroads*, Swedish Geological Society, Series C(375) (translated by J. O. Osterberg). In *Historical Perspectives in Frost Heave Research*, CRREL Special Report 91-23, 41-157.

Black, P. B. (1989). *On the Use of the ϕ-variable to Describe the State of Water in Porous Media*, CRREL Report 89-3, Hanover.

Black, P. B. (1990). *Three Functions that Model Empirically Measured Unfrozen Water Content Data and Predict Relative Hydraulic Conductivity*, CRREL Report 90-5, Hanover.

Black, P. B., and Tice, A. R. (1989). "Comparison of soil freezing curve and soil water curve data for Windsor sandy loam." *Water Resources Research*, 25(10), 2205-2210.

Bouyoucos, G. (1917). *Classification and Measurement of the Different Forms of Water in the Soil by Means of the Dilatometer Method*, Michigan Agricultural College Experiment Station, Technical Bulletin 36, Michigan.

Bouyoucos, G. (1920). "A new classification of the soil moisture." *Soil Science*, 11(1), 33-47.

Bresler, E., and Miller, R. D. (1975). "Estimation of pore blockage induced by freezing of unsaturated soil." *Proc., Conference on Soil-Water Problems in Cold Regions*, American Geophysical Union, Calgary, Alberta, Canada, 161-175.

Brooks, R. H., and Corey, A. T. (1964). "Hydraulic properties of porous media." *Hydrology Paper No. 3, Colorado State University,* Ft. Collins, Colorado.

Brooks, R. H., and Corey, A. T. (1966). "Properties of porous media affecting fluid flow." *Proc. ASCE, Journal of the Irrigation and Drainage Division*, 92(IR2), 61-88.

Brown, G., *ed.* (1961). *The X-ray Identification and Crystal Structures of Clay Minerals*: Mineralogical Society, London.

Brown, J., and Krieg, R. A., eds. (1983). "Guidebook to permafrost and related features along the Elliott and Dalton Highways, Fox to Prudhoe Bay, Alaska." *Guidebook 4, Permafrost: Fourth International Conference*, University of Alaska, Fairbanks, Alaska.

Burt, T. P., and Williams, P. J. (1976). "Hydraulic conductivity in frozen soils." *Earth Surface Processes*, 1(4), 349-360.

Carroll, D. (1970). "Clay minerals: a guide to their x-ray diffraction." USGS Special Paper 126.

Cary, J. W. (1987). "A new method for calculating frost heave including solute effects." *Water Resources Research*, 23(8), 1620-1624.

Casagrande, A. (1931). "Discussion of frost heaving." *Proc. Annual Meeting, Highway Research Board*, 11, 165-177.

Cass, L. A., and Miller, R. D. (1959). *Role of the Electric Double Layer in Mechanism of Frost Heaving*, CRREL Research Report 49, Hanover.

Chalmers, B., and Jackson, K. A. (1970). *Experimental and Theoretical Studies of the Mechanism of Frost Heaving*, CRREL Research Report 199, Hanover.

Chamberlain, E. J. (1981). *Frost Susceptibility of Soil,* CRREL Monograph 81-2, Hanover.

Chamberlain, E. J. (1983). "Frost heave of saline soils." *Proc., Permafrost: Fourth International Conference*, University of Alaska Fairbanks and National Academy of Sciences, Fairbanks, Alaska, 121-126.

Chamberlain, E. J. (1986). *Evaluation of Selected Frost-Susceptibility Test Methods*: CRREL Report 86-14, Hanover.

Chamberlain, E. J. (1987). *A Freeze-Thaw Test to Determine the Frost Susceptibility of Soils*, CRREL Special Report 87-1, Hanover.

Chamberlain, E. J., and Gow, A. J. (1979). "Effect of freezing and thawing on the permeability and structure of soils." *Engineering Geology*, 13, 73-92.

Chen, X., and Wang, Y. (1988). "Frost heave prediction for clayey soils." *Cold Regions Science and Technology*, 15(3), 233-238.

Chen, X. and Wang, Y. (1991). "A new model of frost heave prediction for clayey soils." *Cold Regions Science and Technology*, 19(2), 213-214.

Chen, X., and Wang, Y. (1991b). "A new model of frost heave prediction for clayey soils." *Science in China*, 34(10), 1225-1236.

Chen, X., Wang, Y., Ping, J. (1983). "Influence of penetration rate, surcharge stress, and ground water table on frost heave." *Proc., Permafrost: Fourth International Conference*, University of Alaska Fairbanks and National Academy of Sciences, Fairbanks, Alaska, 131-135.

Cheverev, V. G., Ershov, E. D., Magomedgadzhieva, M. A., Vidyapin, I. Y. (1998). "Results of physical simulation of frost heaving in soils." *Proc., Permafrost: Seventh International Conference*, International Permafrost Association, Yellowknife, Canada, 145-149.

Comparini, E. (1988). "On a model for quasi-steady freezing processes of saturated porous media." *Ground Freezing 88: Proc. of the Fifth International Symposium on Ground Freezing*, Nottingham, England, 41-49.

Cornell University. (1951). *Final Report, Soil Solidification Research, Cornell University 1946 – 1951: Vol. 2 – Fundamental Properties, Clay-Water Systems*, U.S. Department of Commerce, Washington, D.C.

Corte, A. E. (1962). "Vertical migration of particles in front of a moving freezing plane." *Journal of Geophysical Research*, 67(3), 1085-1090.

Croney, D., and Jacobs, J. C. (1967). *The Frost Susceptibility of Soils and Road Materials*, British Ministry of Transport, Road Research Laboratory RRL Report No. 90, Crowthorne, England.

Czurda, K. A., and Schababerle, R. (1988). "Influence of freezing and thawing on the physical and chemical properties of swelling clays." *Ground Freezing 88: Proc. of the Fifth International Symposium on Ground Freezing*, Nottingham, England, 51-58.

Das, B. M. (1997). *Soil Mechanics Laboratory Manual*, 5th Ed., Engineering Press, Austin.

Dash, J. G. (1989). "Thermomolecular pressure in surface melting: motivation for frost heave." *Science*, 246(4937), 1591-1593.

Detterman, R. L., Bowsher, A. L., Dutro, Jr., J. T. (1958). "Glaciation on the Arctic slope of the Brooks Range, northern Alaska." *Arctic*, 11(1), 43-61.

Dirksen, C., and Miller, R. D. (1966). "Closed-system freezing of unsaturated soil." *Proc., Soil Science Society of America*, 30(2), 168-173.

Doré, G., Konrad, J.-M., Bérubé, M.-A. (1998). "The effect of consolidation on frost susceptibility of silty soils." *Proc., Permafrost: Seventh International Conference*, International Permafrost Association, Yellowknife, Canada, 239-244.

Dostovalov, B. N. (1973). "Structures, phase transitions, and properties of free and bound water." *Proc., Permafrost: Second International Conference, USSR Contribution*, National Research Council of Canada, National Academy of Sciences, Yakutsk, U.S.S.R, 287-292.

Dudek, S. J. M., and Holden, J. T. (1979). "A theoretical model for frost heave." *Proc., First International Conference on Numerical Methods in Thermal Problems*, Swansea, United Kingdom, 216-229.

Edlefsen, N. F., and Anderson, A. B. C. (1943). "Thermodynamics of soil moisture." *Hilgardia*, 15(2), 1-298.

Efimov, S. S., Kozhevnikov, N. N., Kurilko, A. S., Nikitina, M., Stepanov, A. V. (1981). "Influence of cyclic freezing-thawing on heat and mass transfer characteristics of clay soil." *Engineering Geology*, 18(1-4), 147-152.

Everett, D. H. (1961). "The thermodynamics of frost damage to porous solids." *Transactions of the Faraday Society*, 57, 1541-1551.

Everett, D. H., and Haynes, J. M. (1965). "Capillary properties of some model pore systems with reference to frost damage." *RILEM Bulletin*, (27), 31-38.

Ferrians, Jr., O. J., Nichols, D. R., Williams, J. R. (1983). "Copper River Basin." In Péwé, T. L., and Reger, R. D., eds., *Guidebook to Permafrost and Quaternary Geology along the Richardson and Glenn Highways, Alaska.* Alaska DGGS, Guidebook 1, 137-175.

Førland, K. S., Førland, T., Ratkje, S. K. (1988). "Frost heave." *Proc., Permafrost: Fifth International Conference*, Norwegian Committee on Permafrost and Norwegian Institute of Technology, Trondheim, Norway, 344-348.

Fowler, A. C. and Noon, C. G. (1993). "A simplified numerical solution of the Miller model of secondary frost heave." *Cold Regions Science and Technology*, 21(4), 327-336.

Fritschen, L. J., and Gay, L. W. (1979). *Environmental Instrumentation*, Springer-Verlag, New York.

Fukuda, M. (1980). "Experimental studies of coupled heat and moisture transfer in soils during freezing." *Cold Regions Science and Technology*, 3(2-3), 223-232.

Fukuda, M., and Huang, S. L. (1991). "Effects of total water content on dynamic properties of frozen soils." *Proc., International Arctic Technology Conference*, Anchorage, Alaska, 621-629.

Fukuda, M., and Nakagawa, S. (1985). "Numerical analysis of frost heaving based upon the coupled heat and water flow model." *Ground Freezing: Proc. of the Fourth International Symposium on Ground Freezing*, Sapporo-shi, Japan, 109-117.

Gardner, W. H. (1986). "Water content." In Klute, A. ed., *Methods of Soil Analysis – Part 1: Physical and Mineralogical Methods*, 2nd Ed., Soil Science Society of America, Madison, Wisconsin.

Gilpin, R. R. (1980). "A model for the prediction of ice lensing and frost heave in soils." *Water Resources Research*, 16(5), 918-930.

Gold, L. W. (1957). "A possible force mechanism associated with the freezing of water in porous materials." *Highway Research Board Bulletin*, 168, 65-73.

Gorelik, J. B., Kolunin, V. S., Reshetnikov, A. K. (1998). "Rigid-ice model and stationary growth of ice." *Proc., Permafrost: Seventh International Conference*, International Permafrost Association, Yellowknife, Canada, 327-333.

Grant, S. A. (2000). *Physical and Chemical Factors Affecting Contaminant Hydrology in Cold Environments*, CRREL Technical Report 00-21, Hanover.

Grant, S. A., Boitnott, G. E., Tice, A. R. (1999). *Effects of Dissolved NaCl on Freezing Curves of Kaolinite, Montmorillonite, and Sand Pastes*, CRREL Special Report 99-2, Hanover.

Greenland, D. J., and Hayes, M. H. B., eds. (1978). *The Chemistry of Soil Constituents*, John Wiley and Sons, New York.

Grim, R. E. (1952). "Relation of frost action to the clay-mineral composition of soil minerals." *Highway Research Board*, 2, 167-172.

Grim, R. E. (1958). "Organization of water on clay mineral surfaces and its implication for the properties of clay-water systems." *National Research Council, Highway Research Board*, 40, 17-23.

Grim, R. E. (1962). *Applied Clay Mineralogy*, McGraw-Hill, New York.

Groenevelt, P. H., and Kay, B. D. (1974). "On the interaction of water and heat transport in frozen and unfrozen soils, II: the liquid phase." *Proc., Soil Science Society of America*, 38(3), 400-404.

Groenevelt, P. J., and Kay, B. D. (1977). "Water and ice potentials in frozen soils." *Water Resources Research*, 13(2), 445-449.

Guymon, G. L., Berg, R. L., Johnson, T. C., Hromadka, II, T. V. (1981). "Results from a mathematical model of frost heave." *Transportation Research Record*, 809, 2-6.

Guymon, G. L., Hromadka II, T. V., Berg, R. L. (1980). "A one-dimensional frost heave model based upon simulation of simultaneous heat and water flux." *Cold Regions Science and Technology*, 3(2-3), 253-262.

Guymon, G. L., and Luthin, J. N. (1974). "A coupled heat and moisture transport model for Arctic soils." *Water Resources Research*, 10(5), 995-1001.

Harlan, R. L. (1973). "Analysis of coupled heat-fluid transport in partially frozen soil." *Water Resources Research*, 9(5), 1314-1323.

Harris, C., and Davies, M. C. R. (1998). "Pressures recorded during laboratory freezing and thawing of natural silt-rich soil." *Proc., Permafrost: Seventh International Conference*, International Permafrost Association, Yellowknife, Canada, 433-439.

Hazen, B., Nixon, J. F., Heuer, C. E., Caldwell, J. B., Brudie, E. L. (1993). "Frost heave predictions for Alaskan soils." *Proc., Permafrost: Sixth International Conference*, Lanzhou Institute of Glaciology and Geocryology, Chinese Academy of Science, Chinese Society of Glaciology and Geocryology, Beijing, China, 244-249.

Heagler, Jr., J. B. (1964). "Clay mineralogy and soil stabilization." *Proc., Fifteenth Annual Highway Geology Symposium*, Missouri Geological Survey and Water Resources, Rolla, MO, 133-142.

Henry, K. S. (1988). *Chemical Aspects of Soil Freezing,* CRREL Report 88-17, Hanover.

Henry, K. S. (2000). *A Review of the Thermodynamics of Frost Heave*, CRREL Technical Report TR-00-16, Hanover.

Hermansson, A. (2000). *Frost Modeling and Pavement Temperatures*, Licentiate thesis, Luleå University of Technology, Luleå, Sweden.

Hermansson, A. (2002). *Modeling of Frost Heave and Surface Temperatures in Roads*, Doctoral thesis, Luleå University of Technology, Luleå, Sweden.

Higashi, A. (1958). *Experimental Study of Frost Heaving*, CRREL Research Report 45, Hanover.

Hillel, D. (1980). *Fundamentals of Soil Physics*, Academic Press, San Diego.

Hoekstra, P. (1966). "Moisture movement in soils under temperature gradients with the cold-side temperature below freezing." *Water Resources Research*, 2(2), 241-250.

Hoekstra, P. (1969). "Water movement and freezing pressures." *Proc., Soil Science Society of America*, 33(4), 512-518.

Hoekstra, P., Chamberlain, E., Frate, A. (1965). *Frost-Heaving Pressures,* CRREL Research Report 176, Hanover.

Holden, J. T. (1983). "Approximate solutions for Miller's theory of secondary heave." *Proc., Permafrost: Fourth International Conference*, University of Alaska Fairbanks and National Academy of Sciences, Fairbanks, Alaska, 498-503.

Holden, J. T., Piper, D., Jones, R. H. (1985). "Some developments of a rigid-ice model of frost heave." *Ground Freezing: Proc. of the Fourth International Symposium on Ground Freezing*, Sapporo-shi, Japan, 93-99.

Hopke, S. W. (1980). "A model for frost heave including overburden." *Cold Regions Science and Technology*, 3(2-3), 111-127.

Horiguchi, K. (1979). "Effect of the rate of heat removal on the rate of frost heaving." *Engineering Geology*, 13(1-4), 63-71.

Horiguchi, K., and Miller, R. D. (1980). "Experimental studies with frozen soil in an "ice sandwich" permeameter." *Cold Regions Science and Technology*, 3(3), 177-183.

Horiguchi, K., and Miller, R. D. (1983). "Hydraulic conductivity functions of frozen materials." *Proc., Permafrost: Fourth International Conference*, University of Alaska Fairbanks and National Academy of Sciences, Fairbanks, Alaska, 504-508.

Hromadka II, T. V. (1980). *Mathematical Model of Frost Heave in Freezing Soils*, Doctoral thesis, University of California Irvine, California.

Hunter, R. J. (2001). *Foundation of Colloid Science*, 2nd Ed., Oxford University Press, New York.

Ingersoll, J., and Berg, R. (1981). "Simulating frost action by using an instrumented soil column." *Transportation Research Record*, 809, 34-42.

Ingersoll, J., and Berg, R. L. (1985). "Hydraulic properties of selected soils." In Anderson, D. M., and Williams, P. J., eds., *Freezing and Thawing of Soil-Water Systems*, ASCE, New York.

Ishizaki, T., and Nishio, N. (1985). "Experimental study of final ice lens growth in partially frozen saturated soil." *Ground Freezing: Proc. of the Fourth International Symposium on Ground Freezing*, Sapporo-shi, Japan, 71-78.

Ishizaki, T, and Nishio, N. (1988). "Experimental study of frost heaving of a saturated soil." *Ground Freezing 88: Proc. of the Fifth International Symposium on Ground Freezing*, Nottingham, England, 65-72.

Ito, Y., Vinson, T. S., Nixon, J. F., Stewart, D. (1998). "An improved step freezing test to determine segregation potential." *Proc., Permafrost: Seventh International Conference*, International Permafrost Association, Yellowknife, Canada, 509-516.

Iwata, S. (1983). "A mechanism for the existence of an unfrozen liquid in the vicinity of a solid surface." *Proc., Permafrost: Fourth International Conference*, University of Alaska Fairbanks and National Academy of Sciences, Fairbanks, Alaska, 25-31.

Jackson, K. A., Chalmers, B., McKay, G. (1957). *Study of Ice Formation in Soils,* Corps of Engineers Technical Report No. 65, Massachusetts.

Jame, Y., and Norum, D. I. (1976). "Heat and mass transfer in freezing unsaturated soil in a closed system." *Proc., Conference on Soil-Water Problems in Cold Regions*, American Geophysical Union, Edmonton, Alberta, Canada, 46-62.

Jame, Y., and Norum, D. I. (1980). "Heat and mass transfer in a freezing unsaturated porous medium." *Water Resources Research*, 16(4), 811-819.

Japan Geotechnical Society. (2003). Test method for frost heave prediction of soils, JGS 0171-2003; and Test Method for frost susceptibility of soils, JGS 0172-2003, Tokyo, Japan.

Jessberger, H. L., and Jagow, R. (1989). "Determination of frost susceptibility of soils." *Proc., International Symposium on Frost in Geotechnical Engineering*, Saariselka, Finland, 95, 449-469.

Jinsheng, Z., and Rong, F. (1983). "Preliminary experimental study of water migration at the ice/soil interface." *Proc., Permafrost: Fourth International Conference*, University of Alaska Fairbanks and National Academy of Sciences, Fairbanks, Alaska, 1469-1472.

Johnson, T. C., Berg, R. L., DiMillio, A. (1986). "Frost action predictive techniques: an overview of research results." *Transportation Research Record*, 1089, 147-161.

Jones, R. H. (1981). "Developments and applications of frost susceptibility testing." *Engineering Geology*, 18(1-4), 269-280.

Jones, R. H., and Dudek, S. J-M. (1979). "Comparison of the precise freezing cell with other facilities for frost-heave testing." *Transportation Research Record*, 705, 63-71.

Jumikis, A. R. (1957). "The effect of freezing on a capillary meniscus." *Highway Research Board Bulletin*, 168, 116-122.

Jumikis, A. R. (1973). "Effect of porosity on amount of soil water transferred in a freezing silt." *Proc., Permafrost: Second International Conference, North American Contribution,* National Research Council of Canada, National Academy of Sciences, Yakutsk, U.S.S.R, 305-310.

Kaplar, C. W. (1968). "New experiments to simplify frost susceptibility testing of soils." *Highway Research Record*, 215, 48-59.

Kaplar, C. W. (1970). "Phenomenon and mechanism of frost heaving." *Highway Research Record*, 304, 1-13.

Kay, B. D., and Groenevelt, P. H. (1974). "On the interaction of water and heat transport in frozen and unfrozen soils: I. basic theory; the vapor phase." *Proc., Soil Science Society of America*, 38(3), 395-400.

Kay, B. D., and Perfect, E. (1988). "State of the art: heat and mass transfer in freezing soils." *Ground Freezing 88: Proc. of the Fifth International Symposium on Ground Freezing*, Nottingham, England, 3-21.

Kazda, J. (1979). "The character of adsorbed water on clayey soils." *Proc., Eighth Conference on Clay Mineralogy and Petrology*, Teplice, Czech Republic, 59-64.

Kemper, W. D. (1960). "Water and ion movement in thin films as influenced by the electrostatic charge and diffuse layer of cations associated with clay mineral surfaces." *Proc., Soil Science Society of America*, 24, 10-16.

Ketcham, S. A., and Black, P. B. (1995). *Initial Results from Small-Scale Frost Heave Experiments in a Centrifuge,* CRREL Report 95-9, Hanover.

Kinosita, S. (1975). "Soil-water movement and heat flux in freezing ground." *Proc., Conference on Soil-Water Problems in Cold Regions*, American Geophysical Union, Calgary, Alberta, Canada, 33-41.

Kiselev, V. F., Kvlividze, V. I., Kurzayev, A. B. (1973). "Surface phenomena at the ice-gas and ice-solid interfaces." *Proc., Permafrost: Second International Conference, USSR Contribution*, National Research Council of Canada, National Academy of Sciences, Yakutsk, U.S.S.R, 339-341.

Klute, A. (1986). "Water retention: laboratory methods." In Klute, A. ed., *Methods of Soil Analysis – Part 1: Physical and Mineralogical Methods*, 2nd Ed., Soil Science Society of America, Madison, Wisconsin.

Konrad, J. M. (1987). "Procedure for determining the segregation potential of freezing soils." *Geotechnincal Testing Journal*, 10(2), 51-58.

Konrad, J. M. (1988). "Influence of freezing mode on frost heave characteristics." *Cold Regions Science and Technology*, 15(2), 161-175.

Konrad, J. M. (1989). "Influence of overconsolidation on the freezing characteristics of clayey silt." *Canadian Geotechnical Journal*, 26(1), 9-21.

Konrad, J. M. (1990). "Segregation potential–pressure–salinity relationships near thermal steady state for a clayey silt." *Canadian Geotechnical Journal*, 27(2), 203-215.

Konrad, J. M. (1990b). "Unfrozen water as a function of void ratio in a clayey silt." *Cold Regions Science and Technology*, 18(1), 49-55.

Konrad, J. M. (1993). "Sixteenth Canadian geotechnical colloquium: frost heave in soils – concepts and engineering." *Canadian Geotechnical Journal*, 31(2), 223-245.

Konrad, J. M., and Duquennoi, C. (1993). "A model for water transport and ice lensing in freezing soils." *Water Resources Research*, 29(9), 3109-3124.

Konrad, J. M., and Morgenstern, N. R. (1980). "A mechanistic theory of ice lens formation in fine-grained soils." *Canadian Geotechnical Journal*, 17(4), 473-486.

Konrad, J. M., and Morgenstern, N. R. (1981). "The segregation potential of a freezing soil." *Canadian Geotechnical Journal*, 18(4), 482-491.

Konrad, J. M., and Morgenstern, N. R. (1982). "Effects of applied pressure on freezing soils." *Canadian Geotechnical Journal*, 19(4), 494-505.

Konrad, J. M., and Morgenstern, N. R. (1982b). "Prediction of frost heave in the laboratory during transient freezing." *Canadian Geotechnical Journal*, 19(3), 250-259.

Konrad, J. M., and Morgenstern, N. R. (1983). "Frost susceptibility of soils in terms of their segregation potential." *Proc., Permafrost: Fourth International Conference*, University of Alaska Fairbanks and National Academy of Sciences, Fairbanks, Alaska, 660-665.

Konrad, J. M., and Nixon, J. F. (1994). "Frost heave characteristics of a clayey silt subjected to small temperature gradients." *Cold Regions Science and Technology*, 22(3), 299-310.

Koopmans, R. W. R., and Miller, R. D. (1966). "Soil freezing and soil water characteristic curves." *Proc., Soil Science Society of America*, 30, 680-685.

Krantz, W. B., and Adams, K. E. (1996). "Application of a fully predictive model for secondary frost heave." *Arctic and Alpine Research*, 28(3), 284-293.

Kudryavtsev, V. A., and Yershov, E. D. (1973). "Moisture transfer and ice formation in frozen and freezing ground." *Proc., Permafrost: Second International Conference, USSR Contribution*, National Research Council of Canada, National Academy of Sciences, Yakutsk, U.S.S.R, 834-835.

Kudryavtsev, V. A., Yershov, E. D., Cheverev, V. G. (1973). "Migration of moisture in fine-grained soil of different composition, structure, and properties." *Proc., Permafrost: Second International Conference, USSR Contribution*, National Research Council of Canada, National Academy of Sciences, Yakutsk, U.S.S.R, 292-298.

Kujala, K. (1989). "Unfrozen water content of Finnish soils measured by NMR." *Proc., International Symposium on Frost in Geotechnical Engineering*, Saariselka, Finland, 94, 301-310.

Kunze, G. W., and Dixon, J. B. (1986). "Pretreatment for mineralogical analysis." In Klute, A. ed., *Methods of Soil Analysis – Part 1: Physical and Mineralogical Methods*, 2nd Ed., Soil Science Society of America, Madison, Wisconsin.

Kuroda, T. (1985). "Theoretical study of frost heaving – kinetic process at water layer between ice lens and soil particles." *Ground Freezing: Proc. of the Fourth International Symposium on Ground Freezing*, Sapporo-shi, Japan, 39-45.

Ladanyi, B. and Shen, M. (1989). "Mechanics of freezing and thawing in soils." *Proc., International Symposium on Frost in Geotechnical Engineering*, Saariselka, Finland, 94, 73-104.

Lambe, T. W. (1953). *Cold Room Studies, Third Interim Report of Investigations, App. D – Mineral and Chemical Studies*, Arctic Construction and Frost Effects Laboratory, Boston.

Lambe, T. W., Kaplar, C. W., Lambie, T. J. (1969). *Effect of Mineralogical Composition of Fines on Frost Susceptibility of Soils*, CRREL Technical Report 207, Hanover.

Leary, R. M., Sanborn, J. L., Zoller, J. H. (1968). "Freezing tests of granular materials." *Highway Research Record*, 215, 60-74.

Ledbetter, R. D. (1959). *Preliminary Materials Investigation – Glenn Highway Reconstruction, Station 16+16[9] to 152+00, Richardson Junction to Moose Creek, F-042-3(5).* Alaska Bureau of Public Roads, Anchorage, Alaska.

Lewis, R. W., and Sze, W. K. (1988). "A finite element simulation of frost heave in soils." *Ground Freezing 88: Proc. of the Fifth International Symposium on Ground Freezing*, Nottingham, England, 73-80.

Lindholm, G. F., Thomas, L. A., Davidson, D. T., Handy, R. L., Roy, C. J. (1957). *Geologic and Engineering Properties of Silts near Big Delta and Fairbanks, Alaska,* Iowa State College, Ames, Iowa.

Linell, K. A., and Kaplar, C. W. (1959). "The factor of soil and material type in frost action." *Highway Research Board Bulletin*, 225, 81-126.

Loch, J. P. G. (1978). "Thermodynamic equilibrium between ice and water in porous media." *Soil Science*, 126(2), 77-80.

Loch, J. P. G. (1979). "Influence of the heat extraction rate on the ice segregation rate of soils." *Frost I Jord*, (20), 19-30.

Loch, J. P. G. (1979b). "Suggestions for an improved standard laboratory test for frost heave susceptibility of soils." *Frost I Jord*, (20), 33-38.

Loch, J. P. G. (1981). "State-of-the-art report – frost action in soils." *Engineering Geology*, 18(1-4), 213-224.

Loch, J. P. G., and Kay, B. D. (1978). "Water redistribution in partially frozen, saturated silt under several temperature gradients and overburden loads." *Soil Science Society of America Journal*, 42(3), 400-406.

Loch, J. P. G., and Miller, R. D. (1975). "Tests of the concept of secondary frost heaving." *Proc., Soil Science Society of America*, 39(6), 1036-1041.

Lomas, K. J., and Jones, R. H. (1981). "Evaluation of a self-refrigerated unit for frost-heave testing." *Transportation Research Record*, 809, 6-13.

Low, P. F., Anderson, D. M., Hoekstra, P. (1968). "Some thermodynamic relationships for soils at or below the freezing point, 1. freezing point depression and heat capacity." *Water Resources Research*, 4(2), 379-394.

McCabe, E. Y., and Kettle, R. J. (1985). "Soil freezing response: influence of test conditions." *Geotechnical Testing Journal*, 8(2), 49-58.

McCabe, E. Y., and Kettle, R. J. (1985b). "Thermal aspects of frost action." *Ground Freezing: Proc. of the Fourth International Symposium on Ground Freezing*, Sapporo-shi, Japan, 47-54.

Mackay, J. R., Konishchev, V. N., Popov, A. I. (1978). "Geologic controls of the origin, characteristics, and distribution of ground ice." *Proc., Third International Conference on Permafrost*, National Research Council of Canada, Edmonton, Alberta, Canada, 2, 1-18.

Mageau, D. W. (1978). *Moisture Migration in Frozen Soil*, Masters thesis, University of Alberta, Edmonton, Alberta, Canada.

Mageau, D. W., and Morgenstern, N. R. (1979). "Observations on moisture migration in frozen soils." *Canadian Geotechnical Journal*, 17(1), 54-60.

Mageau, D. W., and Sherman, M. B. (1983). "Frost cell design and operation." *Proc., Permafrost: Fourth International Conference*, University of Alaska Fairbanks and National Academy of Sciences, Fairbanks, Alaska, 767-772.

Marion, G. M. (1995). *Freeze-Thaw Processes and Soil Chemistry,* CRREL Special Report 95-12, Hanover.

McBride, M. B. (1994). *Environmental Chemistry of Soils*, Oxford University Press, New York.

McGaw, R. W., and Tice, A. R. (1976). "A simple procedure to calculated the volume of water remaining unfrozen in a freezing soils." *Proc., Conference on Soil-Water Problems in Cold Regions*, American Geophysical Union, Edmonton, Alberta, Canada, 114-122.

Michalowski, R. L. (1993). "Phenomenological modeling of frost-susceptible soils." *Proc., Permafrost: Sixth International Conference*, Lanzhou Institute of Glaciology and Geocryology, Chinese Academy of Science, Chinese Society of Glaciology and Geocryology, Beijing, China, 465-470.

Michalowski, R. L., and Voller, V. R. (1991). *Modeling of Frost Heave in Soils*, University of Minnesota, Minnesota.

Miller, R. D. (1963). "Phase equilibria and soil freezing." *Proc., Permafrost International Conference*, National Academy of Sciences, National Research Council, Lafayette, Indiana, 193-197.

Miller, R. D. (1972). "Freezing and heaving of saturated and unsaturated soils." *Highway Research Record*, (393), 1-11.

Miller, R. D. (1973). "Movement of water in frozen ground." *Proc., Permafrost: Second International Conference, USSR Contribution*, National Research Council of Canada, National Academy of Sciences, Yakutsk, U.S.S.R, 846.

Miller, R. D. (1973b). "Soil freezing in relation to pore water pressure and temperature." *Proc., Permafrost: Second International Conference, North American Contribution,* National Research Council of Canada, National Academy of Sciences, Yakutsk, U.S.S.R, 344-352.

Miller, R. D. (1976). "Transport of water and heat in a frozen soil permeameter." *Proc., Conference on Soil-Water Problems in Cold Regions*, American Geophysical Union, Edmonton, Alberta, Canada, 110-113.

Miller, R. D. (1977). "Frost heaving and ice lens formation a capillary model." *EOS*, 58(12), 1130.

Miller, R. D. (1978). "Frost heaving in non-colloidal soils." *Proc., Third International Conference on Permafrost*, National Research Council of Canada, Edmonton, Alberta, Canada, 707-713.

Miller, R. D. (1980). "The adsorbed film controversy." *Cold Regions Science and Technology*, 3, 83-86.

Miller, R. D. (1983). "Thermally induced regelation – a qualitative discussion." *Proc., Permafrost: Fourth International Conference*, University of Alaska Fairbanks and National Academy of Sciences, Fairbanks, Alaska, 61-63.

Miller, R. D., and Koslow, E. E. (1980). "Computation of rate of heave versus load under quasi-steady state." *Cold Regions Science and Technology*, 3(2-3), 243-251.

Miller, R. D., Loch, J. P. G., Bresler, E. (1975). "Transport of water and heat in a frozen permeameter." *Proc., Soil Science Society of America*, 39, 1029-1036.

Miyata, Y. (1988). "A frost heave mechanism model based on energy equilibrium." *Ground Freezing 88: Proc. of the Fifth International Symposium on Ground Freezing*, Nottingham, England, 91-98.

Miyata, Y. (1998). "A thermodynamic study of liquid transportation in freezing porous media." *JSME International Journal*, Series B 41(3), 601-609.

Miyata, Y., and Akagawa, S. (1991). "Factors governing a frost heave ratio." *Ground Freezing 91: Proc. of the Sixth International Symposium on Ground Freezing*, Beijing, China, 55-63.

Miyata, Y., and Akagawa, S. (1997). "An experimental study on static solid-liquid phase equilibrium in the pores of a porous medium." *Heat Transfer – Japanese Research*, 26(2), 69-83.

Miyata, Y., and Akagawa, S. (1998). "An experimental study of dynamic solid-liquid phase equilibrium in a porous medium." *JSME International Journal*, Series B 41(3), 590-600.

Mokwa, R. L. (2004). "Soil response in sub-freezing environments: the frost heave model." *Transportation Research Board, 83rd Annual Meeting*, 83.

Moore, D. M., and Reynolds, Jr., R. C. (1997). *X-ray Diffraction and the Identification and Analysis of Clay Minerals*, 2nd ed., Oxford University Press, Oxford, United Kingdom.

Mu, S., and Ladanyi, B. (1987). "Modeling of coupled heat, moisture and stress field in freezing soil." *Cold Regions Science and Technology*, 14(3), 237-246.

Nakano, Y. (1990). "Quasi-steady problems in freezing soils: I. Analysis on the steady growth of an ice layer." *Cold Regions Science and Technology*, 17, 207-226.

Nakano, Y., and Horiguchi, K. (1985). "Role of phase equilibrium in frost heave of fine-grained soil under negligible overburden pressure." *Advances in Water Resources*, 8(2), 50-68.

Nakano, Y., Tice, A., Oliphant, J. (1984). "Transport of water in frozen soils: III. Experiments on the effects of ice content." *Advances in Water Resources*, 7(1), 28-34.

Nersesova, Z. A. (1961). "Effect of exchange cations on the migration of water and the heaving of soils during freezing (In Russian: Vliyanie obmennykh kationov na migratsiyu vody I puchenie gruntov pri promerzanii)." *Issledovaniya po Fizike I Mekhanike Merzlykh Gruntov*, 4, 22-52.

Nersesova, Z. A., and Tsytovich, N. A. (1963). "Unfrozen water in frozen soils." *Proc., Permafrost International Conference*, National Academy of Sciences, National Research Council, Lafayette, Indiana, 230-234.

Newman, G. P., and Wilson, G. W. (1997). "Heat and mass transfer in unsaturated soils during freezing." *Canadian Geotechnical Journal*, 34(1), 63-70.

Nixon, J. F. (1987). "Ground freezing and frost heave – a review." *The Northern Engineer*, 19(3-4), 8-18.

Nixon, J. F. (1991). "Discrete ice lens theory for frost heave in soils." *Canadian Geotechnical Journal*, 28(6), 843-859.

Nuffield, E. W. (1966). *X-ray Diffraction Methods*, John Wiley & Sons, Inc, New York, New York.

Ohrai, T., and Yamamoto, H. (1985). "Growth and migration of ice lenses in partially frozen soil." *Ground Freezing: Proc. of the Fourth International Symposium on Ground Freezing*, Sapporo-shi, Japan, 79-84.

Oliphant, J. L., Tice, A. R., Nakano, Y. (1983). "Water migration due to a temperature gradient in frozen soil." *Proc., Permafrost: Fourth International Conference*, University of Alaska Fairbanks and National Academy of Sciences, Fairbanks, Alaska, 951-956.

O'Neill, K. (1983). "The physics of mathematical frost heave models: a review." *Cold Regions Science and Technology*, 6, 275-291.

O'Neill, K., and Miller, R. D. (1982). *Numerical Solutions for a Rigid-Ice Model of Secondary Frost Heave,* CRREL Report 82-13, Hanover.

O'Neill, K., and Miller, R. D. (1985). "Explorations of a rigid ice model of frost heave." *Water Resources Research*, 21(3), 281-296.

Odom, I. E. (1984). "Smectite clay minerals: properties and uses." *Philosophical Transactions of the Royal Society, London*, A 311, 391-409.

Orlov, V. O. (1973). "Some heave laws of freezing soils." *Proc., Permafrost: Second International Conference, USSR Contribution*, National Research Council of Canada, National Academy of Sciences, Yakutsk, U.S.S.R, 269-271.

Outcalt, S. (1976). "A numerical model of ice lensing in freezing soils." *Proc., Conference on Soil-Water Problems in Cold Regions*, American Geophysical Union, Edmonton, Alberta, Canada, 63-71.

Outcalt, S. (1979). "The influence of the addition of water vapor diffusion on the numerical simulation of the process of ice segregation." *Frost I Jord*, 20, 45-47.

Padilla, F., and Villeneuve, J. P. (1990). "Modeling the movement of water, heat and solutes in frost-susceptible soils." *Collection Nordicana*, 54, 43-49.

Padilla, F., and Villeneuve, J. P. (1992). "Modeling and experimental studies of frost heave including solute effects." *Cold Regions Science and Technology*, 20(2), 183-194.

Palmer, A. C. (1967). "Ice lensing, thermal diffusion and water migration in freezing soil." *Journal of Glaciology*, 6(47), 681-694.

Patterson, D. E., and Smith, M. W. (1981). "The measurement of unfrozen water content by time domain reflectometry: results from laboratory tests." *Canadian Geotechnical Journal*, 18(1), 131-144.

Penner, E. (1956). "Soil moisture movement during ice segregation." *Highway Research Board Bulletin*, 135, 109-118.

Penner, E. (1957). "Soil moisture tension and ice segregation." *Highway Research Board Bulletin*, 168, 50-64.

Penner, E. (1959). "The mechanism of frost heaving in soils." *Highway Research Board Bulletin*, 225, 1-22.

Penner, E. (1962). "Ground freezing and frost heaving." *Canadian Building Digest*, 26, 1-4.

Penner, E. (1963). "Frost-heaving in soils." *Proc., Permafrost International Conference*, National Academy of Sciences, National Research Council, Lafayette, Indiana, 197-202.

Penner, E. (1967). "Heaving pressure in soils during unidirectional freezing." *Canadian Geotechnical Journal*, 4(4), 398-408.

Penner, E. (1972). "Influence of freezing rate on frost heaving." *Highway Research Record*, 393, 56-64.

Penner, E. (1976). "Grain size as a basis for frost susceptibility criteria." *Proc., Conference on Soil-Water Problems in Cold Regions*, American Geophysical Union, Edmonton, Alberta, Canada, 103-109.

Penner, E. (1981). "Heaving behaviour of soils in the step freezing mode." *Canadian Geotechnical Journal*, 18(4), 583-585.

Penner, E. (1982). *Aspects of Ice Lens Formation*, CRREL Special Report 82-16, Hanover.

Penner, E. (1986). "Aspects of ice lens growth in soils." *Cold Regions Science and Technology*, 13(1), 91-100.

Penner, E., and Goodrich, L. E. (1981). "Location of segregated ice in frost-susceptible soil." *Engineering Geology*, 18(1-4), 231-244.

Penner, E., and Ueda, T. (1978). "A soil frost-susceptibility test and a basis for interpreting heaving rates." *Proc., Third International Conference on Permafrost*, National Research Council of Canada, Edmonton, Alberta, Canada, 722-727.

Penner, E., and Walton, T. (1979). "Effects of temperature and pressure on frost heaving." *Engineering Geology*, 13(1-4), 29-39.

Perfect, E., and Williams, P. J. (1980). "Thermally induced water migration in frozen soils." *Cold Regions Science and Technology*, 3(2-3), 101-109.

Peterson, R. A., and Krantz, W. B. (1998). "A linear stability analysis for the inception of differential frost heave." *Collection Nordicana*, 57, 883-889.

Péwé, T. L. (1955). "Origin of the upland silt near Fairbanks, Alaska." *Geological Society of America Bulletin*, 66(6), 699-724.

Philip, J. R. (1980). "Thermal fields during regelation." *Cold Regions Science and Technology*, 3(2-3), 193-203.

Pietrzyk, K. (1981). "An attempt at a new formulation of the criteria of frost heave." *Engineering Geology*, 18(1-4), 281-290.

Piper, D., Holden, J. T., Jones, R. H. (1988). "A mathematical model of frost heave in granular materials." *Proc., Permafrost: Fifth International Conference*, Norwegian Committee on Permafrost and Norwegian Institute of Technology, Trondheim, Norway, 370-376.

Pusch, R. (1979). "Unfrozen water as a function of clay microstructure." *Engineering Geology*, 13(1-4), 157-162.

Radd, F. J., and Oertle, D. H. (1973). "Experimental pressure studies of frost heave mechanisms and the growth-fusion behavior of ice." *Proc., Permafrost: Second International Conference, North American Contribution,* National Research Council of Canada, National Academy of Sciences, Yakutsk, U.S.S.R, 377-383.

Ratkje, S. K. (1982). *The Hydraulic Conductivity of Soils during Frost Heave*, CRREL Special Report 82-16, Hanover.

Ratkje, S. K., Yamamoto, H., Takashi, T., Ohrai, T., Okamoto, J. (1982). "The hydraulic conductivity of soils during frost heave." *Frost I Jord*, 24, 22-26.

Rawls, W. J., Brakensiek, D. L., Saxton, K. E. (1982). "Estimation of soil water properties." *Transactions, American Society of Agricultural Engineers*, 25(5), 1316-1320.

Reed, M. A., Lovell, C. W., Altschaeffl, A. G., Wood, L. E. (1979). "Frost-heaving rate predicted from pore-size distribution." *Canadian Geotechnical Journal*, 16(3), 463-472.

Reginato, R. J., and van Bavel, C. H. M. (1962). "Pressure cell for soil cores." *Soil Science Society of America*, 26(1), 1-3.

Rempel, A. W., Wettlaufer, J. S., Worster, M. G. (2004). "Premelting dynamics in a continuum model of frost heave." *Journal of Fluid Mechanics*, 498, 227-244.

Riddick, T. M. (1968). *Control of Colloid Stability through Zeta Potential*, Zeta-Meter, Inc., New York.

Rieke, R. D. (1982). *The Role of Specific Surface Area and Related Index Properties in the Frost Susceptibility of Soils,* Masters thesis, Oregon State University, Oregon.

Rieke, R. D., Vinson, T. S., Mageau, D. W. (1983). "The role of specific surface area and related index properties in the frost heave susceptibility of soils." *Proc., Permafrost: Fourth International Conference*, University of Alaska Fairbanks and National Academy of Sciences, Fairbanks, Alaska, 1066-1071.

Rhoades, J. D. (1996). "Salinity: electrical conductivity and total dissolved solids." In Sparks, D. L., et al., eds., *Methods of Soil Analysis – Part 3: Chemical Methods*, Soil Science Society of America, Madison, 417-435.

Ryokai, K. (1985). "Frost heave theory of saturated soil coupling water/heat flow and its application." *Ground Freezing: Proc. of the Fourth International Symposium on Ground Freezing*, Sapporo-shi, Japan, 101-108.

Ryokai, K., Tuchiya, F., Mochizuki, M. (1988). "Frost expansion pressure and displacement of saturated soil analyzed with coupled heat and water flows." *Ground Freezing 88: Proc. of the Fifth International Symposium on Ground Freezing*, Nottingham, England, 115-120.

Saarelainen, S. M. I. (1989). "Evaluation of frost heave properties of soils." *Proc., International Symposium on Frost in Geotechnical Engineering*, Saariselka, Finland, 95, 471-480.

Savel'ev, B. A. (1978). "Investigation of the structure and properties of bound water." *Proc., Permafrost: Third International Conference*, National Research Council of Canada, Edmonton, Alberta, Canada, 1, 132-136.

Schellekens, F. J. (1997). *Fundamentals, Accuracy and Input Parameters of Frost Heave Prediction Models*, Carleton University, Ottawa, Canada.

Schmoll, H. R., Yehle, L. A., Updike, R. G. (1999). "Summary of Quaternary geology of the Municipality of Anchorage, Alaska." *Quaternary International*, 60, 3-36.

Sheeran, D. E., and Yong, R. N. (1975). "Water and salt redistribution in freezing soils." *Proc., Conference on Soil-Water Problems in Cold Regions*, American Geophysical Union, Calgary, Alberta, Canada, 58-69.

Shen, M., and Konrad, J. M. (1993). "Correct use of the segregation potential concept for two-dimensional frost heave simulation." *Proc., Permafrost: Sixth International Conference*, Lanzhou Institute of Glaciology and Geocryology, Chinese Academy of Science, Chinese Society of Glaciology and Geocryology, Beijing, China, 550-555.

Sheng, D., Axelsson, K., Knutsson, S. (1994). "Frost heave due to ice lens formation in freezing soils, 1. theory and verification." *Nordic Hydrology*, 26(2), 125–146.

Sheng, D., Axelsson, K., Knutsson, S. (1995). "Frost heave due to ice lens formation in freezing soils, 2. field applications." *Nordic Hydrology*, 26(2), 147-168.

Sheng, D., and Knutsson, S. (1993). "Sensitivity analysis of frost heave – a theoretical study." *Proc., Second International Symposium on Frost in Geotechnical Engineering*, Anchorage, Alaska, 3-16.

Sheng, Y., and Chen, X. (1991). "A numerical simulation of frost heave under overburden stress." *Ground Freezing 91: Proc. of the Sixth International Symposium on Ground Freezing*, Beijing, China, 175-180.

Sheppard, M. I., Kay, B. D., Loch, J. P. G. (1978). "Development and testing of a computer model for heat and mass flow in freezing soils." *Proc., Third International Conference on Permafrost*, National Research Council of Canada, Edmonton, Alberta, Canada, 75-81.

Smith, M. W. (1985). "Models of soil freezing." In Church, M., Slaymaker, O., eds. *Field and Theory: Lectures in Geocryology*, University of British Columbia Press, Vancouver, 96-120.

Sumner, M. E., and Miller, W. P. (1996). "Cation exchange capacity and exchange coefficients." In Sparks, D. L. et al., eds., *Methods of Soil Analysis – Part 3: Chemical Methods*, Soil Science Society of America, Madison, 1201-1229.

Sutherland, H. B., and Gaskin, P. N. (1973). "Pore water and heaving pressures developed in partially frozen soils." *Proc., Permafrost: Second International Conference, North American Contribution,* National Research Council of Canada, National Academy of Sciences, Yakutsk, U.S.S.R, 409-419.

Svec, O. J. (1989). "A new concept of frost-heave characteristics of soils." *Cold Regions Science and Technology*, 16(3), 271-279.

Svec, O. J., and Chang, Y. (1993). "Critical segregation potential – frost heave upper limit." *Proc., Permafrost: Sixth International Conference*, Lanzhou Institute of Glaciology and Geocryology, Chinese Academy of Science, Chinese Society of Glaciology and Geocryology, Beijing, China, 596-601.

Taber, S. (1929). "Frost heaving." *Journal of Geology*, 37(5), 428-461.

Taber, S. (1930). "The mechanics of frost heaving." *Journal of Geology*, 38(4), 307-317.

Takagi, S. (1963). "Fundamentals of the theory of frost-heaving." *Proc., Permafrost International Conference*, National Academy of Sciences, National Research Council, Lafayette, Indiana, 203-216.

Takagi, S. (1963b). "Theory of freezing-point depression with special reference to soil water." *Proc., Permafrost International Conference*, National Academy of Sciences, National Research Council, Lafayette, Indiana, 216-224.

Takagi, S. (1965). *Principles of frost heaving*, CRREL Research Report 140, Hanover.

Takagi, S. (1979). "Segregation freezing as the cause of suction force for ice lens formation." *Engineering Geology*, 13(1-4), 93-100.

Takagi, S. (1980). "The adsorption force theory of frost heaving." *Cold Regions Science and Technology*, 3(1), 57-81.

Takagi, S. (1982). *Initial Stage of the Formation of Soil-Laden Ice Lenses*, CRREL Special Report 82-16, Hanover.

Takashi, T, Ohrai, T., Yamamoto, H., Okamoto, J. (1982). *Effect of Specimen Height on Frost Heave Ratio in Unidirectional Freezing Test of Soil*, CRREL Special Report 82-16, Hanover.

Takashi, T., Yamamoto, H., Ohrai, T., Masuda, M. (1978). "Effect of penetration rate of freezing and confining stress on the frost heave ratio of soil." *Proc., Third International Conference on Permafrost*, National Research Council of Canada, Edmonton, Alberta, Canada, 736-742.

Tan, K. H. (1998). *Principles of Soil Chemistry*, Marcel Dekker, Inc., New York, New York.

Tarnawski, V. R., and Wagner, B. (1996). "On the prediction of hydraulic conductivity of frozen soils." *Canadian Geotechnical Journal*, 33(1), 176-180.

Taylor, G. S., and Luthin, J. N. (1976). "Numeric results of coupled heat-mass flow during freezing and thawing." *Proc., Conference on Soil-Water Problems in Cold Regions*, American Geophysical Union, Edmonton, Alberta, Canada, 155-172.

Taylor, G. S., and Luthin, J. N. (1978). "A model for coupled heat and moisture transfer during soil freezing." *Canadian Geotechnical Journal*, 15(4), 548-555.

Taylor, S. A., and Ashcroft, G. L. (1972). *Physical Edaphology – The Physics of Irrigated and Nonirrigated Soils*, W. H. Freeman and Company, San Francisco, California.

Tester, R. E., and Gaskin, P. N. (1996). "Effect of fines content on frost heave." *Canadian Geotechnical Journal*, 33(4), 678-680.

Tice, A. R., Black, P. B., Berg, R. L. (1989). "Unfrozen water contents of undisturbed and remolded Alaskan silt." *Cold Regions Science and Technology*, 17(2), 103-111.

Tice, A. R., Burrous, C. M., Anderson, D. M. (1978). "Determination of unfrozen water in frozen soil by pulsed nuclear magnetic resonance." *Proc., Third International Conference on Permafrost*, National Research Council of Canada, Edmonton, Alberta, Canada, 149-155.

Tice, A. R., and Oliphant, J. L. (1984). "The effects of magnetic particles on the unfrozen water content of frozen soils determined by nuclear magnetic resonance." *Soil Science*, 138(1), 63-73.

Tice, A. R., Oliphant, J. L., Nakano, Y., Jenkins, T. F. (1982). *Relationship between the Ice and Unfrozen Water Phases in Frozen Soil as Determined by Pulsed Nuclear Magnetic Resonance and Physical Desorption Data*, CRREL Report 82-15, Hanover.

Torrance, J. K., and Schellekens, F. J. (2003). "A conceptual analysis of chemical factors in soil freezing and frost heave." *Proc., 56th Annual Canadian Geotechnical Conference*, Canadian Geotechnical Society, Winnipeg, Manitoba, Canada (CD-ROM).

Townend, J., Reeve, M. J., Carter, A. (2001). In Smith, K. A., and Mullins, C. E., eds., *Soil and Environmental Analysis: Physical Methods*, 2nd Ed., M. Dekker, New York.

Tyutyunov, I. A. (1963). "Phase transformation of water in soils and the nature of migration and heaving." *Proc., Permafrost International Conference*, National Academy of Sciences, National Research Council, Lafayette, Indiana, 234-238.

Tyutyunov, I. A. (1973). "New concepts of the nature of frozen soils." *Proc., Permafrost: Second International Conference, USSR Contribution*, National Research Council of Canada, National Academy of Sciences, Yakutsk, U.S.S.R, 303-307.

Updike, R. G., and Schmoll, H. R. (1985). *A Brief Résumé of the Geology of Anchorage and Vicinity.* Alaska DGGS Public-data File 85-2, Fairbanks, Alaska.

US Salinity Laboratory Staff. (1954). *Diagnosis and Improvement of Saline and Alkali Soils*, USDA Agriculture Handbook No. 60, US Government Printing Office, Washington, D.C.

van Genuchten, M. Th., Leij, F. J., Yates, S. R. (1991). *The RETC Code for Quantifying the Hydraulic Functions of Unsaturated Soils*, US Salinity Laboratory, US Environmental Protection Agency, Ada, Oklahoma.

Volkova, Y. V. (1973). "Some characteristic features of water migration during freezing of fine soils." *Proc., Permafrost: Second International Conference, USSR Contribution*, National Research Council of Canada, National Academy of Sciences, Yakutsk, U.S.S.R, 324-330.

Vomocil, J. A. (1969). "Porosity." In Black, C. A., ed., *Methods of Soil Analysis, Part 1*, American Society of Agronomy, Wisconsin.

Wahrhaftig, C. (1965). *Physiographic Divisions of Alaska*, USGS Professional Paper 482, Washington, D.C.

Westgate, J. A., Stemper, B. A., Péwé, T. L. (1990). "A 3 m.y. record of Pliocene-Pleistocene loess in interior Alaska." *Geology*, 18, 858-861.

Williams, P. J. (1963). "Suction and its effects in unfrozen water of frozen soils." *Proc., Permafrost International Conference*, National Academy of Sciences, National Research Council, Lafayette, Indiana, 225-229.

Williams, P. J. (1964). "Unfrozen water content of frozen soils and soil moisture suction." *Geotechnique*, 14(3), 231-246.

Williams, P. J. (1966). "Pore pressures at a penetrating frost line and their prediction." *Geotechnique*, 16(3), 187-208.

Williams, P. J. (1976). "Volume change in frozen soils." *Laurits Bjerrum Memorial Volume – Contribution to Soil Mechanics*, 233-246.

Williams, P. J. (1977). "General properties of freezing soils." *In* Williams, P. J., Fremond, M., eds., *Soil Freezing and Highway Construction, Proc.*, Ottawa, Ontario, Canada.

Williams, P. J. (1979). *Pipelines and Permafrost: Physical Geography and Development in the Circumpolar North*, Longman, New York.

Williams, P. J. (1983). "Moisture migration in frozen soils." *Proc., Permafrost: Fourth International Conference*, University of Alaska Fairbanks and National Academy of Sciences, Fairbanks, Alaska, 64-66.

Winston, P. W., and Bates, D. H. (1960). "Saturated solutions for the control of humidity in biological research." *Ecology*, 41(1), 232-237.

Wood, J. A. (1990). "The role of irreversible thermodynamics and rheology in the regelation-flow phenomenon." *Cold Regions Science and Technology*, 18(2), 133-145.

Wood, J. A., and Williams, P. J. (1985). "Further experimental investigation of regelation flow with an ice sandwich permeameter." In Anderson, D. M., and Williams, P. J., eds., *Freezing and Thawing of Soil-Water Systems*, ASCE, New York.

Xu, X., Oliphant, J. L., Tice, A. R. (1987). *Factors Affecting Water Migration in Frozen Soils*, CRREL Report 87-9, Hanover.

Xu, X., Zhang, L., Wang, J., Deng, Y. (1999). *Mechanisms of Frost Heave and Salt Expansion of Soils,* Science Press, Beijing, China.

Yamamoto, H., Ohrai, T., Izuta, H. (1988). "Effect of over consolidation ratio of saturated soil on frost heave and thaw subsidence." *Proc., Permafrost: Fifth International Conference*, Norwegian Committee on Permafrost and Norwegian Institute of Technology, Trondheim, Norway, 522-527.

Yanagisawa, E., and Yao, Y. J. (1985). "Moisture movement in freezing soils under constant temperature condition." *Ground Freezing: Proc. of the Fourth International Symposium on Ground Freezing*, Sapporo-shi, Japan, 85-91.

Yang, D. (1997). *Investigation of the Scaling Laws for Centrifuge Modeling of Frost Heave,* Doctoral thesis, University of Maryland, Maryland.

Yoneyama, K., Ishizaki, T., Nichio, N. (1983). "Water redistribution measurements in partially frozen soil by x-ray technique." *Proc., Permafrost: Fourth International Conference*, University of Alaska Fairbanks and National Academy of Sciences, Fairbanks, Alaska, 1445-1450.

Yong, R. N., Boonsinsuk, P., Tucker, A. E. (1984). "A study of frost-heave mechanics of high-clay content soils." *Journal of Energy Resources Technology*, 106, 502-508.

Yong, R. N., Cheung, C. H., Sheeran, D. E. (1979). "Prediction of salt influence on unfrozen water content in frozen soils." *Engineering Geology*, 13(1-4), 137-155.

Zeta-Meter, Inc. (1975). *Zeta-Meter Manual*, 3rd Ed., Zeta-Meter, Inc., New York.

Zhestkova, T. N. (1978). "Results of experimental studies of the freezing process in very fine-grained soils." *Proc., Permafrost: Third International Conference*, National Research Council of Canada, Edmonton, Alberta, Canada, 1, 156-162.

Zoller, J. H. (1973). "Frost heave and the rapid frost heave test." *Public Roads*, 37, 211-220.

APPENDIX A
SUMMARY OF NOTATION AND SYMBOLS

Table A.1: Summary of notation and symbols

Notation or Symbol	Meaning	Page with Initial Use
AASHTO	American Association of State Highway Transportation Officials	27
AK DOT&PF NRML	Alaska Department of Transportation and Public Facilities Northern Region Materials Laboratory	27
Al^{3+}	aluminum cation	161
AMRL	AASHTO Materials Reference Laboratory	27
ASTM	American Society for Testing and Standards	28
BET	Brunauer, Emmett, and Teller equation	33
BP	before present	24
BSLN	"Baseline" samples	28
C	percent of particles smaller than 2μm	136
$\%Cl$	weight percent of chlorite	149
Ca^{2+}	calcium cation	34
CEC	cation exchange capacity	33
CR	Copper River silty clay	24
CRREL	U.S. Army Cold Regions Research and Engineering Laboratory	24
D^*	dielectric constant	54
d	spacing of mineral reflecting planes	36
DEA	DeArmoun sandy loam	24
DMSO	dimethyl sulfoxide	35
DPT	differential pressure transducer	61
E'	applied electric field	54
EC	electrical conductivity	50

Table A.1 (continued): Summary of notation and symbols

Notation or Symbol	Meaning	Page with Initial Use
Fe^{3+}	iron cation	161
FID	free induction decay	56
FS	Fairbanks silt	24
g	gravitational acceleration	51
$gradT$	temperature gradient in the frozen fringe	17
HR	heave rate	106
HS	Hanover silt loam	24
HV	Happy Valley silt loam	24
HV ORG	HV soil with original organic content	33
ΔH_f	frost heave amount at end of freezing test	17
H_l	sample length prior to freezing	17
h	matric suction	68
K^+	potassium cation	34
$\%Ka$	weight percent kaolinite	155
L_{fs}, L_f	latent heat of fusion per unit mass	5, 5
M_d	final dry mass	49
M_o	primary magnetic field	56
M_r	tare mass	49
M_w	gram molecular weight of water vapor	51
m	empirical parameter	68
MDC	main drying curve	46
Mg^{2+}	magnesium cation	34
MWC	main wetting curve	46
n	empirical parameter, an integer	68, 195
Na^+	sodium cation	34
NMR	nuclear magnetic resonance	9

Table A.1 (continued): Summary of notation and symbols

Notation or Symbol	Meaning	Page with Initial Use
ΔP_a	soil atmosphere pressure	79
P_i, p_i, ΔP_i	ice pressure	4, 5, 79
P_w, p_w, ΔP_w, p_w	water pressure, "total potential" of soil water	4, 5, 79, 83
p	hydrostatic pressure	83
PID	proportional, integral, derivative	61
R	ideal gas constant	51
R^2	coefficient of multiple determination	136
r^2	coefficient of determination	69
r_{iw}	radius of ice-water interface	4
RF	radio-frequency	56
RH	relative humidity	47
RTD	resistance temperature detector	60
$\%Sm$	weight percent smectite	155
S_e	effective saturation	68
SFC	soil freezing characteristic	78
SMC	soil-moisture characteristic	46
SP_o	segregation potential	17
T	absolute temperature	51
T_1	longitudinal relaxation time	57
T_2	transverse relaxation time	57
T_o	melting point of pure water	5
ΔT	temperature deviation from freezing point in °C	5
USDA	United States Department of Agriculture	28
U	freezing rate	17
U_o	soil constant	17

Table A.1 (continued): Summary of notation and symbols

Notation or Symbol	Meaning	Page with Initial Use
u	pore water pressure	14
u_i	pore ice pressure	14
USCS	Unified Soil Classification System	30
$\overline{V}$	specific volume of pore water solution	5
V_f	final water volume	49
$\overline{V_i}$	specific volume of ice	5
V_i	initial water volume	49
V_o	water intake flux	17
v_e	electrokinetic velocity	54
$w_{10^\circ C}$	measured water content at 10°C	58
w_f	final gravimetric soil moisture content	49
w_i	gravimetric soil moisture content	49
w_U	unfrozen water content	58
w_{paste}	moisture content of paste	50
w_{sample}	moisture content of sample	50
WSU	Washington State University	33
$x_{10^\circ C}$	NMR FID signal amplitude at 10°C	58
x_T	NMR FID signal amplitude at measured temperature	58
XRD	x-ray diffraction	8
α	empirical parameter	68
ζ potential	zeta potential or electrokinetic potential	41
η	slope of plot of $\sqrt{\psi_m}$ versus temperature	83
θ	volumetric water content, angle of reflection	68, 195

Table A.1 (continued): Summary of notation and symbols

Notation or Symbol	Meaning	Page with Initial Use
θ_i	volumetric moisture content	49
θ_r	residual volumetric water content	68
θ_s	saturated volumetric water content	68
λ	pore-size distribution index, wavelength of x-ray radiation	68, 195
μ	fluid viscosity	54
ξ	frost heave ratio	16
ξ_o	soil constant	17
π	osmotic pressure	83
ρ_b	dry bulk density	49
ρ_s	density of the solid	5
ρ_w	density of the wetting fluid	49
σ	applied overburden pressure	17
σ_{iw}	surface tension of ice-water interface	4
σ_n	neutral stress	14
σ_o	soil constant	17
Y_o	negative potential	41
Y_δ	negative potential at the Stern layer	41
$\chi(\psi)$	stress partition function	14
ψ_m	matric potential	46
ψ_o	osmotic potential	50
ψ_t	total potential	51

APPENDIX B

MAPS AND PHOTOGRAPHS OF ALASKAN SOIL SAMPLE LOCATIONS

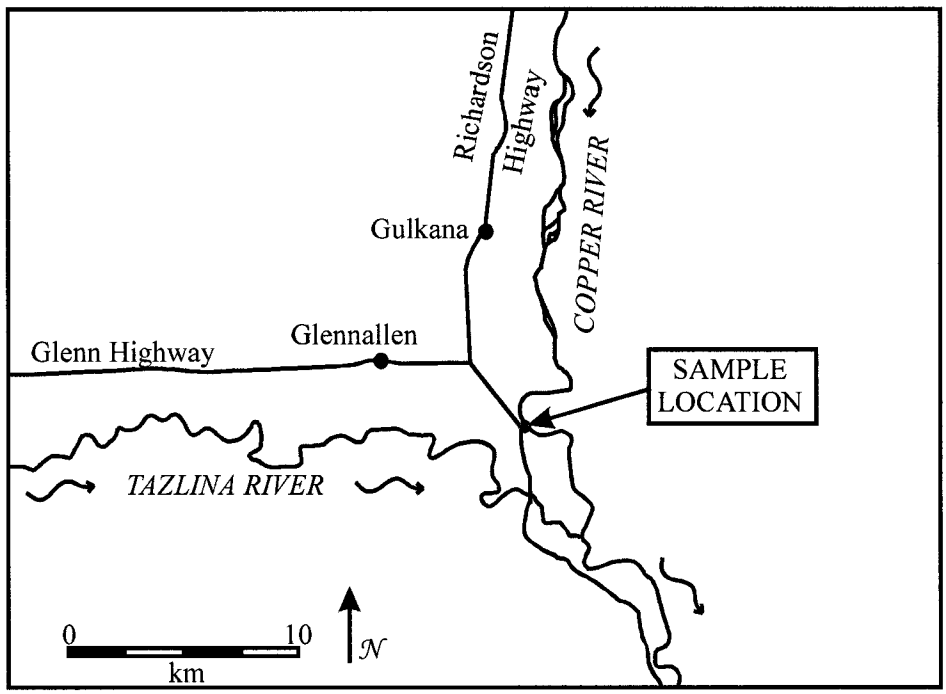

Figure B.1: Generalized map of the CR sample site area

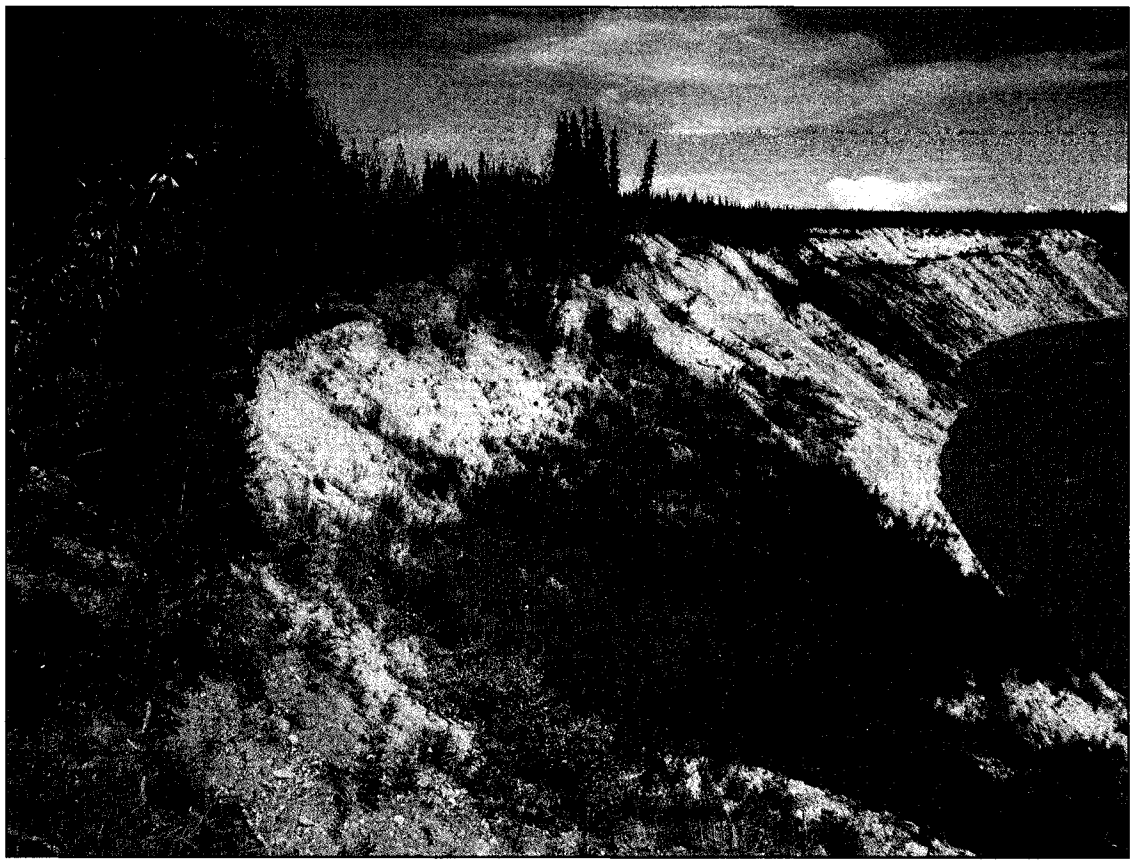

Figure B.2: Copper River silty clay (CR) sample location. The sample site is located immediately to the left of this photograph within the spruce forest. The Copper River is along the right extremity of the photograph, and is approximately 60 m lower in elevation than the ground surface at the left.

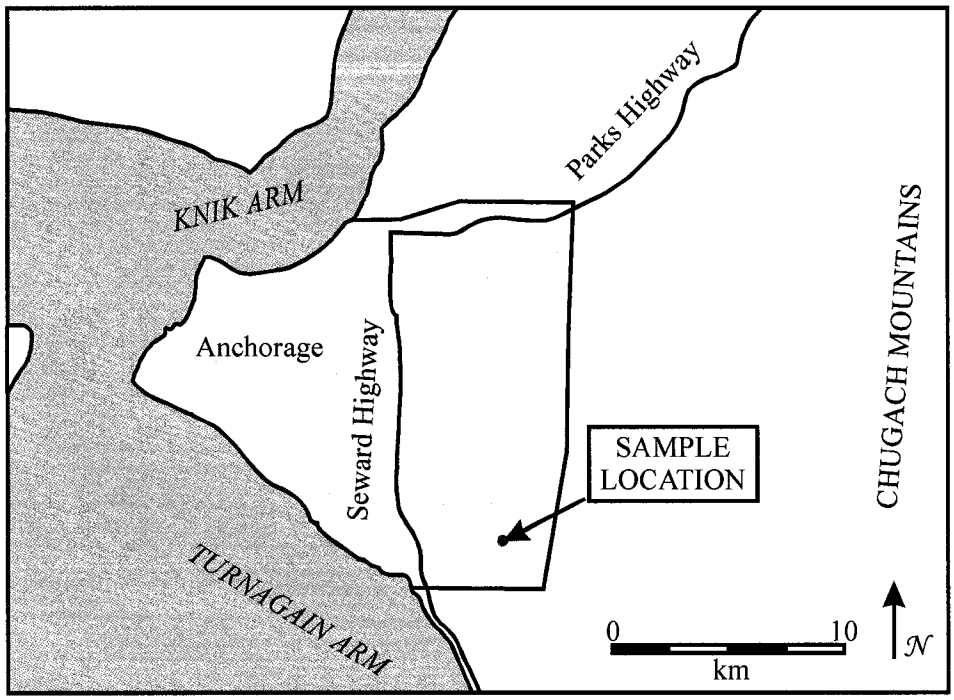

Figure B.3: Generalized map of the DEA sample site area

Figure B.4: DeArmoun sandy loam (DEA) sample location. This photograph shows pavement distress at the intersection of DeArmoun and Von Scheben roads. Soil was taken from the ditch to the left of the embankment in this photograph. The Chugach Mountains are visible in the distance. Photograph by D. Hemstreet, 2003.

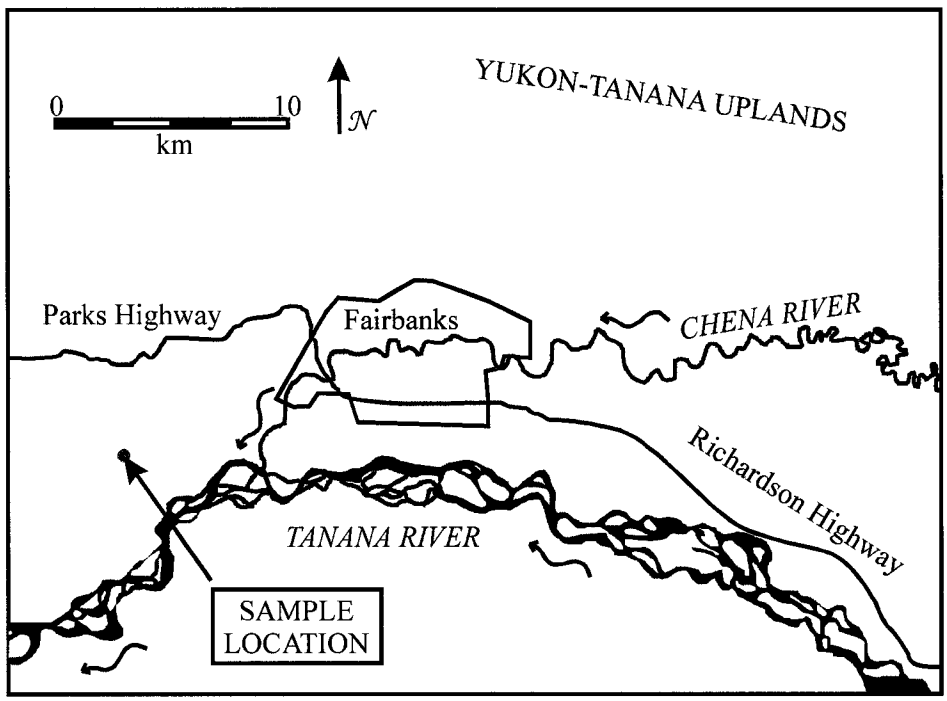

Figure B.5: Generalized map of the FS sample site area

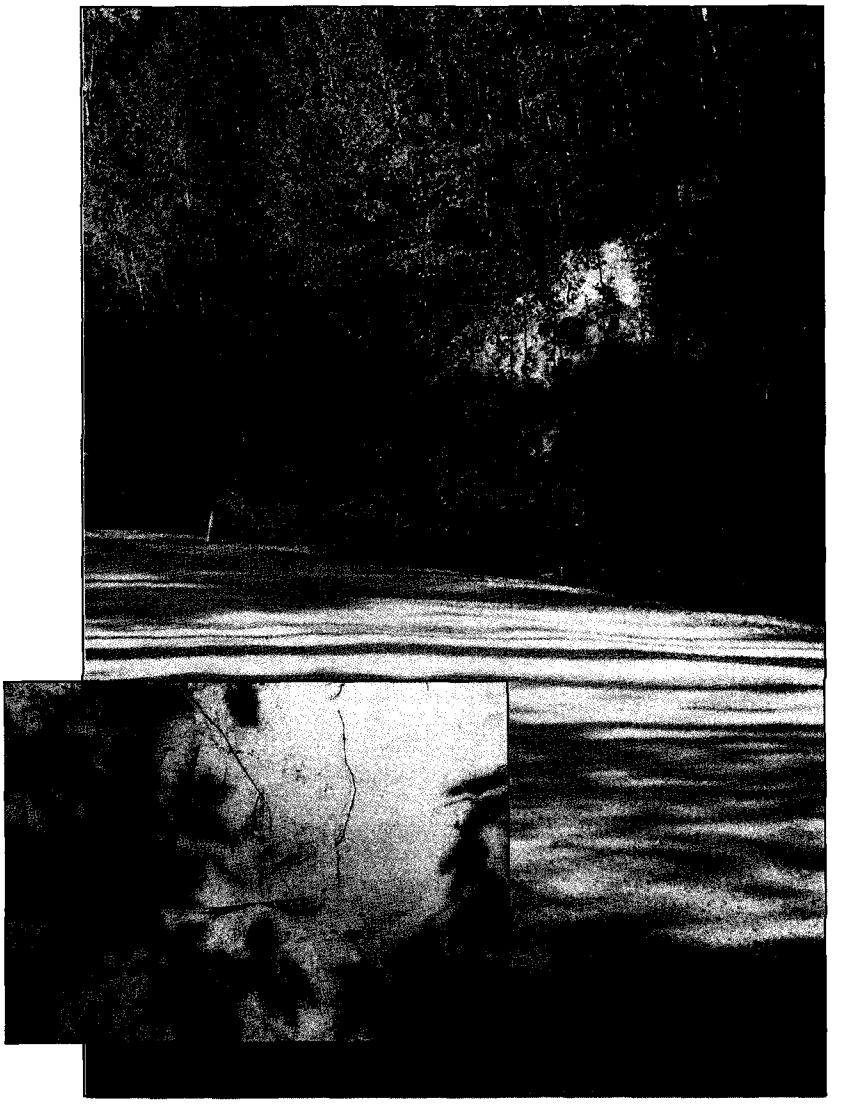

Figure B.6: Fairbanks silt (FS) sample location. The large photograph shows the sampled road cut along Fiddle Way and the inset is a close-up view of the FS soil.

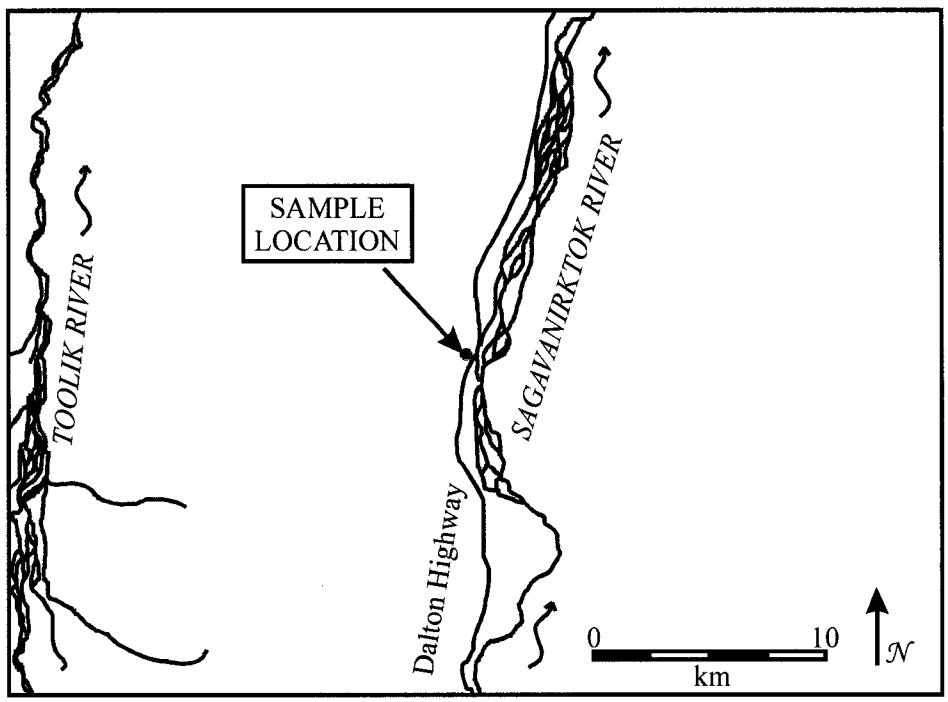

Figure B.7: Generalized map of the HV sample site area

(a) (b)

Figure B.8: Happy Valley silt loam (HV) sample location. The sampled test pit is shown in (a), and (b) is a view of the tundra at Happy Valley. Photographs by J. Bickley, 2004.

APPENDIX C
OVERVIEW OF MINERAL IDENTIFICATION THROUGH X-RAY DIFFRACTION

C.1 Overview of X-ray Diffraction

In the early 20th century, researchers discovered that there is a period arrangement of atoms in crystals, and that crystals will diffract x-rays. The reflected x-ray wavelength from a mineral crystal is related to the lattice plane spacing (Nuffield 1966), and can be described using Bragg's Law:

$$n\lambda = 2d\sin\theta \qquad \text{(C.1)}$$

where n is an integer, λ is the wavelength of the x-ray radiation, d is the spacing of the reflecting planes, and θ is the angle of reflection (see Figure C.1 for a graphical representation of these values).

By knowing the wavelength of the x-rays and by measuring the 2θ angle, one can use Bragg's Law to calculate the d-spacing that produces a specific peak in a diffraction pattern. Each peak in a given diffraction pattern can then be compared to the d-spacing of various minerals, facilitating the identification of the individual minerals in the sample. For optimum clay mineral identification, the mineral grains should be oriented with their c-axes pointing up. This is called preferred orientation, as all of the grains are presenting their (001) planes to the x-rays (Nuffield 1966).

C.2 Mineral Structure and XRD Patterns

C.2.1 Kaolinite – $Al_2Si_2O_5(OH)_4$

Kaolinite is a 1:1 clay, consisting of one silica tetrahedral sheet and one alumina octahedral sheet. These sheets are held together by oxygen atoms that are mutually shared by the silicon and aluminum atoms in their respective sheets (Tan 1998). Repeated dual sheets are then held together by hydrogen bonding, giving it a basal spacing of roughly 7.14 Å (see Figure C.2). Laboratory testing indicates that there is very little isomorphic substitution in kaolinite, which results in a low CEC (10-100 mmol/kg) (Tan 1998).

Kaolinite particles are more resistant to weathering due to the close structural bonds (Tan 1998), making it the most wide-spread aluminosilicate mineral in soils, and in clay and shale deposits (Moore and Reynolds, Jr. 1997). Also because of its close structural bonds,

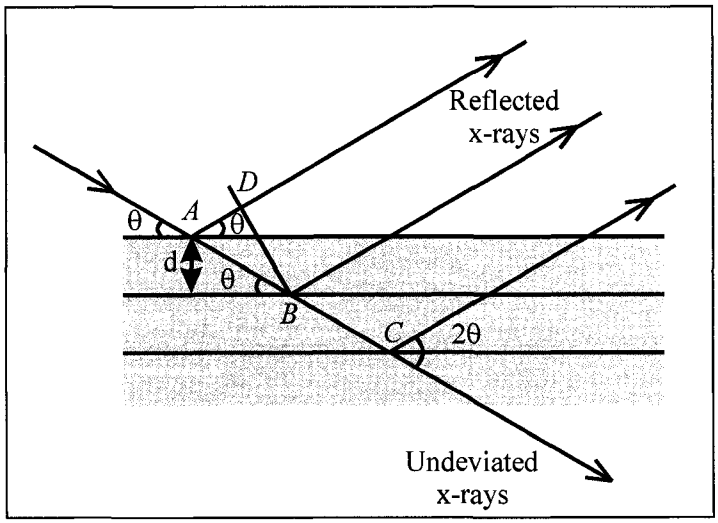

Figure C.1: Schematic of a mineral surface, showing incoming and reflected x-rays. (Adapted from Nuffield (1966)).

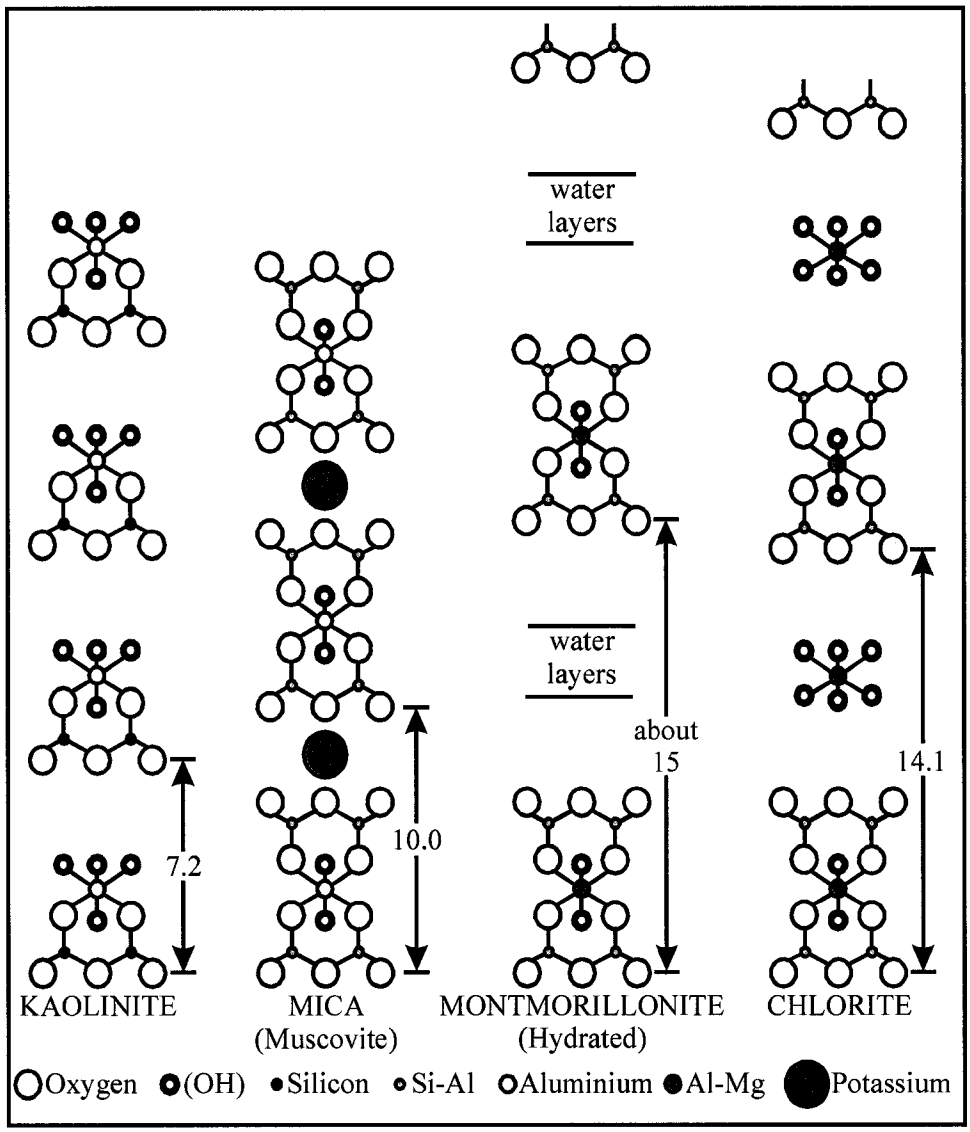

Figure C.2: Diagrammatic representation of layer succession in some layer lattice silicates. Distances between repeating basal units are given in Angstroms. (Adapted from Brown (1961)).

kaolinite exhibits low plasticity and does not shrink and swell (Tan 1998). Kaolinite crystals generally are the largest of the clay minerals, giving it a low specific surface area (7-30 m^2/g).

Kaolinite is usually identified in XRD analysis by its (001) peak at about 7 Å ($2\theta = 12.65°$) and its (002) peak at around 3.57-3.58 Å ($2\theta = 24.87°$). Unfortunately, the chlorite diffraction pattern matches this almost exactly. Therefore, to truly determine the presence of kaolinite, other diagnostic techniques are necessary. If the sample is heated to above 550°C, the hydroxides are forced out of the structure and kaolinite collapses to metakaolinite, which is an x-ray amorphous mineral (Carroll 1970). Thus, the peaks from kaolinite disappear, leaving only those for chlorite and other minerals. Finally, if the sample is intercalated with dimethyl sulfoxide (DMSO) vapor, the (001) peak shifts to 11.2 Å ($2\theta = 7.89°$) (Moore and Reynolds, Jr. 1997). This procedure, although more involved, allows the definitive identification of kaolinite.

C.2.2 Illite and Muscovite – $KAl_2(AlSi_3O_{10})$

Although muscovite is not a clay mineral, it is included here in a discussion of illite because of its structural similarity. Muscovite is the predominate micaceous mineral found in soils, due to its resistance to weathering. For example, biotite has more magnesium and iron than muscovite, which makes its bonds weaker. Typically, biotite is only found in soils near the source rock (Carroll 1970).

Muscovite is a 2:1 mineral, consisting of two silica tetrahedral sheets sandwiching an alumina octahedral sheet (see Figure C.2). The sheets are connected to each other by K^+ ions in 12-fold coordination with the silica tetrahedral oxygen atoms (Carroll 1970). The interlayer K^+ ions give muscovite a basal spacing of roughly 9.95 Å. Muscovite's diffraction pattern begins with the (001) peak at 9.95 Å ($2\theta = 8.89°$), followed by the (002) through (005) peaks at regular intervals. The (003) peak at 3.3 Å ($2\theta = 26.8°$) usually overlaps the main diagnostic peak of quartz.

Illite's structure is similar to that of muscovite, except that illite contains less K^+, and more silicon and water than muscovite. The exact structure is not easy to determine, as the term "illite" may represent a range of minerals, much like the plagioclase series (Moore and Reynolds, Jr. 1997). Some researchers consider illite to be a continuous series between muscovite and smectite, as it often occurs in mixed-layers with smectite (Tan 1998), and its specific surface area ranges between 80 and 150 m^2/g (McBride 1994). Because of the loss of some K^+ ions, the illite structure is not charge-balanced, giving it a CEC of about 300 mmol/kg.

The remaining K^+ ions give illite a basal spacing of about 10 Å, and cause it to have low plasticity and shrinking and swelling abilities (Tan 1998).

Illite can be identified in XRD analysis by its (001) peak at roughly 10 Å ($2\theta = 8.85°$), and successive (00*l*) peaks at regular intervals. These peaks are unaffected by heating to 550°C or by glycerol solvation (Moore and Reynolds, Jr. 1997). Although the peaks of illite are broader than those of muscovite due to mixed-layering, the peaks are nearly identical to those of muscovite and it is impossible to determine if the peaks represent illite or muscovite. Another mineral identification method must be used to make this determination.

C.2.3 Smectite – $(Al_2O_3)(SiO_2)_4(H_2O) + xH_2O$

Smectite is the name for a group of expandable 2:1 clay minerals. The smectite structure is similar to that of muscovite; however, instead of K^+ ions, the interlayers are filled with water surrounding hydrated cations (see Figure C.2). The interlayer water thickness can expand and contract, depending on water conditions, without ruining the structural integrity of the clay (Moore and Reynolds, Jr. 1997). When air-dry, the d-spacing of smectite is roughly 12.4-14 Å. This can vary, however, depending on how much interlayer water is present. In an oven-dry state, the d-spacing is roughly 10 Å.

Isomorphous substitution occurs often in both the tetrahedral and octahedral sheets with nearly an infinite number of combinations of positions and cations (Carroll 1970). This makes the chemical formula difficult to determine. The high isomorphic substitution gives smectite a large CEC (700 mmol/kg). The smectite particles are extremely fine-grained, with a specific surface area of roughly 700-800 m^2/g. The large specific surface area leads to high plasticity and stickiness when wet (Tan 1998). Smectites commonly are formed from the weathering of igneous and metamorphic rocks in an alkaline environment, and can be found in soils in arid areas (Carroll 1970). These minerals often are present in continental and oceanic sediment formed during the Cretaceous and later (Odom 1984).

Because of the reasons stated above, the (001) peak reflection can vary between roughly 10 to 14 Å. Several other minerals have their (001) peak reflections in this same range, making identification of smectite problematic. The solution to this problem is to compare the diffraction patterns of air-dried smectite with an ethylene glycol-solvated or glycerol-solvated diffraction pattern. After the adsorption of ethylene glycol or glycerol, the d-spacing expands to 17 to 18 Å ($2\theta = 5.2°$ to $4.9°$) (Moore and Reynolds, Jr. 1997). Additionally, if the sample is saturated with

K^+ and dried at 300°C, the basal spacing collapses to 10 Å. This can be used as a second identification feature, unless illite and/or muscovite are present in the soil as well.

C.2.4 Chlorite – $(Mg,Fe,Al)_6(Al,Si)_4O_{10}(OH)_8$

Chlorite also has a structure similar to that of muscovite, with an alumina octahedral sheet sandwiched between two silica tetrahedral sheets (see Figure C.2). It differs from muscovite, as the layers are held together with a brucite-like layer. In some texts, this is called a 2:1:1 or a 2:2 structure. Isomorphic substitution occurs within the "mica-like" sheets, allowing chlorite to range from iron-rich to magnesium-rich (Carroll 1970). The negative charge that is formed from this substitution is neutralized by isomorphic substitution of Mg^{2+} by Al^{3+} in the brucite-like interlayer-sheet. Overall, the structure has a small negative charge, resulting in a moderate CEC ranging between 100 and 400 mmol/kg (Grim 1962). Chlorite's specific surface area is approximately 80 m^2/g (Hillel 1980).

As mentioned previously, the peaks in the chlorite diffraction pattern coincide with those of kaolinite and possibly smectite. Its (001) peak is at about 14 Å ($2\theta = 6.3°$) followed by the (002) through (005) peaks at regular intervals. These peaks do not change with heat treatments, or glycerol or ethylene glycol treatments.

Chlorites occur in low-grade schists (giving rise to the name "green schist facies"), metamorphosed iron-bearing sediments, and in pre-Tertiary consolidated sedimentary rocks (Carroll 1970). Chlorites are often found in detrital sediments coming from the glacial erosion of metamorphic rocks.

C.2.5 Mixed-layer Clay Minerals

To further complicate mineral identification, some of the clay minerals will form "mixed-layer" clays, in which structural elements of two different minerals are present in one platelet. The two most common mixed-layer clays in soils are illite/smectite (I/S) and chlorite/smectite (C/S) (Moore and Reynolds, Jr. 1997). The presence of either of these clay minerals can be determined from a shift and/or broadening of peaks in an ethylene glycol- or glycerol-solvated sample as compared to the air-dried sample. The range of 2θ values is large due to the many variations of mixed-layer clays. Moore and Reynolds, Jr. (1997) offer a complete discussion on the identification of mixed-layer clays.

C.2.6 Quartz – SiO_2

Unlike the clay minerals, quartz and other silica minerals can be considered inert in the soil. They have low chemical activity, a nearly absent surface charge, and a very small specific surface area (2-3 m^2/g) (Tan 1998). However, since quartz is present in the clay-sized fraction of soils, its peaks are present in the XRD patterns. The (101) peak occurs at 3.34 Å ($2\theta = 26.7^{\circ}$) with a smaller (θ01) peak at 4.26 Å ($2\theta = 20.8^{\circ}$).

C.2.7 Feldspars

Moore and Reynolds, Jr. (1997) state: "There must be someone who loves feldspars, but to the clay mineralogist they are an unmitigated headache. They have many reflections that interfere with almost anything you want to do beyond a simple qualitative analysis." With this in mind, feldspars will be discussed in very little detail.

APPENDIX D

XRD PATTERNS AND PROCEDURES

D.1 WSU XRD Analysis Charts

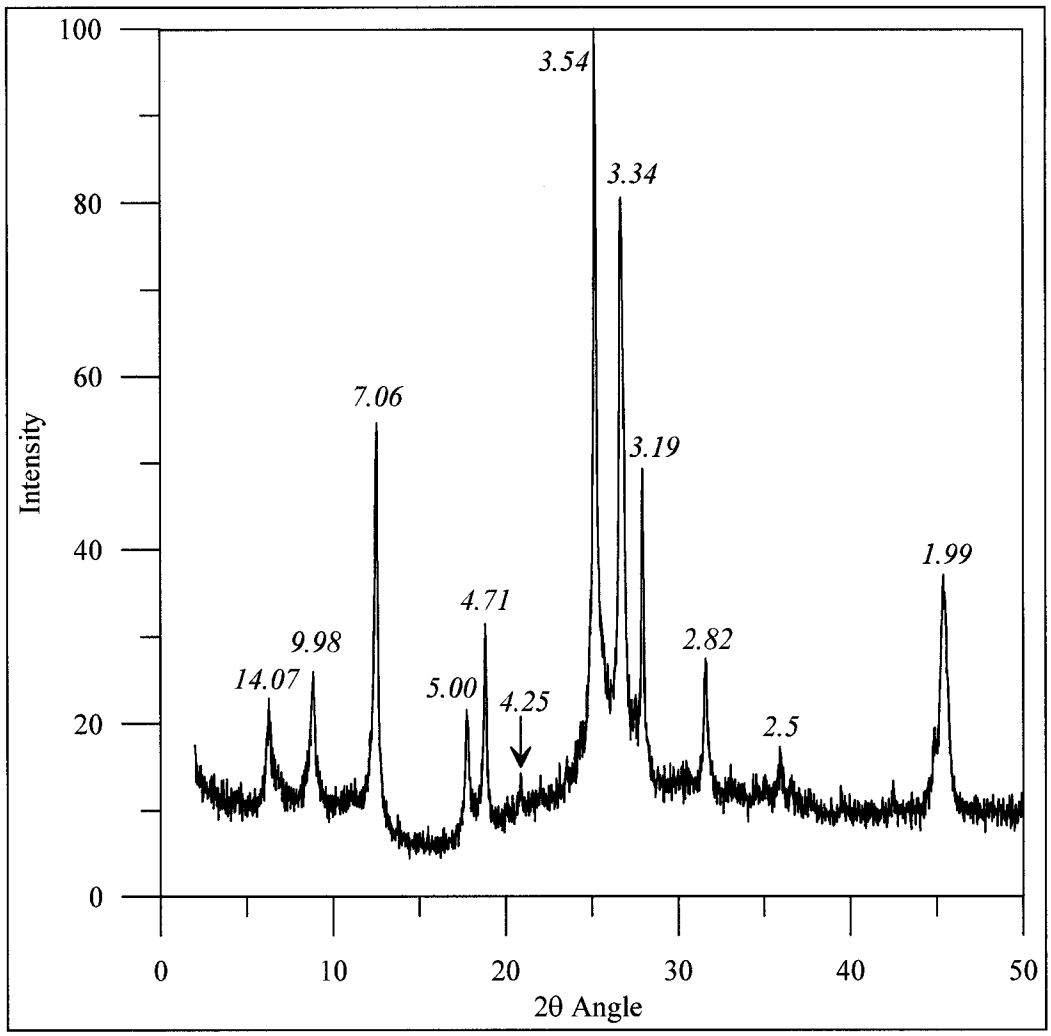

Figure D.1: Full-range XRD pattern for DEA. Annotation above or near each major peak gives the d-spacing in Angstroms.

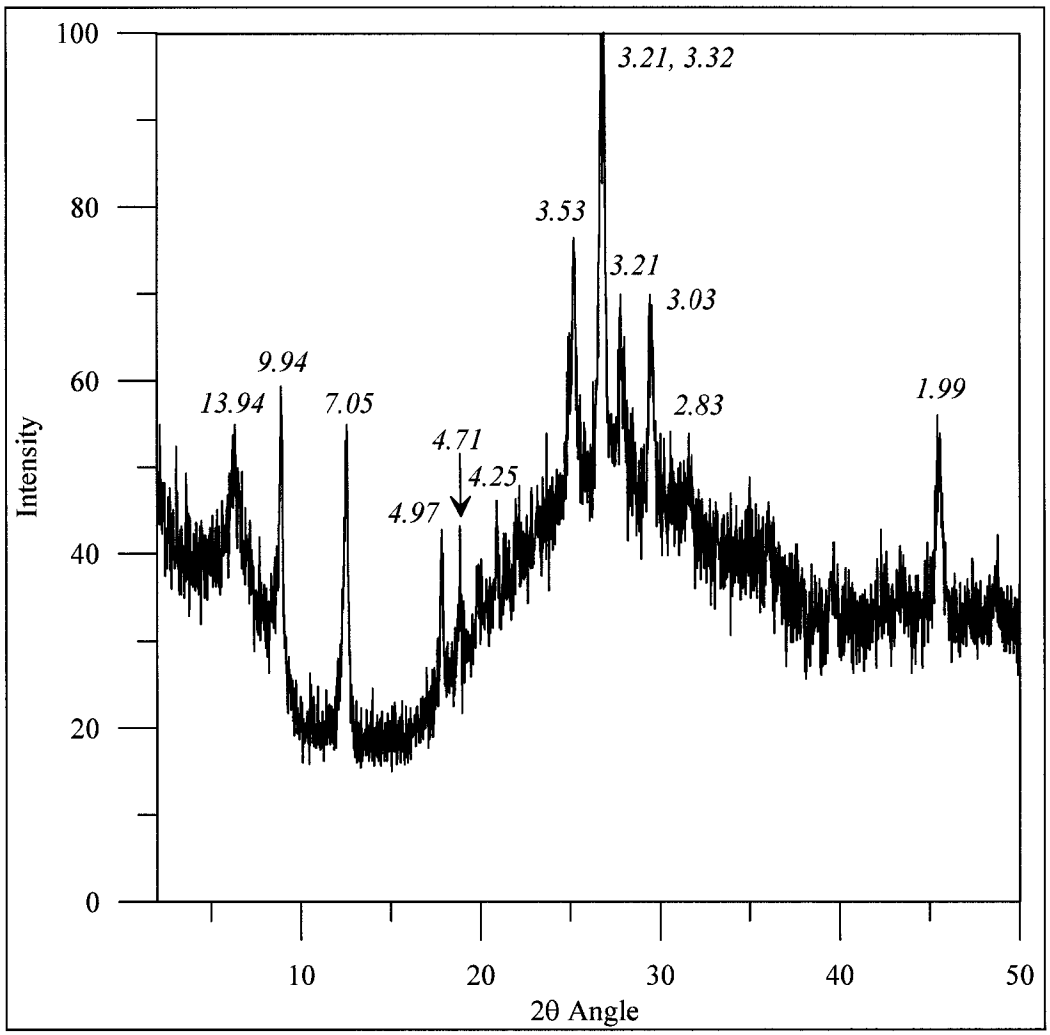

Figure D.2: Full-range XRD pattern for FS. Annotation above or near each major peak gives the d-spacing in Angstroms.

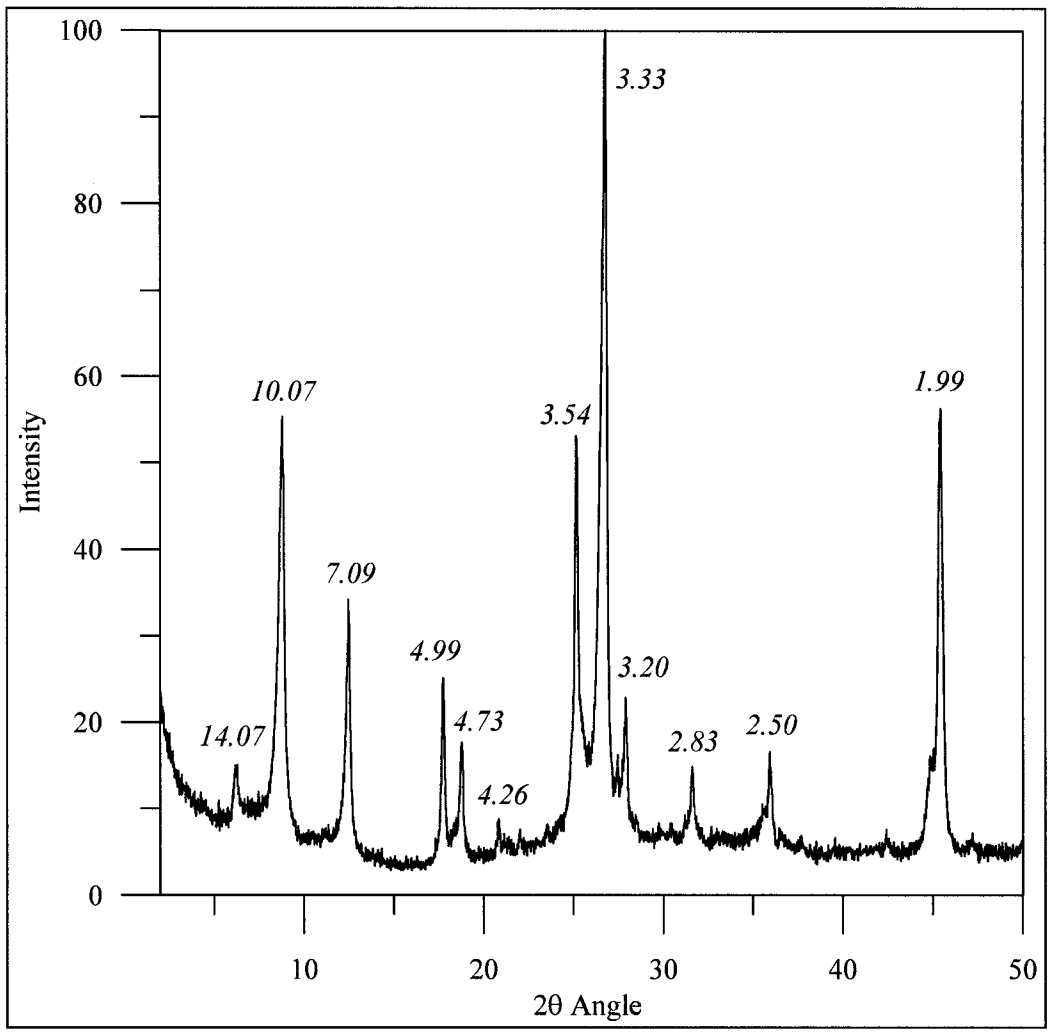

Figure D.3: Full-range XRD pattern for HS. Annotation above or near each major peak gives the d-spacing in Angstroms.

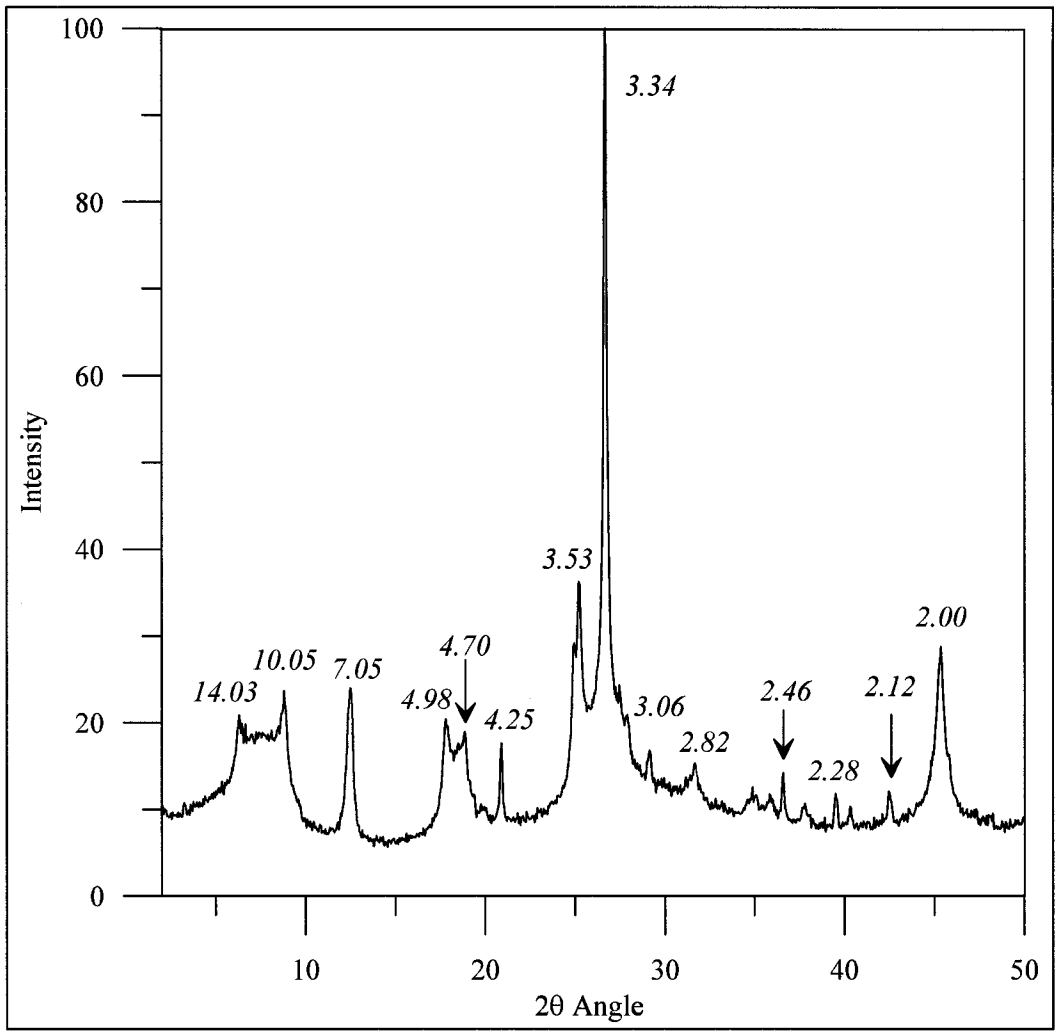

Figure D.4: Full-range XRD pattern for HV. Annotation above or near each major peak gives the d-spacing in Angstroms.

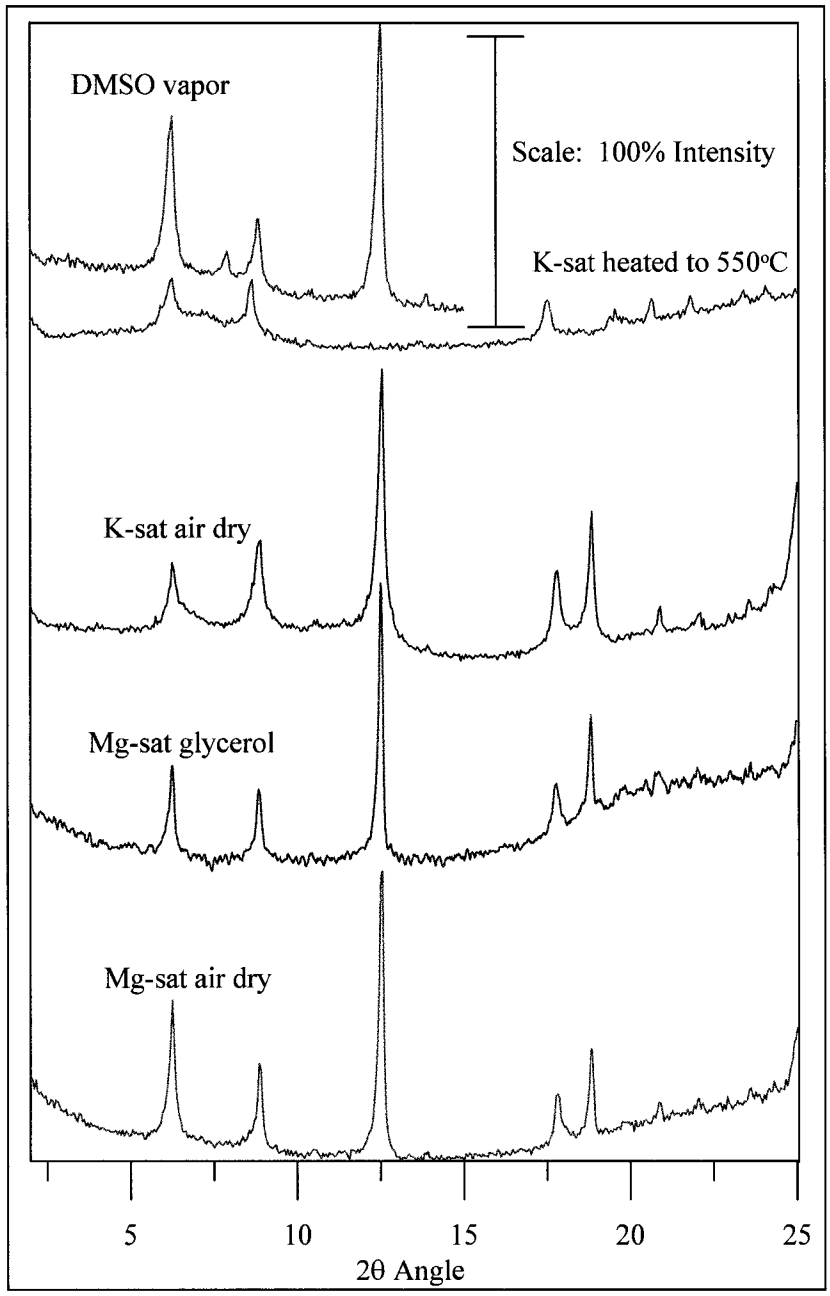

Figure D.5: XRD patterns of the various treatments on DEA soil

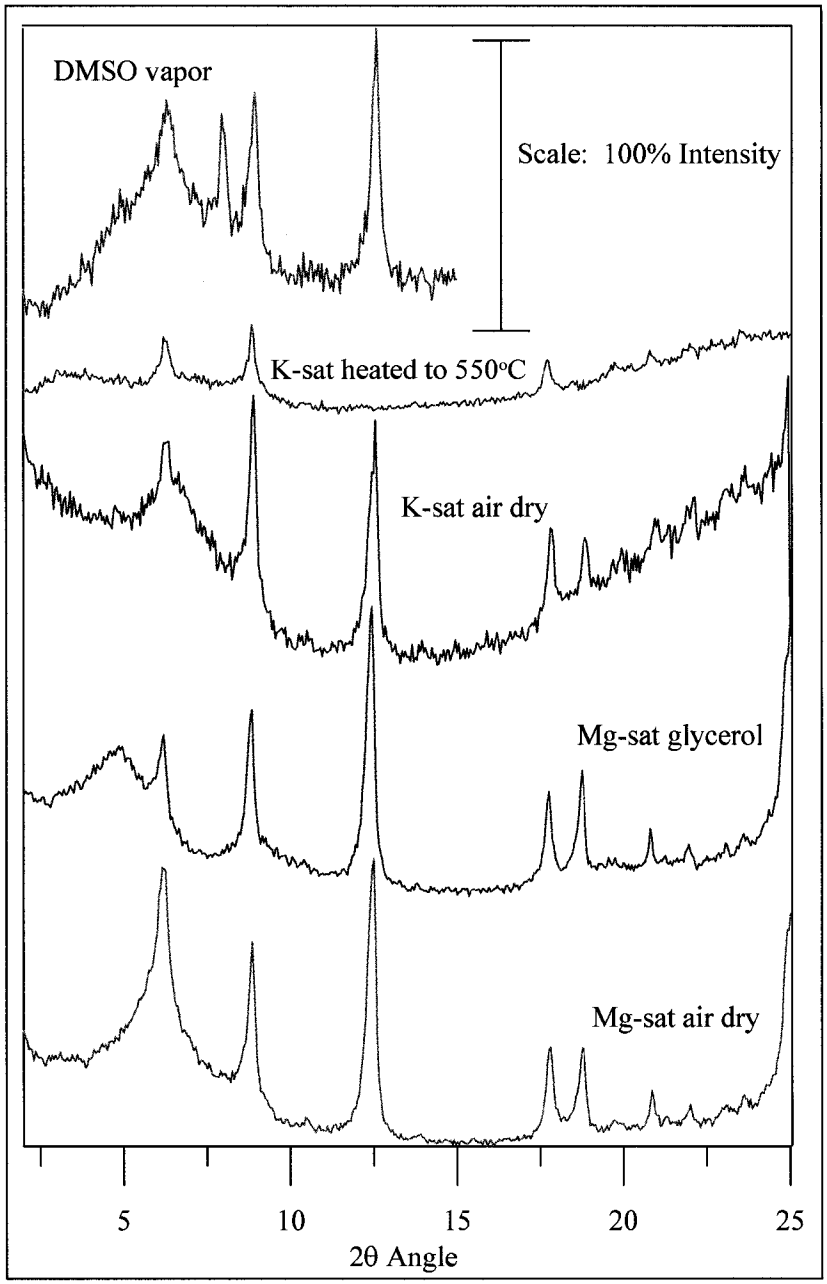

Figure D.6: XRD patterns of the various treatments on FS soil

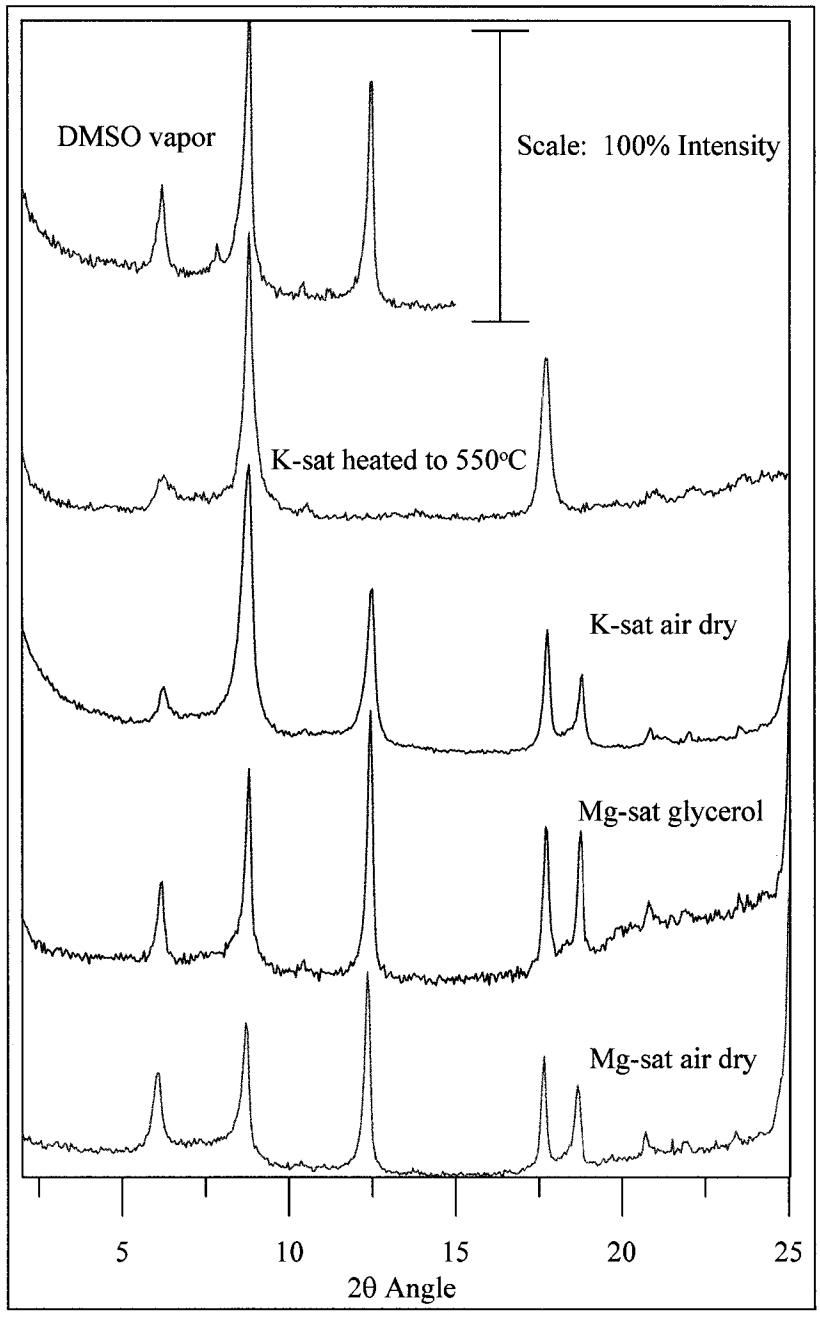

Figure D.7: XRD patterns of the various treatments on HS soil

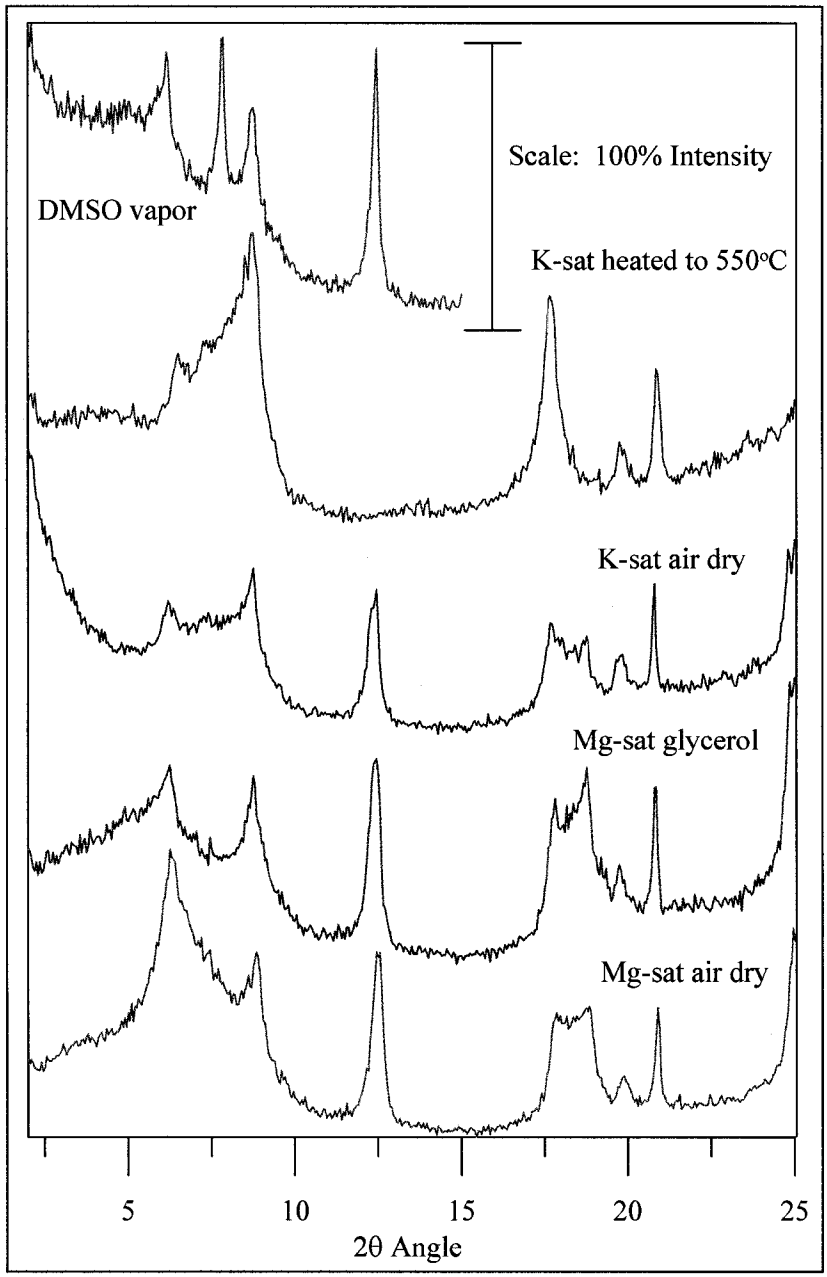

Figure D.8: XRD patterns of the various treatments on HV soil

D.2 K/T GeoServices, Inc. Whole Rock and Clay Fraction XRD, Sample Preparation and Analytical Procedures (Verbatim, 2006)

Samples submitted for whole rock and clay mineral XRD analyses are cleaned of obvious contaminants and disaggregated in a mortar and pestle. A split of each sample is then transferred to distilled water and pulverized using a McCrone micronizing mill. The resultant powder is dried, disaggregated, and packed into a metal sample holder to produce random whole-rock mounts. A separate split of each sample is dispersed in distilled water using a sonic probe. The suspensions are then size fractionated with a centrifuge to isolate clay-size (<4 micron equivalent spherical diameter) materials for a separate clay mount. The suspensions are then vacuum deposited on nylon membrane filters to produce oriented clay mineral mounts. The clay mineral mounts are attached to glass slides and exposed to ethylene glycol vapor for approximately 12 hours.

X-ray Diffraction (XRD) analyses of the samples are performed using a Rigaku automated powder diffractometer equipped with a copper X-ray source (40kV, 35mA) and a scintillation X-ray detector. The whole rock samples are analyzed over an angular range of two to sixty-five degrees two theta at a scan rate of one degree per minute. The glycol solvated oriented clay mounts are analyzed over an angular range of two to thirty six degrees two theta at a scan rate of one degree per minute.

Semiquantitative determinations of whole-rock mineral amounts are done utilizing integrated peak areas (derived from peak-decomposition / profile-fitting methods) and empirical reference intensity ration (RIR) factors determined specifically for the diffractometer used in data collection. The total phyllosilicate (clay and mica) abundance of the samples is determined on the whole-rock XRD patterns using combined {001} and {hkl} clay mineral reflections and suitable empirical RIR factors.

XRD patterns from glycol-solvated clay-fraction samples are analyzed using techniques similar to those described above. The relative amounts of phyllosilicate minerals are determined from the patterns using profile-fitted integrated peak intensities and combined empirical and calculated RIR factors. Determinations of mixed-layer clay ordering and expandability are done by comparing experimental diffraction data from the glycol-solvated clay mounts with simulated one dimensional diffraction profiles generated using the program NEWMOD written by R. C. Reynolds.

D.3 XRD Patterns from K/T GeoServices, Inc.

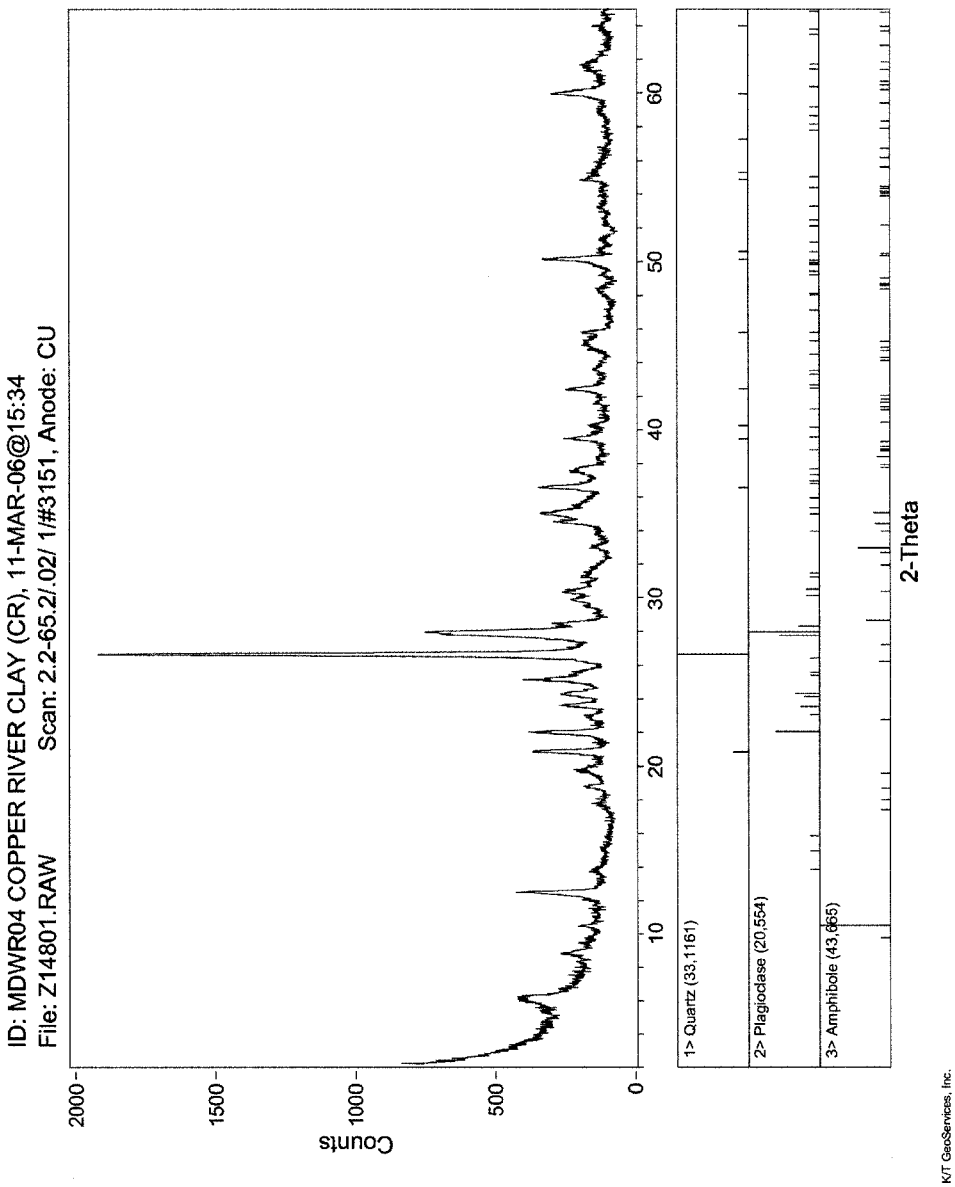

Figure D.9: Whole rock XRD pattern for CR

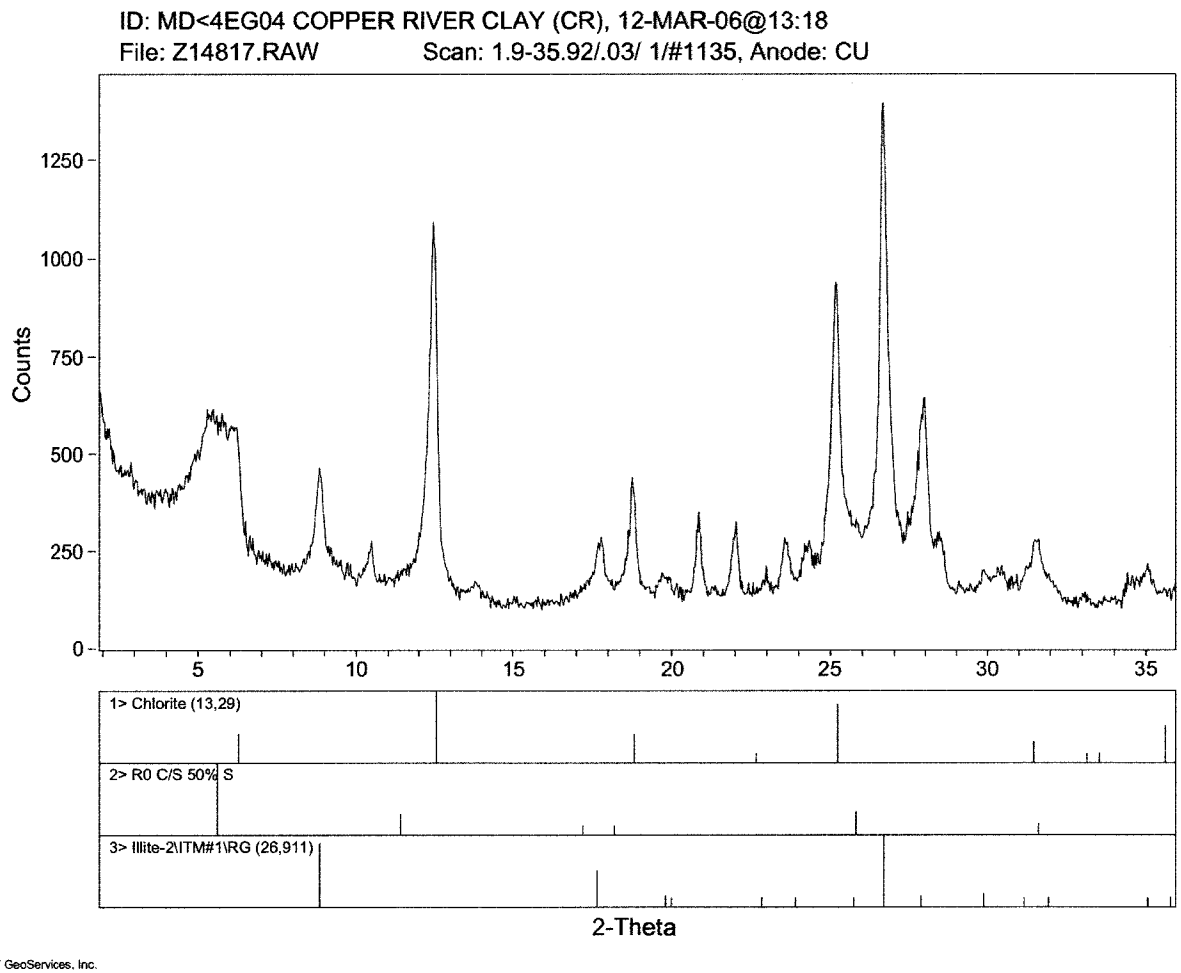

Figure D.10: Ethylene glycol solvated XRD pattern for CR

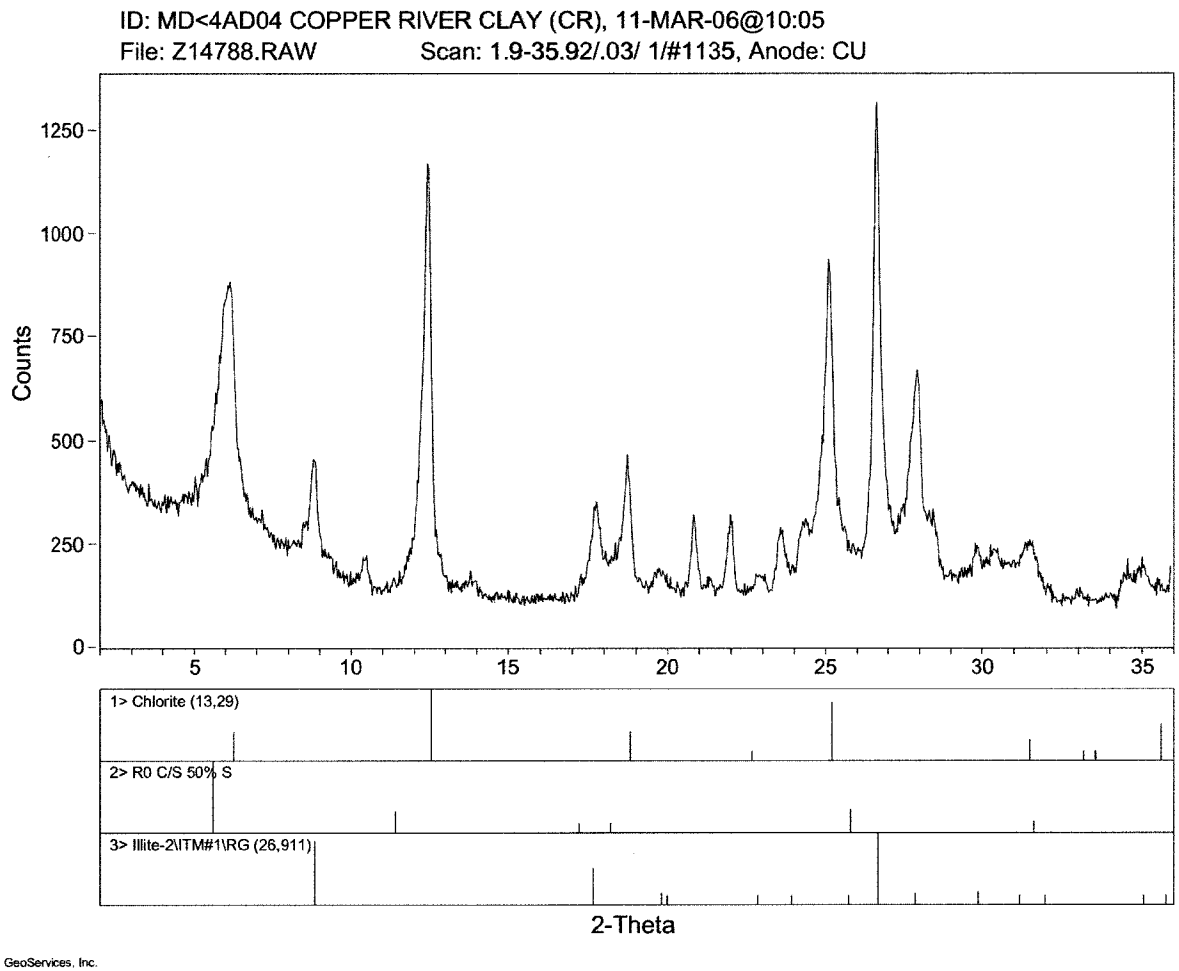

Figure D.11: Air-dried XRD pattern for CR

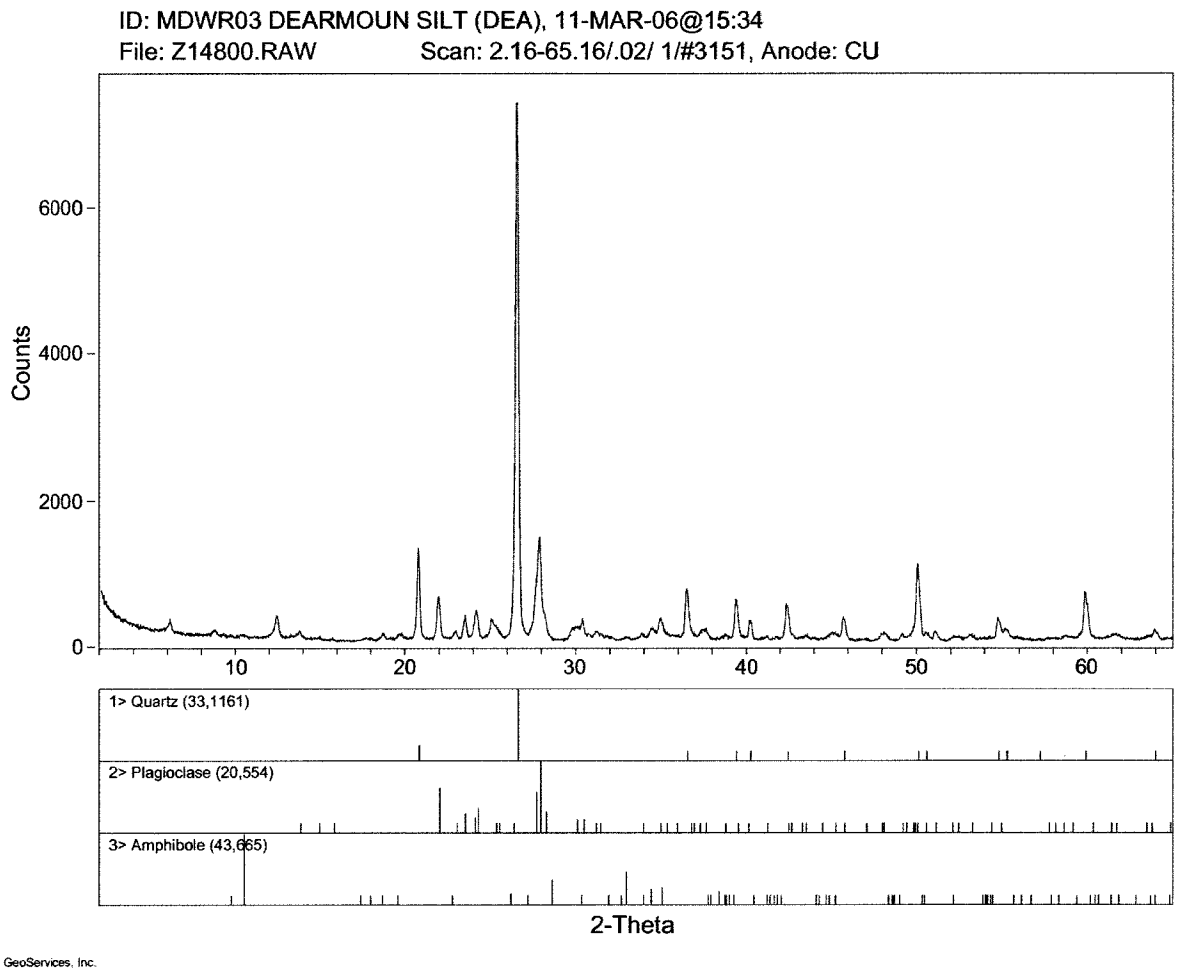

Figure D.12: Whole rock XRD pattern for DEA

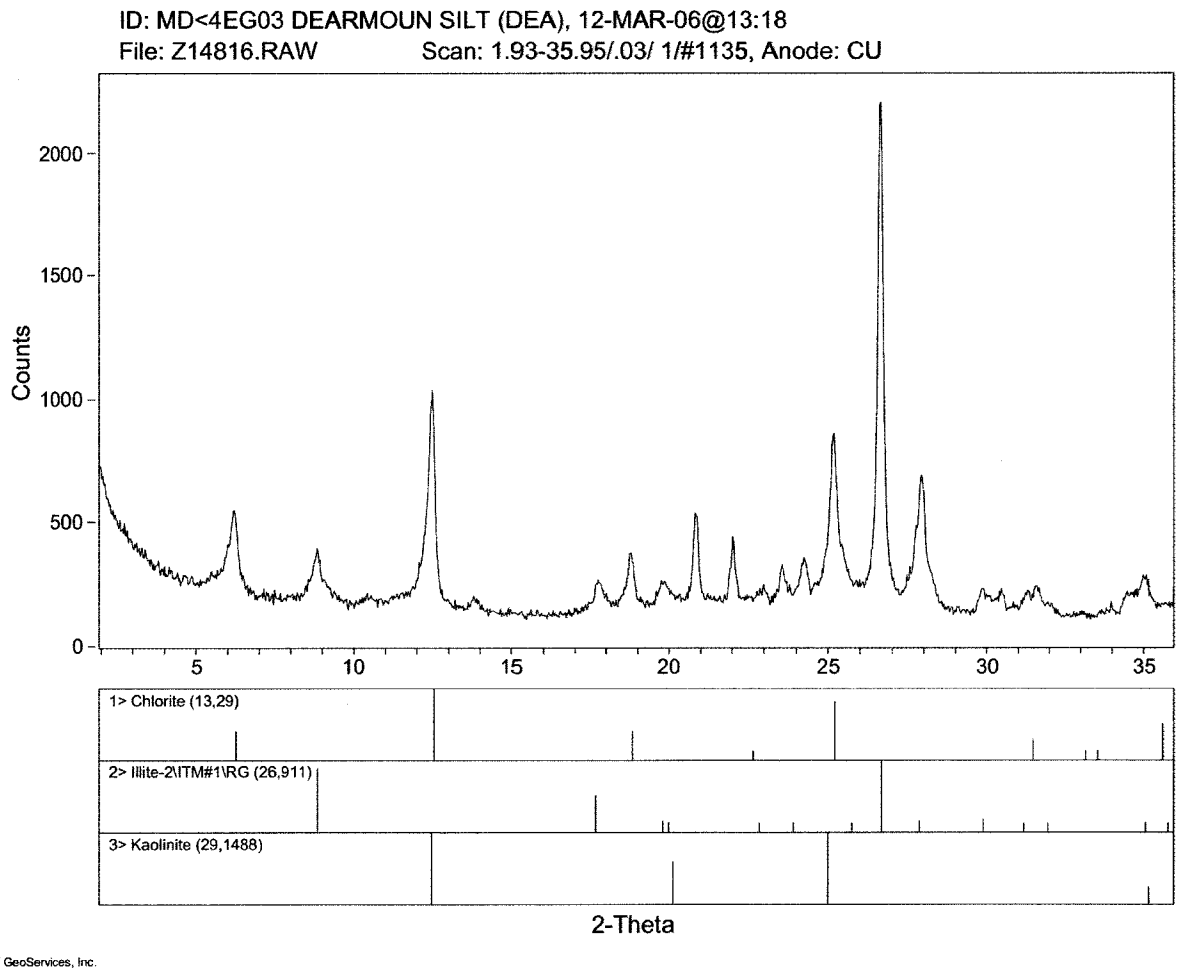

Figure D.13: Ethylene glycol solvated XRD pattern for DEA

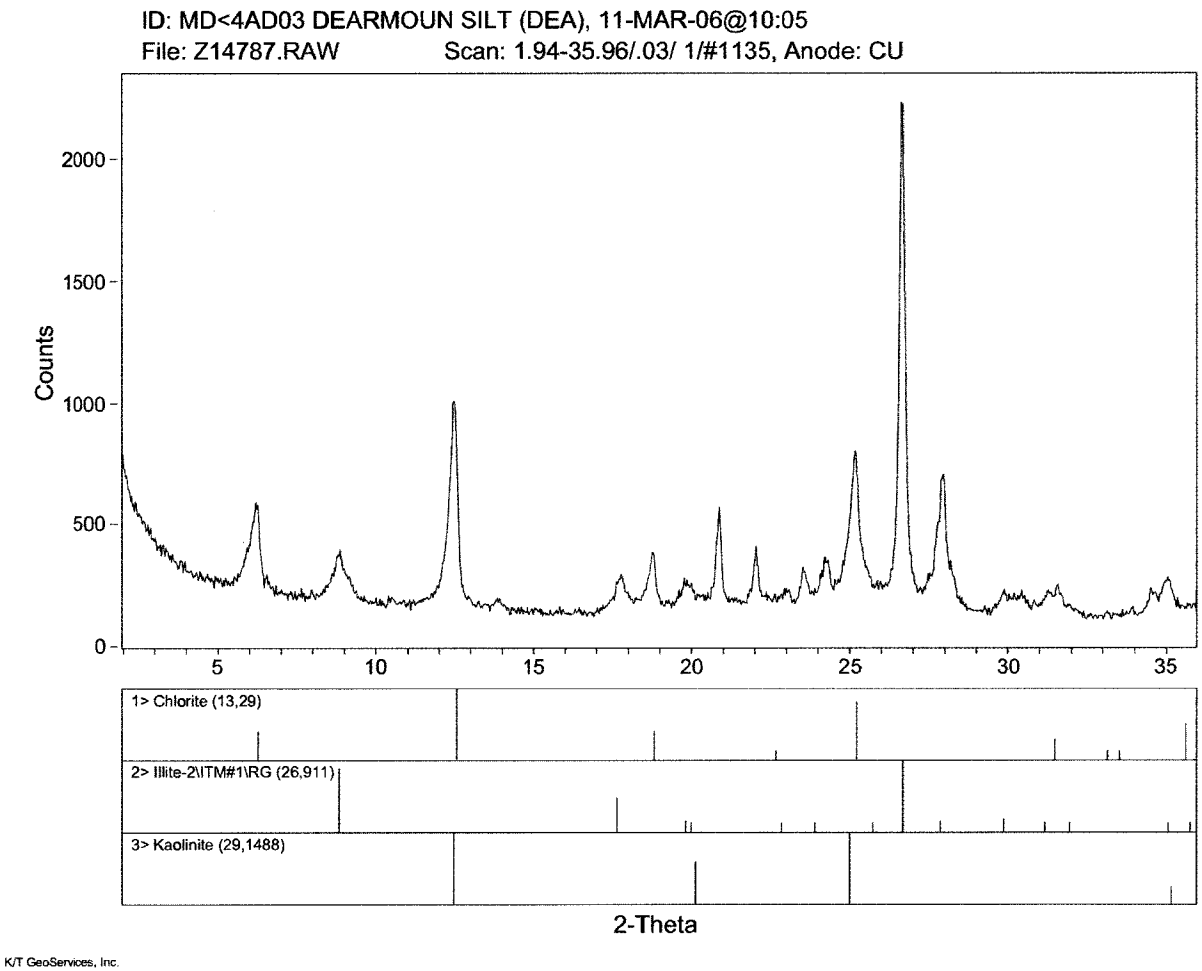

Figure D.14: Air-dried XRD pattern for DEA

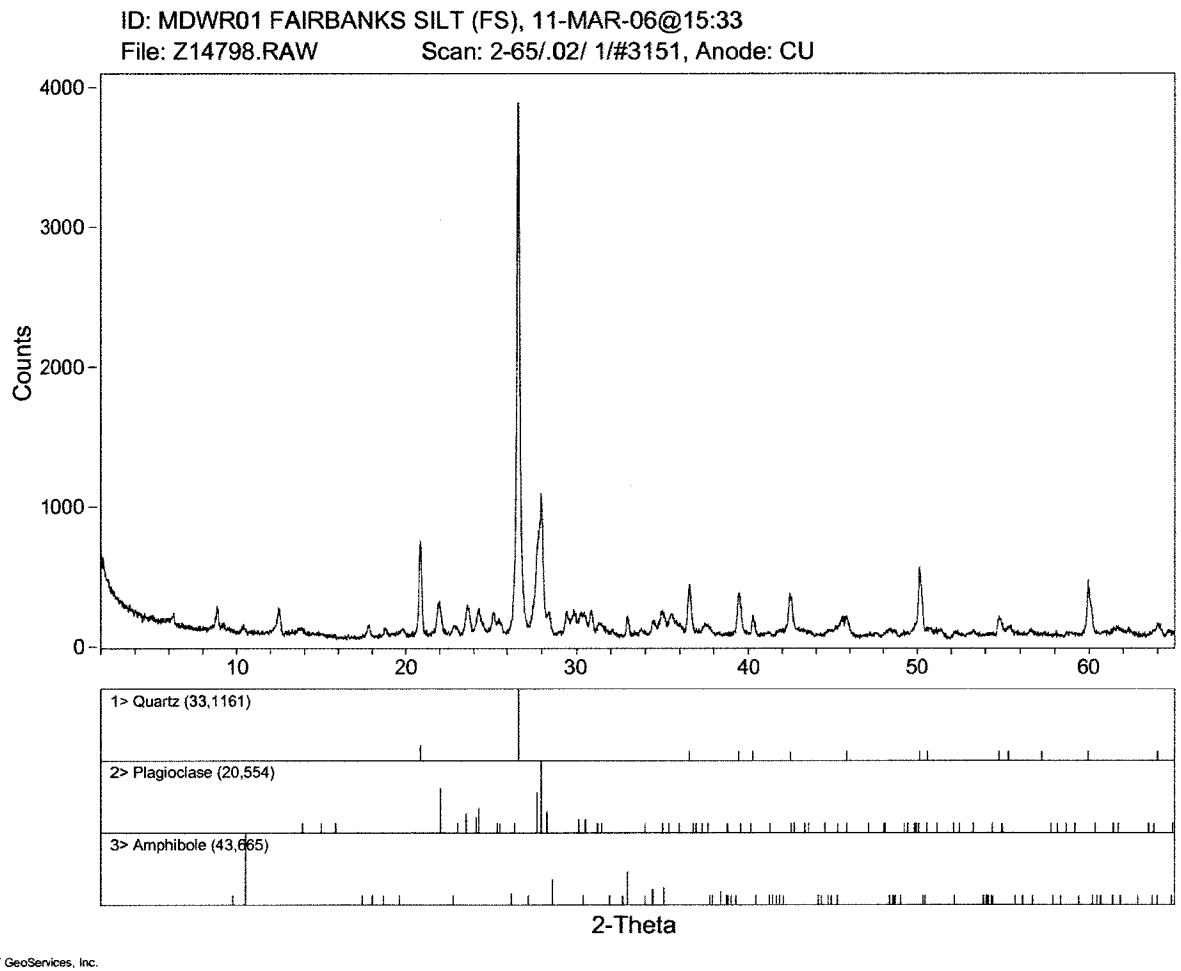

Figure D.15: Whole rock XRD pattern for FS

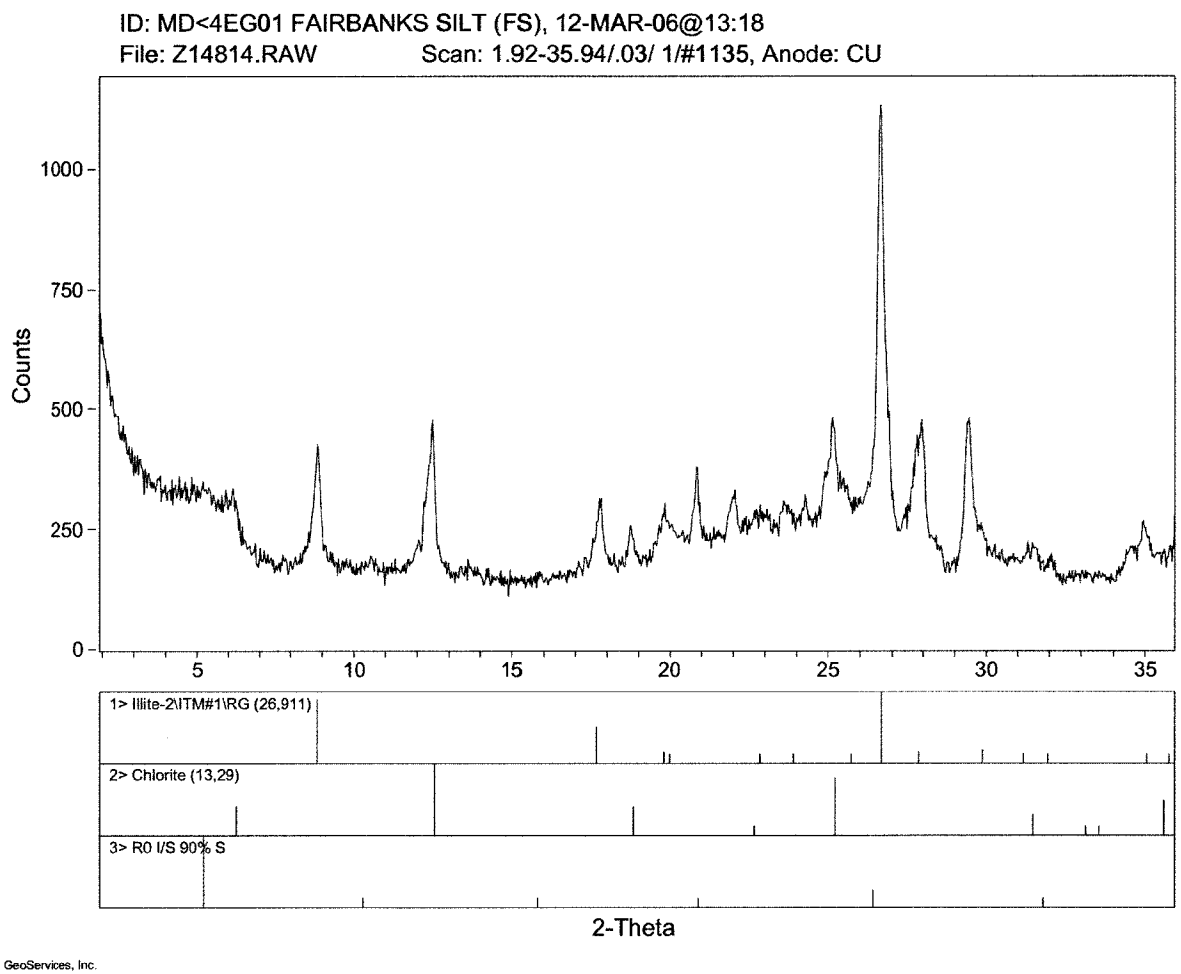

Figure D.16: Ethylene glycol solvated XRD pattern for FS

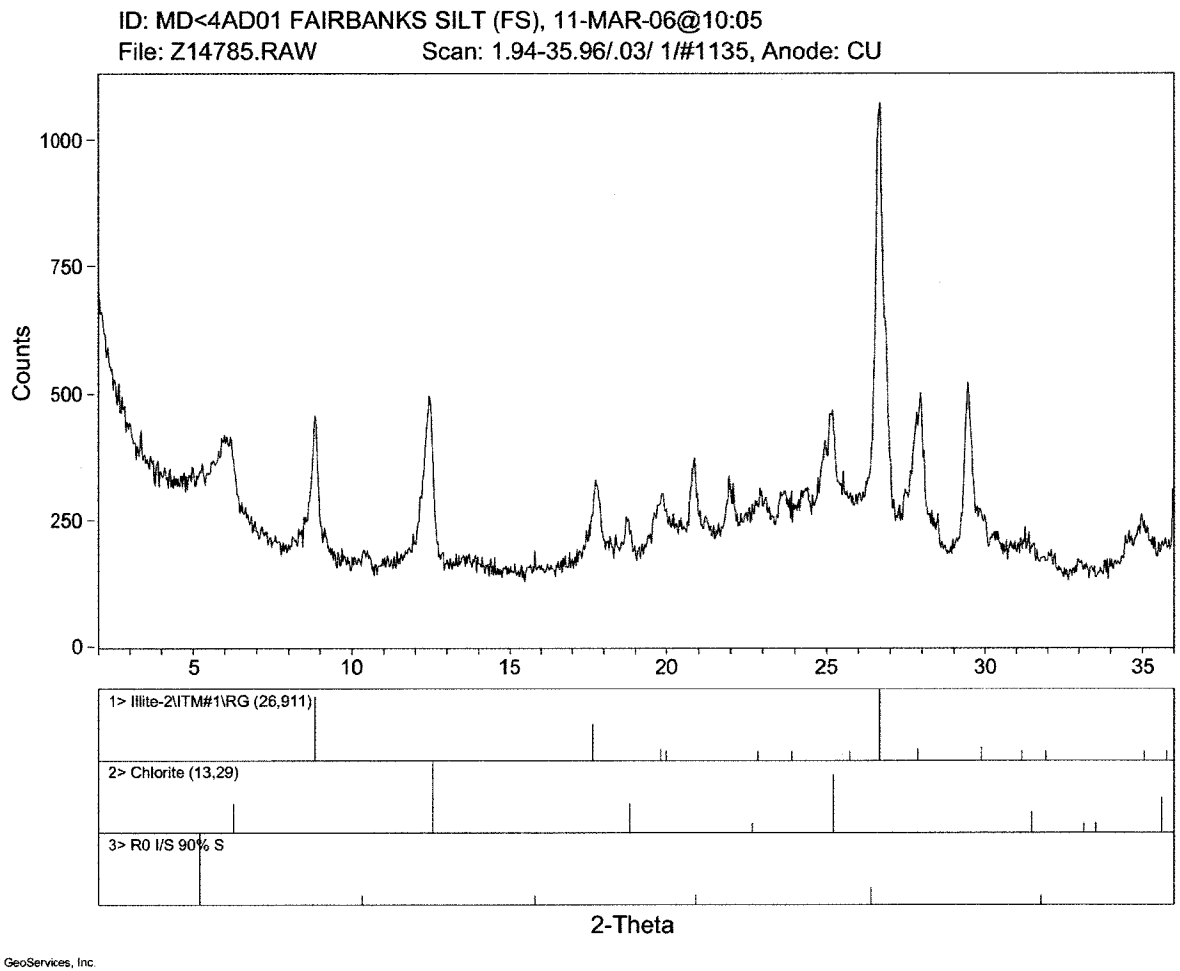

Figure D.17: Air-dried XRD pattern for FS

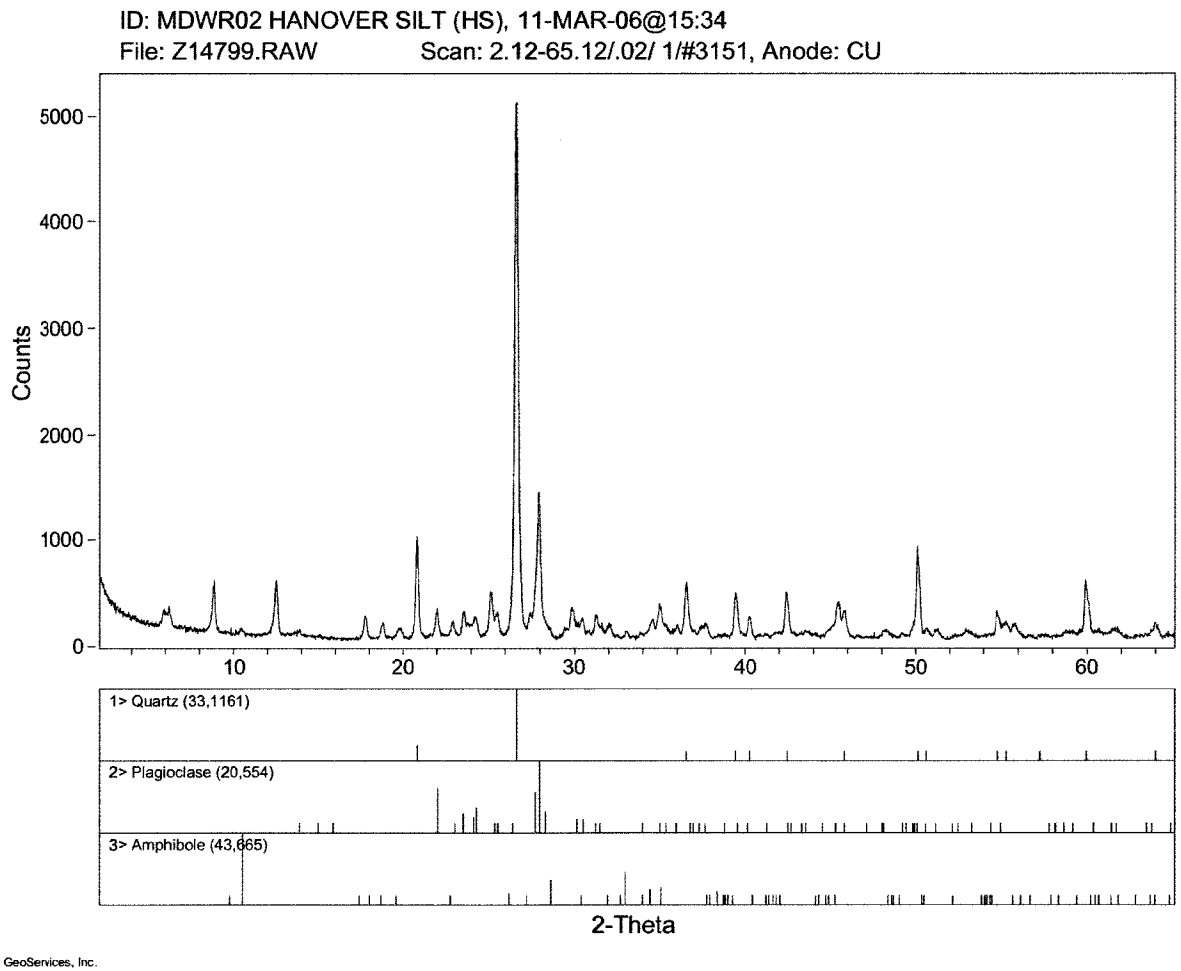

Figure D.18: Whole rock XRD pattern for HS

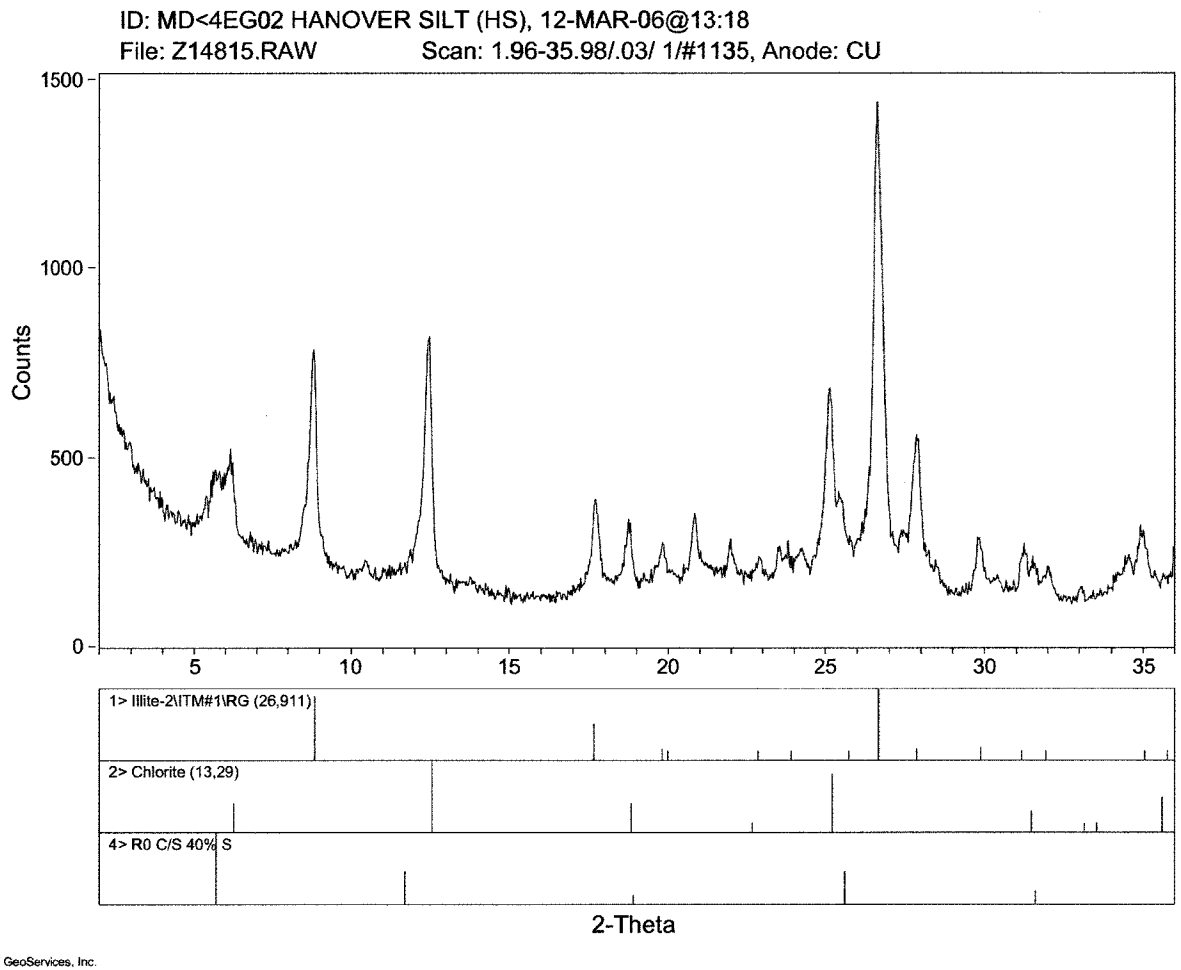

Figure D.19: Ethylene glycol solvated XRD pattern for HS

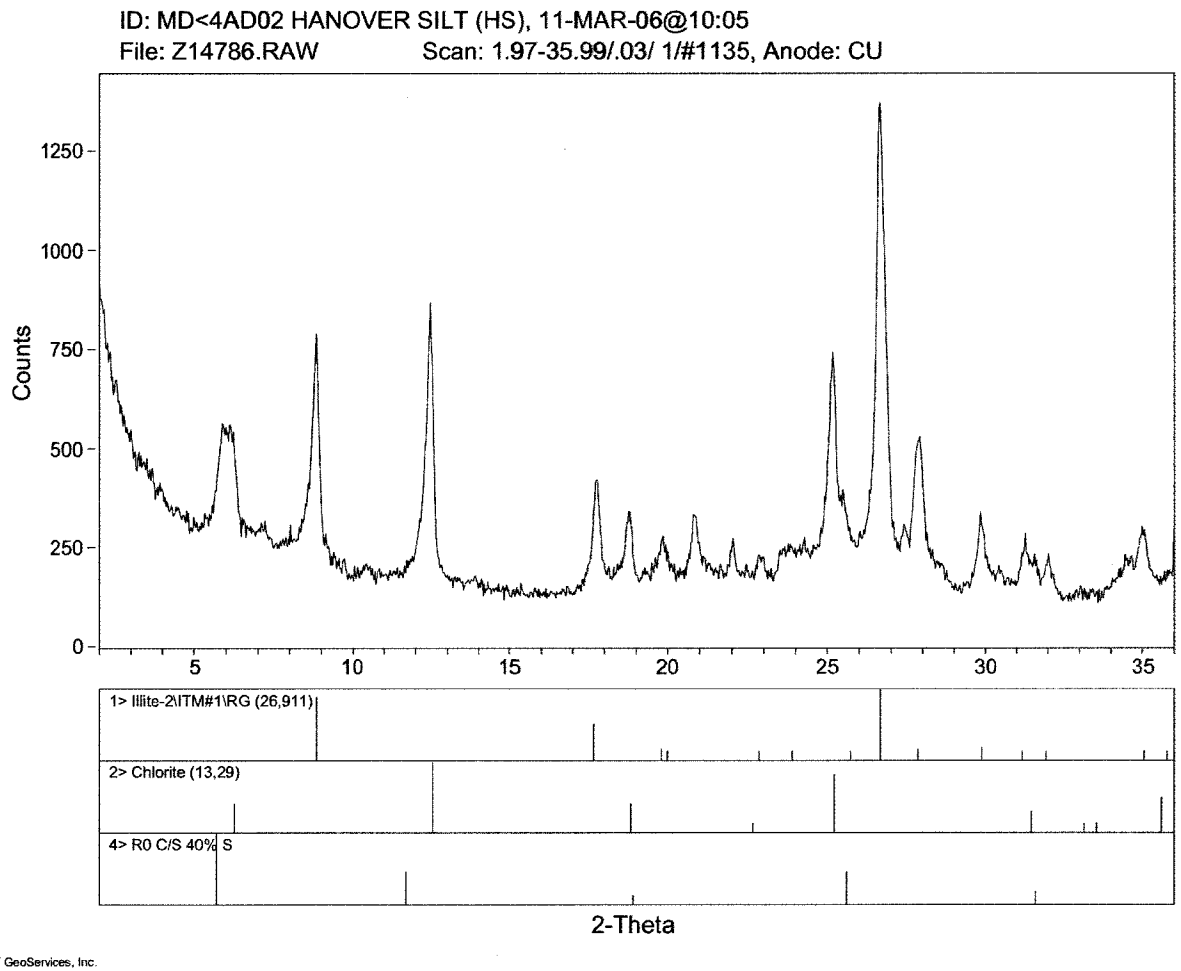

Figure D.20: Air-dried XRD pattern for HS

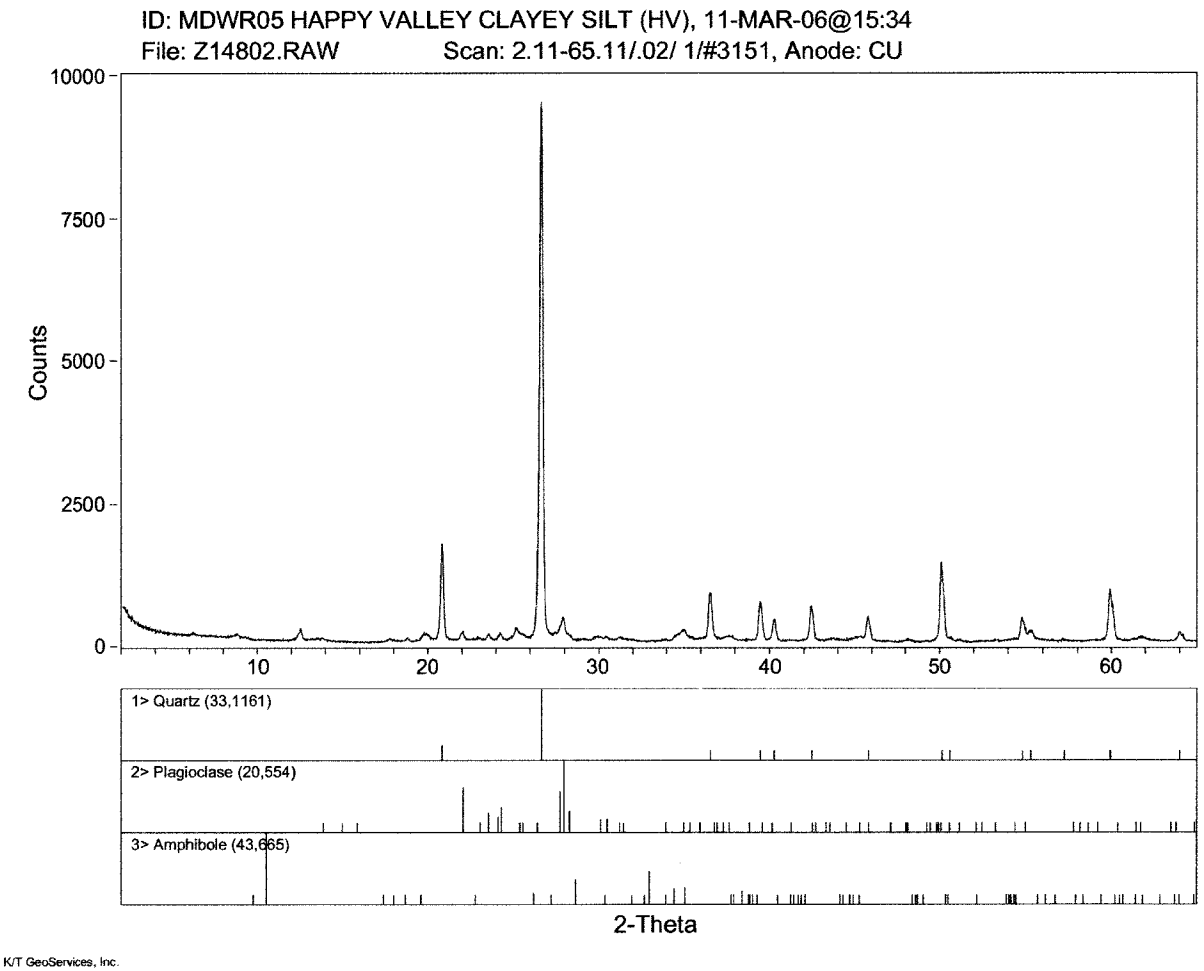

Figure D.21: Whole rock XRD pattern for HV

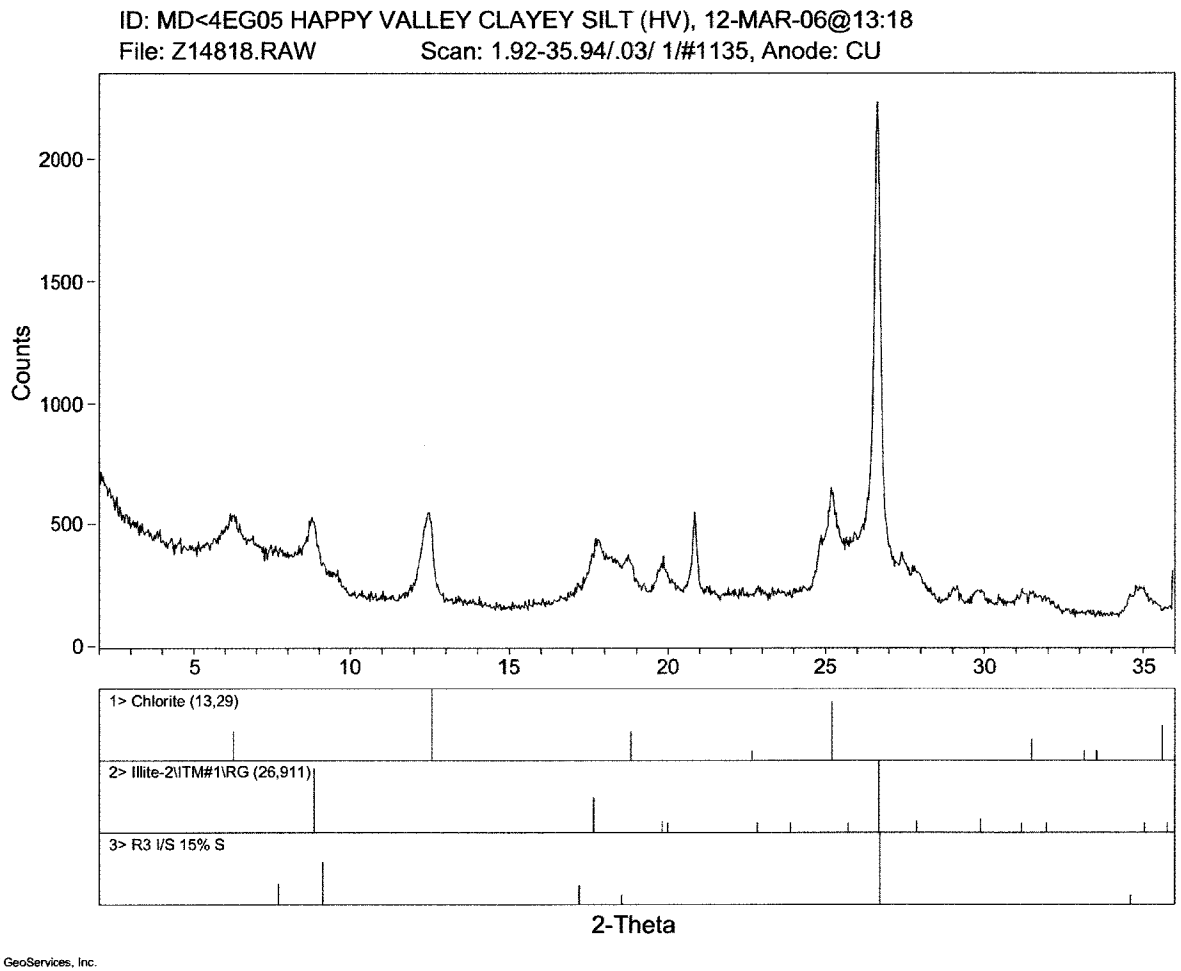

Figure D.22: Ethylene glycol solvated XRD pattern for HV

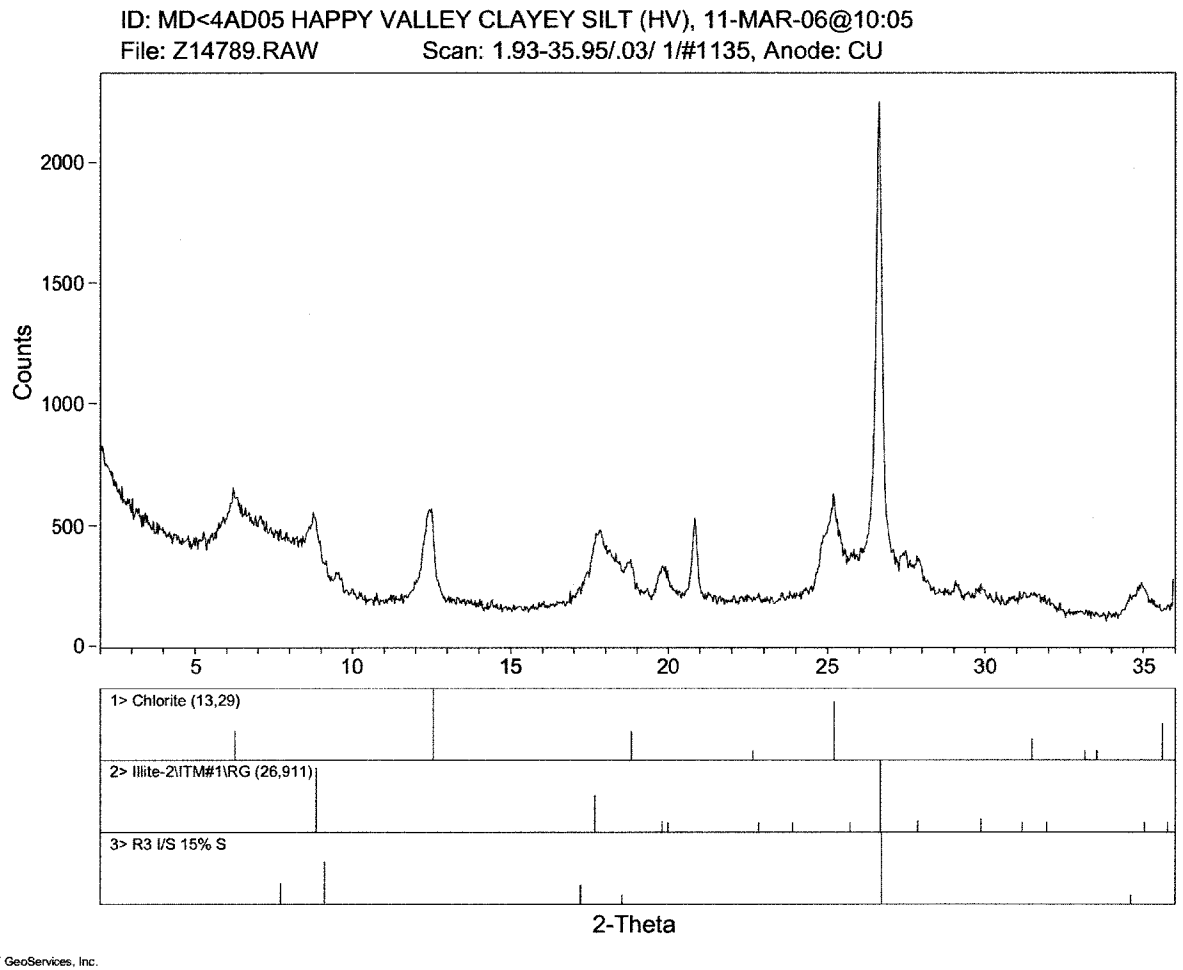

Figure D.23: Air-dried XRD pattern for HV

APPENDIX E

GRAPHICAL PRESENTATION OF RAW FROST HEAVE TEST RESULTS

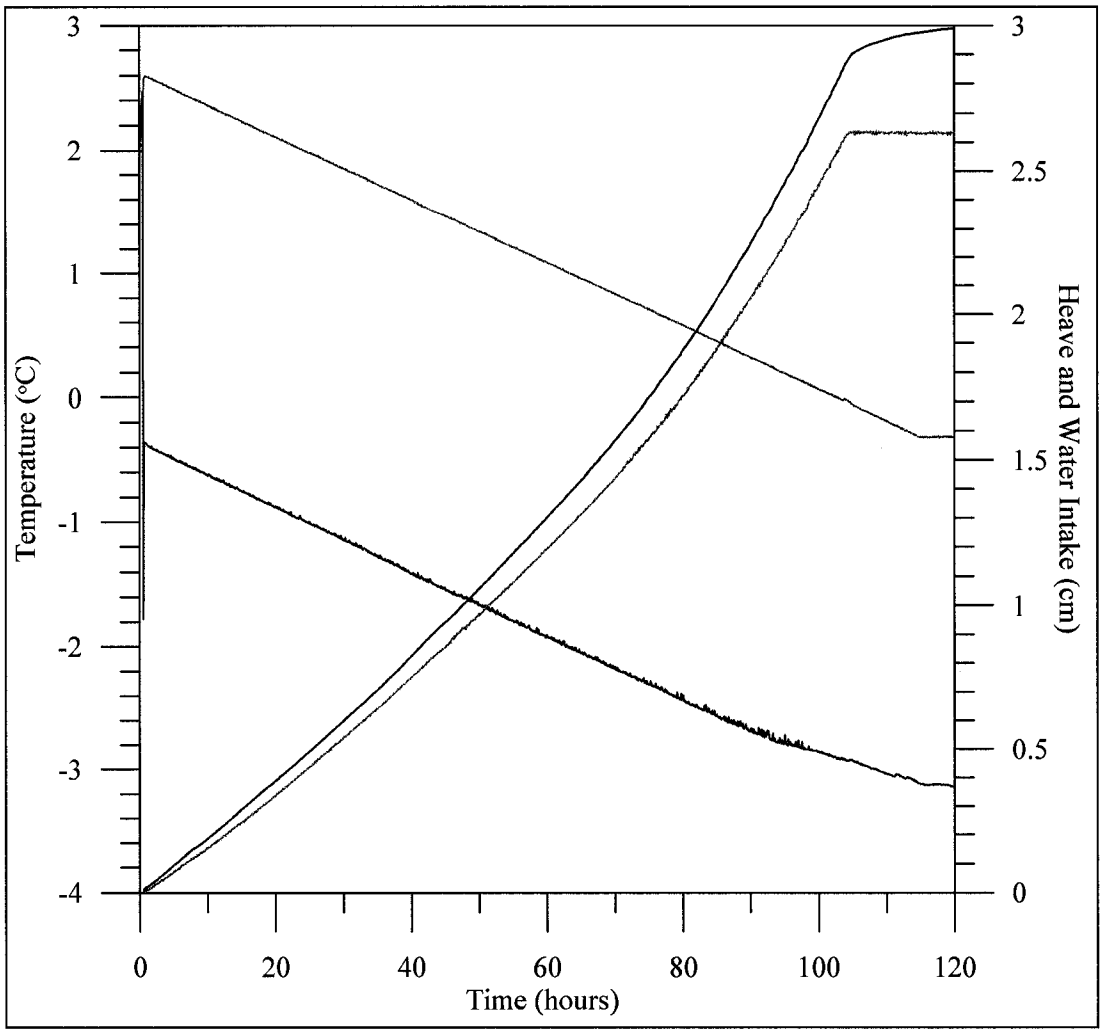

Figure E.1: Raw data for CR-A frost heave test. The top and bottom pedestal temperatures (°C) are shown in dark blue and red, respectively. The amount of heave (cm) is shown in green, and the amount of water intake (cm) is shown in sky blue. The initial sample length was 57 mm. The bottom pedestal temperature reached 0°C at 102.25 hours. The calculated average freezing rate was 0.55 mm/hr.

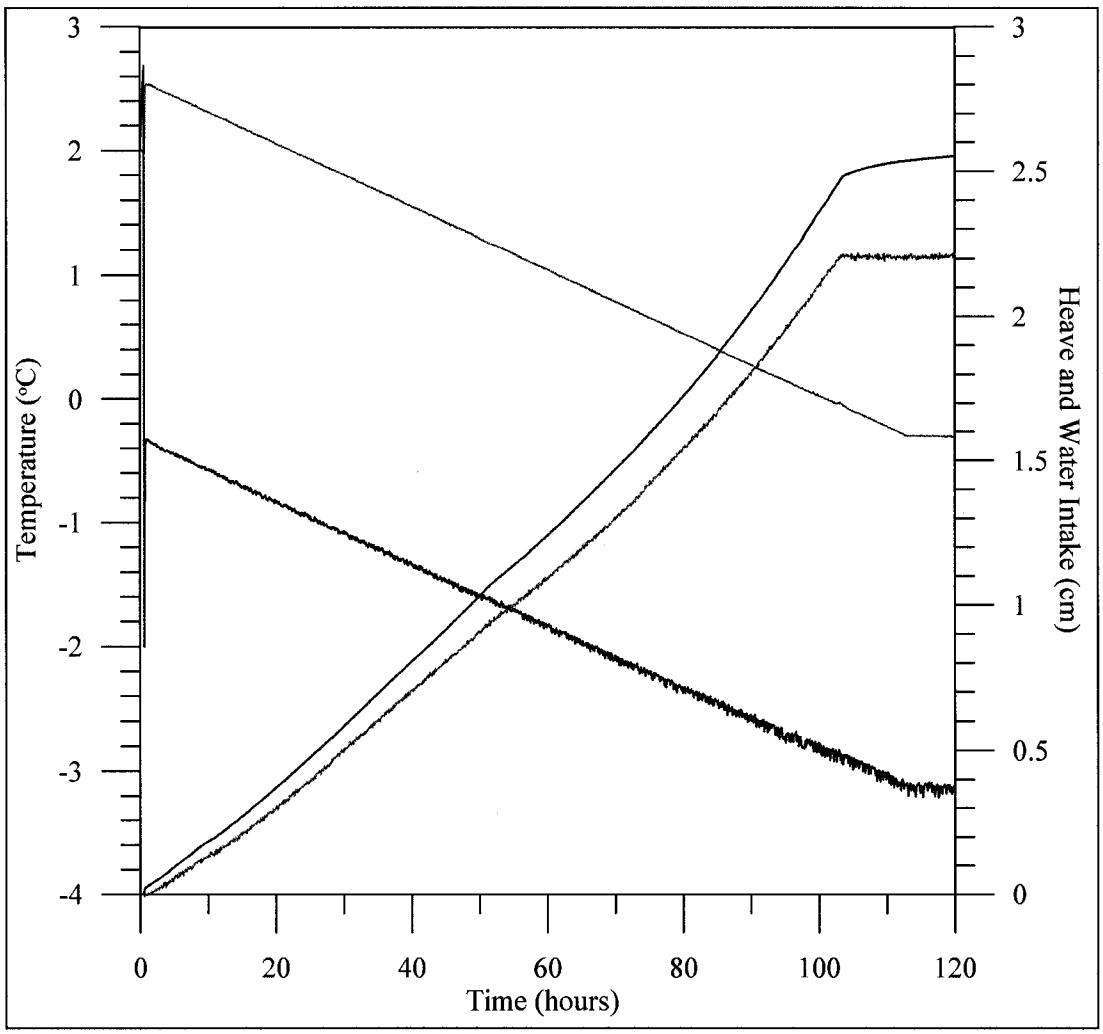

Figure E.2: Raw data for CR-B frost heave test. The top and bottom pedestal temperatures (°C) are shown in dark blue and red, respectively. The amount of heave (cm) is shown in green, and the amount of water intake (cm) is shown in sky blue. The initial sample length was 56 mm. The bottom pedestal temperature reached 0°C at 100.75 hours. The calculated average freezing rate was 0.55 mm/hr.

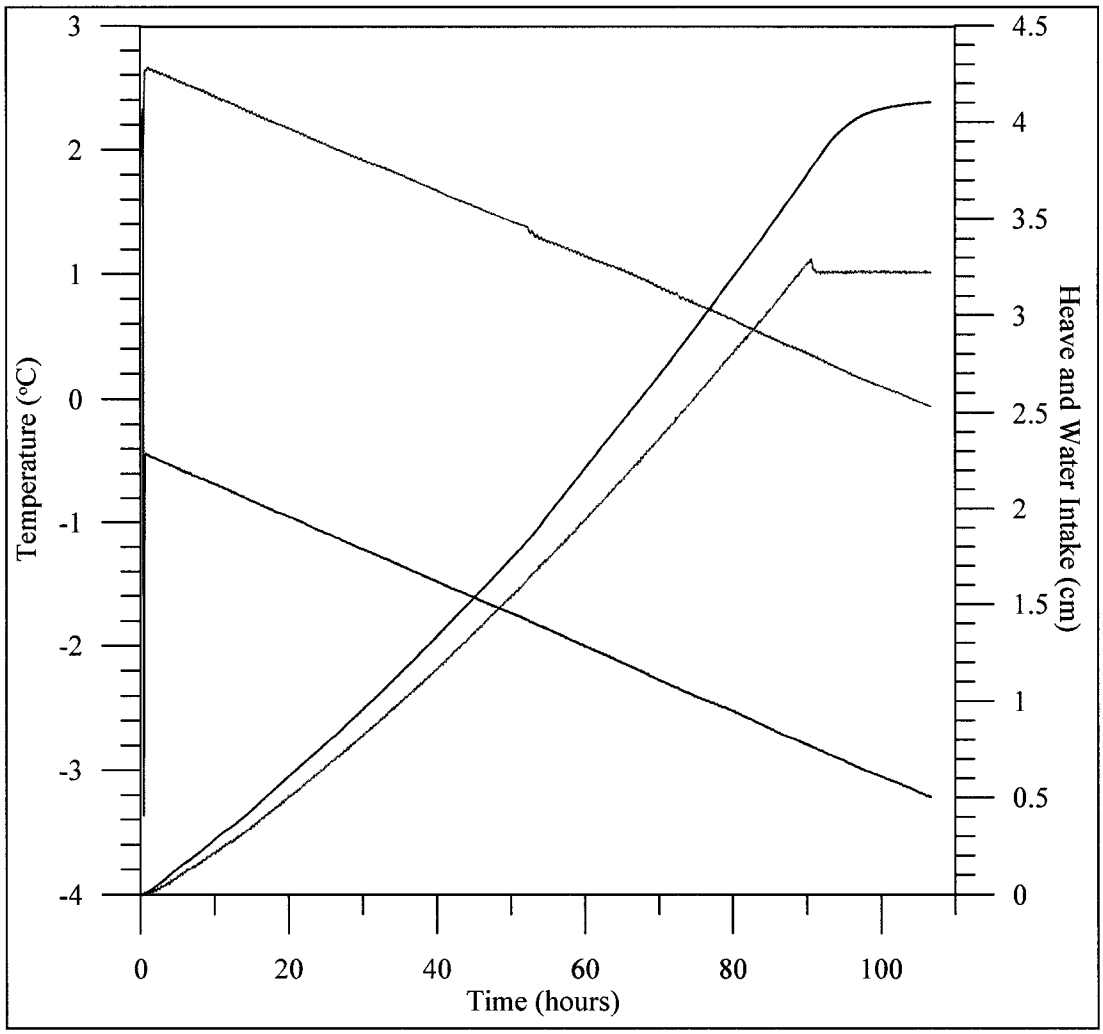

Figure E.3: Raw data for CR Ca^{2+} frost heave test. The top and bottom pedestal temperatures (°C) are shown in dark blue and red, respectively. The amount of heave (cm) is shown in green, and the amount of water intake (cm) is shown in sky blue. The initial sample length was 58 mm. The complete sample length was frozen before the bottom pedestal temperature reached 0°C. For this test, the end was defined at the point when the water intake stopped abruptly at 90.75 hours. The calculated average freezing rate was 0.64 mm/hr.

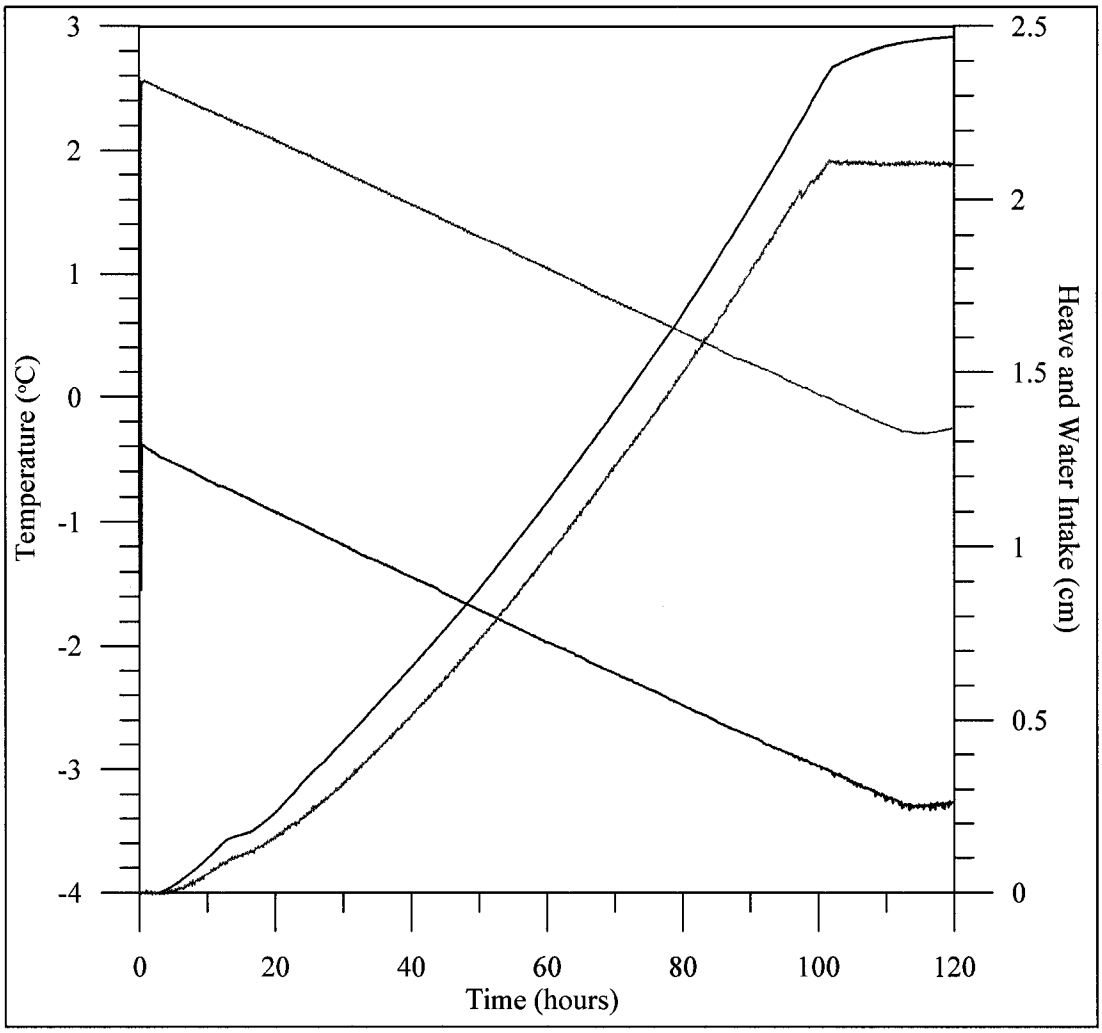

Figure E.4: Raw data for CR Mg^{2+} frost heave test. The top and bottom pedestal temperatures (°C) are shown in dark blue and red, respectively. The amount of heave (cm) is shown in green, and the amount of water intake (cm) is shown in sky blue. The initial sample length was 56 mm. The bottom pedestal temperature reached 0°C at 100.42 hours. The calculated average freezing rate was 0.56 mm/hr.

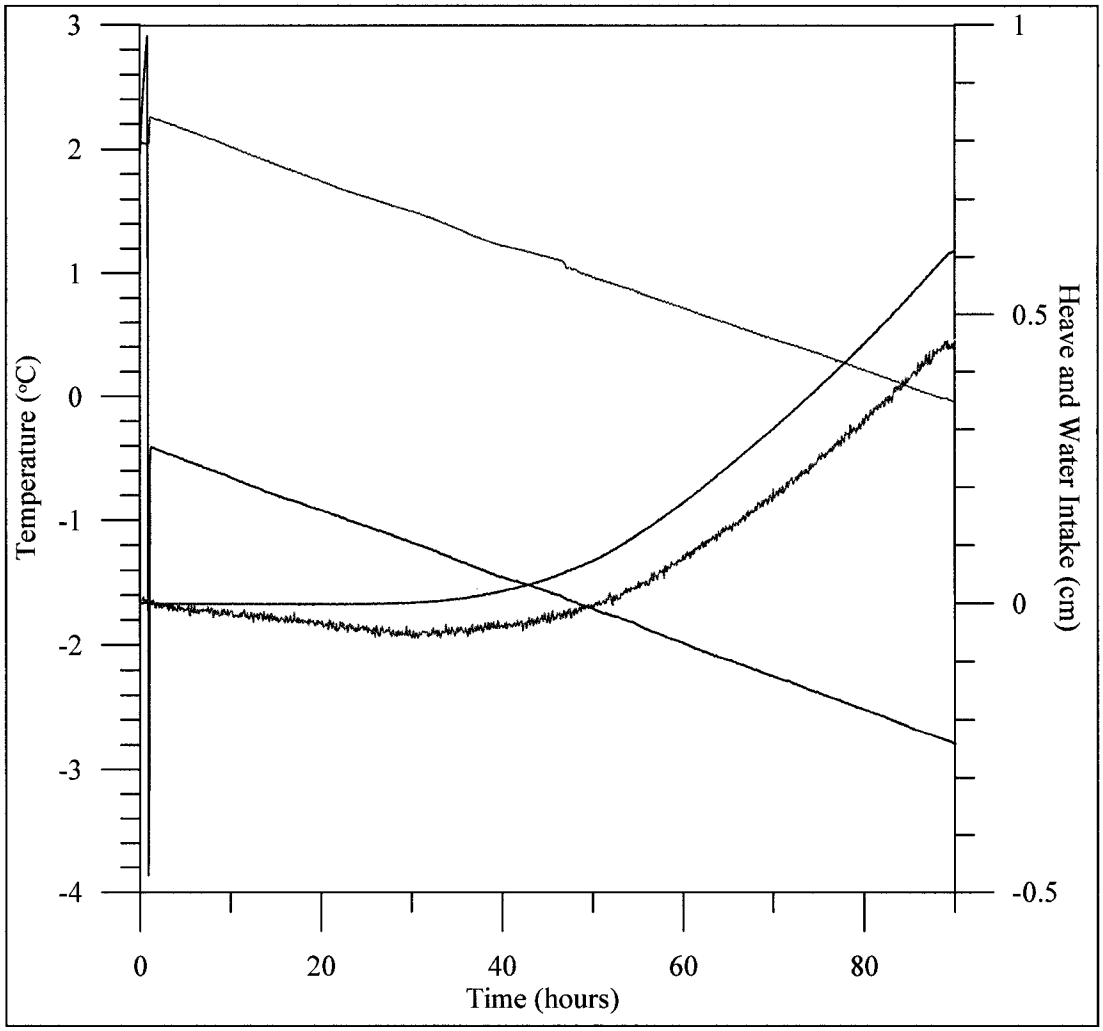

Figure E.5: Raw data for CR Na^+ frost heave test. The top and bottom pedestal temperatures (°C) are shown in dark blue and red, respectively. The amount of heave (cm) is shown in green, and the amount of water intake (cm) is shown in sky blue. The initial sample length was 49 mm. The bottom pedestal temperature reached 0°C at 87.92 hours. The calculated average freezing rate was 0.56 mm/hr.

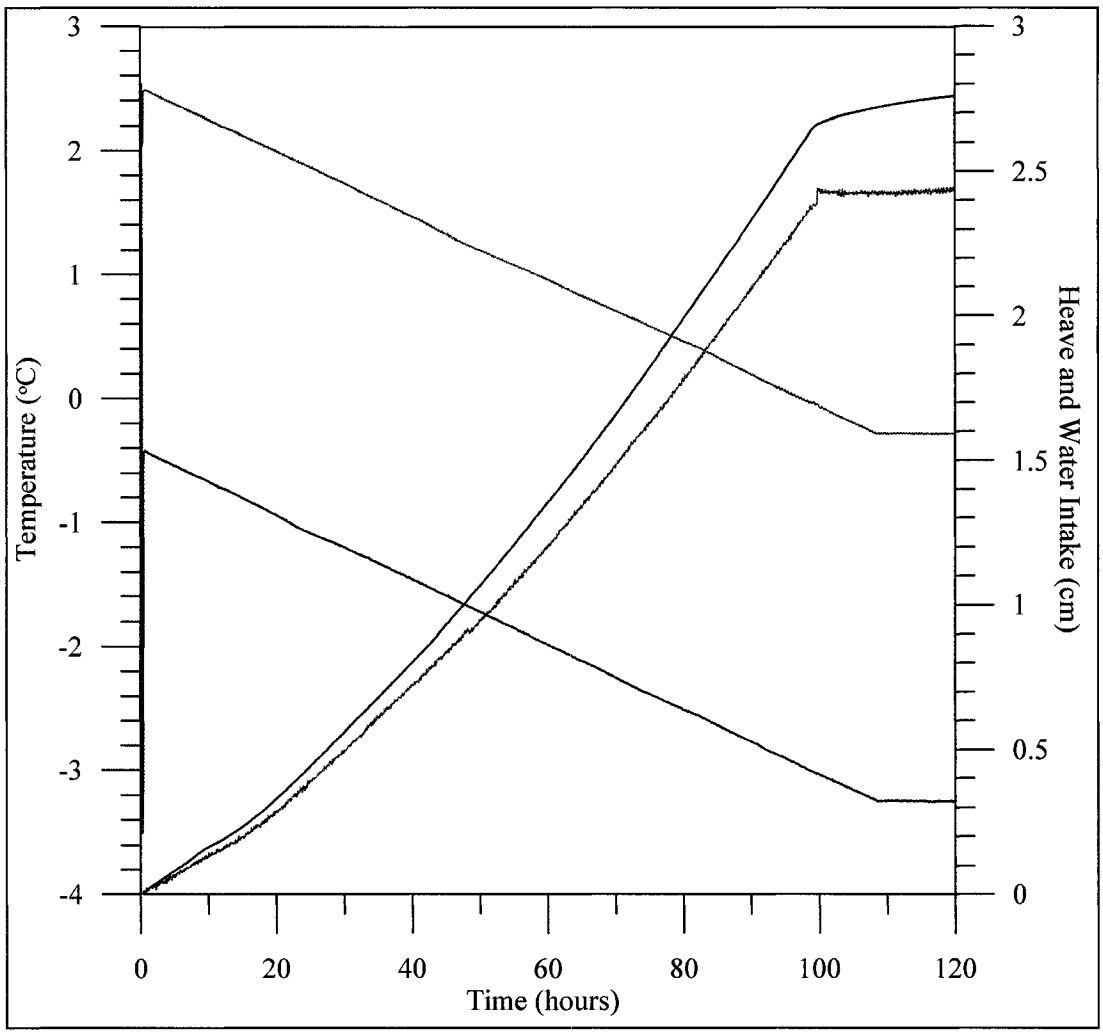

Figure E.6: Raw data for CR K^+ frost heave test. The top and bottom pedestal temperatures (°C) are shown in dark blue and red, respectively. The amount of heave (cm) is shown in green, and the amount of water intake (cm) is shown in sky blue. The initial sample length was 54 mm. The bottom pedestal temperature reached 0°C at 97.0 hours. The calculated average freezing rate was 0.56 mm/hr.

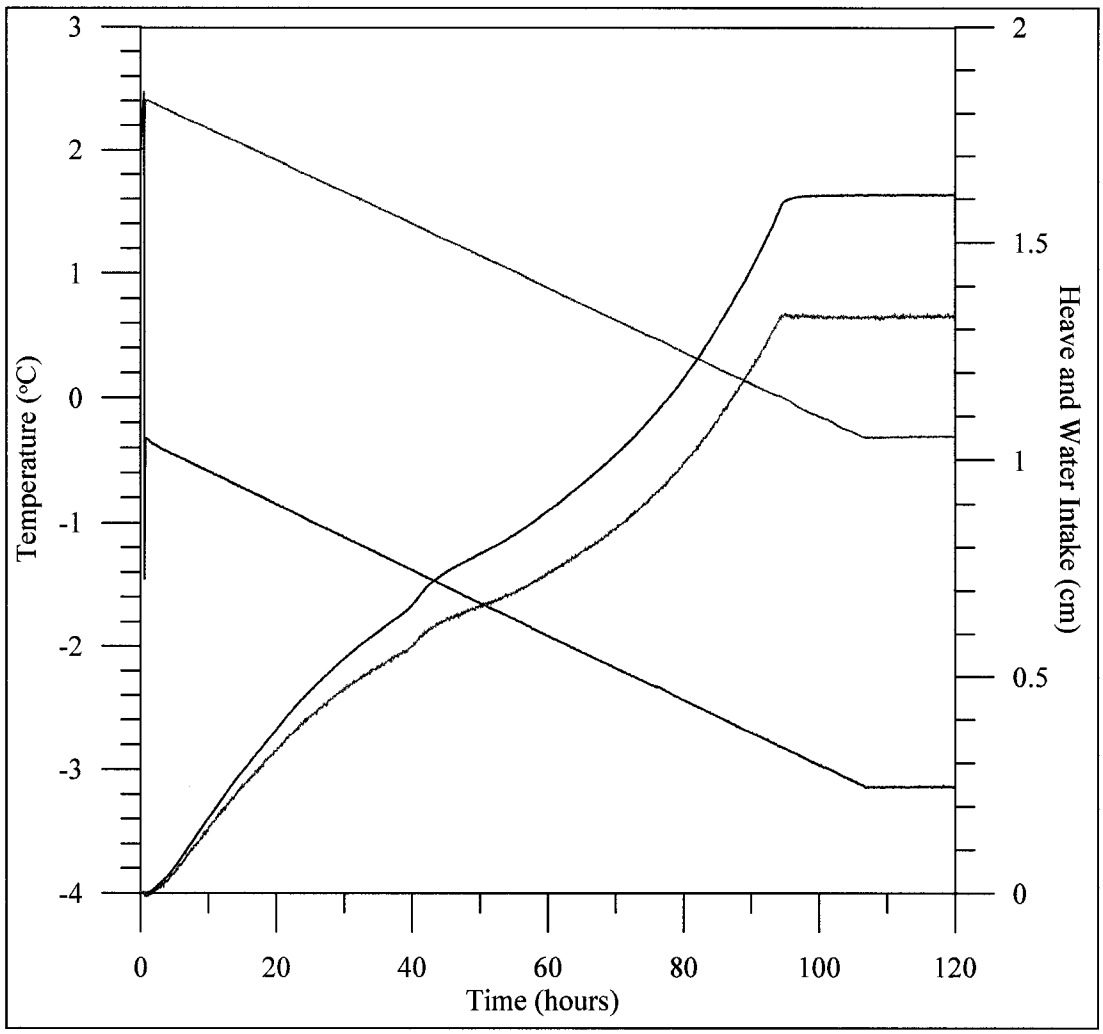

Figure E.7: Raw data for DEA-A frost heave test. The top and bottom pedestal temperatures (°C) are shown in dark blue and red, respectively. The amount of heave (cm) is shown in green, and the amount of water intake (cm) is shown in sky blue. The initial sample length was 52 mm. The bottom pedestal temperature reached 0°C at 94.58 hours. The calculated average freezing rate was 0.55 mm/hr.

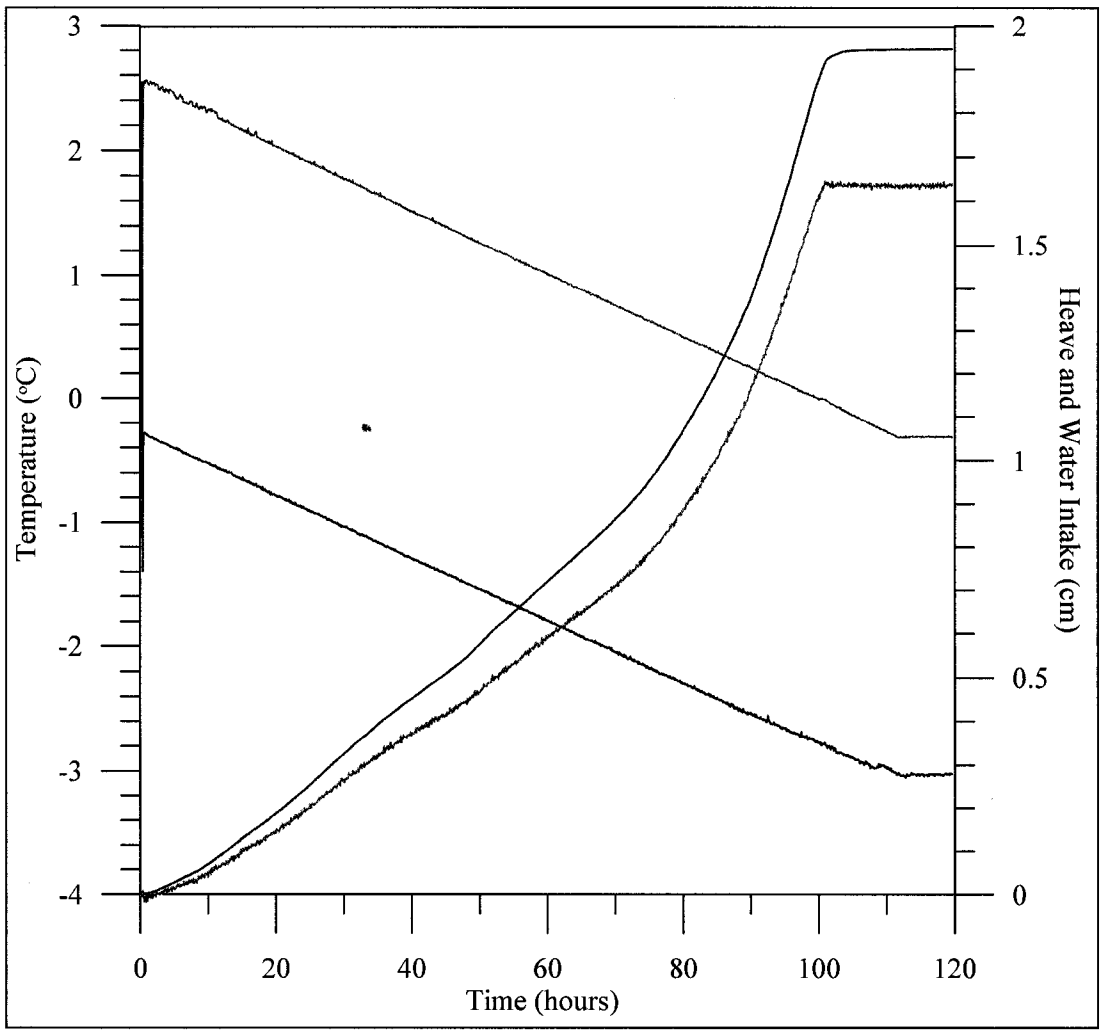

Figure E.8: Raw data for DEA-B frost heave test. The top and bottom pedestal temperatures (°C) are shown in dark blue and red, respectively. The amount of heave (cm) is shown in green, and the amount of water intake (cm) is shown in sky blue. The initial sample length was 55 m. The bottom pedestal temperature reached 0°C at 99.67 hours. The calculated average freezing rate was 0.55 mm/hr.

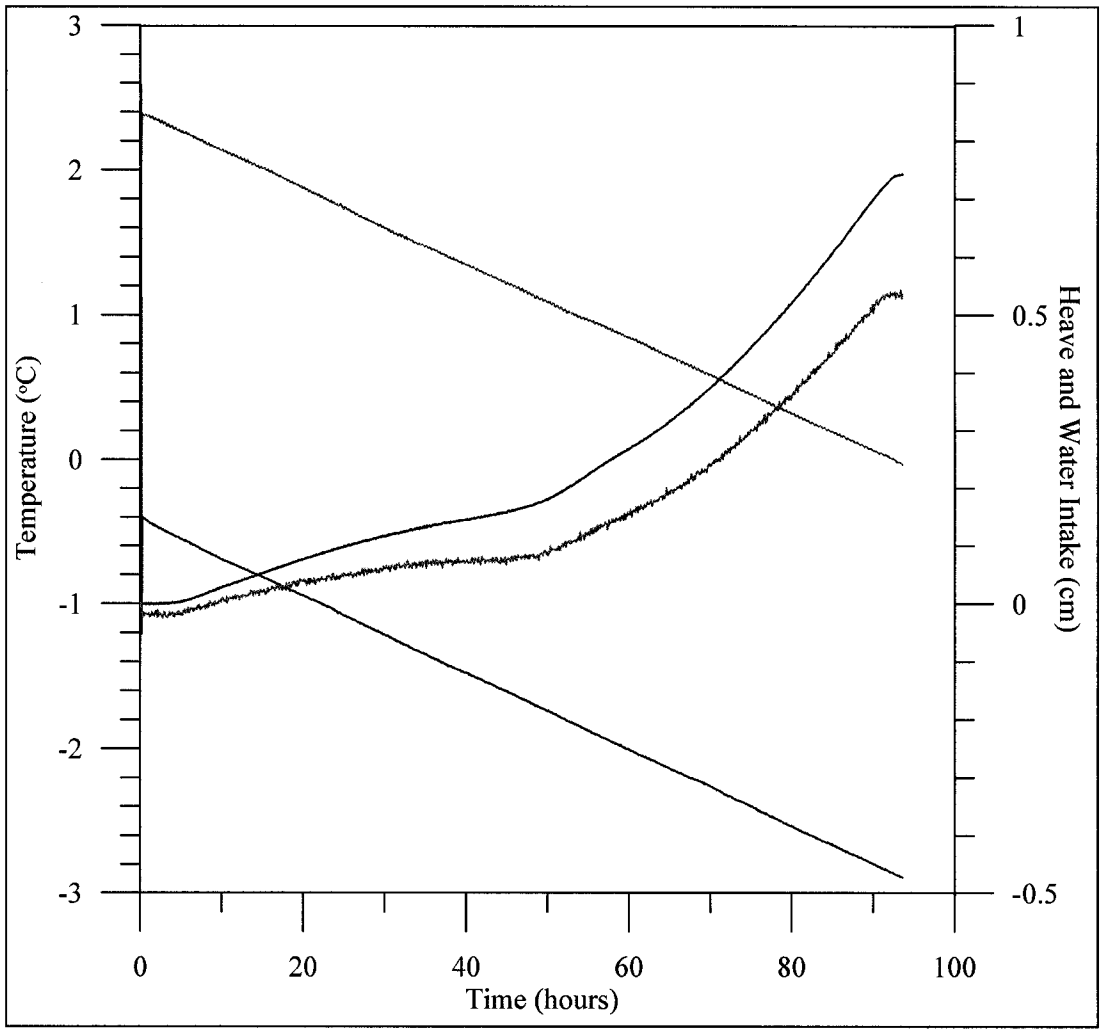

Figure E.9: Raw data for DEA Ca^{2+} frost heave test. The top and bottom pedestal temperatures (°C) are shown in dark blue and red, respectively. The amount of heave (cm) is shown in green, and the amount of water intake (cm) is shown in sky blue. The initial sample length was 52 mm. The bottom pedestal temperature reached 0°C at 92.5 hours. The calculated average freezing rate was 0.55 mm/hr.

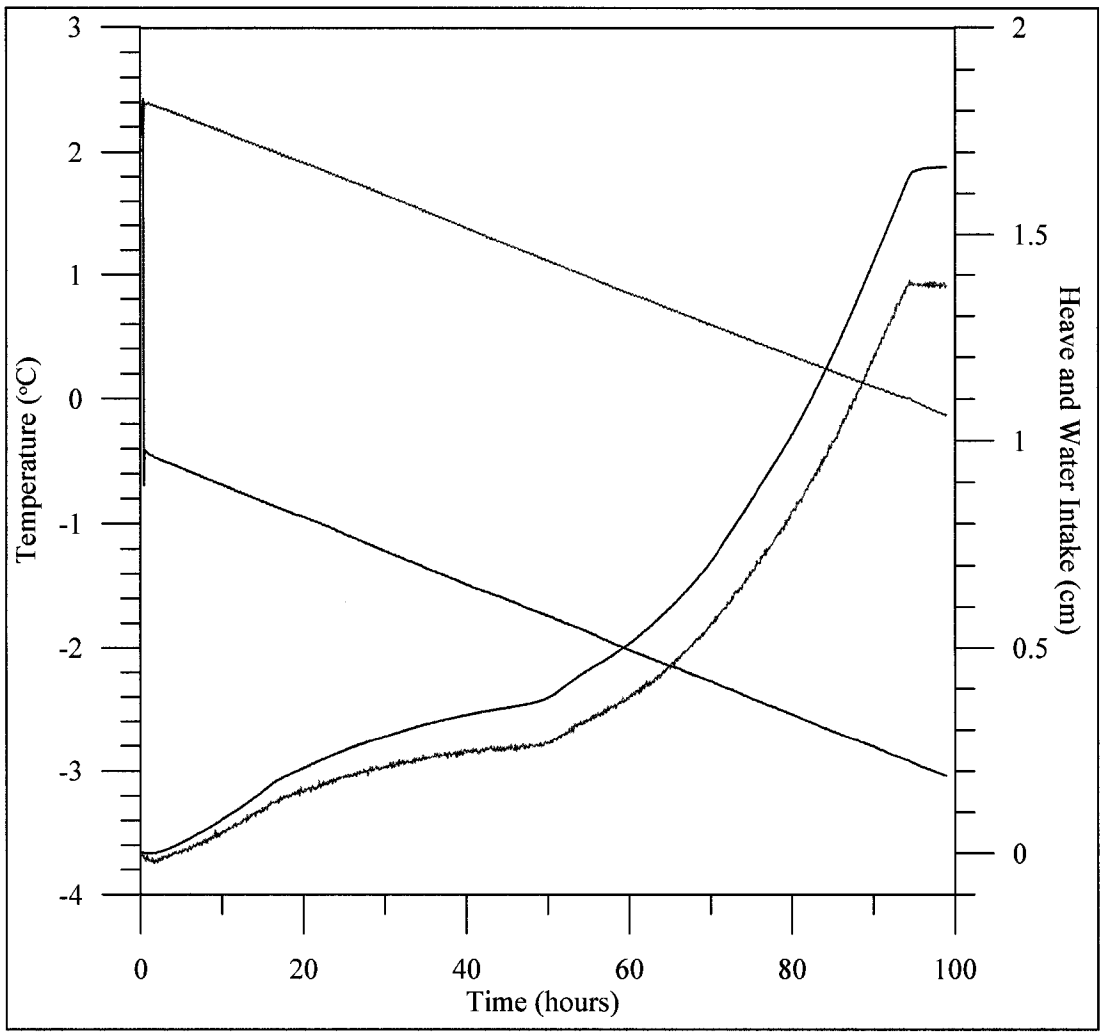

Figure E.10: Raw data for DEA Mg^{2+} frost heave test. The top and bottom pedestal temperatures (°C) are shown in dark blue and red, respectively. The amount of heave (cm) is shown in green, and the amount of water intake (cm) is shown in sky blue. The initial sample length was 53 mm. The bottom pedestal temperature reached 0°C at 94.0 hours. The calculated average freezing rate was 0.56 mm/hr.

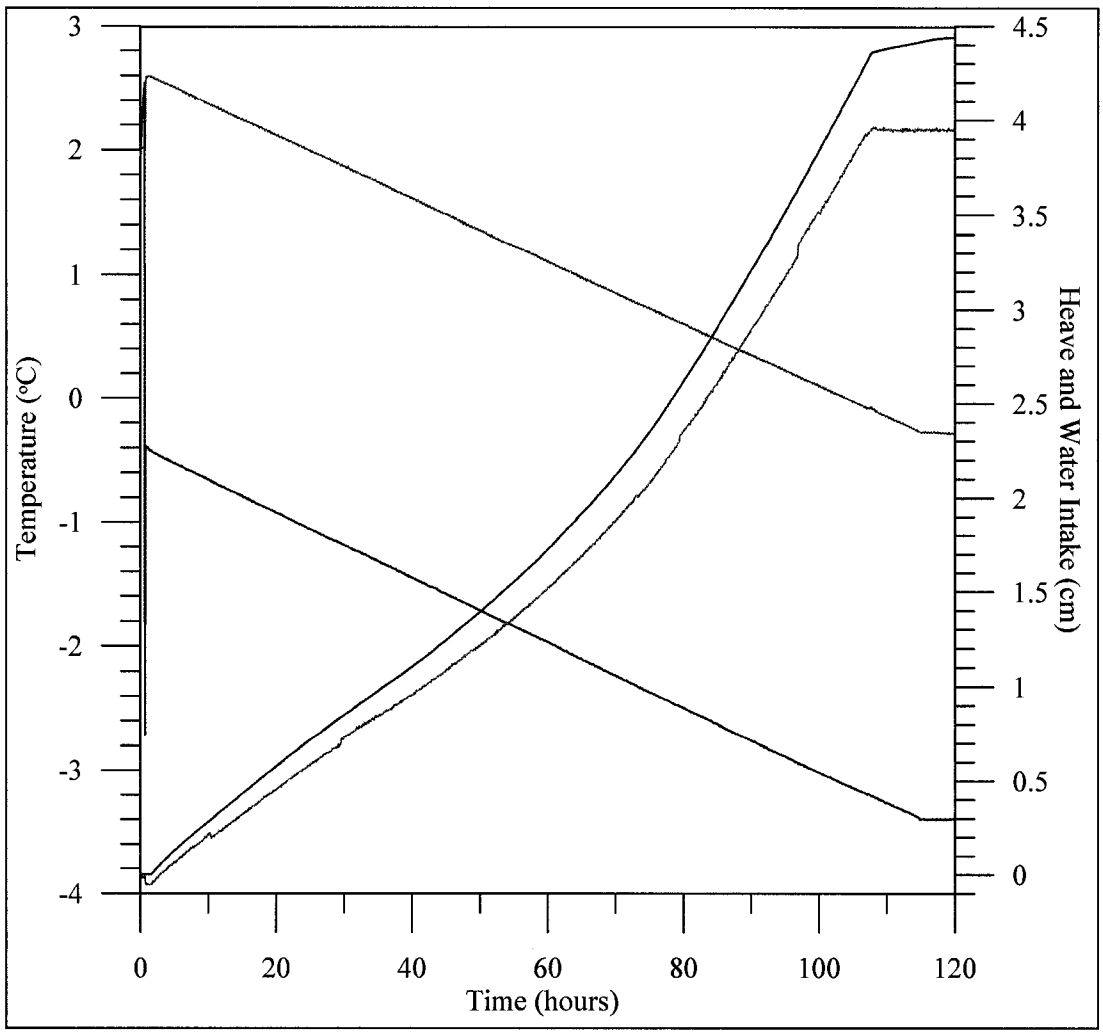

Figure E.11: Raw data for DEA Na^+ frost heave test. The top and bottom pedestal temperatures (°C) are shown in dark blue and red, respectively. The amount of heave (cm) is shown in green, and the amount of water intake (cm) is shown in sky blue. The initial sample length was 57 mm. The bottom pedestal temperature reached 0°C at 103.8 hours. The calculated average freezing rate was 0.55 mm/hr.

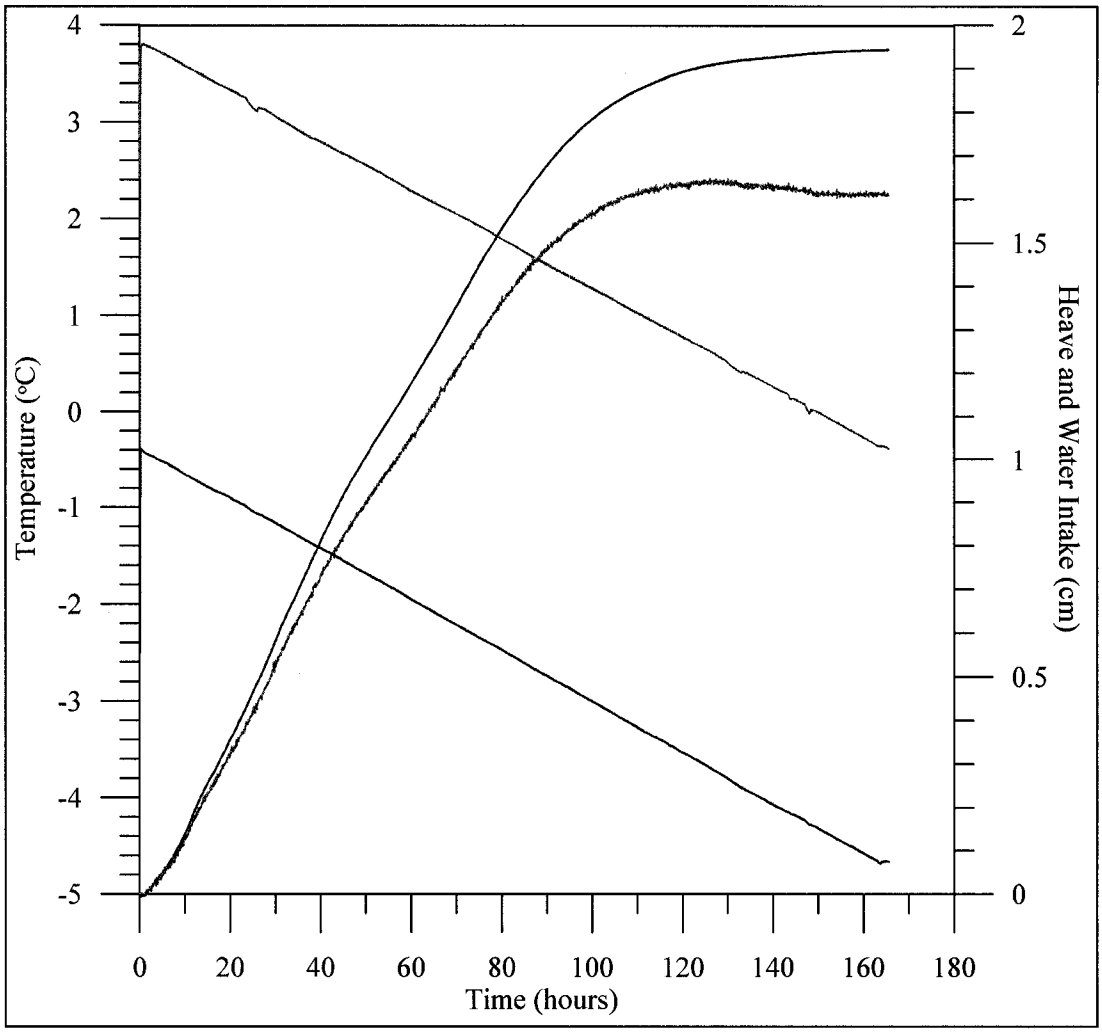

Figure E.12: Raw data for DEA K^+ frost heave test. The top and bottom pedestal temperatures (°C) are shown in dark blue and red, respectively. The amount of heave (cm) is shown in green, and the amount of water intake (cm) is shown in sky blue. The initial sample length was 82 mm. The bottom pedestal temperature reached 0°C at 147.75 hours. The calculated average freezing rate was 0.55 mm/hr.

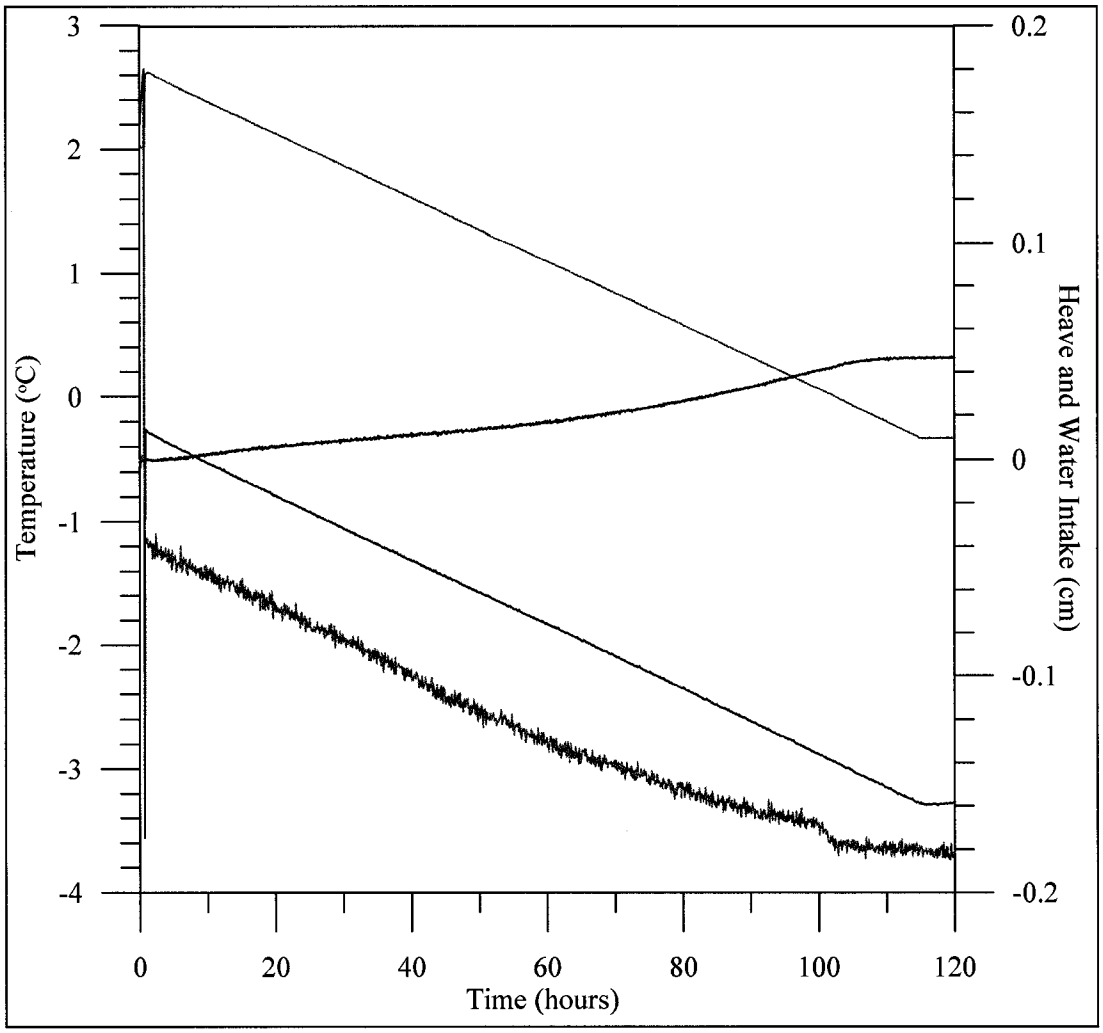

Figure E.13: Raw data for FS-A frost heave test. The top and bottom pedestal temperatures (°C) are shown in dark blue and red, respectively. The amount of heave (cm) is shown in green, and the amount of water intake (cm) is shown in sky blue. The initial sample length was 56 mm. The bottom pedestal temperature reached 0°C at 102.25 hours. The calculated average freezing rate was 0.56 mm/hr.

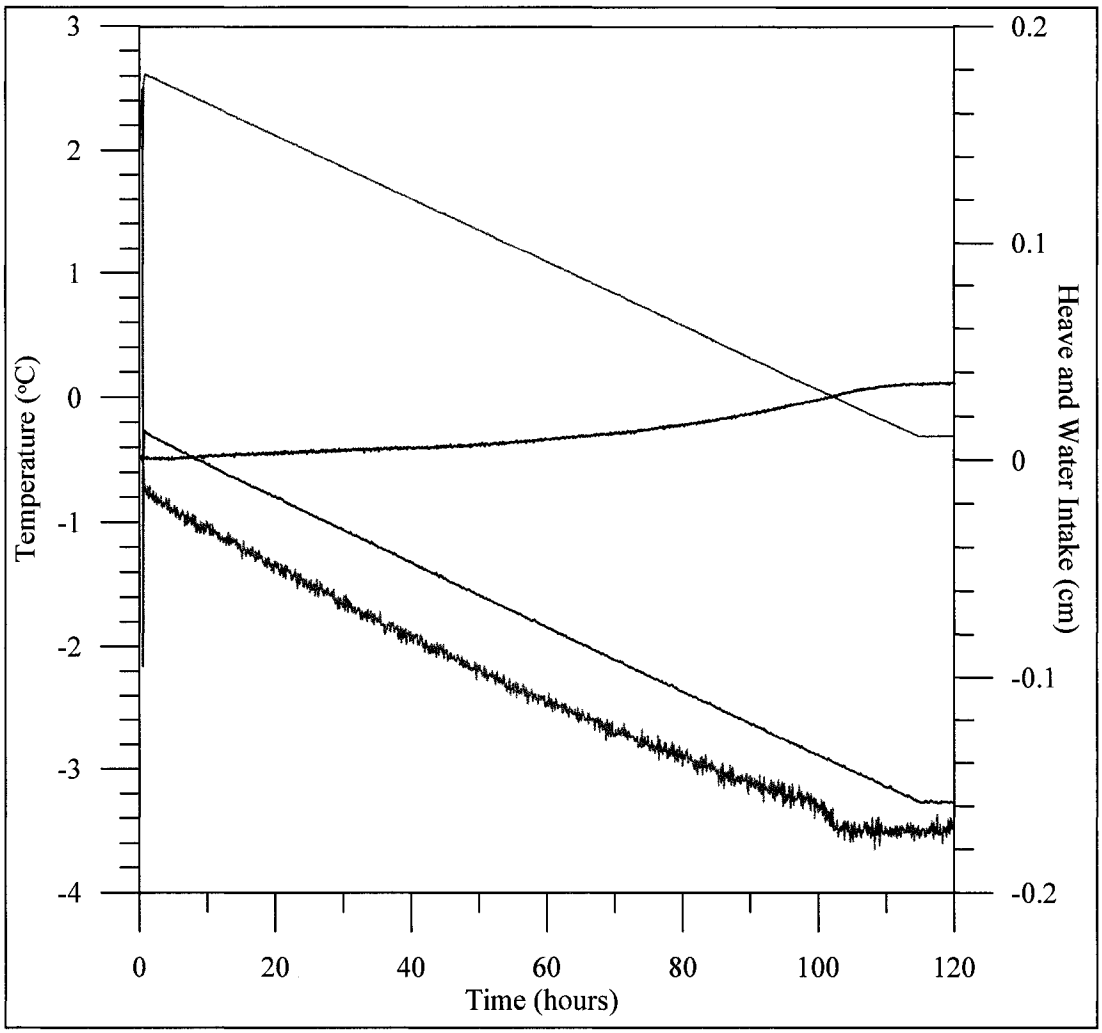

Figure E.14: Raw data for FS-B frost heave test. The top and bottom pedestal temperatures (°C) are shown in dark blue and red, respectively. The amount of heave (cm) is shown in green, and the amount of water intake (cm) is shown in sky blue. The initial sample length was 56 mm. The bottom pedestal temperature reached 0°C at 102.42 hours. The calculated average freezing rate was 0.56 mm/hr.

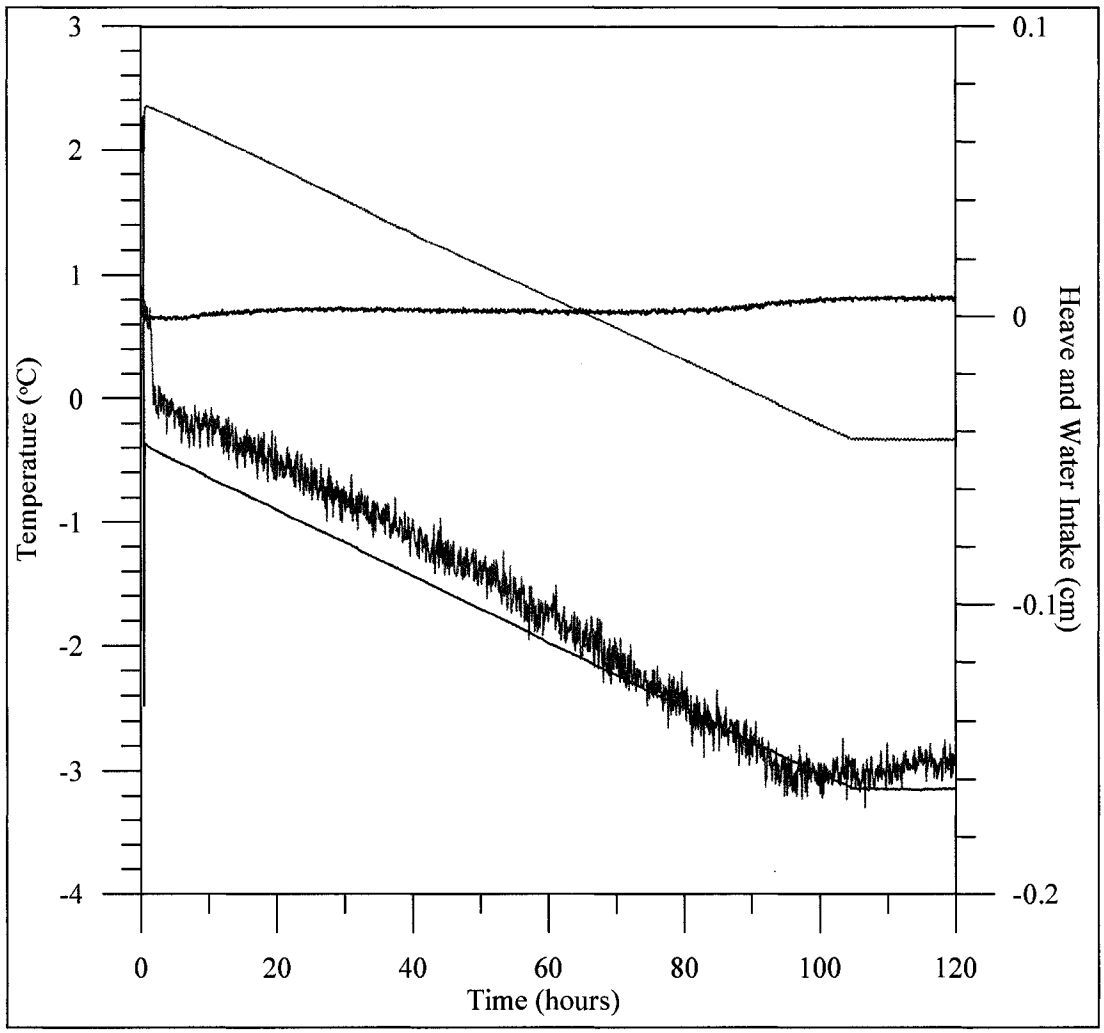

Figure E.15: Raw data for FS Mg^{2+} frost heave test. The top and bottom pedestal temperatures (°C) are shown in dark blue and red, respectively. The amount of heave (cm) is shown in green, and the amount of water intake (cm) is shown in sky blue. The initial sample length was 52 mm. The bottom pedestal temperature reached 0°C at 92.0 hours. The calculated average freezing rate was 0.57 mm/hr.

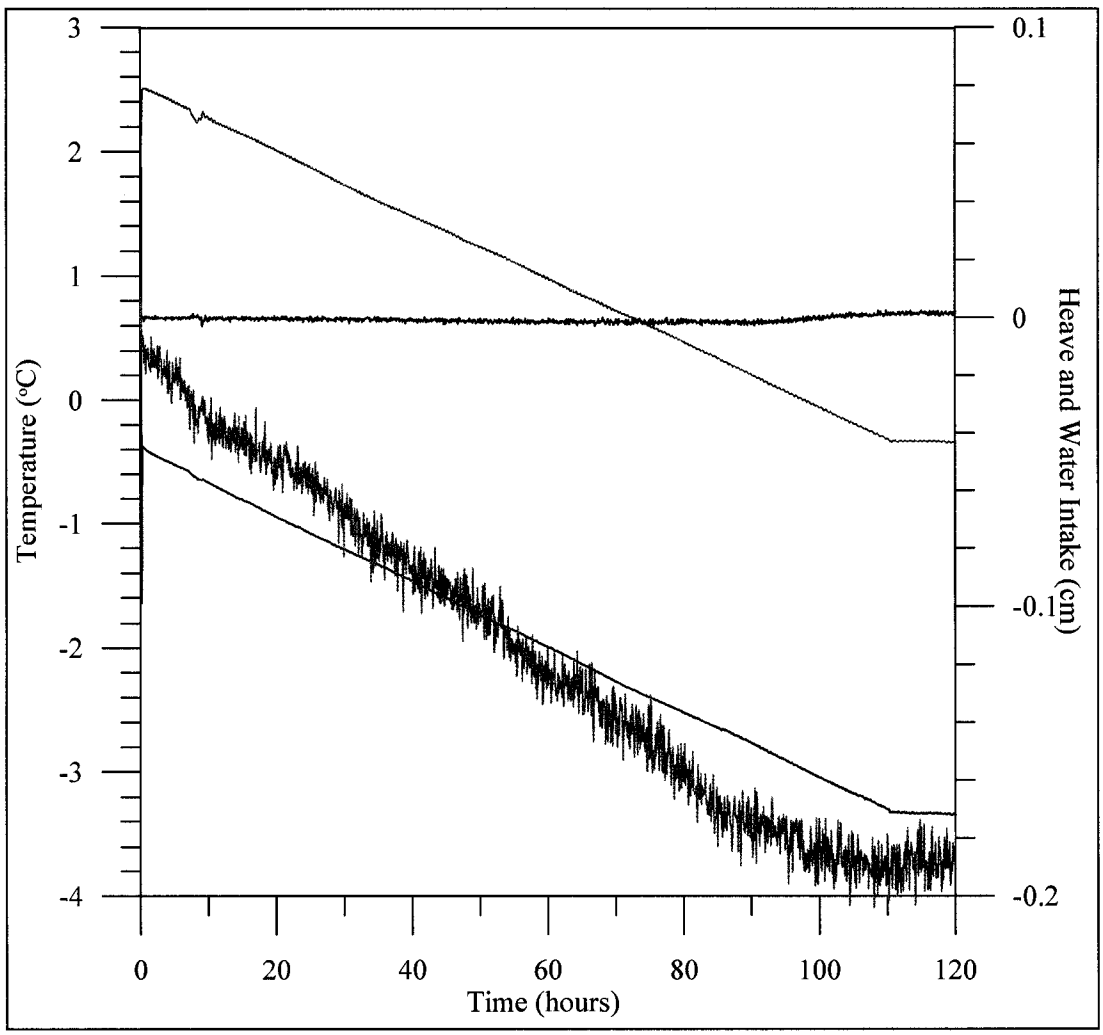

Figure E.16: Raw data for FS Na^+ frost heave test. The top and bottom pedestal temperatures (°C) are shown in dark blue and red, respectively. The amount of heave (cm) is shown in green, and the amount of water intake (cm) is shown in sky blue. The initial sample length was 55 mm. The bottom pedestal temperature reached 0°C at 97.5 hours. The calculated average freezing rate was 0.56 mm/hr.

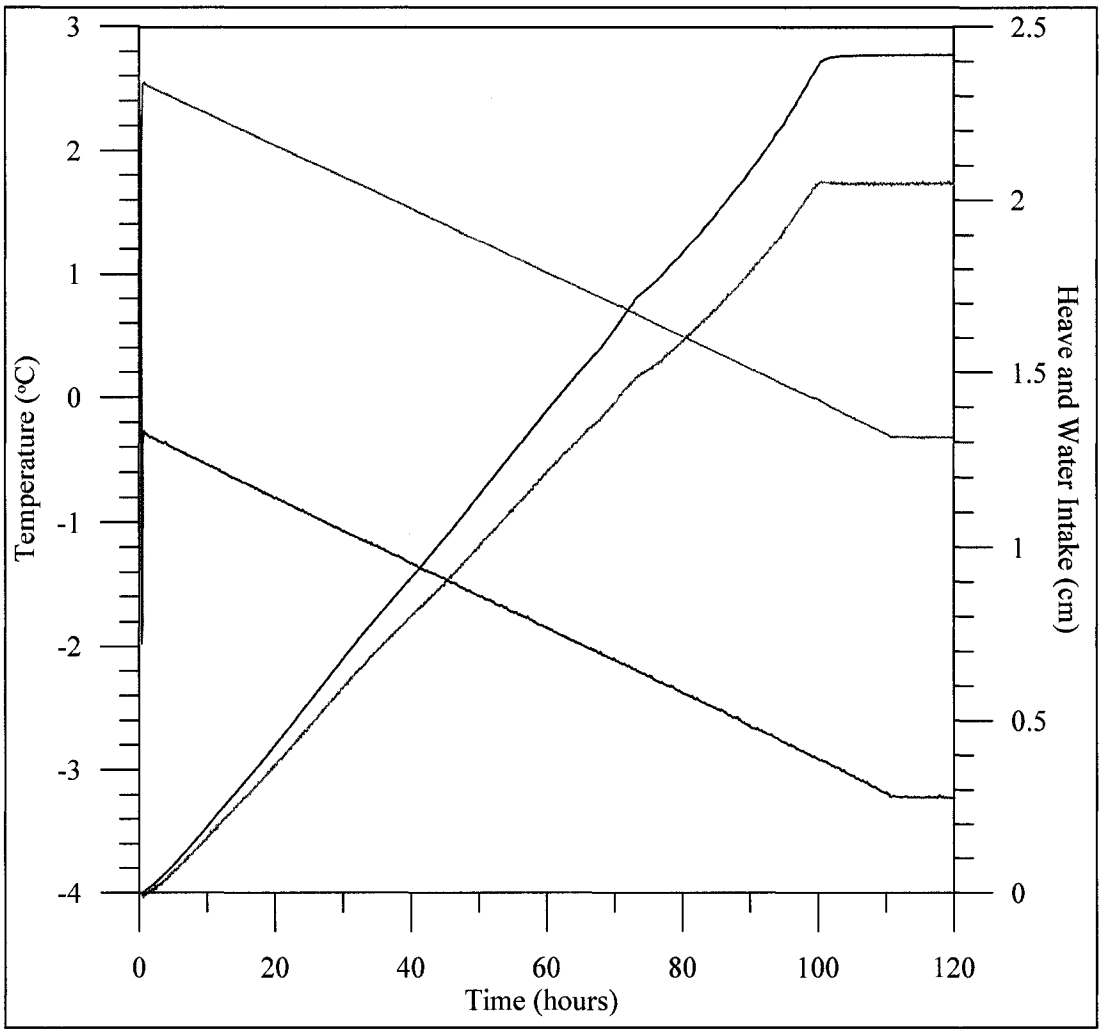

Figure E.17: Raw data for HS-A frost heave test. The top and bottom pedestal temperatures (°C) are shown in dark blue and red, respectively. The amount of heave (cm) is shown in green, and the amount of water intake (cm) is shown in sky blue. The initial sample length was 54 mm. The bottom pedestal temperature reached 0°C at 98.75 hours. The calculated average freezing rate was 0.56 mm/hr.

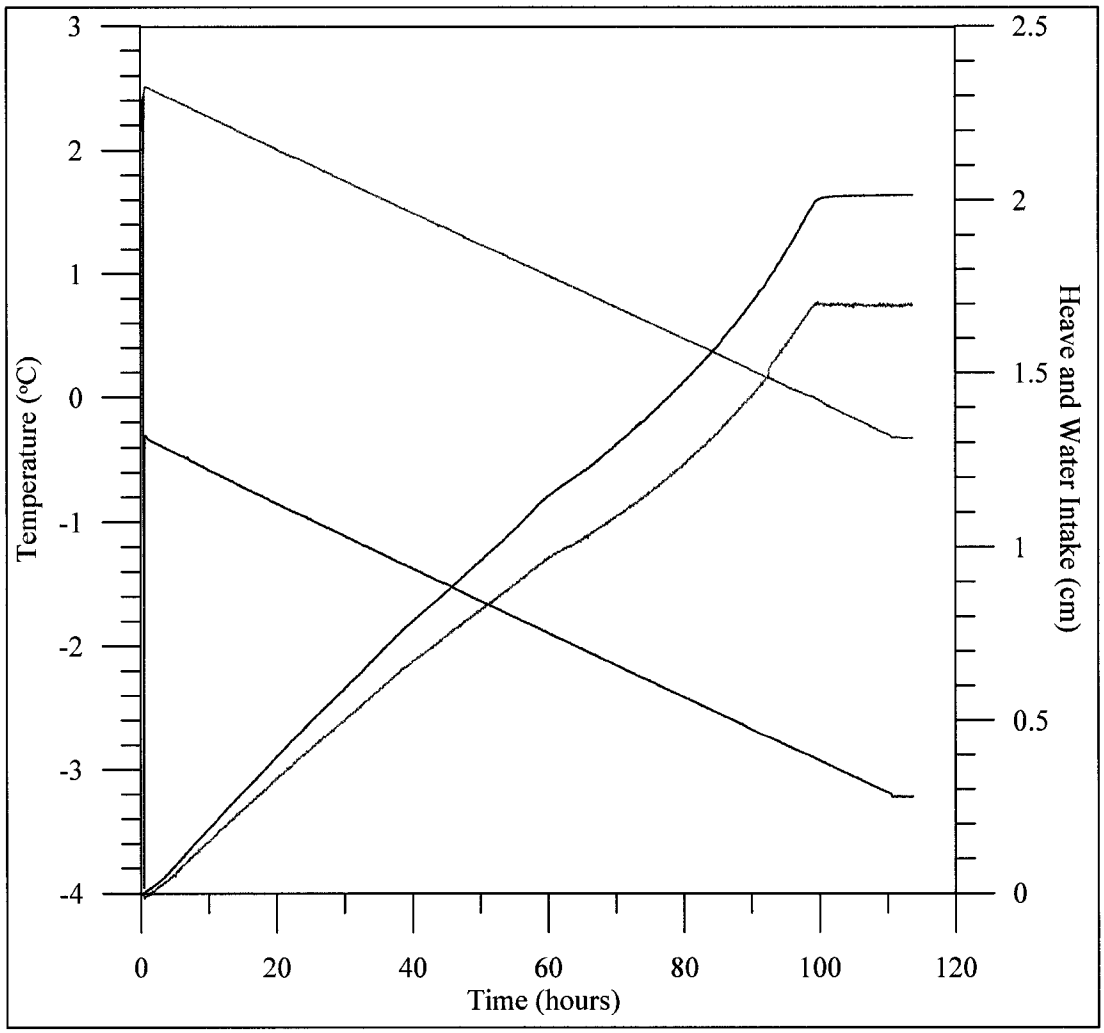

Figure E.18: Raw data for HS-B frost heave test. The top and bottom pedestal temperatures (°C) are shown in dark blue and red, respectively. The amount of heave (cm) is shown in green, and the amount of water intake (cm) is shown in sky blue. The initial sample length was 54 mm. The bottom pedestal temperature reached 0°C at 99.08 hours. The calculated average freezing rate was 0.56 mm/hr.

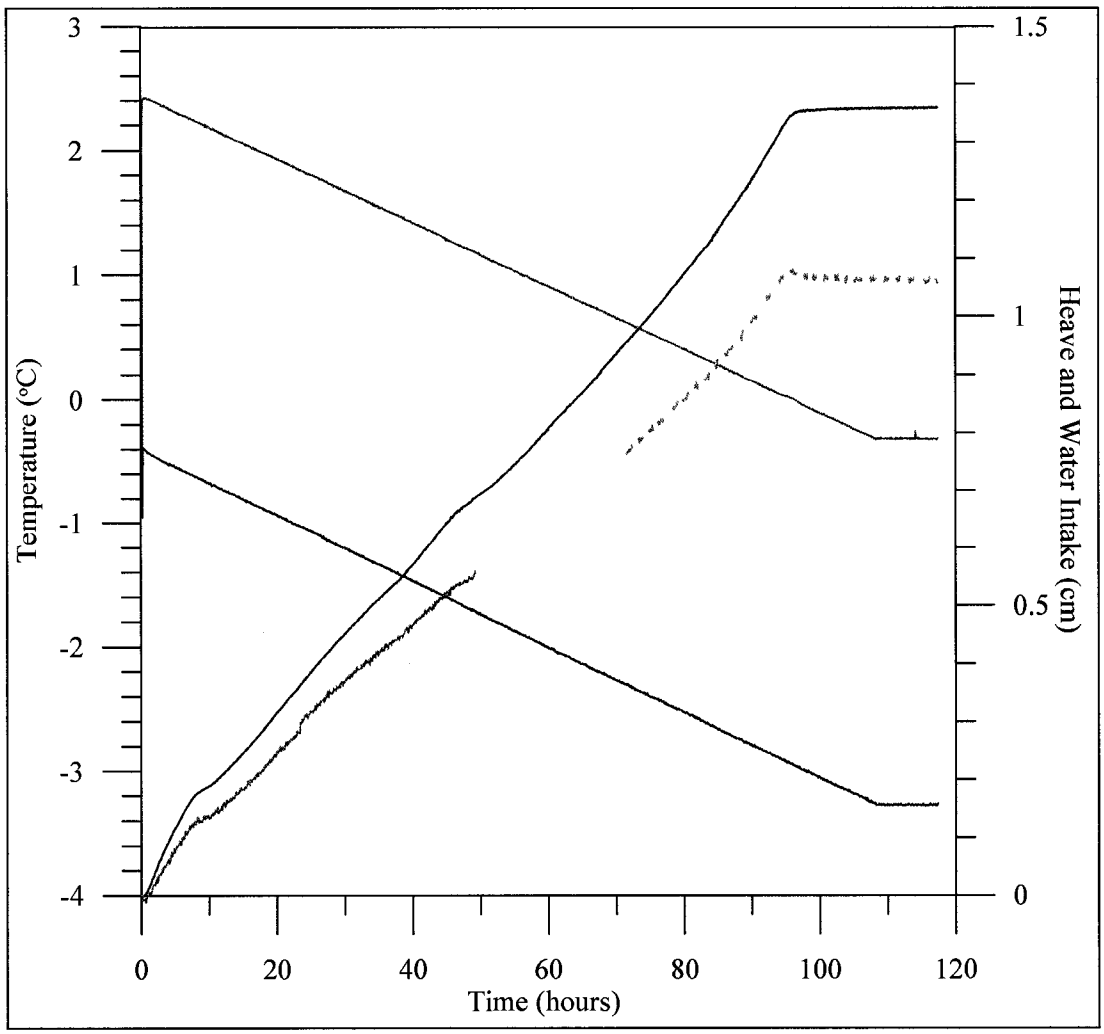

Figure E.19: Raw data for HS Ca^{2+}-A frost heave test. The top and bottom pedestal temperatures (°C) are shown in dark blue and red, respectively. The amount of heave (cm) is shown in green, and the amount of water intake (cm) is shown in sky blue. The initial sample length was 54 mm. The bottom pedestal temperature reached 0°C at 96.08 hours. The calculated average freezing rate was 0.56 mm/hr. At 49.25 hours, the double-walled burette was filled incorrectly, inadvertently introducing pressure into the water system. The problem was corrected at 71.42 hours, and the water intake data after this time (shown as the dashed sky blue line) has been projected, following a linear trend.

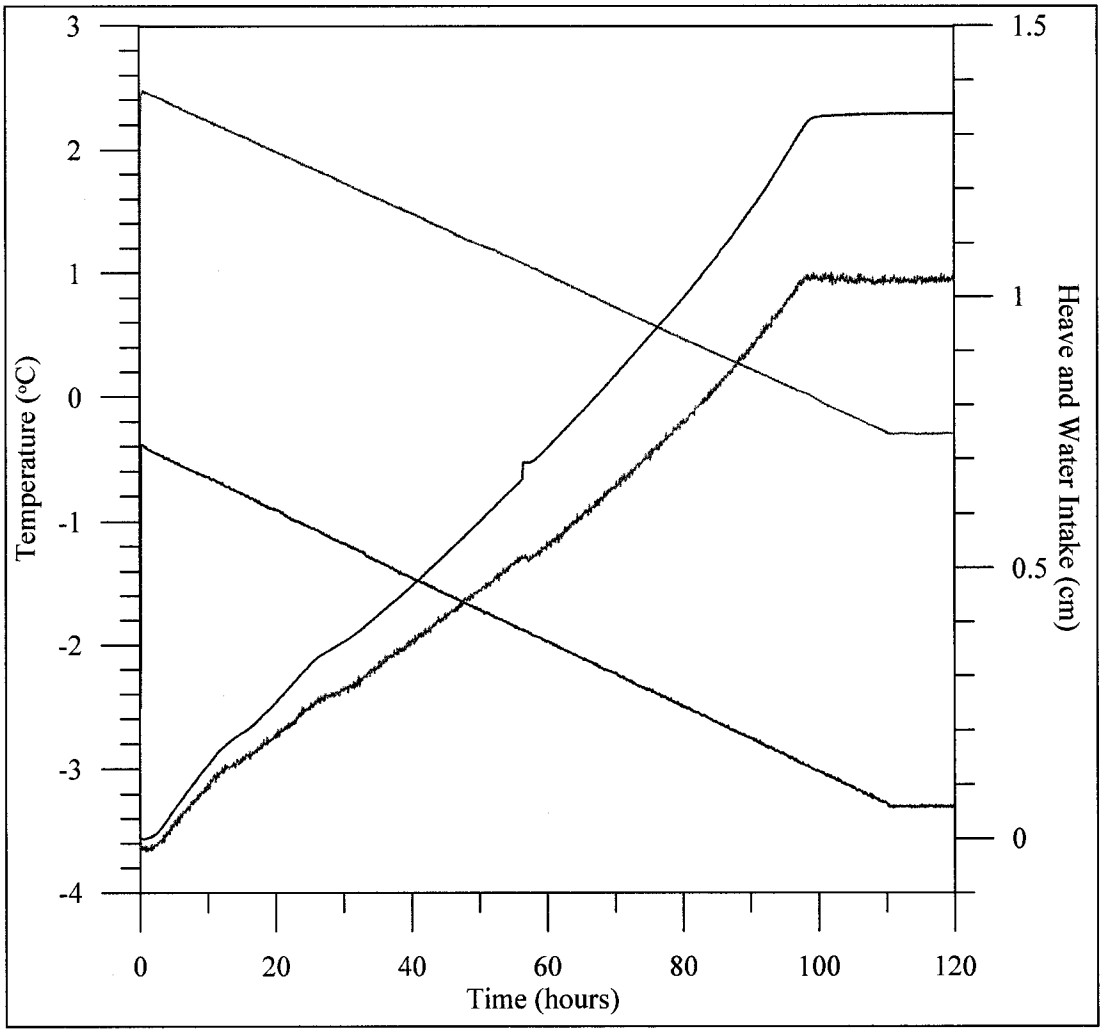

Figure E.20: Raw data for HS Ca^{2+}-B frost heave test. The top and bottom pedestal temperatures (°C) are shown in dark blue and red, respectively. The amount of heave (cm) is shown in green, and the amount of water intake (cm) is shown in sky blue. The initial sample length was 55 mm. The bottom pedestal temperature reached 0°C at 98.92 hours. The calculated average freezing rate was 0.56 mm/hr.

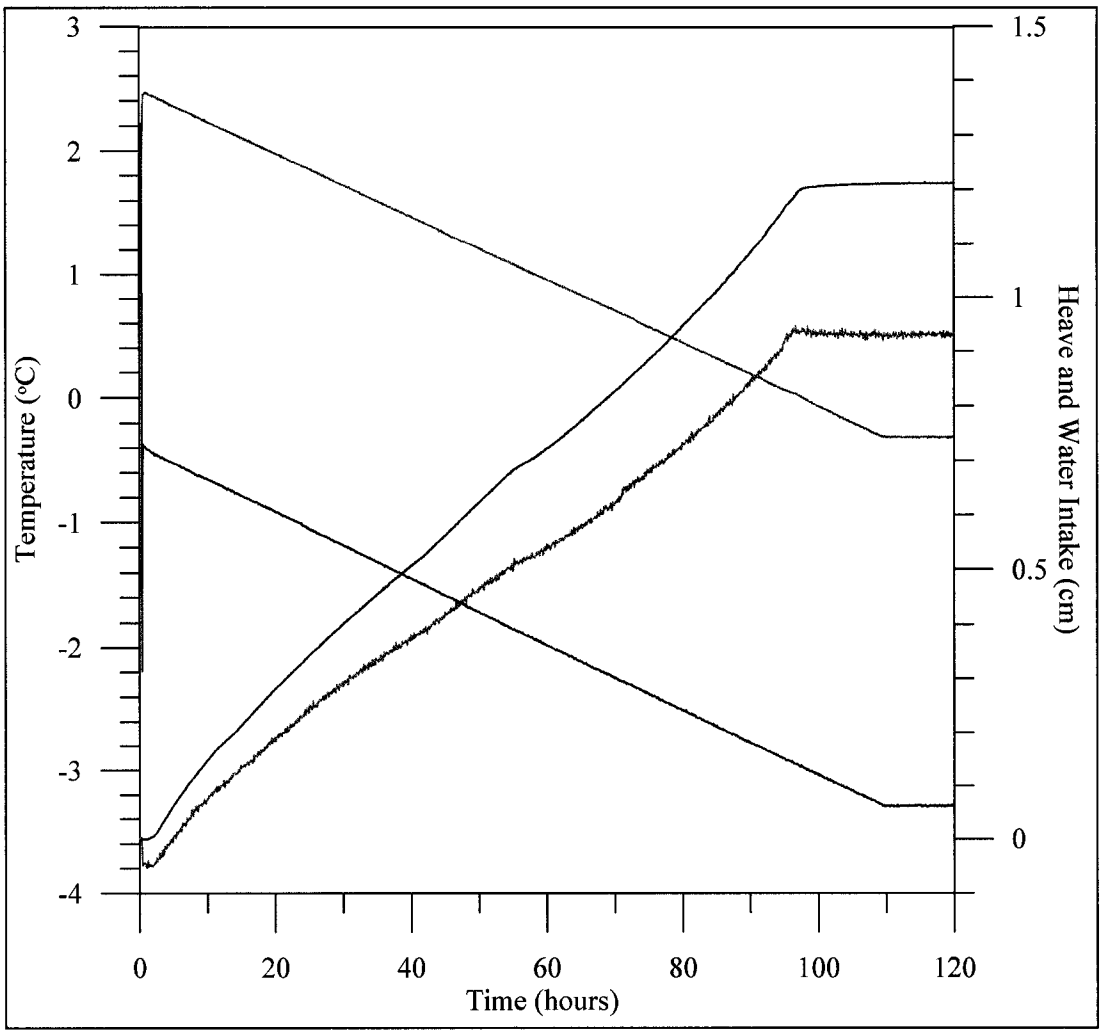

Figure E.21: Raw data for HS Mg^{2+}-A frost heave test. The top and bottom pedestal temperatures (°C) are shown in dark blue and red, respectively. The amount of heave (cm) is shown in green, and the amount of water intake (cm) is shown in sky blue. The initial sample length was 55 mm. The bottom pedestal temperature reached 0°C at 97.58 hours. The calculated average freezing rate was 0.56 mm/hr.

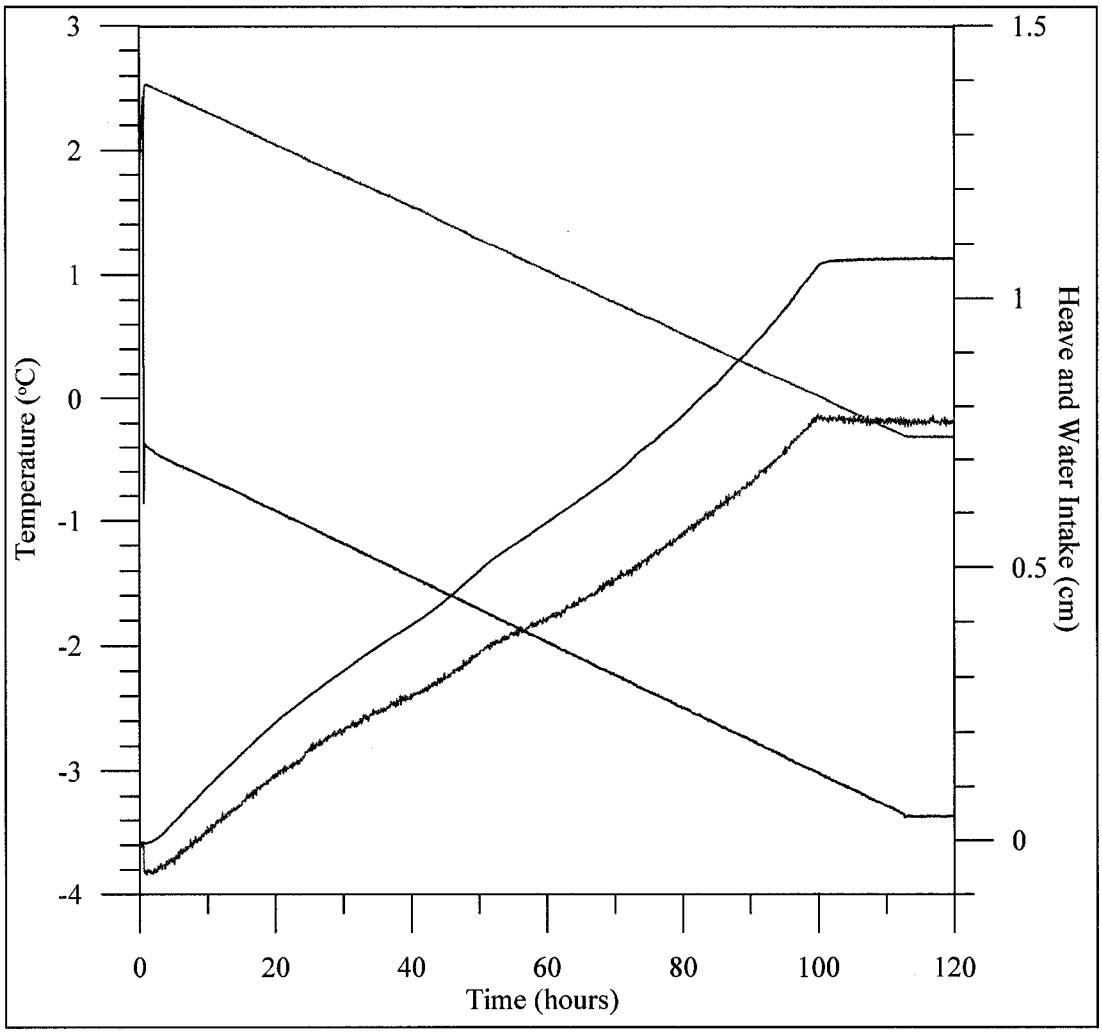

Figure E.22: Raw data for HS Mg^{2+}-B frost heave test. The top and bottom pedestal temperatures (°C) are shown in dark blue and red, respectively. The amount of heave (cm) is shown in green, and the amount of water intake (cm) is shown in sky blue. The initial sample length was 56 mm. The bottom pedestal temperature reached 0°C at 100.83 hours. The calculated average freezing rate was 0.56 mm/hr.

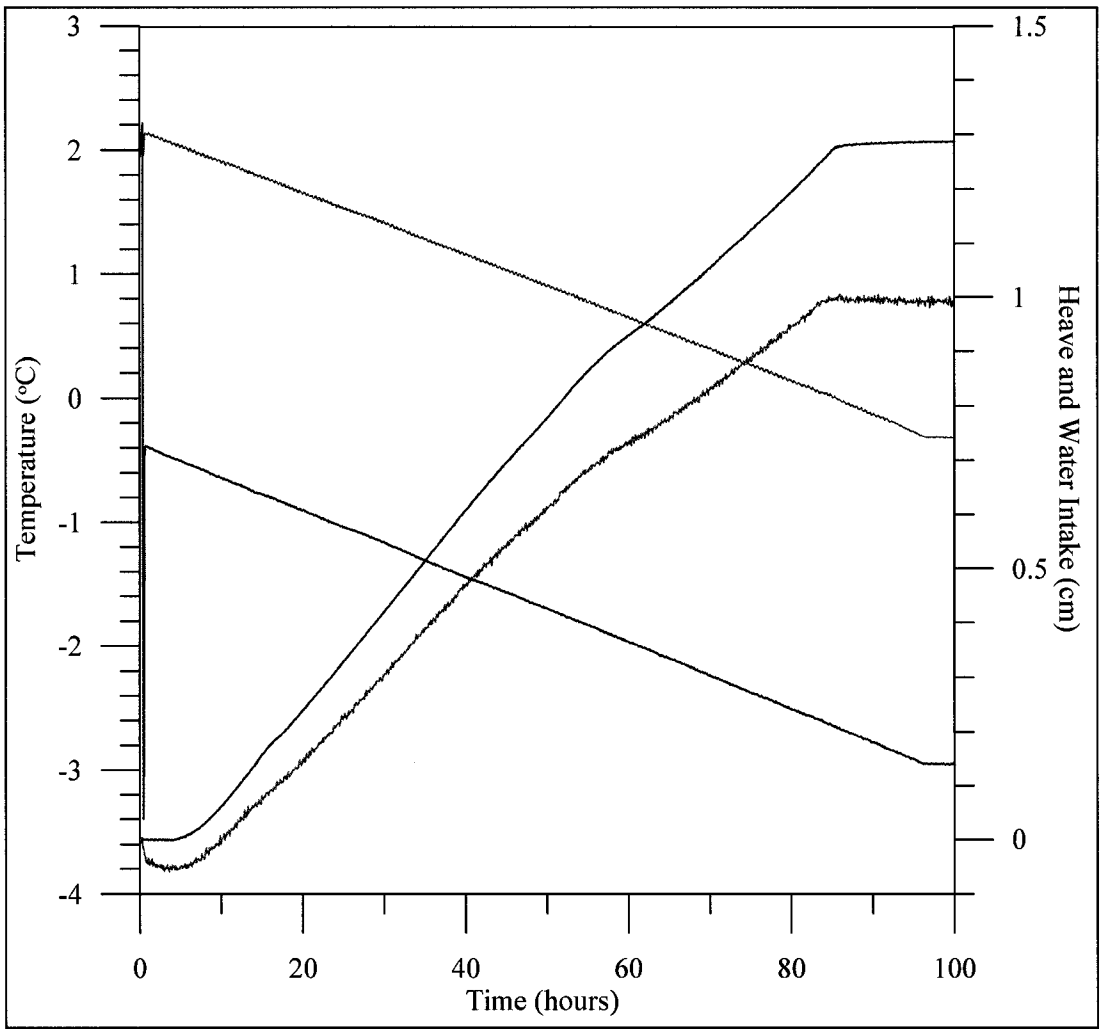

Figure E.23: Raw data for HS Na^+-A frost heave test. The top and bottom pedestal temperatures (°C) are shown in dark blue and red, respectively. The amount of heave (cm) is shown in green, and the amount of water intake (cm) is shown in sky blue. The initial sample length was 48 mm. The bottom pedestal temperature reached 0°C at 85.42 hours. The calculated average freezing rate was 0.56 mm/hr.

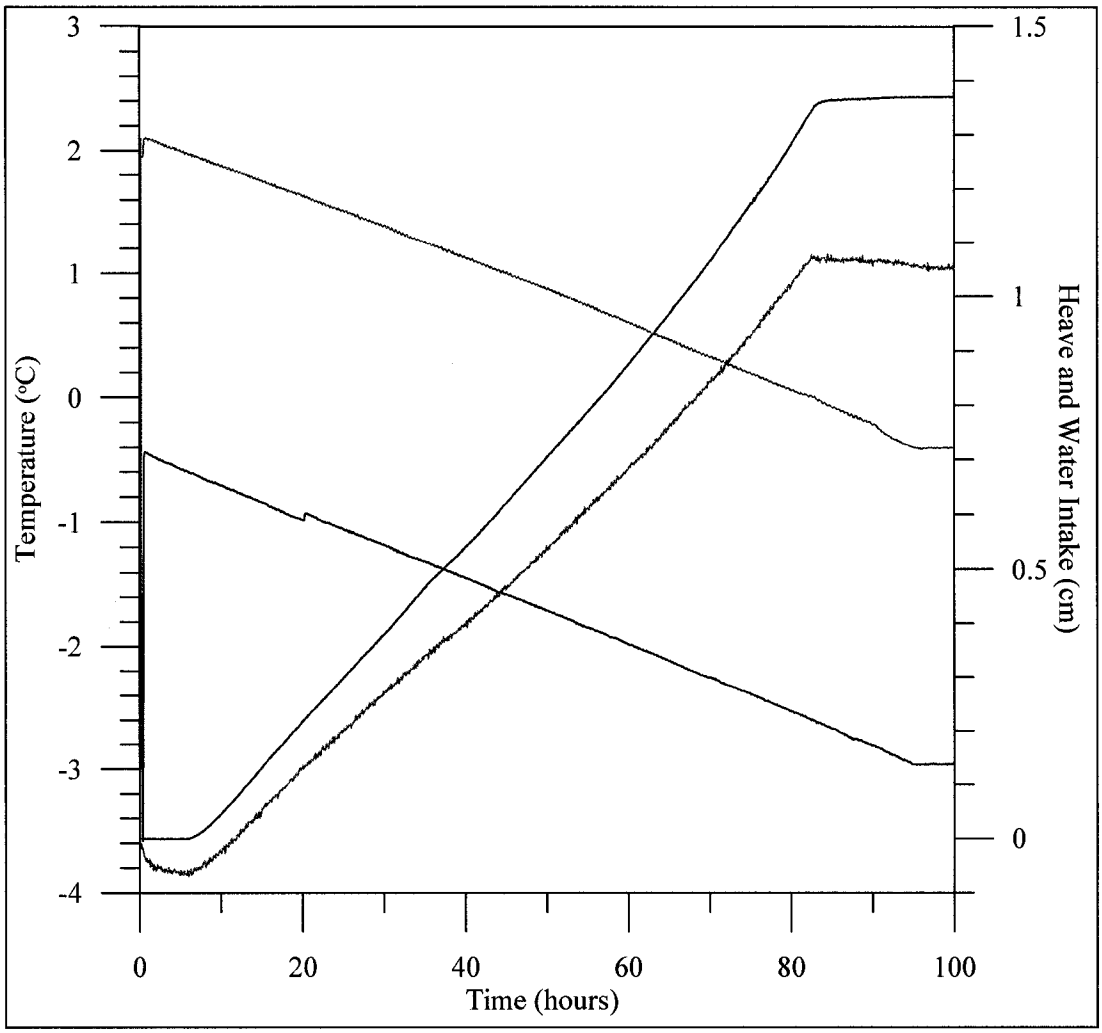

Figure E.24: Raw data for HS Na^+-B frost heave test. The top and bottom pedestal temperatures (°C) are shown in dark blue and red, respectively. The amount of heave (cm) is shown in green, and the amount of water intake (cm) is shown in sky blue. The initial sample length was 48 mm. The bottom pedestal temperature reached 0°C at 82.08 hours. The calculated average freezing rate was 0.58 mm/hr.

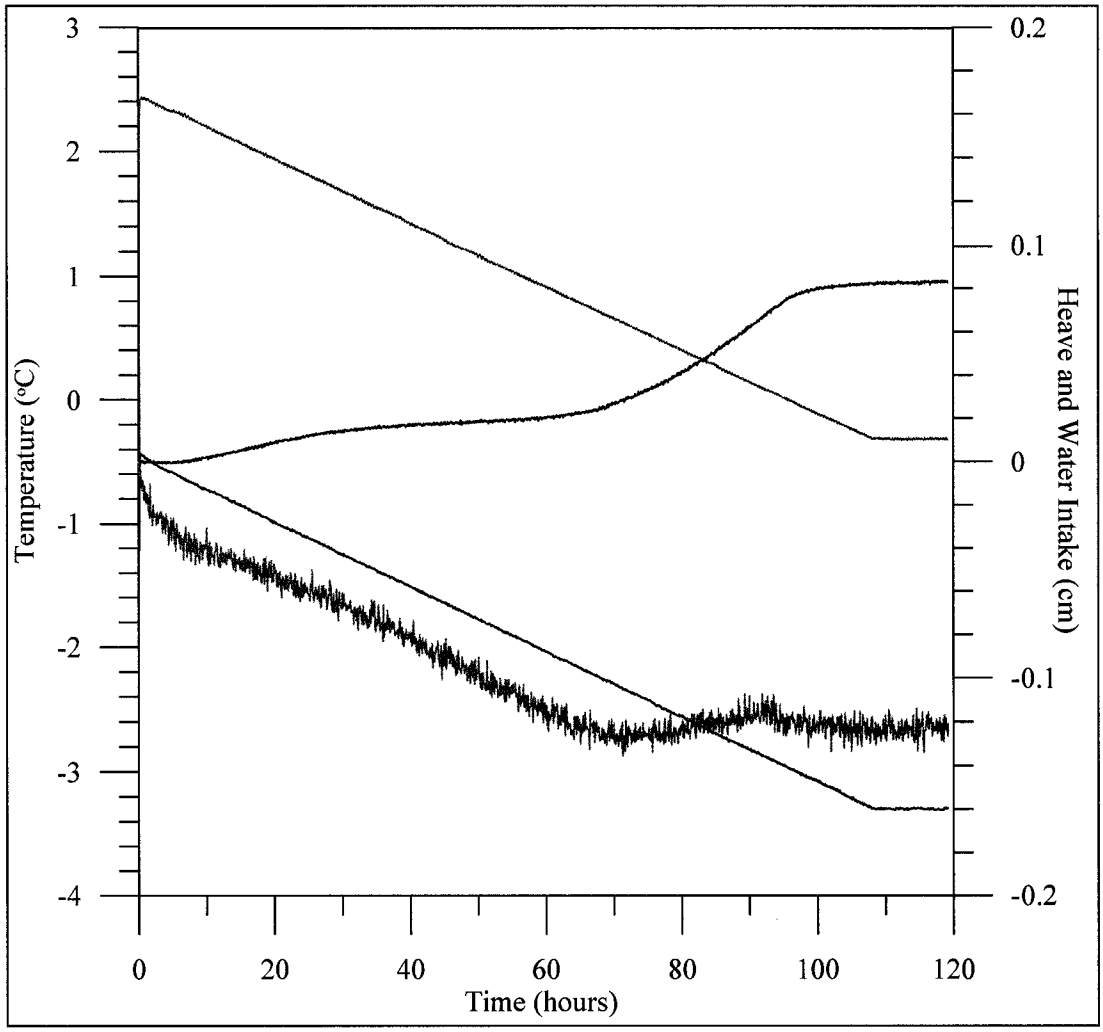

Figure E.25: Raw data for HS K^+-A frost heave test. The top and bottom pedestal temperatures (°C) are shown in dark blue and red, respectively. The amount of heave (cm) is shown in green, and the amount of water intake (cm) is shown in sky blue. The initial sample length was 54 mm. The bottom pedestal temperature reached 0°C at 95.5 hours. The calculated average freezing rate was 0.57 mm/hr.

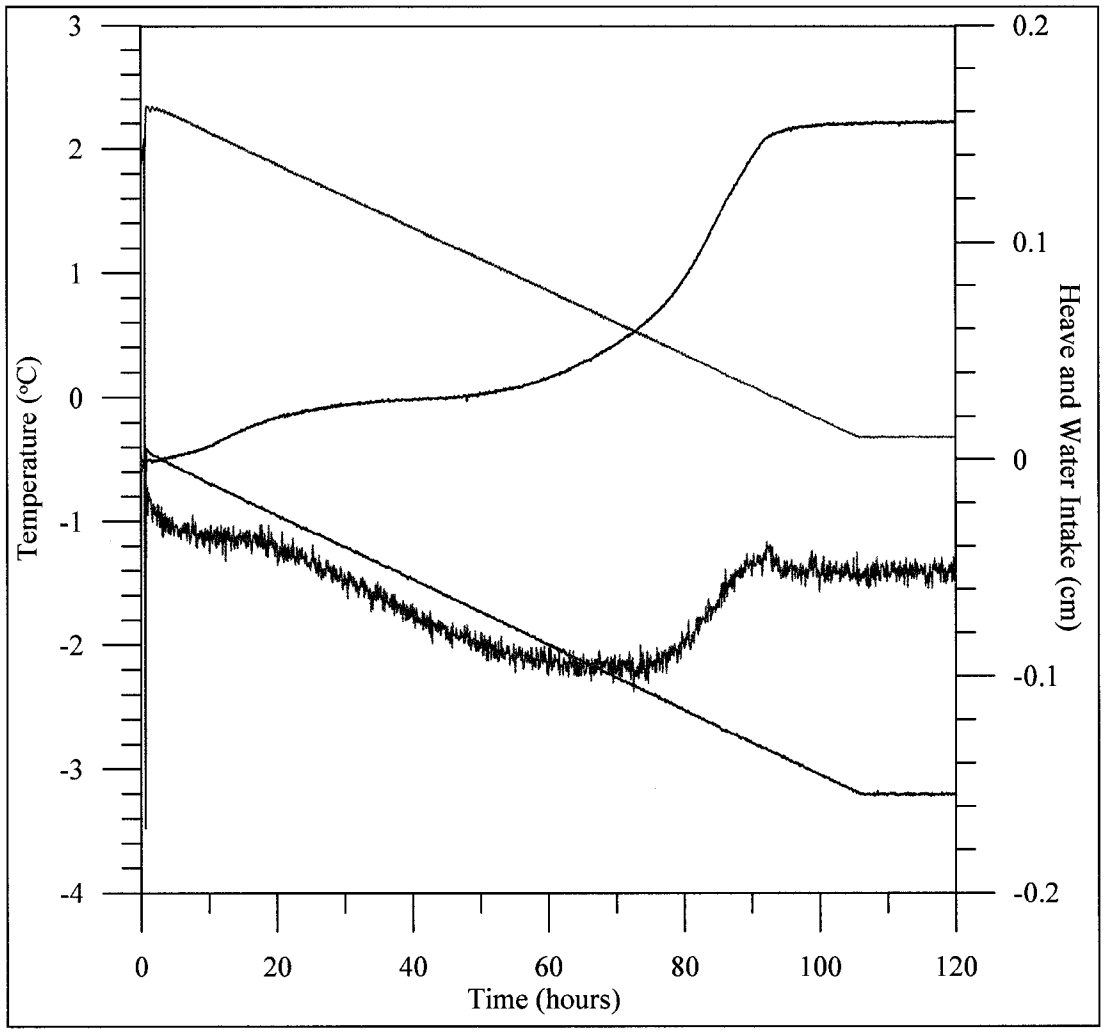

Figure E.26: Raw data for HS K^+-B frost heave test. The top and bottom pedestal temperatures (°C) are shown in dark blue and red, respectively. The amount of heave (cm) is shown in green, and the amount of water intake (cm) is shown in sky blue. The initial sample length was 53 mm. The bottom pedestal temperature reached 0°C at 93.08 hours. The calculated average freezing rate was 0.56 mm/hr.

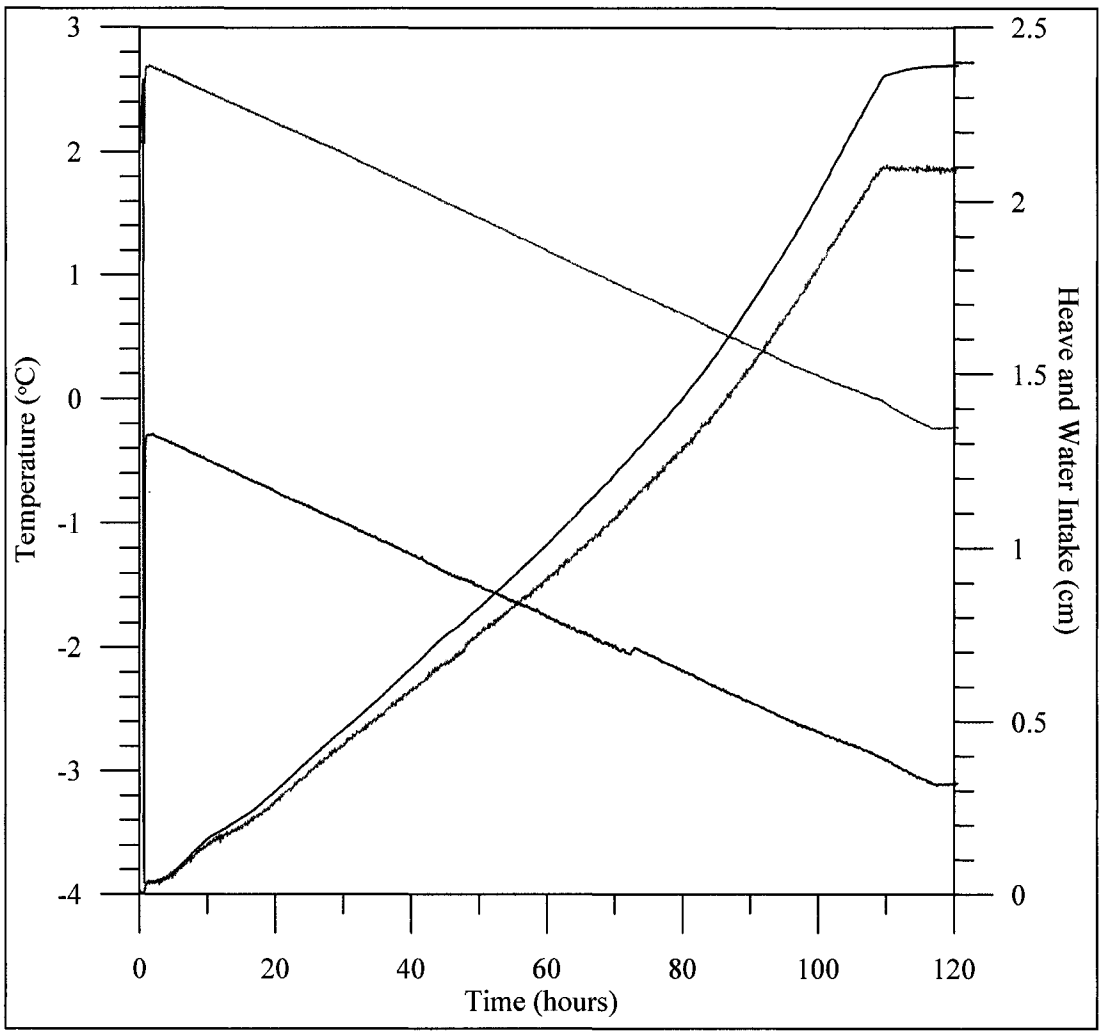

Figure E.27: Raw data for HV-A frost heave test. The top and bottom pedestal temperatures (°C) are shown in dark blue and red, respectively. The amount of heave (cm) is shown in green, and the amount of water intake (cm) is shown in sky blue. The initial sample length was 58 mm. The bottom pedestal temperature reached 0°C at 108.5 hours. The calculated average freezing rate was 0.53 mm/hr.

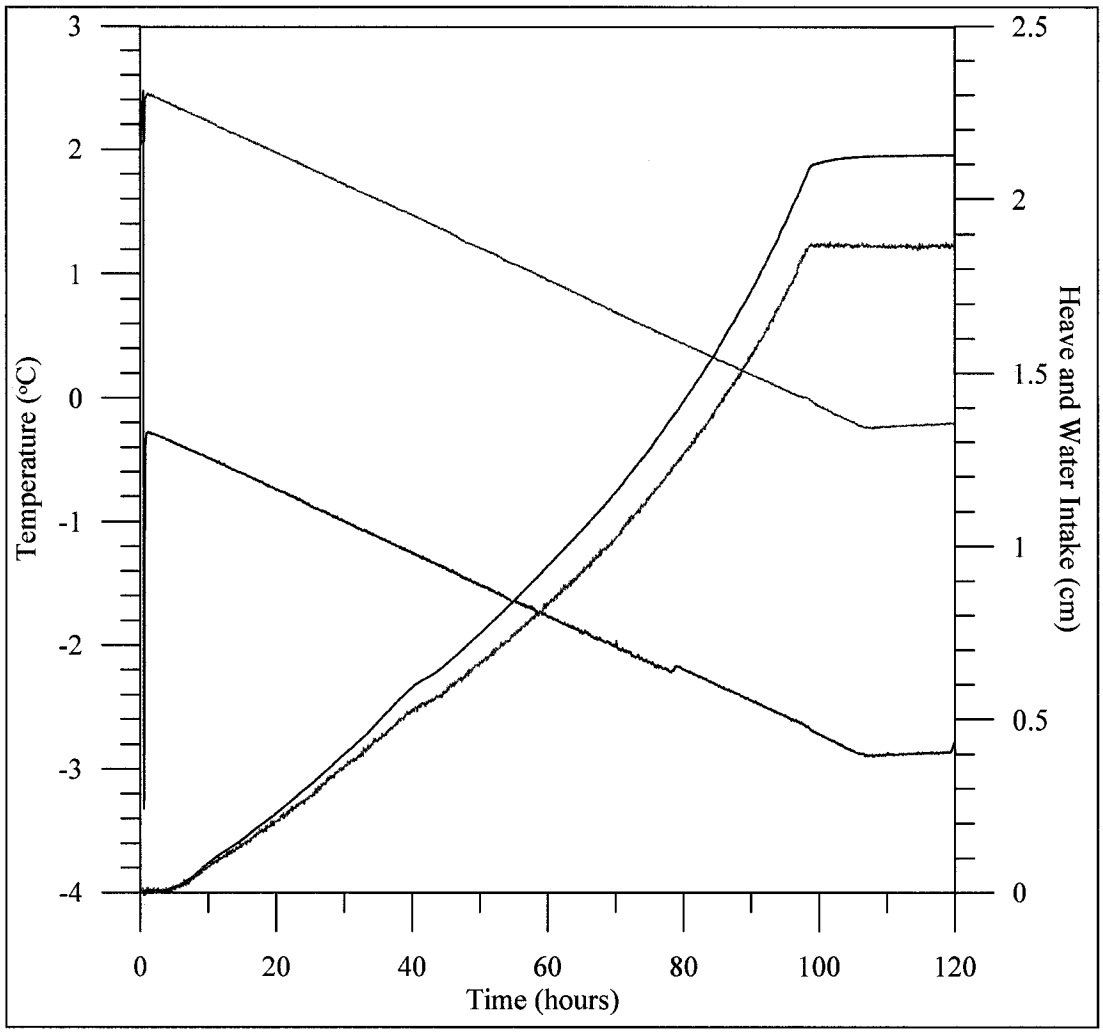

Figure E.28: Raw data for HV-B frost heave test. The top and bottom pedestal temperatures (°C) are shown in dark blue and red, respectively. The amount of heave (cm) is shown in green, and the amount of water intake (cm) is shown in sky blue. The initial sample length was 53 mm. The bottom pedestal temperature reached 0°C at 98.0 hours. The calculated average freezing rate was 0.54 mm/hr.

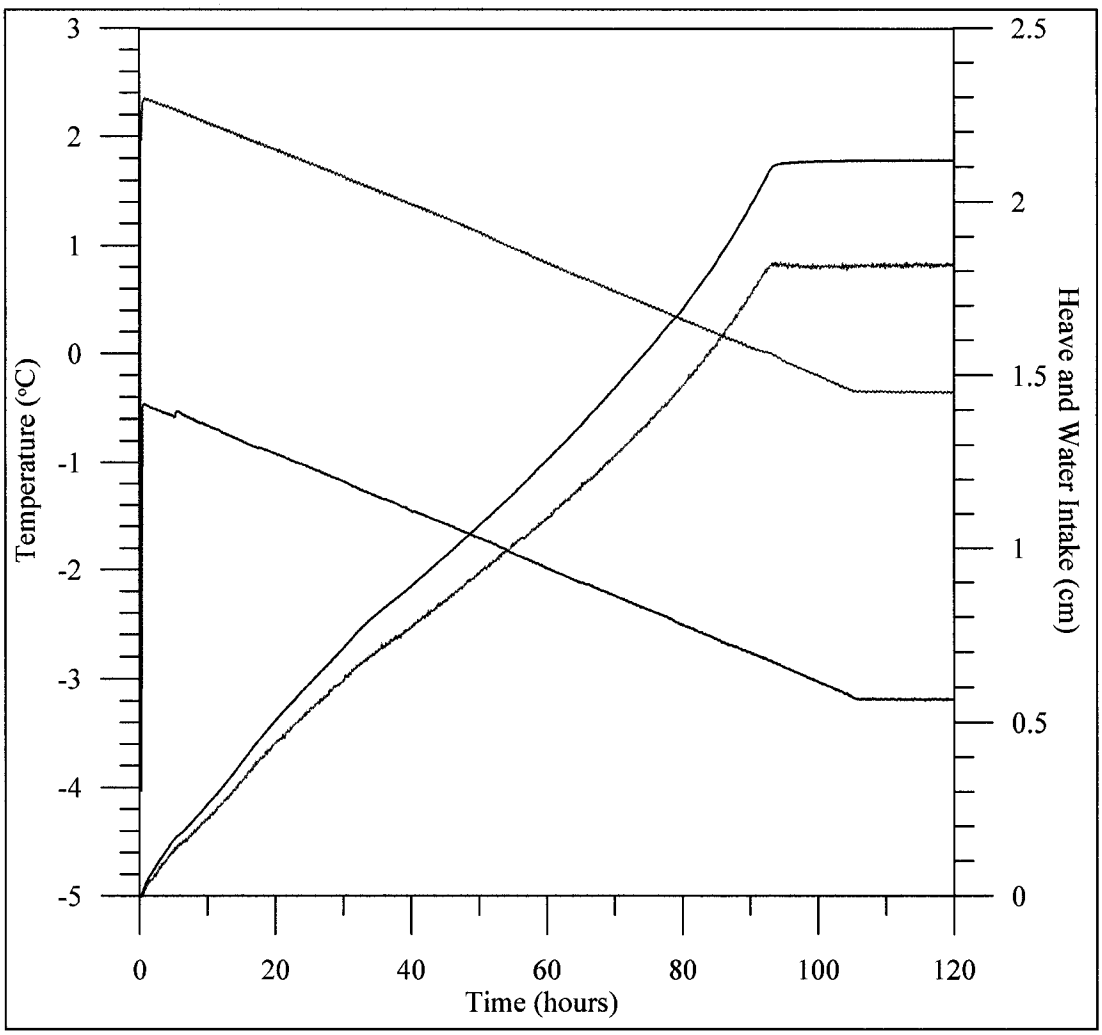

Figure E.29: Raw data for HV Ca^{2+} frost heave test. The top and bottom pedestal temperatures (°C) are shown in dark blue and red, respectively. The amount of heave (cm) is shown in green, and the amount of water intake (cm) is shown in sky blue. The initial sample length was 53 mm. The bottom pedestal temperature reached 0°C at 92.67 hours. The calculated average freezing rate was 0.57 mm/hr.

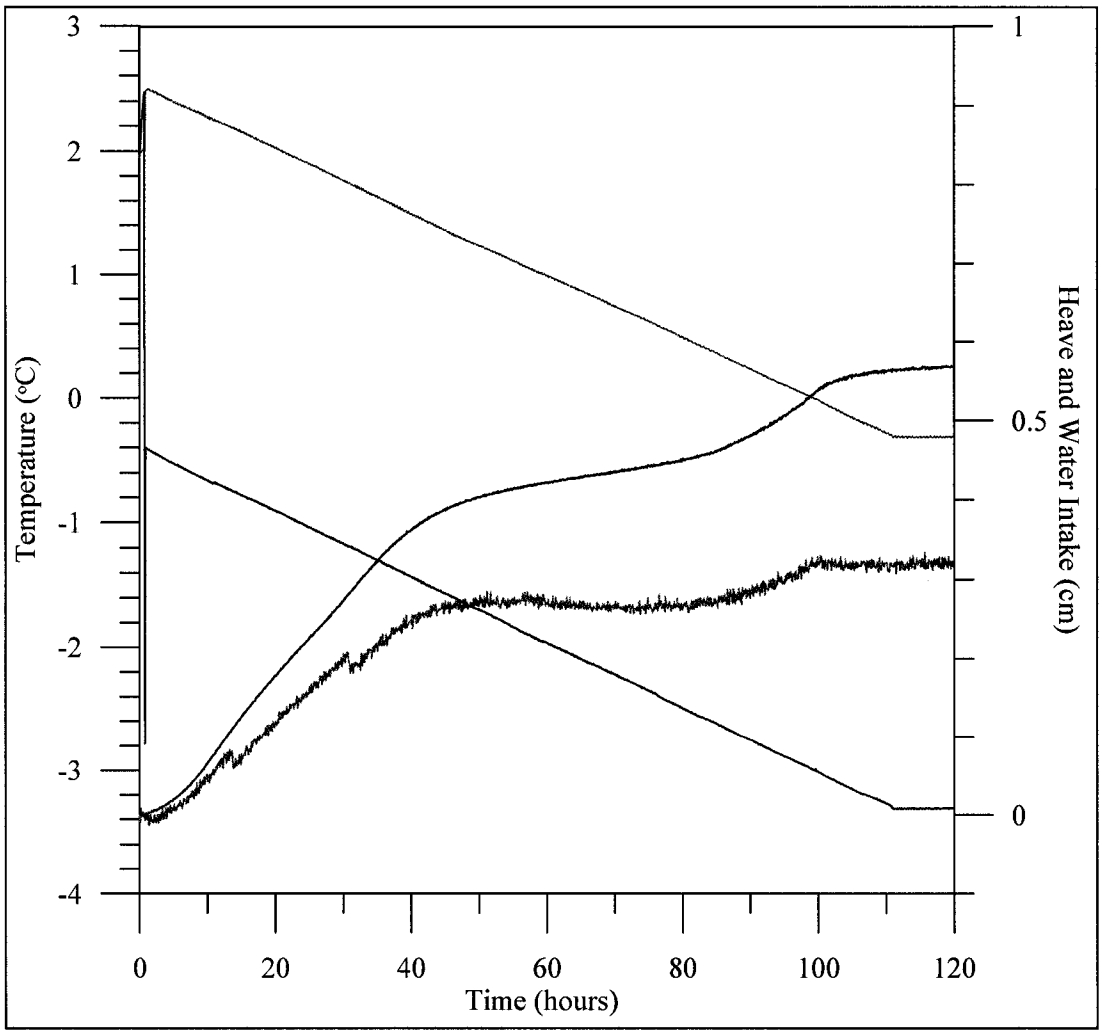

Figure E.30: Raw data for HV Na^+ frost heave test. The top and bottom pedestal temperatures (°C) are shown in dark blue and red, respectively. The amount of heave (cm) is shown in green, and the amount of water intake (cm) is shown in sky blue. The initial sample length was 55 mm. The bottom pedestal temperature reached 0°C at 98.83 hours. The calculated average freezing rate was 0.56 mm/hr.

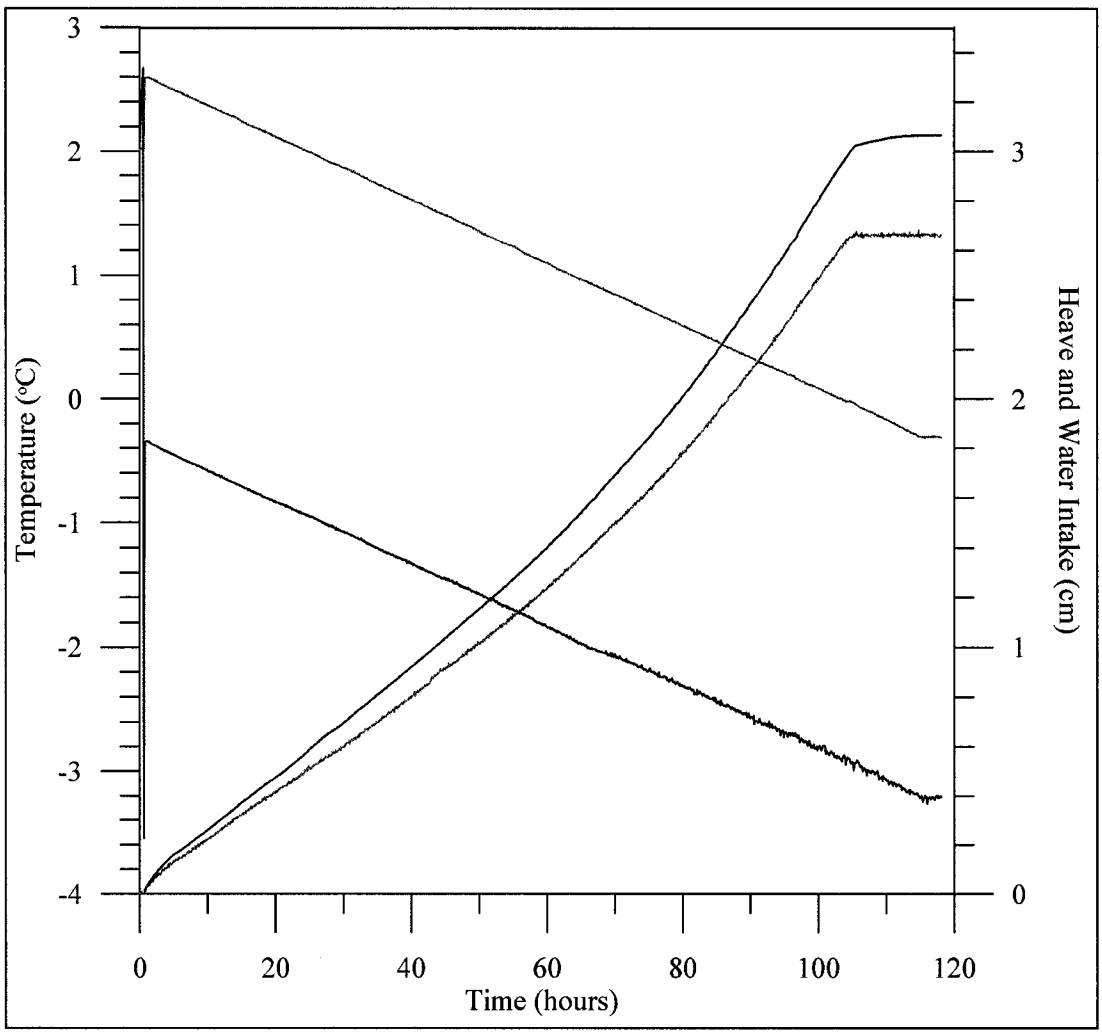

Figure E.31: Raw data for HV ORG-A frost heave test. The top and bottom pedestal temperatures (°C) are shown in dark blue and red, respectively. The amount of heave (cm) is shown in green, and the amount of water intake (cm) is shown in sky blue. The initial sample length was 57 mm. The bottom pedestal temperature reached 0°C at 103.08 hours. The calculated average freezing rate was 0.55 mm/hr.

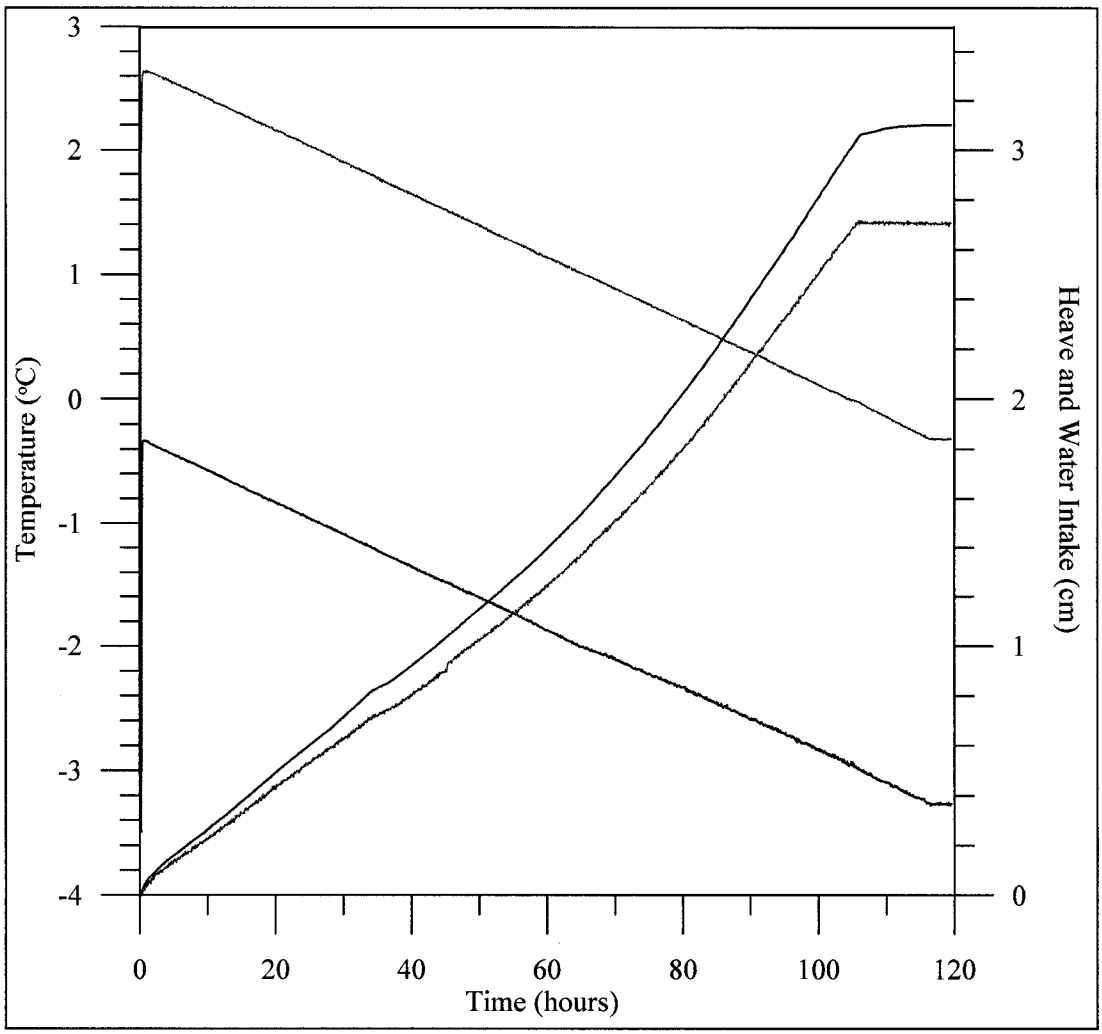

Figure E.32: Raw data for HV ORG-B frost heave test. The top and bottom pedestal temperatures (°C) are shown in dark blue and red, respectively. The amount of heave (cm) is shown in green, and the amount of water intake (cm) is shown in sky blue. The initial sample length was 58 mm. The bottom pedestal temperature reached 0°C at 104.0 hours. The calculated average freezing rate was 0.56 mm/hr.